Molecular Biomarkers in the Biosphere, Geosphere and Archaeosphere

Dissertation

zur Erlangung des Doktorgrades
der Mathematisch-Naturwissenschaftlichen Fakultät
der Christian-Albrechts-Universität
zu Kiel

vorgelegt von

Jan Hendrik Weber

Kiel, 2020

Erster Gutachter:	Prof. Dr. Lorenz Schwark
Zweiter Gutachter:	Prof. Dr. Volker Thiel
Tag der mündlichen Prüfung:	19.06.2020

Abstract

Biomarkers are molecular compounds from a once living organism (plant, microbe or animal), which can be used to trace a specific source organism, a group of organisms, or a particular process in geological and archaeological media. In this thesis, organic geochemical techniques including the biomarker approach and stable isotopes were applied to different research areas of the biosphere, geosphere and archaeosphere to characterise the origin of the organic matter. The biomarkers provide essential knowledge about environmental and climatic changes, and about the diet and rites of ancient cultures.

Paleoclimate and associated paleovegetation exert a major influence on present to prehistoric human activities and therefore are of paramount importance to investigate ancient human living conditions. Early reforestation after the last glacial shaped human living space and was dominated by pioneer plants including four birch species. These differ in habitat conditions but their differentiation by palynology poses a problem due to similar pollen shape and size. Here an alternative approach of birch species identification based on their epicuticular wax composition was ascertained for potential application in especially Late Glacial and Holocene sediments. A chemotaxonomic separation of the four Europen birch species based on a suite of wax lipids could be achieved. In addition to previous studies employing recent plant wax *n*-alkane distribution only, the potential contribution of *n*-alkanes, which in an ontogentic to diagentic continuum can be released from precursor lipids via secondary and tertiary degradation of *n*-alkyl esters (and their degradation products like *n*-alkanoic acids and *n*-alcohols) were assessed. The early release of bound wax lipids carries a high potential to modulate the pool of free lipids, which should be considered when interpreting wax lipids of potentially mixed origin and their isotopic signatures in soils and sediments.

Lake sediment from Lake Steisslingen (SW-Germany) has been investigated to characterise the biotic response of organisms during the Younger Dryas cold period (12,680 – 11,590 BP) at the Pleistocene/Holocene transition. Based on biomarker distributions representing specific organism groups including diatoms, haptophyte algae, heterocyte cyanobacteria, heterotrophic bacteria and terrestrial plants, a separation of the Younger Dryas in three phases was defined.

In a second case study, lacustrine sediments from Lake Stymphalia (Peleponnes, Southern Greece) were investigated to study the local environmental and climatic changes between 15,000 to 2,000 a BP. Heterocyte glycolipids (HGs) and glycerol dialkyl glycerol tetraethers (GDGTs) have been applied to characterise the (aquatic) microbial community and to determine paleotemperature changes in the study area. Epicuticular wax lipids yielded information on development of paleovegetation and revealed a human impact on land-use and ecosystem evolution.

The second part of this PhD thesis deals with the application of biomarkers and their compound-specific carbon isotope values in the archaeosphere. These techniques facilitate reconstructing the diet of past cultures and to trace animal husbandry practisess. Modern animal adipose fats and dairy fats from pigs, cattle, sheep, and goats from Ukraine can be distinguished by their $\delta^{13}C$ values of palmitic ($C_{16:0}$) and stearic ($C_{18:0}$) acid. These individual fatty acids are also found in pottery vessels from Cucuteni-Trypillia culture, suggesting that most samples are from ruminant animal origin, but also from another potential source such as horses. Beside the animal fats, lipids indicative for beeswax have been detected in the pottery samples from Ukraine and Moldova, but also in ancient ceramic pots from the Wartberg culture of central Germany. Here, the individual lipid composition could be connected to the shape and function of most pots.

In archaeological sites from the Baltic in Northern Germany, pottery use based its organic residue content could be compared between everyday use pottery from a domestic dwelling site (Oldenburg-Dannau) and specific grave gift pottery recovered from a nearby megalithic tomb (Wangels). Highly decorated, unglazed ceramic vessels from the Funnelbeaker and Globular Amphora culture were found as intact burial gifts containing cattle meat and milk fats, but no common cereals or aquatic resources, although located close to the shoreline. Additionally, a fatty acid distribution indicative for Sea Buckthorn oil was found in samples from exclusively the latest burial phase, which may have served as an exclusive burial gift. Contrary, the mainly undecorated pots from the coeval adjacent dwelling site Oldenburg-Dannau contained a mixed composition of plant and milk resources. Thus, the exclusive use of cattle meat in the burial indicate the important role of cattle in the ritual and spiritual sphere of Neolithic societies in northern Germany.

Zusammenfassung (German Abstract)

Biomarker sind molekulare Verbindungen aus einem ehemals lebenden Organismus (Pflanzen, Mikroben oder Tiere), die zur Bestimmung eines spezifischen Organismus, einer Organismengruppe oder eines bestimmten Prozesses in geologischen und archäologischen Medien verwendet werden können. In dieser Doktorarbeit wurden organisch-geochemische Techniken, einschließlich die Verwendung von Biomarkern und stabilen Isotope, auf verschiedene Forschungsbereiche der Biosphäre, Geosphäre und Archäosphäre angewandt, um die Herkunft des organischen Materials zu charakterisieren. Biomarker liefern ein wesentliches Verständnis über Umwelt- und Klimaveränderungen in der Vergangenheit, sowie über die Ernährung und Riten alter Kulturen.

Das Paläoklima und die damit verbundene Paläovegetation üben einen großen Einfluss auf die gegenwärtigen und prähistorischen menschlichen Aktivitäten aus und sind daher von größter Bedeutung für die Erforschung der prähistorischen Lebensbedingungen des Menschens. Die erste Wiederaufforstung nach dem letzten Glazial prägte den menschlichen Lebensraum und wurde von Pionierpflanzen, wie den vier europäischen Birkenarten, dominiert. Diese unterscheiden sich zwar in ihren Lebensraumbedingungen, aber ihre palynologische Differenzierung ist aufgrund der ähnlichen Pollenform und -größe problematisch. Daher wurde in dieser Thesis ein alternativer Ansatz zur Identifizierung von Birkenarten auf der Grundlage ihrer epikutikulären Wachszusammensetzung für eine mögliche Anwendung insbesondere in spätglazialen und holozänen Sedimenten gewählt. Eine chemotaxonomische Trennung der vier europäischen Birkenarten konnte mit Hilfe von unterschiedlichen Wachslipiden erreicht werden. Im Vergleich zu früheren Studien wurde der Schwerpunkt auf den sekundären und tertiären Abbau von *n*-Alkylestern und deren Abbauprodukten wie *n*-Fettsäuren und *n*-Alkoholen gelegt. Die Freisetzung dieser zuvor gebundenen Lipide beeinflusst die Zusammensetzung der bereits freien Lipide signifikant, welches bei der späteren Interpretation von Wachslipiden in Böden und Sedimenten zu berücksichtigen ist.

Die Seesedimente des Steißlinger Sees (SW-Deutschland) wurden organisch-geochemisch analysiert, um die biotische Reaktion der Organismen während der Kaltzeit der Jüngeren Dryas (12,680 – 11,590 a BP) am Übergang des Pleistozän/Holozäns zu charakterisieren. Basierend auf der Verteilung von Biomarkern, die spezifische Organismen bzw. Organismengruppen einschließlich heterozyten Cyanobakterien, Diatomeen, haptophyten Algen, Bakterien und terrestrischen Pflanzen repräsentieren, wurde eine Aufteilung der Jüngeren Dryas in drei Phasen definiert.

In einer zweiten Studie wurde ein lakustrischer Sedimentkern aus dem Stymphalia See (Peleponnese, Südgriechenland) untersucht, um die lokalen Umwelt- und

Klimaveränderungen von ca. 15,000 bis 2000 vor heute zu rekonstruieren. Anhand der epikutikulären Wachslipidverteilung im Sedimentkern konnte die Vegetation im Einzugsgebiet des Stymphalia Sees charakterisiert werden und ein menschicher Einfluss in den jüngeren Sedimenten erkannt werden. Zusätzlich wurden heterozyte Glykolipide (HGs) und Glycerol-Dialkyl Glycerol-Tetraethers (GDGTs) zur Charakterisierung der (aquatischen) mikrobiellen Gemeinschaft und zur Bestimmung der Temperaturveränderungen während der letzten ca. 15.000 Jahre in Südgriechenland verwendet.

Der zweite Teil dieser Doktorarbeit befasst sich mit der Anwendung von Biomarkern und den Kohlenstoffisotopenwerten individueller Lipide in der Archäosphäre, um die Ernährung vergangener Kulturen und deren Tierhaltung zu rekonstruieren. Moderne tierische Fett- und Milchprodukte von Schwein, Rind, Schaf und Ziege aus der Ukraine lassen sich durch ihre $\delta^{13}C$-Werte von Palmitin- ($C_{16:0}$) und Stearinsäure ($C_{18:0}$) unterscheiden. Diese Fettsäuren wurden ebenfalls in Keramikgefäßen der Cucuteni-Trypillia-Kultur aus der Ukraine und Moldawiens detektiert. Die Ergebnisse weisen darauf hin, dass die meisten Proben Fette von Wiederkäuern enthalten, aber auch von einer unbekannten Quelle, die nicht in den modernen Referenzfetten vorkommend ist. Diese Fette könnten möglicherweise von Pferden stammen. Neben den tierischen Fetten wurden in den Keramikproben aus der Ukraine und Moldawien, aber auch in Töpfen aus Zentraldeutschland der Wartbergkultur eine Lipidsignatur detektiert, die für Bienenwachs indikativ ist. In den letztgenannten Proben der Wartbergkultur konnte zusätzlich die individuelle Lipidzusammensetzung mit der Form und Funktion der meisten Töpfe in Verbindung gebracht werden.

Die Verwendung von Alltagskeramik aus einer häuslichen Wohnstätte (Oldenburg-Dannau) aus dem Ostseeraum Norddeutschlands wurde mit Keramikgefäßen aus einem nahegelegenen Megalithgrab (Wangels) verglichen. Im Grab wurden primär reichlich verzierte und ornamentierte Keramikgefäße aus der Trichterbecher- und Kugelamphoren-Kultur Norddeutschlands hauptsächlich als intakte Grabbeigaben gefunden. Diese Gefäße enthielten hauptsächlich Rinderfette und Milchprodukte, jedoch kein Getreide oder aquatischen Produkte, obwohl der Fundplatz nahe der Küste lag. Zusätzlich wurde in Proben aus der letzten Bestattungsphase eine Fettsäureverteilung gefunden, die auf Sanddornöl hinweist, welches als exklusive und wertvolle Grabbeigabe gedient haben könnte. Im Gegensatz dazu enthielten die überwiegend schlicht ornamentierten Gefäße aus der benachbarten, gleichaltrigen Siedlung Oldenburg-Dannau eine gemischte Zusammensetzung aus Pflanzen- und Milchprodukten. Die ausschließliche Verwendung von Rinderfetten in den Grabbeigaben deutet somit auf die wichtige Rolle des Rindes in der rituellen und spirituellen Sphäre der neolithischen Gesellschaften in Norddeutschland hin.

I. Publications

The following chapters of this thesis have been accepted, submitted or prepared for publications:

Weber, J., Schwark, L. Epicuticular wax lipid composition of endemic European *Betula* species in a potential ontogenetic/diagenetic continuum and its application to chemotaxonomy and paleobotany. In review in *Science of the Total Environment*.

Weber, J., Bauersachs, T., Schwark, L. A multiphasic Younger Dryas cold period recorded in sediments of Lake Steisslingen, SW-Germany: A biomarker perspective. In review in *Quaternary International*.

Weber, J., Nadeau, M.-J., Bauersachs, T., Unkel, I., Schwark, L. Holocene and late Pleistocene vegetation and environmental history of Lake Stymphalia (Peloponnese/Greece). In preparation for *Palaeogeography, Palaeoclimatology, Palaeoecology*

Weber, J., Brozio, J.-P., Müller, J., Schwark, L. 2020. Grave gifts manifest the ritual status of cattle in Neolithic societies of northern Germany. Accepted for publication in *Journal of Archaeological Science* (March 2020).

Weber, J., Shatilo, L., Hofmann, R., Schwark, L. Organic residue analysis on ceramic vessels from Cucuteni-Trypillia sites in Ukraine and Moldova. In preparation for *Journal of Archaeological Science*

The following chapters forming parts of the Appendix of this thesis have been published or are prepared for publication:

Talma, M., **Weber, J.**, Gütter, S., Holzheid, A., Rinne, C., Schwark, L., Urz, R. Organic Residue Analysis on pottery vessels from the Wartberg culture in central Germany. In preperation

Seguin, J., Bintliff, J. L., Grootes, P. M., Bauersachs, T., Dörfler, W., Heymann, C., Manning, S.W., Müller, S., Nadeau, M.-J., Nelle, O., Steier, P., **Weber, J.**, Wild, E.-M., Zagana, E., Unkel, I. 2019. 2500 years of anthropogenic and climatic landscape transformation in the Stymphalia polje, Greece. *Quaternary Science Reviews* 213, 133-154, doi: 10.1016/j.quascirev.2019.04.028

Additional publication not included in this thesis:

Dreibrodt, S., Krüger, S., **Weber, J.**, Feeser, I. Limnological response to the Laacher See eruption (LSE) in an annually laminated Allerød sediment sequence from the Nahe palaeolake (northern Germany). In review in *Boreas.*

II. Index of contents

III. Index of figures

IV. Abbreviations

$\delta^{13}C_{TOC}$= stable carbon isotope composition of total organic carbon
$\delta^{15}N$= stable nitrogen isotope composition of organic matter
$\delta^{18}O$= stable oxygen isotope composition of bulk carbonates
a.s.l.= above sea level
ACL= average chain-lengths
ASE= accelerated solvent extraction
APAA= ω-(*o*-alkylphenyl)alkanoic acid
BC= before Christ
BIT= branched and isoprenoid tetraether index
BP= before present
brGDGTs= branched glycerol dialkyl glycerol tetraether
BSTFA= *N,O*-bis(trimethylsilyl)trifluoroacetamide
BDE= Bligh & Dyer extraction
CBT= cyclisation of branched tetraethers
CPI= carbon preference index
DAG= diacylglycerol
DCM= dichloromethane
Et= ethyl
FAME= fatty acid methyl ester
GC-C-IRMS= gas chromatography-combustion-isotope ratio Mass spectrometry
GC-MS= gas chromatography-mass spectrometry
GDGTs= glycerol dialkyl glycerol tetraether
HBI= highly branched isoprenoid
HGs= heterocyte glycolipids
HPLC= high-performance liquid chromatography
HTGC-MS= high temperature gas chromatography-mass spectrometry
isoGDGTs= isoprenoid glycerol dialkyl glycerol tetraether
LCA= long-chain alkenone
LST= Laacher See Tephra
M+= Molecular ion
MAAT= mean annual air temperature
MAG= monoacylglycerol
MBT'_{5ME}= methylation index of the 5-methyl isomers of brGDGTs
Me= methyl
MeOH= methanol
m/z= mass/charge-ratio
OM= organic matter
P_{aq}= proxy for aquatic macrophytes
PTFE= polytetrafluoroethylene
SWT= surface water temperature
TAG= triacylglycerol
TC= total carbon
TIC= total inorganic carbon
TLE= total lipid extract
TN= total nitrogen
TOC= total organic carbon

tr= traces
TS= total sulfur
U^{K}_{37}= alkenone unsaturation index
V-PDB= Vienna PeeDee Belemnite
XRF= X-ray fluorescence

1. Introduction

Organic geochemistry is a relatively young discipline of the natural sciences, which deals with the study of the origin, composition and transformation of organic matter (OM), whether of biological or man-made origin, in the bio- and geosphere (Killops and Killops, 2005). The biosphere comprises a comprehensive ecosystem, where life on earth takes places, while the geosphere represents the solid part of the earth (lithosphere). The more intensive research in the field of organic geochemistry began in the middle of the 20th century with the research of the origin and characterisation of petroleum (Durand, 2003; Kvenvolden, 2006). It was discovered that organic constituents of shales, bitumen and crude oils were remnants synthesized by ancient plants (Treibs, 1934; Blumer and Omenn, 1961). Later, the newly invented methods like separation of molecular compounds by chromatographic columns used in petroleum chemistry and subsequent identification by mass spectrometry (e.g. Kimble et al., 1974; Seifert and Michael Moldowan, 1978), were transferred to numerous other disciplinary fields so that the use of organic geochemical methods spread increasingly. These fields include environmental geochemistry, paleoclimatology in marine and terrestrial archives, geobiology, evolution of organisms, forensic science, archaeology and many more. All these sub-disciplines above combine the use of so-called “biomarkers”.

1.1. The biomarker approach

Biomarkers or biological markers are “chemical fossils”, more precisely organic molecules produced from a once living organism, which have survived intact or slightly altered over time (Eglinton and Calvin, 1967). They are complex organic compounds mainly built of carbon (C), hydrogen (H) and minor hetero-elements like oxygen (O), sulphur (S) and nitrogen (N) (Peters et al., 2005). Biomarkers occur in geological media like sediments, rocks, and oils and survive over geological time (Peters et al., 2005). Further, biomarkers can also be found in archaeological pottery after storage or cooking of nourishment in the pots (Evershed, 2008). Biomarkers comprise many different types of molecules, which is why recent organic material is studied to understand their chemical or biological transformation from biological precursors to geological products. Recent functional biomolecules alter over time by loosing functional groups and/or undergo structural rearrangement, which is why there is a wide variety of structures. Individual biomarkers or biomarker classes can be related to a particular source organism, a group of organisms, or to a particular process (e.g. photosynthesis or biomass burning) and thus offer a wide range of applications in different scientific fields (Castañeda and Schouten, 2011). Most biomarkers are derived from cell membrane lipids of prokaryotic (bacteria and archaea) or eukaryotic organisms which serve as interfaces between intercellular and extracellular environment (Peters et al., 2005). Wax lipids from terrestrial plant

leaves are another significant source of lipids in sediments while fats from animal tissue or plant oils are very common in archaeological pottery. From these different types of archives, either intact biological, geological or archaeological media, biomarkers can be isolated by different solvent extraction methods and measured by different analytic tools, making the origins of multiple constituents in samples discernible. Typical state-of-the-art analytical methods are used including gas chromatography-mass spectrometry (GC-MS), gas chromatography-combustion-isotope ratio mass spectrometry (GC-C-IRMS) and high-performance liquid chromatography (HPLC) coupled to mass spectrometry (HPLC-MS) for separation, characterisation, identification and further interpretation of biomarkers or their stable isotope ratios in modern, but also in ancient samples.

In the following two chapters, an overview is given to outline organic geochemical techniques in paleobotany and environmental/climatic reconstruction (chapter 1.2) as well as in archaeology (1.3), with focus on biomarkers and stable isotopes.

1.2. Biomarkers from biosphere to geosphere

Biomarkers in the biosphere are organic compounds of known origin, which are preserved in geological archives and therefore store the information about their source organism in the geosphere for further interpretation (Eganhouse, 1997). For instance, leaf remnants or palynology have mostly been used for the vegetation reconstruction of the biosphere on species level (Mortensen et al., 2011), whereby an identification on sub-species level might be challenging (Mäkelä, 1996). In this case, biomarkers like *n*-alkanes, *n*-alcohols, *n*-alkanoic acids, *n*-alkyl esters and *n*-ketones are important constituents of epicuticular plant leaf waxes, which can be used for paleovegetation reconstruction and landscape evolution, since they have a high chemotaxonomic potential (Eglinton et al., 1962; Cranwell, 1973; Schwark et al., 2002; Bush and McInerney, 2013; Guo et al., 2018). However, mostly only long-chain *n*-alkanes were used for this application since they are robust against diagenesis and easily detectable by GC-MS, albeit, often used without prior study of the biomarker composition of local recent vegetation. It has been postulated that woody plants can be distinguished from graminoids by comparing the relative abundances of nC_{27}, nC_{29} and nC_{31} (Schwark et al., 2002). However, recent studies demonstrated that all three chain-lengths are highly variable in both groups (Bush and McInerney, 2013). Additionally, little is known about the degradation mechanisms of, in particular, *n*-alkyl esters, *n*-alcohols and *n*-alkanoic acids and how they might affect the pool of already free lipids in soils and sediments. This may be one reason why biomarker data and palynology do not coincide in some studies (Farrimond and Flanagan, 1996; Ficken et al., 1998). Therefore, recent vegetation and the pathways of secondary

generated lipids, either on bio-ontogenetic or geo-diagenetic stages, need to be understood better as they may hamper the interpretation of source species or organism in the geosphere. Furthermore, since organic molecules primarily consist of carbon and hydrogen, the carbon ($\delta^{13}C$) and hydrogen ($\delta^{2}H$ or δD) isotopic composition of bulk OM, individual *n*-alkanes and other individual compounds are frequently used in paleoclimate and paleoenvironmental reconstruction to determine the formation and degradation of OM (Ficken et al., 1998; Sachse et al., 2006, 2012). $\delta^{13}C$ can be used to distinguish plants utilizing different metabolic pathways. C_3 plants fix CO_2 via the Calvin-Cycle resulting in bulk $\delta^{13}C$ values ~-27‰, while C_4 plant bulk $\delta^{13}C$ values are more enriched in ^{13}C due to the Hatch-Slack-Cycle pathway leading to average values of $\delta^{13}C$= ~-13‰ (O'Leary, 1988). Compound specific $\delta^{13}C$ on *n*-alkanes show a similar pattern with slightly lower values of ~-21 for C_3 and ~-35‰ for C_4 plants, respectively (Castañeda et al., 2009a). However, a global study on 334 species of C_3 plants revealed a wide range of $\delta^{13}C$ values from -34.9 to -21.4‰ with overlapping ranges compared to the values postulated for C_4 plants, which might lead to misinterpretation of (paleo)vegetation (Diefendorf et al., 2010).

δD values of leaf waxes, especially *n*-alkanes, have been frequently used to examine changes in aridity and precipitation (Sachse et al., 2006; Rach et al., 2014; Berke et al., 2019). Apart from the δD values of the source water, there are many other factors that influence the δD values of leaf waxes including water-use efficiencies, relative humidity, photosynthetic pathway or plant life-form (Castañeda and Schouten, 2011 and references therein). Since the hydrogen isotopic composition differs between different plant forms, e.g. trees and grasses, again the evaluation and identification of the source organism is of great interest (Chikaraishi and Naraoka, 2003; Tipple and Pagani, 2013). This again encourages the analysis of modern vegetation homologues to rule out further uncertainties and to understand better the biosphere-geosphere interactions.

In contrast to the hydrocarbons of terrestrial plant origin, their homologues from planktonic microorganism are mostly characterized by shorter-chain lengths (<nC_{20}) (Meyers, 2003). Other important biomarkers used in this thesis are bacteria and archaea-derived membrane lipids whose composition varies with mean annual air temperature (MAAT) and pH. These compounds called glycerol dialkyl glycerol tetraethers (GDGTs) are fossilized membrane lipids of archaea and some bacteria and are ubiquitously distributed in marine and terrestrial environments such as lakes, soils, peats and bogs across the globe (Schouten et al., 2013a). They are commonly used to infer past mean annual air and water temperatures (Schouten et al., 2002; Weijers et al., 2007), soil pH (Weijers et al., 2007), organic matter source (Hopmans et al., 2004) and microbial community assemblage (Lipp and Hinrichs, 2009). In general, there are two classes of GDGTs: branched GDGTs (brGDGTs) and isoprenoid GDGTs (isoGDGTs), which represent allochthonous terrestrial and autochthonous aquatic provenances. However,

several studies demonstrated that brGDGTs are at least partly also produced in-situ in lakes (Tierney and Russell, 2009; Sinninghe Damsté et al., 2012a; Naeher et al., 2014; Weber et al., 2015). In order to identify the source of the GDGTs, the branched and tetraether (BIT) index has been introduced, which expresses the proportion of mainly soil-derived brGDGTs to aquatic-derived *Thaumarchaeota* (Hopmans et al., 2004). IsoGDGTs are mainly derived from *Thaumarchaeota*, a cluster of the archaea domain and more abundant in marine settings (Schouten et al., 2013a). On the contrary, brGDGTs, which are produced by a wide variety of *Acidobacteria* living in soil and presumably other bacteria, are used to reconstruct continental paleotemperature (Sinninghe Damsté et al., 2011, 2014, 2018a). It has been shown that the degree of methyl branching (MBT) depends primarily on the mean annual air temperature, while the number of cyclopentane moieties (CBT) of brGDGTs correlates with soil pH (Weijers et al., 2007; Peterse et al., 2012; De Jonge et al., 2014). Recently, a new set of structural brGDGT isomers, the 6-methyl brGDGTs occurring at position 6, have been identified, which coelute with 5-methyl brGDGTs at position 5 when using traditional HPLC methods (De Jonge et al., 2013). By using the recently improved chromatographic separation method, it has been shown that the 5-methyl isomers (expressed as MBT'_{5ME}) have a stronger correlation with temperature, while the amount of 6-methyl isomers have a better correlation with pH (De Jonge et al., 2014; Naafs et al., 2017a, 2017b; Russell et al., 2018).

Similar to archaea and bacteria, other microorganisms like heterocyet cyanobacteria produce unique biomarkers called heterocyte glycolipids (HGs). Their composition is highly variable, which is why the individual components have a high chemotaxonomic potential (Gambacorta et al., 1998; Bauersachs et al., 2009a, 2014a, 2019). Laboratory experiments and a field study on a freshwater lake have also demonstrated that the HG composition correlates with growth temperature (Bauersachs et al., 2014b; Bauersachs et al., 2015) and thus can be used to trace paleotemperature changes.

In the following chapter typical biomarkers of the archaeosphere are introduced.

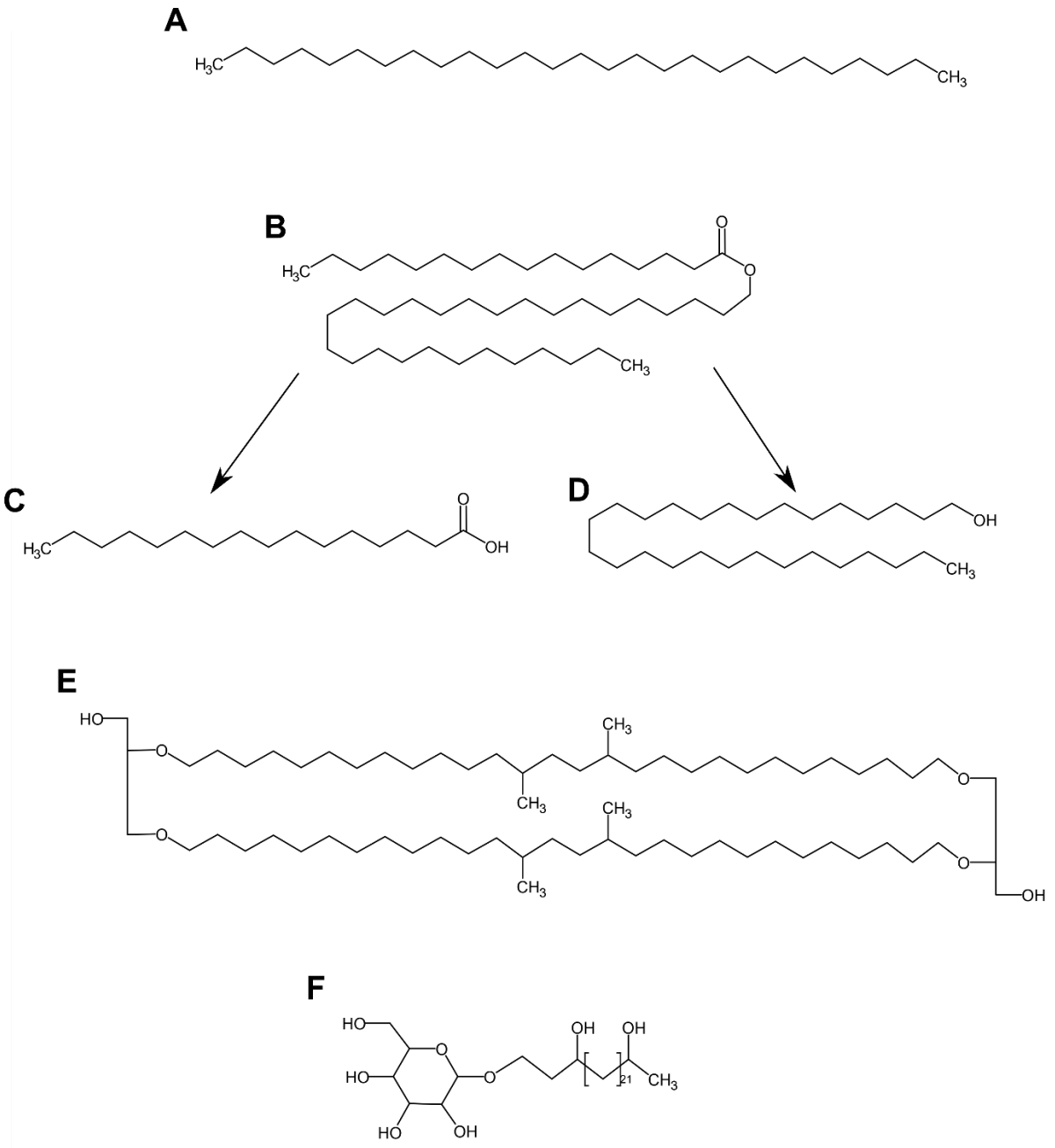

Figure 1.1: Important biomarker used in this thesis including A: nC$_{27}$ alkane derived from plant leaves. B: nC$_{44}$ alkyl ester constituted of nC$_{16}$ alkanoic acid (B) and nC$_{28}$ alcohol (C), which are both important leaf wax lipids, but are also released upon hydrolysis of the alkyl ester at early diagenetic stages. E: bacteria-derived branched GDGT-Ia. F: HG$_{26}$ diol, which is exclusively produced by heterocyte cyanobacteria.

1.3. Biomarkers from biosphere to archaeosphere

Organic substances on archaeological objects mainly occur as residues from food and medicines or as adhesives and binders in paint (Colombini and Modugno, 2009). These residues can occur as charred surface residue, which adheres to the interior or the exterior of the vessel. During cooking of food in unglazed clay pots, organic molecules can also be absorbed into the pores of the clay vessels and survive there over time (Needham and Evans, 1987). However, most lipids do not survive intact, but rather are transformed into defunctionalized and more resistant forms, which are, however, less indicative.

During the early 1990s, the Bristol (UK) chemistry unit around Prof. Dr. Richard Evershed increased the range of applications and analytic techniques of organic (geo)chemistry on archaeological objects to characterize how specific pots were used (Evershed et al., 1990, 1991a, 1991b; Heron et al., 1991). With this important information, ancient human diet and early animal husbandry and domestication could be reconstructed. An early overview of the chemistry of lipids important in archaeology was given by Evershed (1993). Contemporary experimental studies were carried out to improve the understanding of the alteration processes during deposition and early diagenesis on the organic material in the ceramic samples. For this purpose, meat samples from different animals, such as cattle, pigs and fish, but also vegetables or cereals were exposed to different conditions such as temperature and/or oxygen content over time to simulate different burial conditions (Evershed et al., 1995; Raven et al., 1997; Hansel et al., 2004; Hammann and Cramp, 2018). Over the last three decades the number of studies from different research groups increased and important updates on organic residue analysis on pottery were developed. Today, organic substances like animal adipose (ruminant vs. non-ruminant) and dairy fats, marine oils, plant epicuticular waxes and oils, cereals, bark tars and resins, bitumen, wine and beeswax can be identified based upon their biomolecular fingerprints and carbon isotope values in archaeological pottery vessels.

Animal fats and plant oil fats are mixtures of triacylglycerols (TAGs), which are esters of glycerol and three fatty acids of various chain-length and other minor compounds like sterols and free fatty acids (Fig. 1.2 and 1.3). The fatty acids of TAGs are usually unbranched with an even number of carbon atoms and can be saturated or unsaturated, having one (monounsaturated) or more double bonds (polyunsaturated). The carbon number distribution of TAGs can be used to differentiate between modern animal fats. Fresh milk fats contain a very broad distribution of TAGs ranging from 28 to 54 carbon atoms, while adipose fats either from ruminants like cattle and sheep or from non-ruminant fats from pigs have a narrower distribution from C_{46} to C_{54}, with minor contribution of C_{42} and C_{44} (Mukherjee et al., 2007). Unfortunately, the distribution of TAGs transformes over time due the loss of the short-chain acyl moieties during hydrolysis with the result that diagenetically overprinted adipose and dairy fats can no longer be distinguished by their carbon number distribution (Dudd and Evershed,

1998). The hydrolysis of TAGs leads to the formation of diacylglycerols (DAGs) and monoacylglycerols (MAGs) through the loss of fatty acids, which are added to the pool of existing free fatty acids. Finally, degraded fats are characterized by the presence of only a minor amount of acylglycerols, if they are not completely degraded and have a high concentration of free fatty acids and glycerol. Since short-chain fatty acids (C_4-C_{12}) are more water soluble than their long-chain homologues, short-chain fatty acids do not survive in archaeological pottery through leaching or volatilization over archaeological time scales (Bell, 1973; Dudd and Evershed, 1998). Therefore, mainly medium-chain length fatty acids like palmitic ($C_{16:0}$) and stearic ($C_{18:0}$) acid are found in archaeological samples (Pollard et al., 2007). Simple ratios of $C_{16:0}$/$C_{18:0}$ fatty acids were introduced to distinguish between animal and plant origin with vegetable oils having a ratio greater than three and animal products having a ratio between one and two (Copley et al., 2001). However, these values were determined on recent samples, which is why the ratio should only be used with caution since the complicated degradation processes from the biosphere to the archaeosphere are not fully understood.

The commonly high amounts of $C_{16:0}$ and $C_{18:0}$ fatty acids in archaeological samples, however, can be used to measure the carbon isotopic composition ($\delta^{13}C$) of these two individually fatty acids to determine their origin. Studies revealed the differentiation of various animal fats like from ruminant, non-ruminant and dairy fats as well as from marine and freshwater resources (Dudd and Evershed, 1998; Copley et al., 2003; Cramp et al., 2019). Differences in $\delta^{13}C$ values of the major fatty acids of modern terrestrial animals are due to differences in metabolism and digestive physiology of different organisms (Copley et al., 2003; Mukherjee et al., 2007). The two aquatic sources are not easily to distinguish by their $\delta^{13}C$ values since individual species or groups have similar ranges (Cramp and Evershed, 2014). Aquatic resources can be deduced when complementary biomarkers are detectable in the same sample. Aquatic biomarkers include dihydroxy fatty acids, long-chain mono- and polyunsaturated fatty acids, in particular $C_{20:1}$, $C_{22:1}$, $C_{20:5}$ and $C_{22:6}$, isoprenoid fatty acids and ω-(*o*-alkylphenyl)alkanoic acids (APAAs) ranging from 16 to 22 carbon atoms (Cramp and Evershed, 2014). The latter are formed during heating (~270°C) of especially polyunsaturated fatty acids (e.g. $C_{18:3}$, $C_{20:3}$, $C_{22:3}$), which are commonly found in aquatic species (Hansel et al., 2004). Later, other studies, however, revealed that APAAs are also formed by mono- and diunsaturated fatty acids (Evershed et al., 2008a). Since many vegetable oils also contain a high concentration of predominantly polyunsaturated C_{18} fatty acids, APAAs with 18 carbon atoms can be produced also during cooking of plant material (Rossell, 1991). Since vegetable oils contain only traces of unsaturated C_{20} and C_{22} fatty acids, the detection of C_{20} and C_{22} APAAs is a strong evidence for the processing of aquatic resources in pottery vessels (Craig et al., 2007; Evershed et al., 2008a).

Other important biomarkers for ruminant animals are significant amounts of pentadecanoic ($C_{15:0}$) and heptadecanoic ($C_{17:0}$) acids and their equivalent iso- and anteiso-isomers, which are formed in the rumen of e.g. cattle, sheep and goats (Baeten et al., 2012). Cholesterol and its oxidation products are typical animal products, while phytosterols like sitosterol and campesterol are indicative of a plant origin. Nevertheless, these biomarkers are also produced by bacteria and algae and can therefore originate from microorganisms during burial. A complex mixture of *n*-alkanes, *n*-fatty acids, *n*-alcohols and *n*-acyl wax esters is indicative for beeswax, while *n*-alkylresorcinols are ubiquitous biomarkers in modern cereals (Ross et al., 2003; Roffet-Salque et al., 2015). The latter are rarely detected in archaeological samples (Colonese et al., 2017) as *n*-alkylresorcinols are only preserved under anoxic conditions in significant concentrations and a very sensitive detection method has to be used to detect traces of these compounds (Hammann and Cramp, 2018). Wine as one of the most important beverages produced, traded and consumed in recent and ancient times is identifiable by the presence of tartaric, citric, malic, succinic and fumaric acids (Pecci et al., 2013).

As a result of human activity, various biological materials were mixed in pots, especially during food preparation, which increased the complexity of identifying the original contents. In addition, complex alteration processes and decay of lipids during burial increase the need for further development of analytic techniques in molecular archaeology (Evershed, 2008).

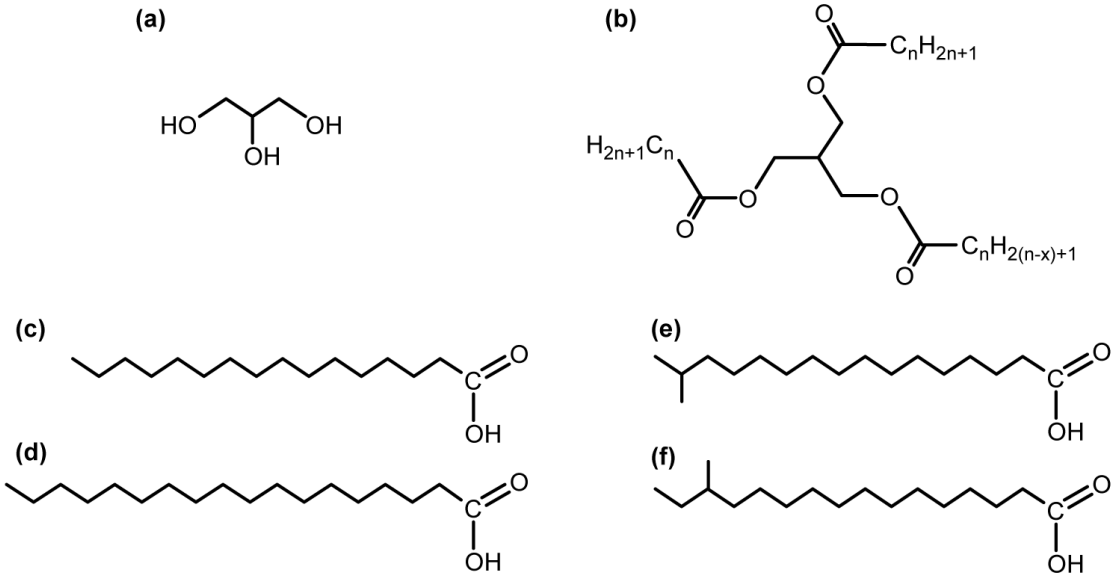

Figure 1.2: Structure of glycerol (a); general structure of triacylglycerol (b) with two saturated and one unsaturated fatty acid moiety (with x: number of double bonds and n: number of carbon atoms). Examples of fatty acids structures (c) palmitic acid, $C_{16:0}$; (d) stearic acid, $C_{18:0}$; and (e-f) heptadecanoic acid, $C_{17:0}$ (respectively, iso-and anteiso) Adapted from (Salque, 2012).

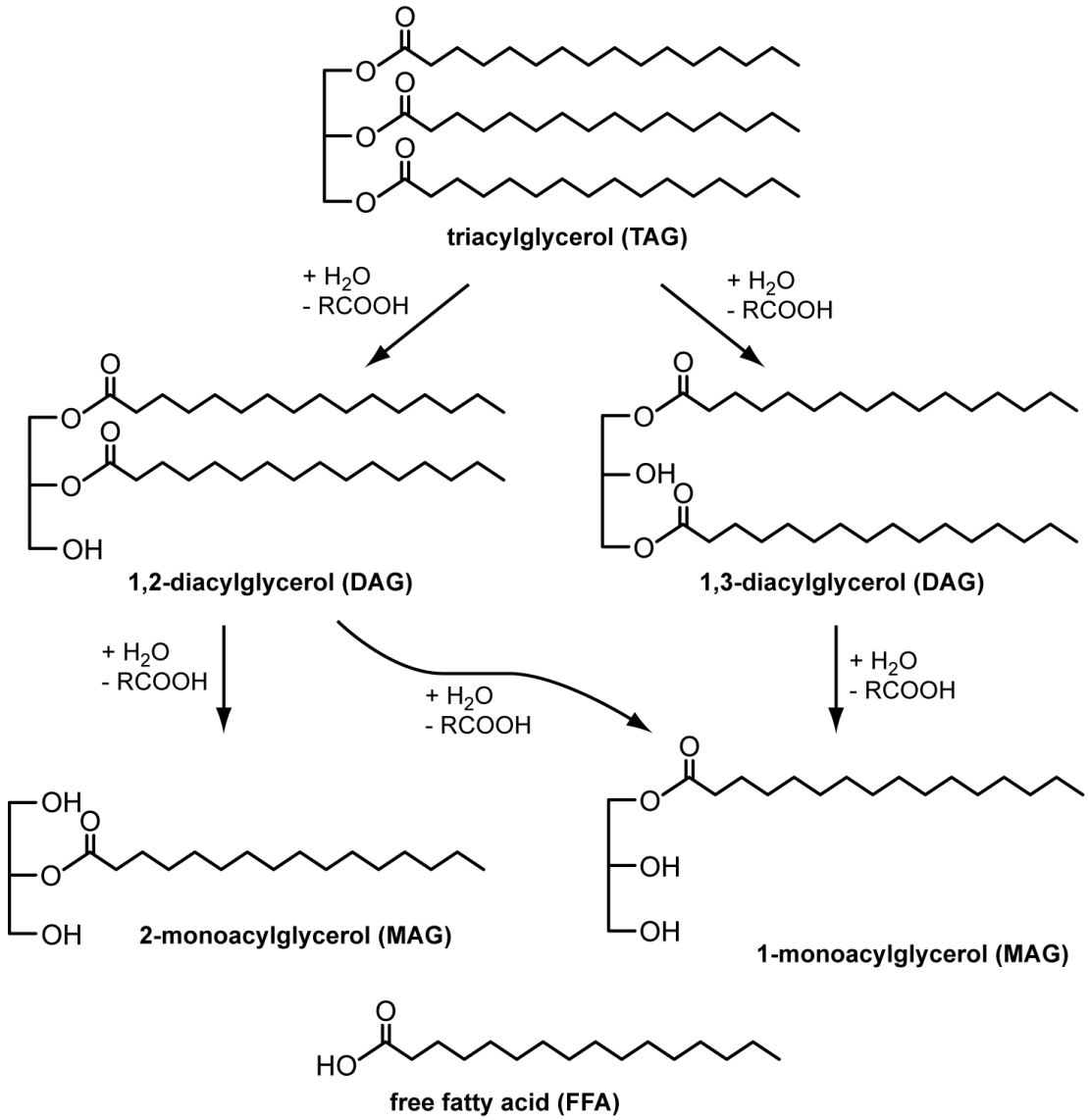

Figure 1.3: Degradation pathways of triacyclglycerols (TAGs). Adapted from Evershed et al. (2002).

1.4. Aims and thesis outline

This PhD thesis is integrated in the Collaborative Research Center (CRC) 1266: “Scales of Transformation – Human-Environmental Interaction in Prehistoric and Archaic Societies” founded by the German Research Foundation (DFG). As this work is embedded in the CRC 1266, numerous interdisciplinary cooperation could be conducted, thus not only “typical” geoscientific questions were dealt with. The aim of this work was to apply different state of the art methods of organic geochemistry in different scientific fields including paleobotany, paleolimnology, paleoclimatology, paleoenvironmental reconstruction and archaeology. In the following chapters, the main results of this thesis are presented for the different scientific fields and locations (Fig. 1.4). This thesis is composed of seven main chapters including an introduction, five chapters that have been published, submitted or are in preparation for publication in international peer-reviewed scientific journals and a final conclusion.

Chapter 1 introduces in the general scientific background of biomarkers in organic geochemistry and provides an overview of the scientific field. **Chapter 2** describes the wax lipid composition of the four European birch species and the interaction of these lipids between biosphere and geosphere. In **Chapter 3** a sediment core from Lake Steisslingen (SW-Germany) comprising Late Glacial and Early Holocene sediments is investigated to characterize especially the Younger Dryas cold period. Here, biomarker and isotopic data indicate that the cold period of roughly 1,000 years was not uniform, but that the ecosystem was highly variable, leading to a subdivision of the Younger Dryas based on the different response of aquatic and terrestrial ecosystem. **Chapter 4** deals with the characterisation of the sediments from Lake Stymphalia (Greece) comprising the Late Pleistocene and almost the entire Holocene. Epicuticular wax lipids (*n*-alkanes) as well as heterocyte cyanobacteria-derived (HGs) and bacteria-derived (brGDGTs) membrane lipids are used to determine the ancient vegetation, microbial community and temperature changes. In **Chapter 5** modern animal fats from cattle, sheep, goats and pigs are reported as modern reference material to compare their lipid and isotopic signature with those extracted from ancient pottery vesselsof the Cucuteni-Trypillia culture excavated in Ukraine and Moldova. The lipid and isotopic signature extracted from Funnel Beaker culture (Trichterbecherkultur) and Globular Amphora culture (Kugelamphorenkultur) potteries of Northern Germany is described in **Chapter 6**. Here, significant lipid contents of the burial gift containing vessels from a Megalith grave differed characteristically from those from the corresponding settlement. Finally, **Chapter 7** provides a summary and outlook for further research. In addition, an **appendix A** is attached in which preliminary results are presented, which form a contribution to a further publication. In a second **appendix B**, a manuscript is added containing GDGT data from the younger part of the Lake Stymphalia sediment record.

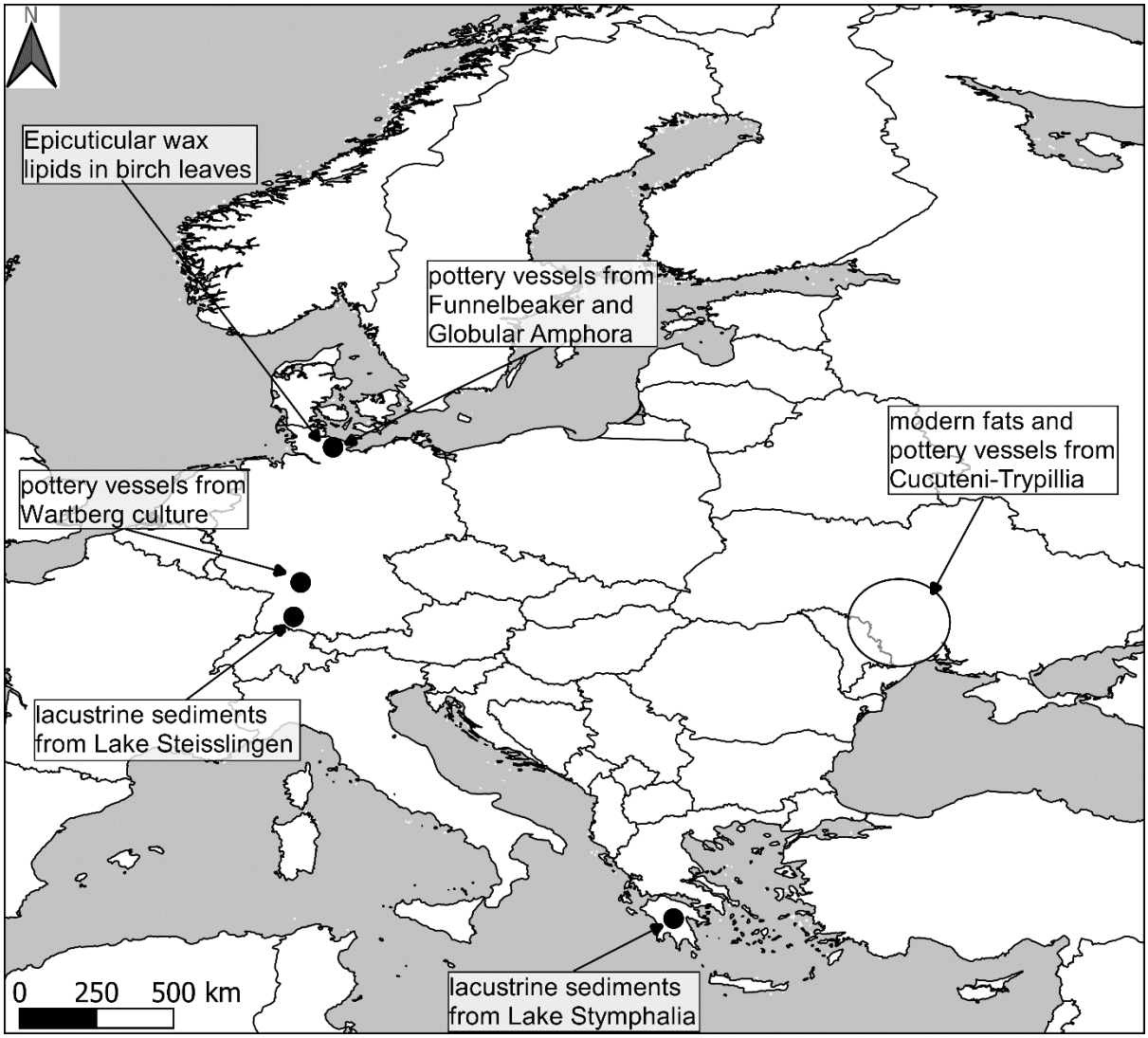

Figure 1.4: Study areas of subprojects investigated within this PhD project.

2. Epicuticular wax lipid composition of endemic European *Betula* species in a potential ontogenetic/diagenetic continuum and its application to chemotaxonomy and paleobotany

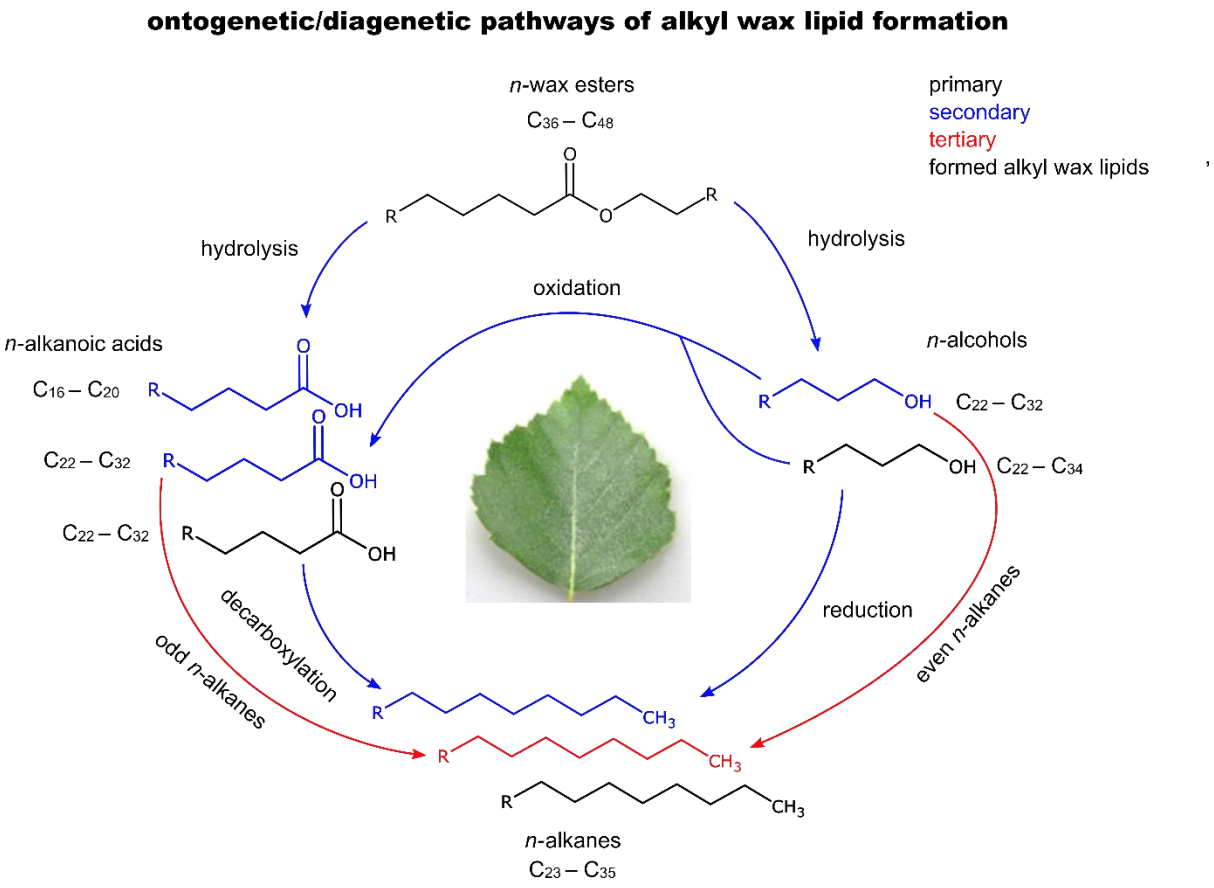

Abstract

Plants are excellent climate indicators and their macro-remains or pollen accumulating in geological archives serve as recorders of environmental change. In Europe birch trees contribute importantly to Holocene plant successions. They constitute the dwarf species *Betula nana* and *B. humilis*, representing colder and two tree birches, *B. pubescens* and *B. pendula* indicative of more temperate climate. Birch pollen are highly similar preventing species differentiation. We obtained unambiguous chemotaxonomic differentiation of four European birch species via cuticular wax lipids. Dominating lipid classes in recent epicuticular birch waxes were *n*-alkanes (nC_{23} to nC_{33}), *n*-alcohols and *n*-alkanoic acids (nC_{20} to nC_{32}), and long-chain wax ester (nC_{36} to nC_{48}) differing in amount and distribution. After plant senescence and in geological archives lipids undergo diagenetic alteration modifying the distributions

found in recent plants. Long-chain wax esters become hydrolysed and release bound alcohols and fatty acids, which add to the fraction of their free analogues. This modification of primary lipid patterns commonly is unaccounted for in paleovegetation studies. Proceeding diagenesis by decarboxylation will convert these functionalized primary and secondary lipids into their corresponding *n*-alkanes, the compound class mostly applied in paleoenvironment reconstruction. Hereby, not only molecular but also isotopic composition is then determined on *n*-alkanes of different origin. We assessed the potential contribution of secondary (free lipid decarboxylation) and tertiary (bound lipid decarboxylation) wax metabolites and compared the cumulative *n*-alkane patterns with birch *n*-alkane distributions reported in the literature. Two statistically different patterns were separated, one dominated by primary, the other by secondary and tertiary formed *n*-alkanes. This may explain the inconsistency in previous birch wax analysis reported and needs to be considered in paleoenvironment reconstruction.

2.1 Introduction

Environmental demands, in particular climate, govern the present-day habitat and distribution of trees, which in turn facilitate determination of climate regimes in the contemporaneous as well as in the fossil domain. Taxonomy of present-day trees is based on anatomical, morphological, genetic and biochemical studies, whereby such features in the fossil record are best preserved in pollen distributions, due to a higher recalcitrance of pollen versus other plant organs, e.g. leaves and rare findings of other macro-remains, e.g. fruits. Under special conditions of preservation though fossil remains can be found in sediments dating back to the Eocene (Crane and Stockey, 1987). Paleovegetation and related paleoclimate reconstruction thus heavily relies on palynology, accompanied by analysis of marco-remains when present. Genetic (Järvinen et al., 2004; Schenk et al., 2008; Bina et al., 2016) and biochemical approaches (Julkunen-Tiitto et al., 1996; Keinänen et al., 1999; Orav et al., 2011; Depciuch et al., 2018) are rare, except for molecular and isotopic investigation of leaf/needle wax, the latter rarely conducted on the species level.

Birches (*Betula* L., *Betulaceae*) are common broadleaf trees and shrubs occurring in diverse habitats of the boreal and the cold-temperate zones of the Northern Hemisphere (Furlow, 1990; Maliouchenko et al., 2007). Ranging from temperate zones in Northern America over Eurasia to East Asia and the circumpolar regions, birches populate different habitats including forests, swamps, tundra and mountainous terrains (Wang et al., 2016). The number of species belonging to the genus *Betula* and their relationships is still under debate ranging from 30 to 60 different taxa within 4 to 6 subgenera (Winkler, 1904; De Jong, 1993; Skvortsov, 2002; Schenk et al., 2008; Ashburner and McAllister, 2013). Of these, four *Betula* species are endemic to Europe. The two tree birches, *B. pubescens* (downy birch) and *B. pendula* (silver

birch) occur throughout most of Europe, whereby *B. pubescens* has a more northerly and easterly distribution, while *B. pendula* reaches more southern regions such as the Iberian Peninsula, Italy and Northern Greece (Maliouchenko et al., 2007; Ashburner and McAllister, 2013). Two dwarf/shrubby birch species, namely *B. nana* (arctic dwarf birch) and *B. humilis* (dwarf birch) thrive in Europe as well but are confined to a much smaller growth range. *B. nana* is preferentially located at higher elevations like the Alps and Carpathian Mountains or in perennial colder regions like Northern Europe from Iceland over northern Scotland to Scandinavia (Maliouchenko et al., 2007; Ashburner and McAllister, 2013). *B. humilis* has a wide distribution from western Germany to eastern Siberia and Korea, but its occurrence is very scattered with only a few habitats left in Central Europe (Ashburner and McAllister, 2013). As an important component of plant succession found in highly contrasting climate and growth regimes, these *Betulaceae* and their respective habitat demands are sensitive (paleo)climate and (paleo)environmental indicators, provided that they can be taxonomically differentiated.

Recent birch species can be distinguished by their leaf and catkin/fruit even when fossilized in sediments shape (van Dinter and Birks, 1996; Freund et al., 2001), whereby their evolutionary relation and phylogeny is difficult to assess due to intensive hybridization in nature. Extensive hybridization and introgression has been investigated not only within a subgenus but also across *Betula* species of different subgenera (Thomson et al., 2015; Tsuda et al., 2017). Precise classification is complicated by a spatial overlap of natural habitats for European birch species enabling natural hybridization (Thórsson et al., 2001). The identification of birch remains in geological archives for paleovegetation reconstruction is limited by a common lack of well-preserved leaves or catkins occurring in statistically relevant quantities. However, the identification of birch vegetation over time is of great interest, especially during the Late Glacial and Early Holocene (approx. 15,000 – 9,000 yr BP), to understand early colonization and forest/shrub expansion in deglaciated landscapes as well as the adaptation of vegetation to climate variability and perturbation. Macrofossil findings revealed a dominance of tree birches, like *B. pubescens*, during temperate phases, whereas upon glacial stages *B. nana* was the most abundant birch species, serving as a tundra indicator (Tralau, 1963).

Most commonly, paleovegetation reconstruction in sedimentary archives like lakes, peats and bogs is based on palynological approaches, since macro remains are mostly absent (Lotter et al., 1992; Lotter, 1999; Jahns, 2000; Eusterhues et al., 2002; Tarasov et al., 2009; Mortensen et al., 2011; Veski et al., 2012; Rösch and Lechterbeck, 2016; Krüger and Damrath, 2019). However, differentiation of birch species by pollen is challenging, due to similar morphological traits, e.g. shape, diameter and depth of pores in pollen within the genus *Betula*, which leads to overlap in pollen-size distribution (Birks, 1968; Mäkelä, 1996; Caseldine, 2001; Karlsdóttir et al., 2007; de Klerk et al., 2017). In addition, pollen morphology can also be affected by the

chemicals used upon preparation, pollen maturity, type of mounting medium, but also a latitudinal and altitudinal effect cannot be excluded (reviewed in Mäkelä, 1996).

Terrestrial plant leaves are covered by a hydrophobic barrier to protect against the loss of water due to evaporation, mechanical damage, ultraviolet radiation and bacterial or fungal pathogens (Jenks et al., 1994; Sieber et al., 2000; Long et al., 2003; Jetter and Kunst, 2008). This barrier consists of an epicuticular wax layer, composed of long-chain alkyl compounds including amongst others *n*-alkanes, *n*-alcohols, *n*-alkanoic acids, *n*-alkyl esters, *n*-aldehydes, *n*-ketones and others (Eglinton and Hamilton, 1967; Jetter and Kunst, 2008). Their composition is highly variable in quality and quantity across plant species and therefore has high chemotaxonomic potential (Eglinton et al., 1962; Herbin and Robins, 1969; Gülz, 1994; Maffei, 1996; Schwark et al., 2002; Buschhaus et al., 2007; Diefendorf et al., 2011, 2015; Bush and McInerney, 2013; Mueller-Niggemann and Schwark, 2015; Guo et al., 2018). *n*-Alkanes with carbon chain-length between nC_{25} and nC_{35} are associated with higher plants with a strong odd-over-even predominance (expressed as the carbon preference index - CPI), while their shorter chain homologues ($<nC_{20}$), especially nC_{17}, are mainly found in aquatic microorganisms (Blumer et al., 1971; Cranwell et al., 1987). Intermediate chain-length *n*-alkanes with nC_{23} and nC_{25} predominance are primarily found in aquatic macrophytes and in mosses of the genus *Sphagnum* (Ficken et al., 2000; Pancost et al., 2002; Bush and McInerney, 2013). Both, *n*-alcohols and *n*-alkanoic acids in contrast to the *n*-alkanes hold an even-over-odd predominance in carbon chain-lengths, which typically ranges from nC_{20} to nC_{32} (Jetter and Kunst, 2008). Alkyl esters consist of even-numbered *n*-alkanoic acids, which are esterified to even-numbered *n*-alcohols, generating long-chain aliphatic compounds with on average 38 to 52 carbon atoms (Shepherd et al., 1999). Among these lipid classes, the *n*-alkane abundances are most frequently reported in vegetation reconstruction, since they are very robust against alteration processes due to the lack of functional groups. Such *n*-alkanes can be found in a variety of geological archives including peats, soils, limnic and marine sediments of different ages ranging from modern times up to several million years (Schwark et al., 2002; Schouten et al., 2007; Smith et al., 2007; Schellekens and Buurman, 2011) and are easily extracted from sediments and leaves by geochemical methods (Jetter and Kunst, 2008). Therefore, most studies conducted to investigate paleovegetation history employing leaf wax lipids are based on *n*-alkanes (Jansen and Wiesenberg, 2017). However, the use of several lipid classes instead of a single will increase the discriminative power and representativeness of the wax lipid composition. Studies involving *n*-alkanoic acids, *n*-alcohols or *n*-alkyl ester for paleovegetation reconstruction are highly underrepresented (Jansen et al., 2013; Wiesenberg et al., 2015), as these lipids are usually not reported from modern plant homologues and their degree of preservation in natural archives may vary (Lockheart et al., 2000). Following incorporation into soil or sediment, wax esters can be hydrolysed, releasing

free *n*-alcohols and *n*-alkanoic acids. These in turn can be converted into *n*-alkanes by decarboxylation and reduction, respectively (e.g. Jansen and Wiesenberg, 2017). Diagenetic fate of functionalized lipids may vary depending on various factors such as oxygen availability and *p*H affecting microbial reworking, but the potential of functionalized lipid classes in paleobotany has been proven for sediments of up to Miocene age (Huang et al., 1995; Lockheart et al., 2000).

As Kirkels et al. (2013) in a previous publication in *The Holocene* emphasized "*Additional focus on biomarker-potential of other cuticular-derived compounds (e.g. n-alcohols, fatty acids, ketones, etc.) and on biomarkers upon senescence/degradation are important research prospects*". Here, we address both an extended epicuticular leaf wax analysis including four different compound classes (*n*-alkanes, *n*-alcohols, *n*-alkanoic acids, and long-chain wax ester) and investigate the potential release of secondary and tertiary metabolites from those functionalized wax lipids present in recent birch plants. We then compare the *n*-alkanes cumulatively releasable from functionalized precursor molecules in recent birch wax with bulk *n*-alkane distributions reported in the literature to investigate if previous chemotaxonomic assessments may have been affected by secondary and tertiary wax alteration.

An improved understanding of the diagenetic effects impacting on leaf waxes may guide in future molecular and isotopic application to paleovegetation reconstruction.

2.2 Material and Methods

2.2.1 Leaf samples and collection

Fresh leaf samples were collected in the Botanical Garden at Kiel University in September 2017. Three samples per birch species were collected as field replicates from branches at different sites of the tree at a height between 1 and 3 m. To avoid contaminations during sampling, gloves were worn and leaves were stored in glass container or aluminium foil until extraction. Subsequently to sampling leaves were dried at 35°C in an oven for 48h. The mean annual air temperature for Kiel-Holtenau is about 9.34°C and the total annual precipitation is about 744 mm (1987-2018) (DWD, 2019).

2.2.2 Lipid extraction

Lipids were extracted by immersing a composite sample, obtained from 3 to 5 individual leaf sections (0.02 – 0.27 g), for 60 s in a 30-50 ml hexane/dichloromethane solution (1:1 v/v). The resulting solution was filtered through $NaSO_4$, evaporated under vacuum at 50°C in a Büchi solvent evaporator and transferred into pre-weighted vials. Per species three leaf composite samples were extracted to calculate standard deviation of lipid concentration and composition. Replicate analyses were not executed on identical extracts as often done in biogeochemistry

but derive from different field samples reflecting full environmental variability. Prior to analyses, an aliquot of the total lipid extract (TLE) was treated with 35 µl *N,O*-bis(trimethylsilyl)trifluoroacetamide (BSTFA) and 5 µl pyridine at 70°C for 1 h to convert the *n*-alkanoic acids and *n*-alcohols to their corresponding trimethylsilyl (TMS) derivates. 10 µg of perdeuterated tetracosane (nC_{24}), octadecanol (nC_{18}), and eicosanoic acid (nC_{20}) were added as internal standard for quantification. All samples were analysed by gas chromatography-mass spectrometry (GC/MS).

2.2.3 Gas chromatography-mass spectrometry (GC-MS)

The wax lipids were analysed using an Agilent 7890A (GC) equipped with an Agilent DB-5 column (30m x 0.25mm x 0.25µm) coupled to an Agilent 5975 B (MS). The oven program started at 60°C for 4 min, followed by a ramp to 140°C at 10°C/min and subsequently to 325°C at 3°C, followed by an isothermal period of 45 min. The MS operated with a scanning mass range of *m/z* 50-850 at an ionization energy of 70 eV. All compounds were identified by using authentic standards, NIST 14 library or their specific fragmentation pattern.

2.2.4 Leaf wax characteristic calculations

The *n*-alkane content of plant species was calculated as µg/g dry weight (d.w.) of leaf based on mean values of triplicate analysis with standard deviation (Fig. 1).

Average chain length (ACL) for *n*-alkanes with 23 to 33 carbon atoms was calculated as:

$$ACL = \frac{(23 \times nC_{23} + 25 \times nC_{25} + 27 \times nC_{27} + 29 \times nC_{29} + 31 \times nC_{31} + 33 \times nC_{33})}{(nC_{23} + nC_{25} + nC_{27} + nC_{29} + nC_{31} + nC_{33})}$$

with C_n as relative abundance of *n*-alkanes with the chain length *n* (Poynter and Eglinton, 1990). This proxy is used as weighted mean of *n*-alkane carbon chain length, which is supposed to vary with climate. The carbon preference index (CPI) outlines the relative abundance of odd-over-even carbon chain lengths, whereby values >1 indicate a predominance of odd carbon chain lengths homologues. CPI values for *n*-alkanes with 24 to 34 carbon atoms were calculated according to:

$$CPI = 0.5 \times \left[\frac{(nC_{25} + nC_{27} + nC_{29} + nC_{31} + nC_{33})}{(nC_{26} + nC_{28} + nC_{30} + nC_{32} + nC_{34})} + \frac{(nC_{25} + nC_{27} + nC_{29} + nC_{31} + nC_{33})}{(nC_{24} + nC_{26} + nC_{28} + nC_{30} + nC_{32})}\right]$$

For further statistical analysis of wax lipid results see supplementary materials S1.

2.2.5 Wax ester quantification

For total wax ester quantification, the respective wax ester peaks in the GC-MS chromatograms were integrated and quantified against an internal standard (deuterated tetracosane). For a wax ester of the type RCOOR' the diagnostic fatty acid ion is $RCOOH_2^+$, indicative for the alkanoic acid chain length. R'- 1^+ derives from the corresponding alcohol moiety, however, its intensity is low and difficult to detect. Therefore, the diagnostic acid fragments ($RCOOH_2^+$) of peaks containing co-eluting alkyl esters of identical total mass but variable combinations of alcohol and alkanoic acid moieties were integrated to determine the percentage of the respective isomer contribution. Multiplication of isomer percentages by analogue abundances led to the proportion of the esterified acids. The proportional amount of esterified alcohol was obtained by subtracting the esterified acid from the corresponding total wax ester homologue.

2.3 Results and discussion

2.3.1 Alkyl lipid distribution of plants from the Botanical Garden of Kiel University

One focus of this study lies on the determination of the primary epicuticular wax compositions of the four birches endemic to Europe. The leaf wax compound classes *n*-alkanes, *n*-alcohols, *n*-alkanoic acid and *n*-alkyl ester were present in all species at variable composition distributions (Fig. S2.1). Epicuticular alkyl lipid abundances are reported as µg/g dry weight (d.w.) of leaf.

The lowest total amount of epicuticular waxes was observed in the artic dwarf birch *B. nana* with 538.3 µg/g d.w., followed by *B. pendula* with 1293.8 µg/g d.w., 3131.7 µg/g d.w. in *B. pubescens* and *B. humilis* with 4187.9 µg/g d.w..

2.3.2 *n*-Alkanes of *Betula* epicuticular wax

The carbon atom chain-lengths of *n*-alkanes varied from nC_{23} to nC_{33} and maximized either at nC_{27} or nC_{31}. A predominance of nC_{27} was noted for *B. humilis* with 413.2±91.1 µg/g d.w.. In relative proportion, nC_{27} was the dominant *n*-alkane homologue in *B. nana*, though it occurred in minor absolute concentrations (7.8±2.5 µg/g d.w.) only. The *n*-alkanes of two tree birches, *B. pubescens* and *B. pendula*, maximised at nC_{31} with 799.0±133.3 and 183.0±103.8 µg/g d.w., respectively, whereby the latter species additionally contained large proportions of nC_{25} and nC_{27} alkanes. The average chain-lengths for odd-carbon-numbered *n*-alkanes in the range from nC_{23} to nC_{33} ($ACL_{23\text{-}33}$) varied from 26.7 in *B. humilis* to 29.7 in *B. pubescens*, while *B. pendula* und *B. nana* had intermediate ACL values of 28.0 and 28.5, respectively. As expected, in the recent leaves a typical odd-over-even predominance was detected, which is expressed in high CPI values. Highest CPI values were found in *B. pendul*a averaging 41.3,

followed by *B. pubescens* with 36.4 and *B. nana* with 11.1. The CPI for *B. humilis* could not be calculated due to the lack of even-numbered *n*-alkanes but consequently preference of odd-numbered homologues (CPI) is exceptionally high. The high *n*-alkane CPI values indicated that there was no significant contamination by sedimentary (e.g. via dust) or petroleum-derived *n*-alkanes.

The birch trees examined in this study grew under identical environmental conditions in the Botanical Gardens of Kiel University, thus a possible influence of climate or soil condition on the wax lipid distribution should be minimal for each species. The *n*-alkane compositions in all four *Betula* species exhibited a dominance of longer-chain lengths homologues (nC_{27}, nC_{29}, nC_{31}) with a mean ACL of ca. 28, as typical of deciduous trees (Bush and McInerney, 2013). However, some species had only one dominant homologue (*B. pubescens, B. humilis*), whilst others had a more bimodal distribution with two dominant homologues (*B. nana, B. pendula*) (Fig. 2.1). The ACL has been used in geological archives as a climate and plant species indicator. For example, it has been recognized that higher ACL values correlated with higher temperatures in sediments of Lake Malawi (east Africa), potentially as protection against heat to increase the melting point of epicuticular waxes (Castañeda et al., 2009b). However, Diefendorf et al. (2017) in their compilation study could not confirm a significant temperature control on ACL neither in C_3 woody plants nor in C_3/C_4 grasses. Higher ACL values, due to a higher proportion of nC_{31}, nC_{33} and partially nC_{35}, were observed in C_4 grasses (*Poaceae*) of arid zones in Africa, which distinguished them from C_3 species from Peru and Australia (Rommerskirchen et al., 2006). No correlation between the preferred habitat of the four birches from our study (arctic/alpine vs. temperate zone) and ACL exists, since especially the two cold tolerant dwarf birches showed markedly different n-alkane distributions. However, the measured ACL values were in accordance with the expected values, since no extended long-chain n-alkanes with 33 or even 35 carbon atoms, typically for arid grasses, were found.

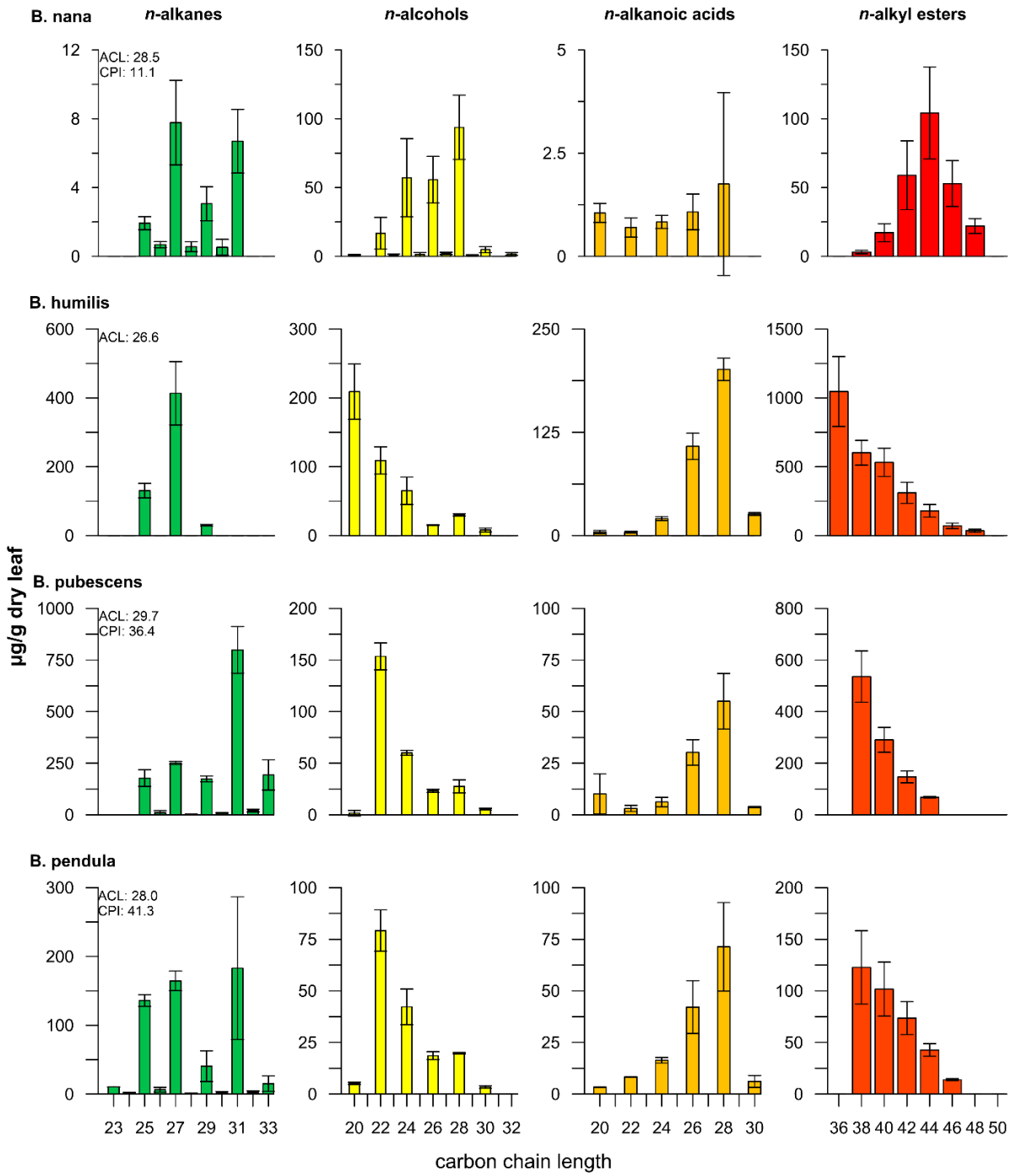

Figure 2.1: Distribution of *n*-alkanes, *n*-alcohols, *n*-alkanoic acids and *n*-alkyl esters (µg/g dry leaf) from epicuticular waxes of four European birch species collected from the Botanical Garden of Kiel (Germany). Note the different scale of the y-axis for each row.

2.3.3 *n*-Alcohols of *Betula* epicuticular wax

As with the *n*-alkane distribution, a typical terrestrial higher plant pattern was observed for *n*-alcohols, yielding a strong even-over-odd dominance in carbon chain-lengths (Otto and Simpson, 2005). The *n*-alcohol chain-lengths ranged from nC_{16} to nC_{32} with a predominance in long-chain alcohols (>nC_{20}) in all birches. As short chain-lengths *n*-alcohol homologues (<nC_{20}) are primarily synthesised by microbes or algae (Han and Calvin, 1969), we based epicuticular wax analysis on the long-chain homologues. The primary *n*-alcohols showed the closest range in overall concentrations of all lipid classes (Fig. 2.1). The cumulative *n*-alcohol concentration extended from 168.5±22.0 µg/g in *B. pendula* to 436.4±84.7 µg/g in *B. humilis*. The three birches *B. humilis, B. pubescens* and *B. pendula* revealed a gradually decreasing concentration with increasing chain-lengths, whereby *B. humilis* maximized at nC_{20} with 209.0±40.2 µg/g d.w. and the latter two at nC_{22} with 153.5±12.9 and 79.2±10.0 µg/g d.w., respectively. *B. nana* was characterized by a narrower distribution, peaking at nC_{28} with 99.7±23.3 µg/g d.w.. Our results demonstrate that the concentration of *n*-alcohols either increased (*B. nana*) or decreased (all other species) gradually with increasing carbon chain-length, whereby only one homologue dominated (Fig. 2.1). Both tree birches, *B. pubescens* and *B. pendula*, revealed similar alcohol patterns and differed in absolute concentrations only. In contrast to the tree birches, however, the two shrub birches showed a markedly different *n*-alcohol distribution and were well distinguishable.

Diefendorf et al. (2011, 2015) reported that the average concentrations of *n*-alcohols in leaves of deciduous angiosperm trees from the U.S. commonly were twice as high as those of *n*-alkanes. In our study *B. nana* exclusively revealed about 10 times higher concentrations of *n*-alcohols compared to *n*-alkanes. The other three species produced two to four times lower amounts of *n*-alcohols than *n*-alkanes. Previous studies have shown that grasses are mainly characterized by nC_{26}, nC_{28} and nC_{32} alcohols (Jansen et al., 2006; Rommerskirchen et al., 2006). This corresponds closely to generally low amounts of these homologues in favour of the high proportions of the shorter alcohols nC_{20} or nC_{22} in *B. humilis*, *B. pubescens* and *B. pendula*. Only the leaves of *B. nana* produced a higher proportion of nC_{26} and nC_{28} alcohols.

2.3.4 *n*-Alkanoic acids of *Betula* epicuticular wax

The *n*-alkanoic acid abundances were characterized by a strong even-over-odd dominance in carbon chain-lengths in the range of nC_{12} to nC_{30}. Similar to the *n*-alcohols, short-chain homologues (<nC_{20}) were not significant for higher plants since these compounds are also produced by a variety of organisms including bacteria and algae or derive from cellular membranes rather than waxes. Here, in all four birches species alkanoic acids in the range of nC_{12} to nC_{30} were observed to peak at nC_{16} or nC_{28}. In the range of the long-chain fatty acids

(>nC$_{20}$), the four *Betula* species maximized exclusively at nC$_{28}$, whereby their concentrations differed by two orders of magnitude (Fig. 2.1). Thus, *B. nana* yielded only 1.75±2.2 µg/g d.w. of nC$_{28}$, while *B. humilis* produced 201.2±13.4 µg/g d.w. of C$_{28}$. *B. pubescens* and *B. pendula* showed intermediate concentrations of 34.3±2.4 and 34.7±4.0 µg/g d.w., respectively. *B. nana* produced more short chain alkanoic acids than long-chain homologues, with highest concentration at nC$_{16}$ with 44.3±6.1 µg/g d.w. and nC$_{18}$ with 20.8±1.3 µg/g d.w..

The relative distribution patterns of long-chain alkanoic acids in the four birches were too similar to allow for differentiation. These basic findings were consistent with a litter and topsoil transect experiment in which deciduous forest sites also showed a dominance of nC$_{28}$ alkanoic acids and differed from conifer (nC$_{24}$) and grasslands sites (nC$_{32}$ and nC$_{34}$) (Schäfer et al., 2016). Therefore, nC$_{28}$ alkanoic acid preponderance may serve to distinguish wax lipid inputs of birches from those of grasses and conifers, like pines. This may be applicable for sediments in periods such as the Late Glacial and Early Holocene in Central Europe, where successions were characterised by a minor diversity in plant species. In contrast, Diefendorf et al. (2011) observed that the *n*-alkanoic acid distributions across plant groups from the east coast of the USA, both angiosperms and gymnosperms, were similar with no dominant homologue present.

2.3.5 *n*-Alkyl esters of *Betula* epicuticular wax

Wax esters are dimeric wax compounds build by a *n*-alcohol and a *n*-alkanoic acid moiety, whereby each *n*-alkyl ester isomer can be composed of several different combinations of *n*-alcohol and *n*-alkanoic acid homologues (Fig. S2.2) (Franich et al., 1985). Saturated wax ester homologues were identified according to their characteristic molecular ions (M^+) (Sümmchen et al., 1995). Straight-chain wax esters in the range of nC$_{38}$ to nC$_{48}$ were detected in all four species, which is typical for higher plants (Koch and Ensikat, 2008) (Fig. 2.1). Additionally, *B. humilis* produced minor quantities of the nC$_{36}$ homologue. The alkyl ester composition of *B. nana* maximized at nC$_{44}$ with 104.2±33.4 µg/g d.w. with an almost normal distribution. *B. humilis* peaked at nC$_{36}$ with 1047.1±254.0 µg/g d.w., followed by a linear decrease in concentration of longer-chain wax esters up to nC$_{48}$. Wax esters chain lengths of *B. pubescens* and *B. pendula* leaves ranged from nC$_{38}$ to nC$_{46}$, whereby the concentrations decreased with an increase in chain-lengths. Concentrations of nC$_{38}$ wax ester of *B. pubescens* and *B. pendula* yielded 535.7±99.4 and 122.7±35.5 µg/g d.w., respectively.

2.3.6 Isomer distribution of wax esters and potential input to free *n*-alkanoic acids and *n*-alcohols

Wax esters are easily hydrolizable primary wax lipids that upon diagenesis will convert into their secondary alcohol and carboxylic acid metabolites. A further aspect of this study aimed at an assessment of the amount and distribution of these bound lipids and a prediction of the cumulative compositions that may result from pooling free and bound alcohols and carboxylic acids. The mass spectral analysis of wax esters by GC/MS allowed to determine their corresponding bound *n*-alcohol and *n*-alkanoic acids (Fig. 2.6, Tables S2.1-S2.4).

In all four species, only even-chain alkanoic acids in the range of nC_{14} to nC_{28} and alcohol moieties ranging from nC_{18} to nC_{32} were observed resulting in even-chain alkyl esters. In *B. nana*, nC_{20} was the overall dominant ester-bound alkanoic acid moiety with 62.2 µg/g d.w. and nC_{24} the most prominent ester-bound alcohol with 58.9 µg/g d.w.. In the shorter nC_{38} and nC_{40} esters shorter ester-bound alkanoic acids with 14 and 16 carbon atoms as well as shorter ester-bound alcohols like nC_{22} occurred. The ester homologues of *B. humilis*, *B. pubescens* and *B. pendula* were dominated by short-chain nC_{16} bound alkanoic acid moieties (841.5, 368.8, 75.7 µg/g d.w.), while nC_{20} was the most dominant alkanoic acid homologue in the long-chain alkanoic acid fraction (190.6, 38.0, 33.4 µg/g d.w.). However, compared to the short-chain alkanoic acids, the long-chain homologues were less abundant in concentrations up to factor of 10. The major esterified alcohol within the three species varied significantly. *B. humilis* was dominated by nC_{20} (744.2 µg/g d.w.), *B. pubescens* by nC_{22} (346.6 µg/g d.w.) and *B. pendula* by nC_{24} (82.7 µg/g d.w.) and nC_{22} (81.2 µg/g d.w.) bound alcohols.

The bound *n*-alkanoic acid and *n*-alcohol moieties of wax esters might be released during hydrolysis upon leaf senescence, incorporation of alkyl esters into soil or during early burial stages in sediments. As consequence, the amount of hydrolysis-released, previously ester-bound *n*-alkanoic acids and *n*-alcohols in a geoarchives will impact on the quantity and distribution pattern of free *n*-alkanoic acids and *n*-alcohols derived from leaf waxes (Jansen et al., 2006) and needs to be considered in paleovegetation reconstruction. However, intact wax esters can survive in sediments and can be used for paleovegetation reconstruction (Cranwell and Volkman, 1981; van Bergen et al., 1997; Lockheart et al., 2000) as well.

To test the potential release of *n*-alcohols and *n*-alkanoic acids from esters two different scenarios were calculated. In the first scenario, 50% of the esterified *n*-alkanoic acids and *n*-alcohols were released and added to their corresponding free homologues (Fig. 2.2). In the second scenario, the maximum release of 100% of the bound lipids and addition to the free analogues was used. Since the wax esters of all four birches consisted mainly of short-chain fatty acids, they do not significantly increase the pool of long-chain fatty acids (>nC_{20}) typical for terrestrial higher plants. Solely in *B. nana*, the alkanoic acid distribution changed from a previously rather balanced distribution of nC_{20} to nC_{28} with 1 to 2 µg/g d.w. to a dominance of

nC_{20} with >60 µg/g d.w., due to the release of the esterified homologues. A dominance of *n*C_{28} alkanoic acid was still observed for the other three birches when 50% of the esterified alkanoic acids had been released. Only upon 100% release of the bound long-chain alkanoic acids, a bimodal distribution maximizing at *n*C_{20} and *n*C_{28} could be noted for *B. pubescens*, which would complicate a source identification in sediments.

The bound *n*-alcohols of the alkyl esters in the four European birches ranged from *n*C_{20} to *n*C_{32}. Sometimes, the dominant esterified *n*-alcohol was found to be the same as the dominant free homologue in the same species (Fig. 2.3). For example, in *B. humilis n*C_{20} and in *B. pubescens n*C_{22} were the dominant free and esterified *n*-alcohol, respectively. The release of 100 % bound *n*-alcohols of both species increased the total amount by about 25%. However, the relative distributions remained comparable. The previously identified dominance of the free *n*C_{22} alcohol in *B. pendula* was reduced by the release of a high proportion of *n*C_{24}. In contrast, the distribution in *B. nana* changed from a dominance of *n*C_{28} to a bimodal distribution maximizing at *n*C_{24} and *n*C_{28} due to the addition of ester-bound *n*-alcohols. The dominance of free *n*C_{22} alcohol in *B. pendula* was reduced by the release of the high proportion of *n*C_{24}.

Our model indicates that the decay of the *n*-alkyl ester can significantly affect the original free lipid composition of birch leaves, which in sediments may complicate an unambiguous assignment based on *n*-alcohol and *n*-alkanoic acids.

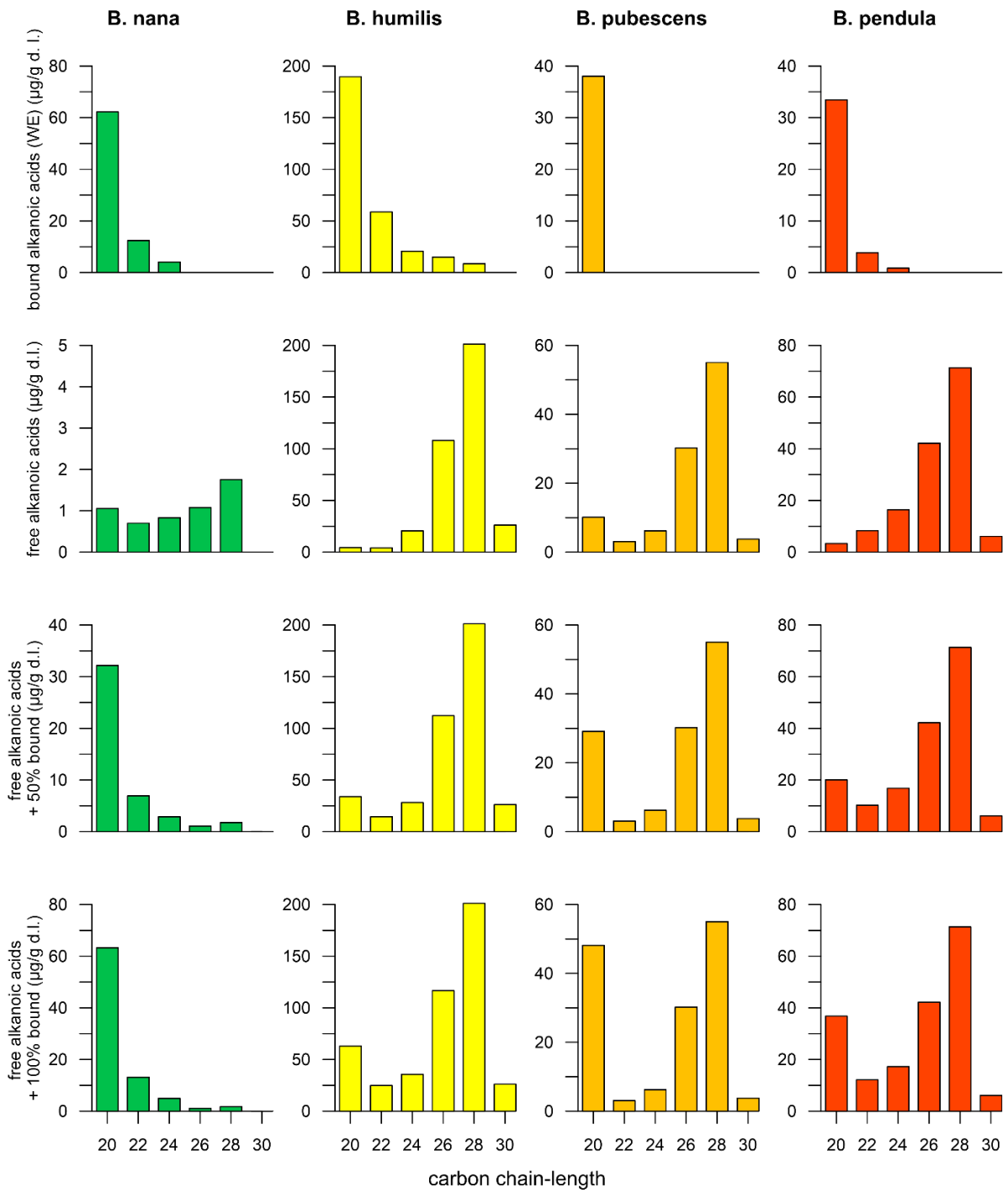

Figure 2.2: Distribution of esterified (bound) alkanoic acids in alkyl esters and their corresponding free homologues. The two lower rows depict the summed concentration of free fatty acids plus an additional 50% or 100% bound fatty acids released by hydrolysis, respectively.

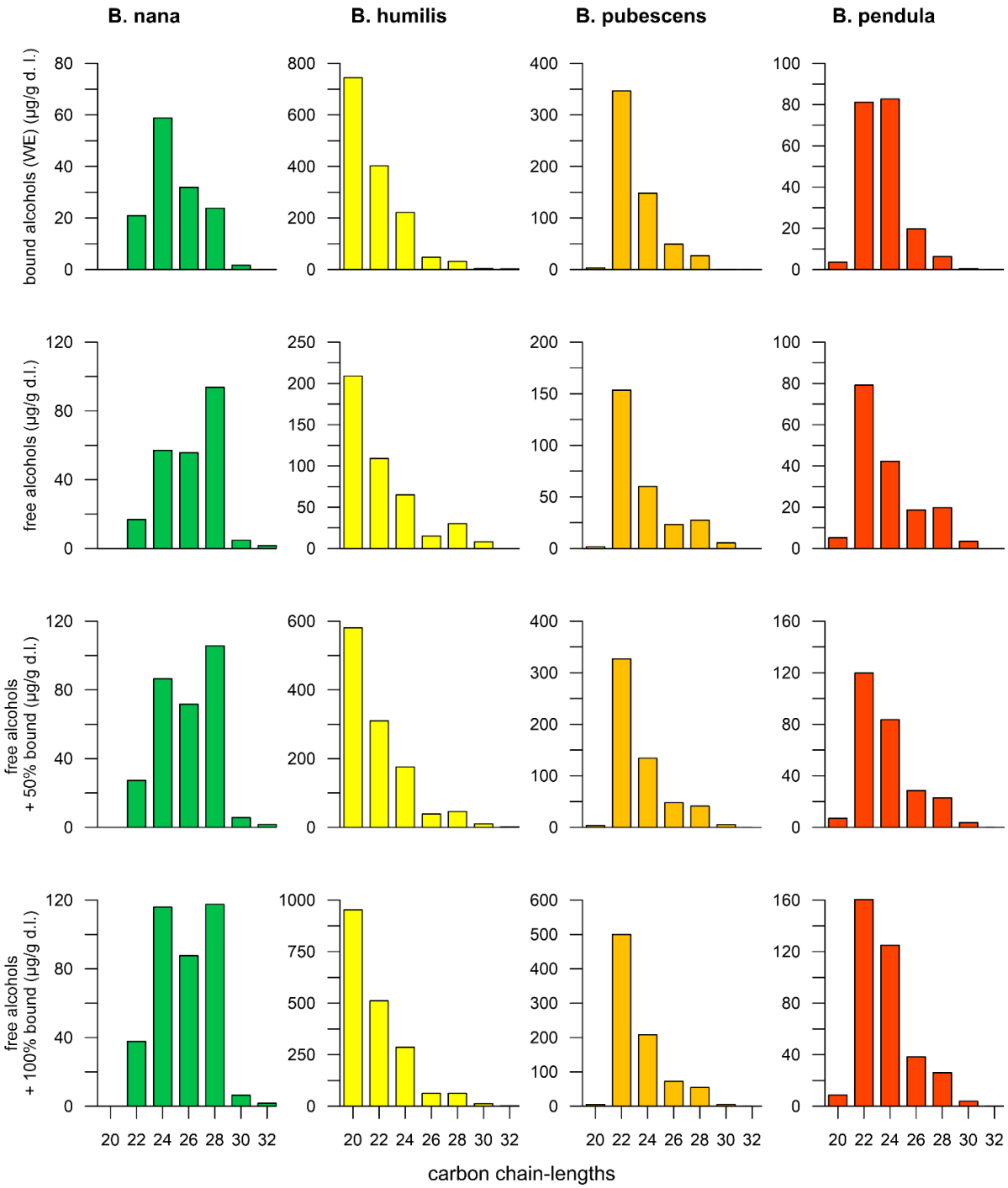

Figure 2.3: Distribution of esterified (bound) alcohols in alkyl esters and their corresponding free homologues. The two lower rows depict the summed concentration of free fatty acids plus an additional 50% or 100% bound fatty acids released by hydrolysis, respectively.

2.3.7 Global variability in *Betula* wax lipids and comparison with those from Kiel

To consolidate the application of the lipid composition of the four European birches for chemotaxonomic differentiation, diagenetic alteration assessment and paleovegetation reconstruction, we compared our wax lipid data of birch trees grown in the Botanical Garden

in Kiel with previously published results (Table 2.1). However, solely the *n*-alkane composition of *B. nana, B. pubescens* and *B. pendula* can be compared, as to the best of our knowledge, the other wax lipid classes were not examined in full in previous studies. We were unable to locate previous studies on the wax lipid composition of *B. humilis* leaves; thus, we do not have any complementary data for comparison. For a better comparison of published data, we have recalculated the distributions given in absolute concentrations into relative abundances, to exclude variation in absolute concentration due to different extraction techniques or analytical protocols. Different extraction techniques and analytic procedures used in the cited studies are briefly described here:

- Extraction of epicuticular waxes by immersion of the hole leaf into solvent mixture with or without ultrasonic bath, e.g. DCM:hexane (1:1) or pure DCM (this study; Lihavainen et al., 2017);
- Prior to extraction, grounding or milling of leaves into a fine powder, followed by ASE (extraction under elevated temperature and pressure) or Soxhlet extraction (Zech et al., 2010; Tarasov et al., 2013; Berke et al., 2019); here, intra-cuticular waxes potentially have been extracted;
- Hydrolysis (10% KOH in ethanol) of ground leaves to extract bound lipids (Mayes et al., 1994); esterified alkanoic acids and alcohols were released and increased the pool of their free homologues.

Most leaves from B. *nana* are characterized by a variable distribution of *n*-alkanes ranging from nC_{23} to nC_{33}. Samples from very northern latitudes such as Greenland, Alaska, Siberia and Norway had a high proportion of nC_{27} to nC_{31} homologues (Mayes et al., 1994; Daniels et al., 2017; Berke et al., 2019). Conversely, *B. nana* leaves from Siberia and Norway can be distinguished from the other *B. nana* samples as these showed significant abundances of mid-chain nC_{23} and nC_{25} alkanes depressing relative amounts of nC_{29} and nC_{31} homologues (Ronkainen et al., 2015; Balascio et al., 2018). Leaf *n*-alkanes of *B. pubescens* from Scotland were bimodally distributed with maxima at nC_{27} and nC_{31} (Rao et al., 2003). In contrast, a unimodal distribution with a maximum at nC_{27} was reported from Pagani et al. (2006), Ronkainen et al. (2015), and Balascio et al. (2018), with variable proportions of nC_{23} and nC_{25}, respectively. A dominance of nC_{27} alkane in leaves from *B. pubescens* has also been reported from Schwark et al. (2002) and Sachse et al. (2006). The latter author stated that only in birches (both *B. pubescens* and *B. pendula*) from northern Scandinavia nC_{27} is the dominant homologue, while species from southern Scandinavia and Germany maximized at nC_{31}. This shift in *n*-alkane carbon chain-length was also expressed in an increasing ACL from North to South (Sachse et al., 2006). In contrast to this, Mayes et al. (1994) found a prevalence of nC_{25} in leaves from Norway.

Similar to the leaves of *B*. *pubescens*, those of *B. pendula* contained high proportions of nC$_{25}$, if the distribution maximized at nC$_{27}$ and then constituted only minor long-chain homologues with more than 29 carbon atoms (Dawson et al., 2004; Zech et al., 2010; Tarasov et al., 2013; van den Bos et al., 2018). Two *B. pendula* species from Estonia and the UK, when grown under artificial laboratory conditions had a distinct bimodal distribution with maxima at nC$_{27}$ and nC$_{31}$ (Huang et al., 1999; Lihavainen et al., 2017).

Due to the complexity of the *n*-alkane patterns both within a single species and between different species, we subdivided the data according to distributions of *n*-alkanes in each species into two groups to improve comparison. The data published for each species were subdivided into two groups (type I and type II) based on similarity in composition and compared with the lipid distribution of the birches from Kiel (Fig. 2.4, Table 2.2, Fig. S2.5). In order to test the robustness of this classification by statistical analysis we conducted an ANOVA and a hierarchical cluster analysis. Type I of each species had a wax lipid composition similar to the *Betula* species from Kiel and was characterized by a dominance of long-chain *n*-alkanes (nC$_{27}$, nC$_{29}$, nC$_{31}$). In contrast, type II of each species was defined by a high presence of mid-chain *n*-alkanes (nC$_{23}$, nC$_{25}$), but also nC$_{27}$, and only minor quantities of long-chain *n*-alkanes with more than 29 carbon atoms.

One-way ANOVA confirmed that the two groups are significantly different at p<0.001 and hierarchical cluster analysis separated the two populations as shown in Fig. S2.5. The two different clusters could not be attributed to a climate gradient or other known environmental driving factors or different work-up procedures. A discussion of potential reasons is given below.

All *Betula* tree species from Kiel and from globally distributed type I were distinct from grasses and shrubs by a prominent prevalence of the nC$_{27}$ alkane (Fig. 2.1 and 2.4). Grasses are mainly dominated by very long-chain *n*-alkanes with nC$_{31}$ and nC$_{33}$ or even nC$_{35}$, and therefore are characterized by a high ACL (>30) (Maffei, 1996; Rommerskirchen et al., 2006; Bush and McInerney, 2013). Typical pioneer shrubs of the late glacial period such as A*rtemisia sp*. or *Juniperus sp.* are also characterized by a dominance at nC$_{31}$ to nC$_{35}$, which is not prevalent in *Betula* species (Schwark et al., 2002; Maffei et al., 2004; Rajčević et al., 2014). Other prominent species such as *Pinus sp.*, which are probably the most widely spread conifer species in Europe, synthesize *n*-alkanes with a predominance in the range from nC$_{27}$ and nC$_{31}$ (Schwark et al., 2002; Ali et al., 2005). However, the quantitative amounts are significantly lower, pointing to subordinate proportions of sedimentary *n*-alkanes originating from pines (Diefendorf et al., 2011).

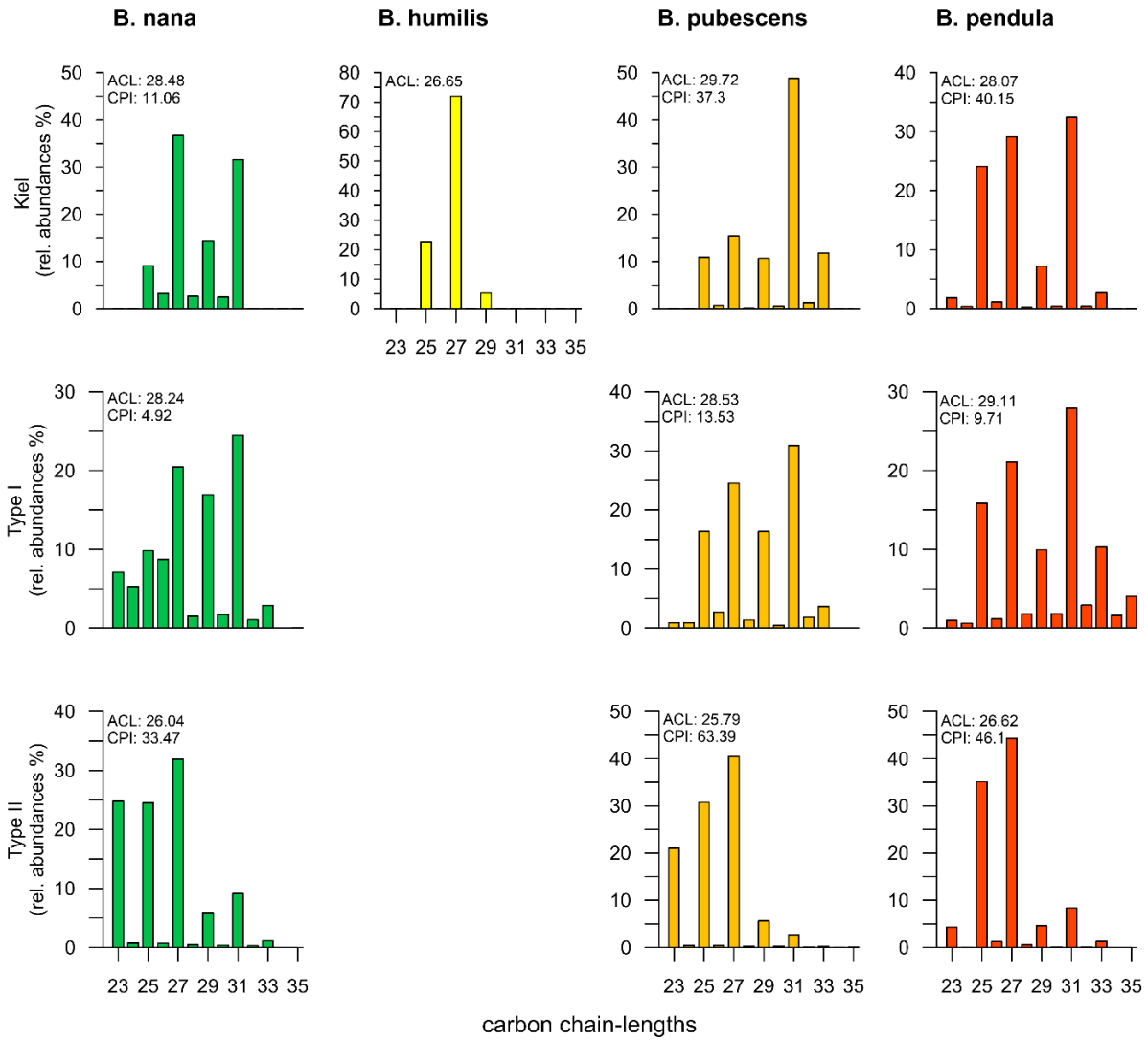

Figure 2.4: Relative abundance patterns of *n*-alkanes for *B. nana, B. humilis, B. pubescens* and *B. pendula*. Samples from Kiel compared with literature data divided into two subgroups (type I and type II; see text for details) separated by ANOVA p>0.001. Note, to the best of our knowledge there are no previous studies reporting the epicuticular wax composition of *B. humilis*.

The type II birch species had *n*-alkane distributions similar to aquatic macrophytes and non-emergent (submerged and floating) aquatic plants, with a prevalence of mid-chain *n*-alkanes (nC_{23}, nC_{25}). These homologues can be a major source to geological archives, especially in lake sediments, often expressed in the P_{aq} proxy (Ficken et al., 2000; Aichner et al., 2010). It has been postulated that terrestrial plants correspond to $P_{aq} < 0.1$, emergent macrophytes to P_{aq} 0.1 - 0.4 and non-emergent macrophytes to P_{aq} 0.4 - 1.0 (Ficken et al., 2000). Each type II birch species, as well as *B. humilis* from our study, showed a P_{aq} value in excess of 0.75, corresponding to a non-emergent macrophyte. Therefore, when applying the P_{aq} proxy in the study of lake sediments receiving birch input, it must be considered that mid-chain *n*-alkanes may derive from either aquatic macrophytes or alternatively from (birch) trees.

n-Alkane abundance or chain-length based indicators like ACL have been used as a proxy for temperature, aridity, geographic location, or vapour pressure deficit (Eley and Hren, 2018; Hoffmann et al., 2013; Kirkels et al., 2013; Lihavainen et al., 2017; Tipple and Pagani, 2013). The variation of the ACL compiled for *B. nana* did not show a trend with climatic drivers. The *B. nana* trees listed, mostly derived from cold environments such as Alaska, Greenland or Siberia and varied in their ACL between 26.4 and 28.9 (Ronkainen et al., 2015; Daniels et al., 2017; Berke et al., 2019). Even two samples both originating from Norway varied by over 2 units in their ACL (Balascio et al., 2018; Lihavainen et al., 2017; Mayes et al., 1994). The *B. nana* investigated from Kiel, and therefore from the warmest region, did not reveal the highest ACL, but rather values between those of leaves from Greenland and Alaska. The ACL distributions of *B. pubescens* revealed higher values in samples from a moderate climate (Kiel, Scotland), whereas samples from colder regions (Siberia, Norway) had a lower ACL. Under certain assumptions, this can be attributed a geographical or temperature effect. The origin for the *B. pubescens* leaves from the study by Pagani et al. (2006) were not reported. Similar to *B. nana*, no latitudinal or temperature trend in the *n*-alkane distribution of *B. pendula* wax was observed.

Overall, a high variability of wax *n*-alkanes within the individual species was noted without recognition of an environmental (e.g. temperature) or geographical trend. This may suggest that genetic differences between the populations control wax lipid composition, preferentially. It is conceivable that not only "pure-bred" birches of the respective species were examined in these studies, but also subspecies or varieties. For example, *B. pubescens* has several varieties that occur naturally in a narrow space like *var. pubescens, var. fragrans, var. litwinowii* and *var. pumila* (Ashburner and McAllister, 2013). Wild hybridization may also affect leaf wax composition, whereby hybridization readily occurs between species with the same chromosome number like *B. pendula* × *B. nana* (diploid × diploid), but there are also reports of interploidy-level hybrids like *B. pendula* × *B. pubescens* (diploid × tetraploid) (Elkington, 1968; Palme et al., 2004). Therefore, future studies may address the association between ploidy level and wax lipid composition of *Betula* species to investigate species determination.

2.3.8 Effect of decarboxylation of *n*-alcohols and *n*-alkanoic acids on the free *n*-alkane pool

Diagenesis may impact on *n*-alkane distributions via the reduction and decarboxylation of *n*-alcohols and *n*-alkanoic acids (e.g. Jansen and Wiesenberg, 2017). Similar to the wax ester degradation as described above, two different scenarios were calculated (Fig. 2.5). In the first scenario, 50% of all free and esterified *n*-alkanoic acids and *n*-alcohols were converted into *n*-alkanes and added to the free pool. In the second scenario, 100% of both lipid classes are

converted and pooled with the free *n*-alkanes. The *n*-alkane distributions of each species then changed significantly in quantity and quality, mainly due to an increase in relative proportions of nC_{23} to nC_{27} alkanes (Fig. 2.5). This resulted in *n*-alkane patterns contrasting with those of the free *n*-alkanes (Fig. 2.1) but being similar to those of *n*-alkanes reported in the literature for group II birches (Fig. 2.4). The adulterated *n*-alkanes distribution mimicked *n*-alkane fingerprints of mosses or aquatic macrophytes described above.

Ontogenetic changes in wax lipid composition have been described previously for a variety of plants but these studies did not include *Betulaceae* (Busta et al., 2017). For *Arabidopsis* species ontogenetic changes in wax constituent classes and in homologue distributions within classes were attributed to enzymatic activities of the CER6-elongase (Busta et al., 2017). Leaf wax developmental stages and in particular wax compositions close to leaf senescence are thus of paramount importance when comparing results generated at various sites and ontogenetic stages. If applied to paleoenvironment analysis the continuation in leaf wax alteration occurring upon earliest diagenesis in soils and sediments must be included as well, as both the bio-ontogenetic as well as geo-diagenetic stages contribute to a continuum of wax lipid compositions present in the biogeosphere. We consider this aspect as critical in all aspects of wax lipid interpretation, including the potential effects on leaf wax δD/H- and $\delta^{13}C$-isotope signatures that are widely applied in paleoclimate reconstruction (see Aichner et al., 2015; Diefendorf and Freimuth, 2017; Sachse et al., 2012 for review). In this case isotope determination on *n*-alkanes of primary, secondary or tertiary origin will have to be tested for potential influence of isotopic differences between the original compound classes, i.e. free or bound functionalized *n*-alkyl lipids.

Table 2.2: Relative *n*-alkane abundances of grouped Betula species

				Relative abundance %													
Species	**Article**	**Location**	**Typ**	**23**	**24**	**25**	**26**	**27**	**28**	**29**	**30**	**31**	**32**	**33**	**34**	**35**	**ACL**
B. nana	This study	Kiel	Kiel	0	0	9	3	37	3	14	2	32	0	0	0	0	28.49
B. nana	Berke et al. (2019)	Greenland	I	9	7	14	10	17	1	15	1	24	1	2	0	0	27.95
B. nana	Daniels et al. (2017)	Alaska (USA)	I	1	4	5	9	24	3	17	3	26	3	5	0	0	28.94
B. nana	Mayes et al. (1994)	Norway	I	12	4	10	7	20	0	19	1	23	0	2	0	0	27.88
B. nana	Ronkainen et al. (2015)	Siberia (Russia)	II	20	1	22	1	34	1	7	1	12	0	1	0	0	26.45
B. nana	Balascio et al. (2018)	Norway	II	30	0	27	0	30	0	5	0	6	0	1	0	0	25.65
B. humilis	This study	Kiel	Kiel	0	0	23	0	72	0	5	0	0	0	0	0	0	26.65
B. pubescens	This study	Kiel	Kiel	0	0	11	1	15	0	11	1	49	1	12	0	0	29.72
B. pubescens	Rao et al. (2003)	Scotland (UK)	I	1	1	16	3	25	1	16	0	31	2	4	0	0	28.53
B. pubescens	Ronkainen et al. (2015)	Siberia (Russia)	II	19	1	25	2	42	1	5	0	4	0	0	0	0	26.00
B. pubescens	Pagani et al. (2006)	?	II	5	0	23	0	73	0	0	0	0	0	0	0	0	26.36
B. pubescens	Mayes et al. (1994)	Norway	II	35	0	48	0	4	0	9	0	3	0	0	0	0	24.94
B. pubescens	Balascio et al. (2018)	Norway	II	25	0	27	0	43	0	3	0	1	0	0	0	0	25.53
B. pendula	This study	Kiel	Kiel	2	0	24	1	29	0	7	0	32	0	3	0	0	28.07
B. pendula	Huang et al. (1999)	Solar Dome (UK)	I	0	0	20	0	25	0	12	0	37	0	7	0	0	28.72
B. pendula	Lihavainen et al. (2017)	Estonia	I	2	1	12	2	18	4	7	4	19	6	14	3	8	29.60
B. pendula	Zech et al. (2010)	Russia	II	0	0	30	2	50	1	5	1	10	1	1	0	0	26.96
B. pendula	Dawson et al. (2004)	UK	II	6	0	34	0	38	0	6	0	12	0	3	0	0	26.88
B. pendula	Tarasov et al. (2013)	Siberia (Russia)	II	0	0	45	3	49	1	2	0	0	0	0	0	0	26.09
B. pendula	van den Bos et al. (2018)	Netherlands	II	11	0	31	0	40	0	6	0	11	0	1	0	0	26.56

Table 2.2: Relative *n*-alkane abundances of grouped Betula species

		relative abundance (%)													
Species	**Type**	**23**	**24**	**25**	**26**	**27**	**28**	**29**	**30**	**31**	**32**	**33**	**34**	**35**	**ACL**
B. nana	Kiel	0	0	9	3	37	3	14	2	32	0	0	0	0	28.49
B. nana	I	7	5	10	9	20	1	17	2	24	1	3	0	0	28.24
B. nana	II	25	1	25	1	32	1	6	0	9	0	1	0	0	26.04
B. humilis	Kiel	0	0	23	0	72	0	5	0	0	0	0	0	0	26.65
B. pubescens	Kiel	0	0	11	1	15	0	11	1	49	1	12	0	0	29.72
B. pubescens	I	1	1	16	3	25	1	16	0	31	2	4	0	0	28.53
B. pubescens	II	21	0	31	0	40	0	6	0	3	0	0	0	0	25.79
B. pendula	Kiel	2	0	24	1	29	0	7	0	32	0	3	0	0	28.07
B. pendula	I	1	1	16	1	21	2	10	2	28	3	10	2	4	29.11
B. pendula	II	4	0	35	1	44	1	5	0	8	0	1	0	0	26.62

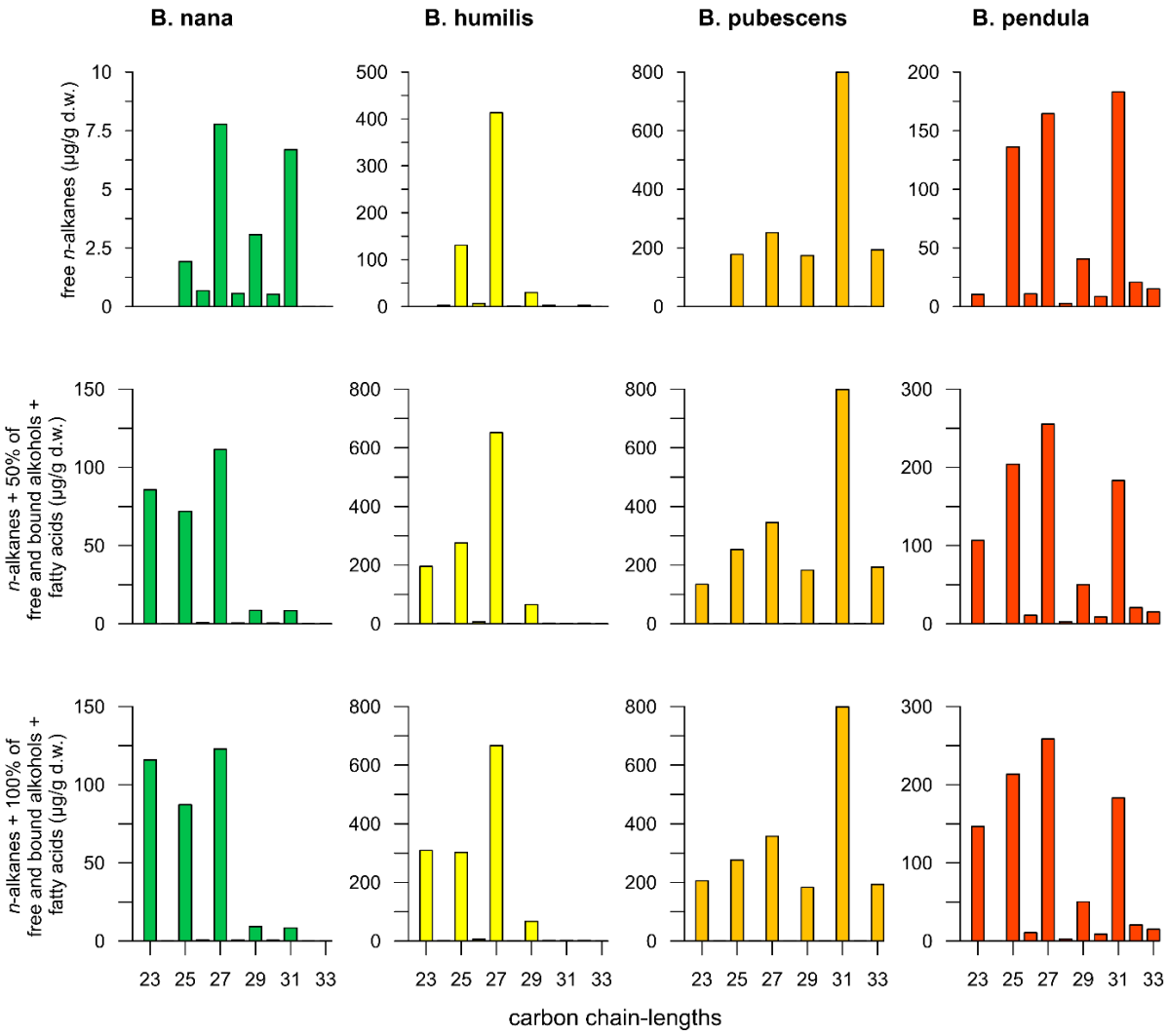

Figure 2.5: Distribution of free *n*-alkanes versus cumulative free plus ontogenetic and diagenetic analogues in the four *Betula* species. The latter were assessed from corresponding functionalized precursor lipids based on 50 and 100 % conversion rates; see text for details.

2.3.9 Analytical and extraction protocols used in previous *Betula* studies

Different analytic protocols have been used to extract the plant lipids as briefly descripted above. Previous studies have shown that the length of the extraction time, as well as the solvent used, had an influence on extraction yield or lipid extract composition (Buschhaus et al., 2007; Jetter and Kunst, 2008). Thus, *n*-alkanes and *n*-alcohols were extracted earlier than *n*-alkanoic acids and long-chain homologues earlier than the shorter ones (Stammitti et al., 1996). Jetter et al. (2008) indicated extraction yields of *n*-alkanes depended on polarity of binary solvent mixtures. Moreover, saponification upon extraction (Mayes et al., 1994) hydrolysed wax esters leading to enhanced release of bound *n*-alcohols and *n*-alkanoic acids adding to the proportion of the free homologues. Since this comparative investigation used *n*-alkane distributions from different studies with different extraction methods, the results are not

unequivocally comparable. For a better comparability of future work, the influence of the extraction method on the other lipid classes including *n*-alcohols, *n*-alkanoic acids and *n*-alkyl esters should be investigated and a standard extraction protocol established.

2.4 Conclusion

The leaves of four endemic European *Betula* species, *B. nana, B. humilis, B. pubescens, B. pendula* were studied, aiming at an extended and more representative chemotaxonomy of their epicuticular wax lipid composition via inclusion of functionalized *n*-alkyl lipids. The following conclusions can be drawn from this study. The free *n*-alkane compositions in leaves of *Betula* species from Kiel were found to be specific, allowing unambiguous differentiation. Birch wax *n*-alcohol and *n*-alkyl ester composition allowed a distinction to be made between the shrubs *B. nana* and *B. humilis* versus the two birch trees. However, the latter two cannot be easily distinguished from each other due to a similar wax lipid fingerprint. The *n*-alkanoic acids seemed to be less suitable for species differentiation since all four species were dominated by the nC_{28} alkanoic acid, however with variations in concentration of about two orders of magnitude. A flowchart (Fig. 2.6) provides a simple means for discrimination of epicuticular waxes from the four birches from Kiel University.

The *n*-alkyl esters consisted of different isomers with varying *n*-alcohol and *n*-alkanoic acid moieties. In the species *B. humilis* and B. *pubescens*, the dominant esterified alcohol matched the dominant free alcohol. Therefore, the birch *n*-alcohol patterns in sediments would not be disturbed by hydrolysis of the wax esters. In *B. nana* and *B. pendula*, the *n*-alcohol distribution changed substantially upon ester hydrolysis, when bound homologues were released. Due to the preponderance of short-chain ester-bound alkanoic acids in wax esters, the distribution of free long-chain alkanoic acids was only slightly impaired. The ratio was influenced in *B. nana* only, as large amounts of bound nC_{20} were released.

Compilation of literature data on *Betula n*-alkane composition revealed a high degree of variability that may complicate application of wax composition in paleoenvironment studies. When comparing the *n*-alkane composition of the *Betula* waxes collected in Kiel with data published for other regions, no trend in geographical location or temperature could be identified. Differences in *n*-alkane compositions can be attributed to various factors. It appears that *Betula* wax composition is genetically controlled, and differences occur due to presence of plant hybrids or variants. An influence of methodological approaches on wax lipid compositions, including secondary alteration reactions is feasible. The most important aspect in leaf wax heterogeneity may result from a continuum of bio-ontogenetic and geo-diagenetic alteration of primary leaf wax composition occurring in nature. This aspect should receive more attention in future studies on plant wax-based chemotaxonomy as well as paleobotany.

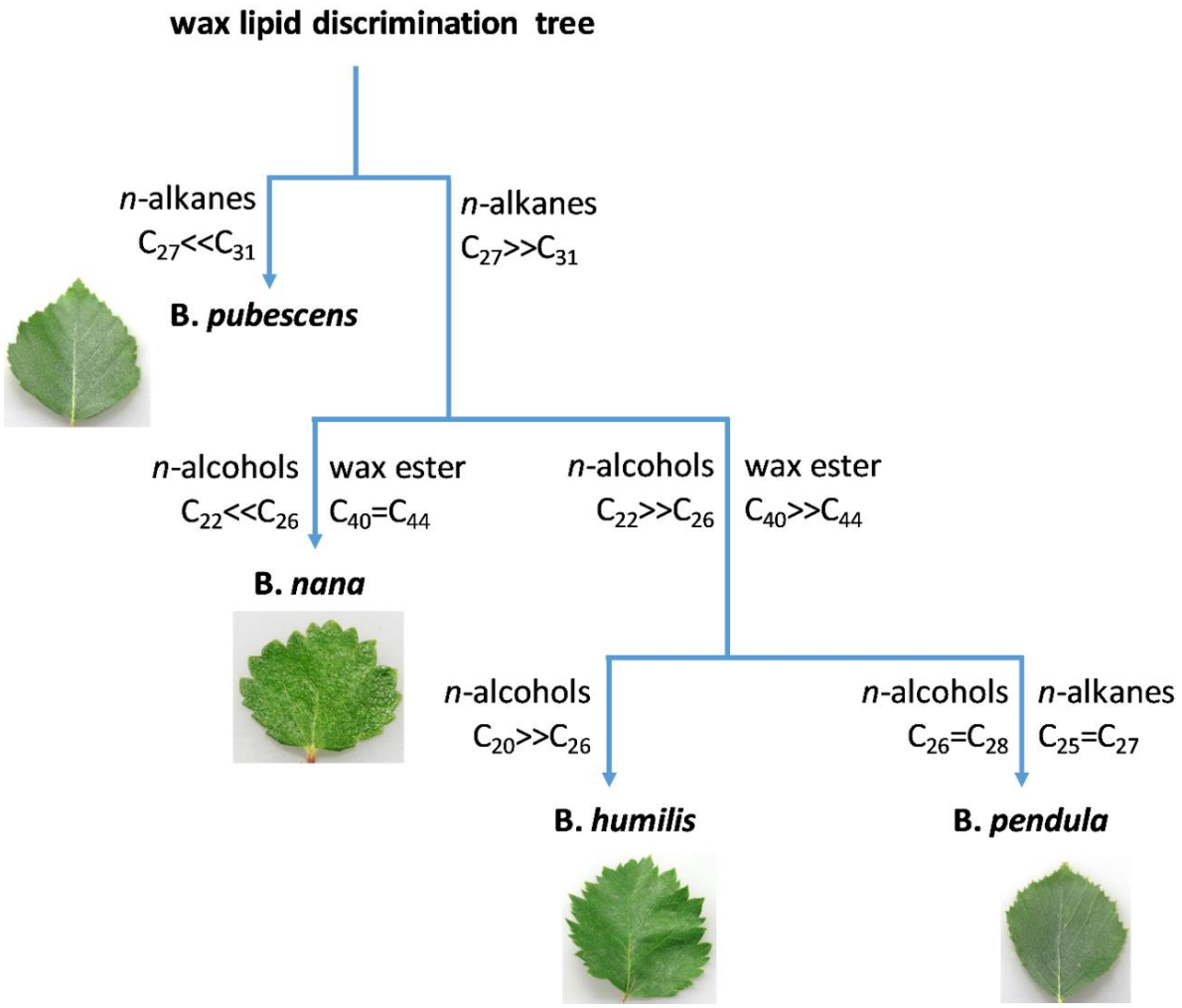

Figure 2.6: Decision making tree for chemotaxonomic differentiation of four European *Betula* species based on epicuticular wax composition

Acknowledgements

T. Martens and V. Grote are thanked for laboratory assistance during lipid extraction. Dr. S. Petersen is thanked for her advice during leaf sampling in the Botanical Garden of Kiel University.

2.5 Supplementary material

S2.1: Statistical Analysis

Principal-component analysis (PCA) and clyster analysis (CA) were carried out based on the absolute concentrations of all wax lipids of the investigated birch species using the software "PAST Paleontological Statistics v. 3.25". The performed PCA visualized the variability in epicuticular wax lipid composition of the four European birch species (Fig. S2.3). The first and second components explain 74.78 and 22.23%, respectively, of the total variance. The figure indicates that all four species are distinguishable based on their lipid distribution and the three triplicates are close to each other. *B. nana* shows negative values for PC1 and PC2, while *B. humilis* loads positive on PC1 and negative PC2. Contrary, *B. pubescens* shows strong positive PC2 values, while the values of *B. pendula* are more diverse (Fig. S2.3). PC1 is mainly characterized by nC$_{31}$ and minor contribution of nC$_{29}$ and nC$_{33}$ alkanes. The variance in PC2, in contrast, is associated with the absolute abundances of the nC$_{27}$ alkane, nC$_{20}$ alcohol and nC$_{28}$ alkanoic acid.

The CA were performed using the Euclidian distance with single-linkage method based on the absolute abundance of the epicuticular wax lipids and reveals further differentiation of the birch species (Fig. S2.4). The CA indicates two main clusters, one consisting of *B. humilis* and the other of *B. nana*, *B. pendula* und *B. pubescens*. Interestingly, both dwarf birches are separated from each other and *B. pendula* is very close to *B. nana*. This is explained by the exclusively high proportion of short-chain wax esters in *B. humilis.* The very close spacing of the triplicates again demonstrates the homogeneity within and reproducibility of the individual species.

Additionally, a CA was performed using Euclidian distance with single-linkage method based on the relative *n*-alkane abundances of all birches from Kiel and literature data (Fig. S2.5). B. pendula from Estonia (Lihavainen et al., 2017) is an outlier potentially due to unusual vapor pressure deficit generated during the execution of the experiment.

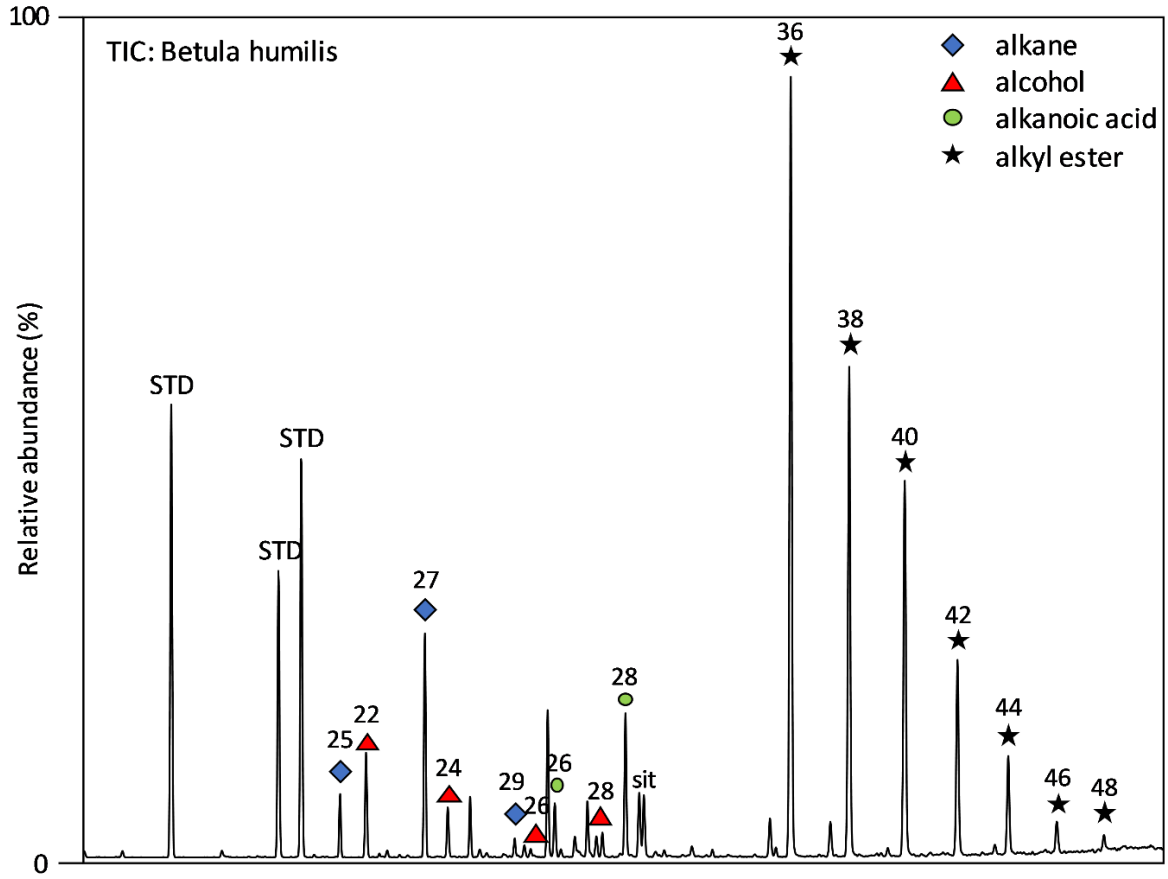

Figure S2.1: Total ion chromatogram of a *Betula humilis* leaf with the most abundant components.

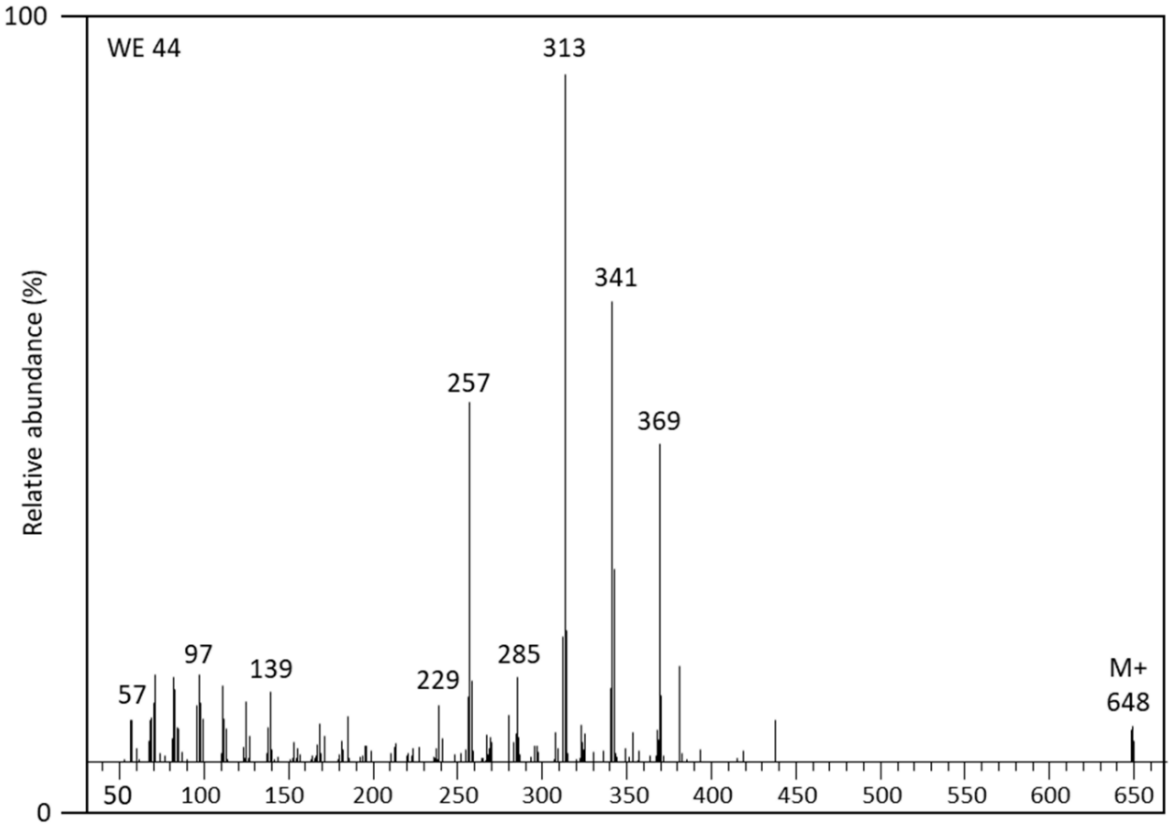

Figure S2.2: Mass spectrum of a C_{44} alkyl ester mixture (RCOOR') of *Betula humilis*. The diagnostic ions are shown for the acid fragments $(RCO_2H_2)^+$ and the molecular ion (M+).

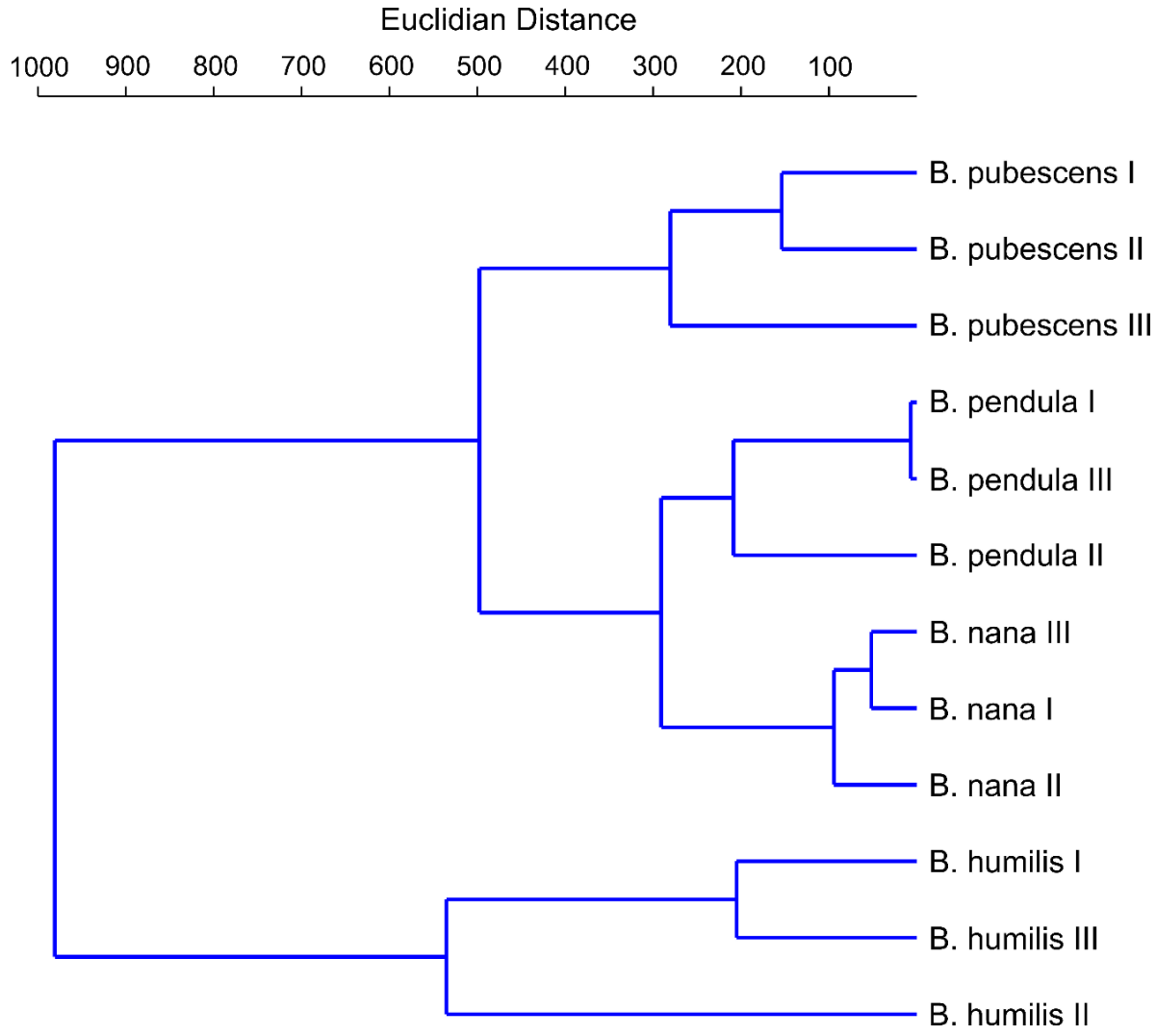

Figure S2.3: Principal components analysis.

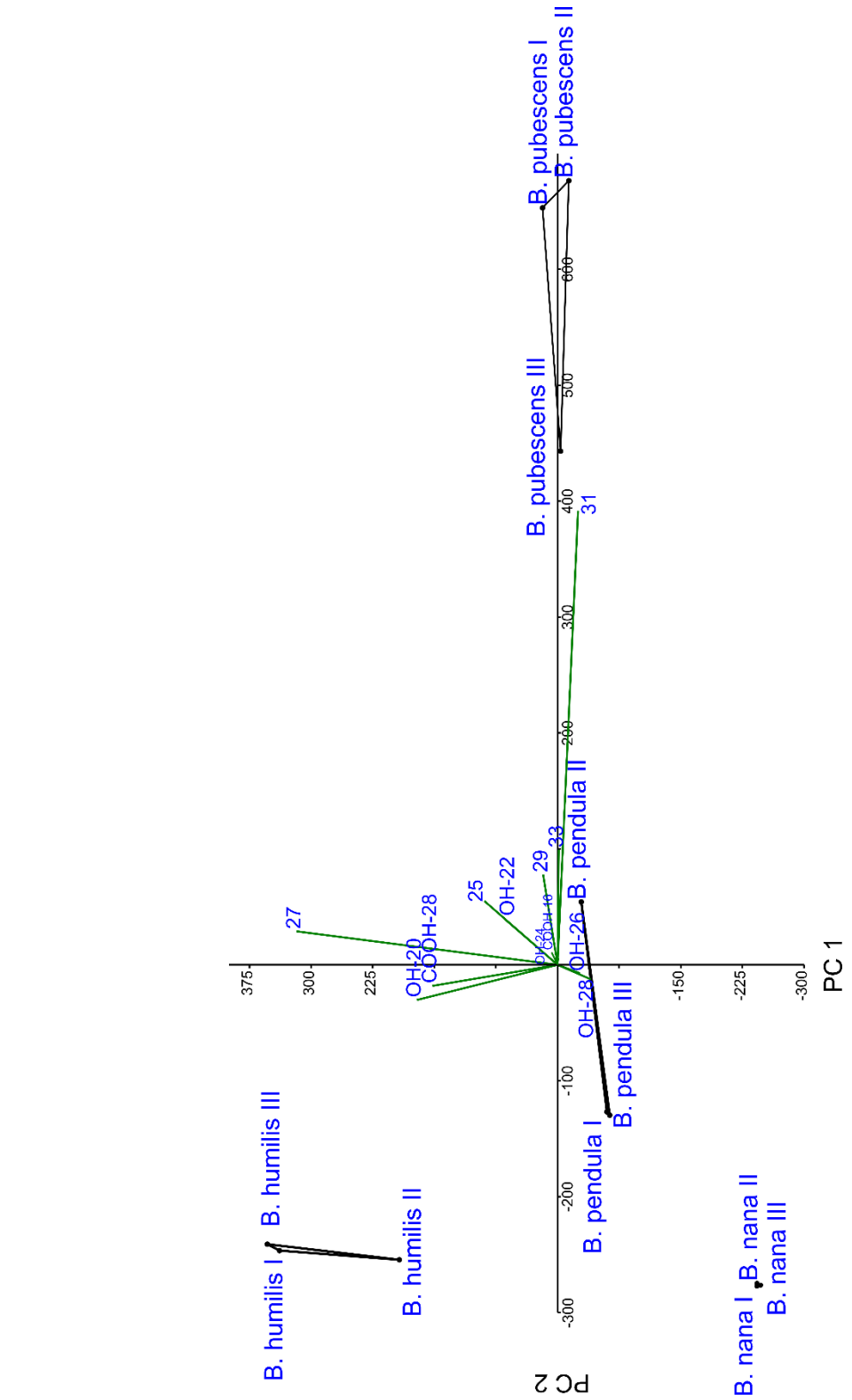

Figure S2.4: Cluster Analysis of Kiel data

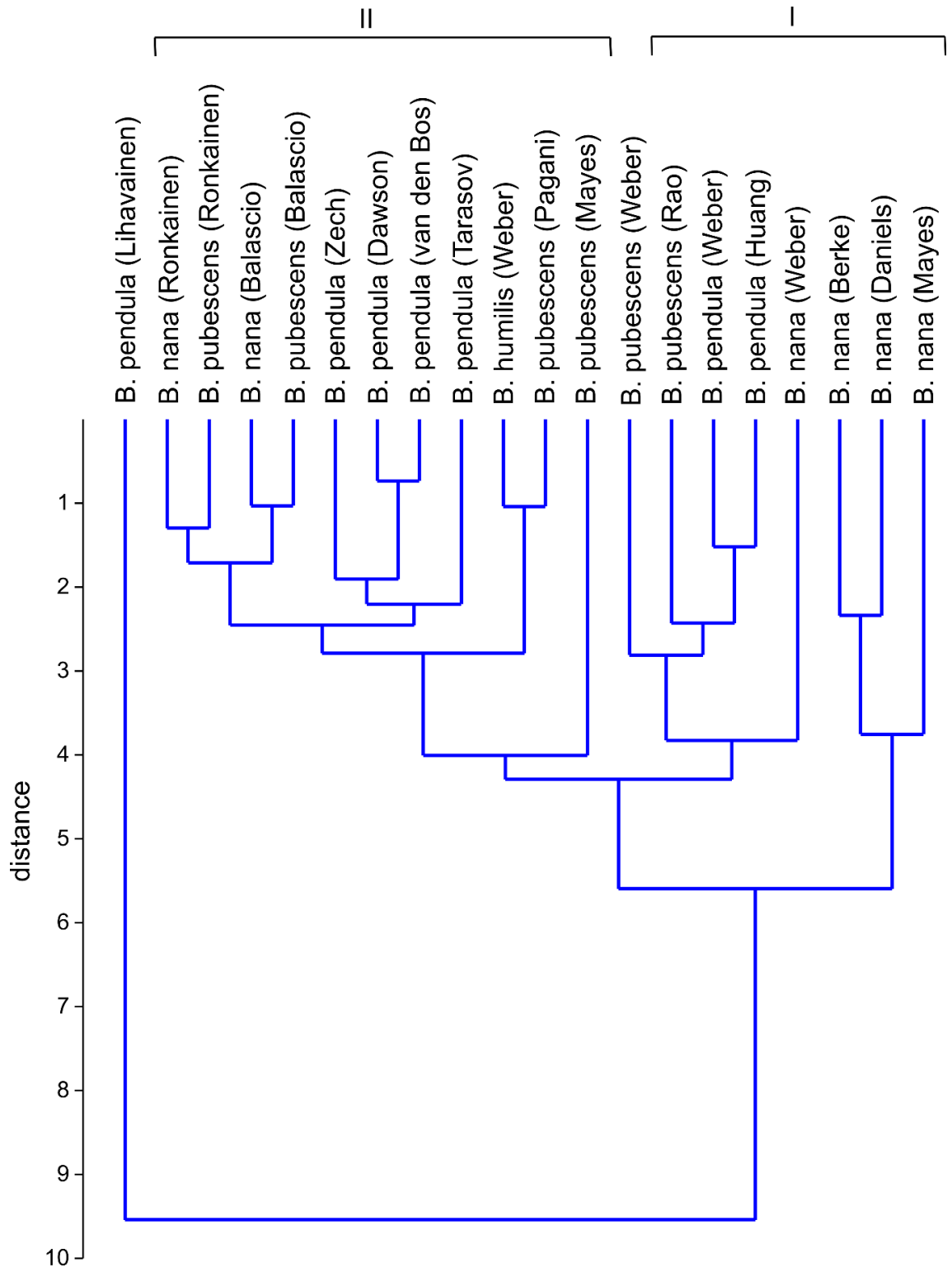

Figure S2.5: Hierarchical cluster analysis of birch wax *n*-alkane distributions obtained from literature data. The two populations (Type I and Type II; see text for details) of birch wax composition samples are fully separated. The outlying wax composition measured by Lihavainen et al. (2017) are due to specific cultivation conditions.

Table S2.1: Composition of *n*-alkyl esters from epicuticular waxes of *Betula nana.*

Ester chain length	M^+	Mass (µg/g d.w.)	Acid chain length	Alcohol chain length	Amount of isomer (µg/g d.w.)
38	564	3.06	14	24	0.78
			16	22	2.28
40	592	17.1	14	26	1.05
			16	24	10
			18	22	4.95
			20	20	1.2
42	620	58.9	14	28	1.73
			16	26	11.8
			18	24	22.9
			20	22	21.9
			22	20	0.16
			24	18	0.34
44	648	104.2	14	30	0.6
			16	28	14.6
			18	26	14.4
			20	24	63.4
			22	22	10.4
			24	20	0.78
46	676	52.8	14	32	0.13
			16	30	1.99
			18	28	8.54
			20	26	27.9
			22	24	11.4
			24	22	2.86
48	704	22.1	20	28	16.1
			22	26	2.35
			24	24	3.62

Table S2.2: Composition of *n*-alkyl esters from epicuticular waxes of *Betula humilis*

Ester chain length	M^+	Mass (µg/g d.w.)	Acid chain length	Alcohol chain length	Amount of isomer (µg/g d.w.)
36	536	1047	14	22	6.5
			16	20	1040
38	564	601	14	24	7.5
			16	22	420
			18	20	173
40	592	532	14	26	3
			16	24	254
			18	22	123
			20	20	150
42	620	310	14	28	2.4
			16	26	57.7
			18	24	57.9
			20	22	147
			22	20	44.7
44	648	180	16	28	39.7
			18	26	10.9
			20	24	59.2
			22	22	49.3
			24	20	21.1
46	676	70	16	30	6.9
			18	28	5.6
			20	26	10.2
			22	24	16.6
			24	22	11.3
			26	20	19.8
48	704	35	16	32	3.62
			20	28	6.03
			24	24	4.95
			26	22	6.18
			28	20	14.2

Table S2.3: Composition of *n*-alkyl ester from epicuticular waxes of *Betula pubescens*

Ester chain length	M^+	Mass (µg/g d.w.)	Acid chain length	Alcohol chain length	Amount of isomer (µg/g d.w.)
38	564	535	14	24	13.6
			16	22	519
			18	20	2.73
			20	18	0.57
40	592	290	14	26	7.29
			16	24	208
			18	22	71.5
			20	20	4.06
42	620	147	14	28	4.85
			16	26	67.3
			18	24	22.8
			20	22	52.4
44	648	68.4	16	28	39.7
			18	26	9.65
			20	24	19

Table S2.4: Composition of *n*-alkyl ester from epicuticular waxes of *Betula pendula*

Ester chain length	M^+	Mass (µg/g d.w.)	Acid chain length	Alcohol chain length	Amount of isomer (µg/g d.w.)
38	564	122.7	14	24	31.3
			16	22	91.5
40	592	101.7	14	26	6.2
			16	24	59.1
			18	22	29.3
			20	20	7.08
42	620	73.6	14	28	2.16
			16	26	14.7
			18	24	28.7
			20	22	27.4
			22	20	0.2
			24	18	0.42
44	648	42.7	14	30	0.25
			16	28	5.98
			18	26	5.92
			20	24	26
			22	22	4.26
			24	20	0.32
46	676	13.9	14	32	0.03
			16	30	0.52
			18	28	2.25
			20	26	7.36
			22	24	3.01
			24	22	0.75

3. A multiphasic Younger Dryas cold period recorded in sediments of Lake Steisslingen, SW-Germany: A biomarker perspective

Abstract

The Younger Dryas (12,680 – 11,590 yr BP) was the last millennial scale cold event of the Quaternary, when a mean annual temperature decline of 3 to 5°C impacted severely on the environment. Whereas pollen distributions document changes in land vegetation, details of limnic ecosystem responses to the cooling event and to its recovery are still not well known. Here, we studied the laminated sediments of Lake Steisslingen (SW-Germany) deposited between 13,500 to 11,100 yr BP in order to investigate the evolution of an aquatic ecosystem. Bulk sediment and organic matter composition mark onset and termination of the Younger Dryas, but remain monotonous through this interval, requiring application of organic and isotope geochemical techniques to follow past ecosystem dynamics. The Younger Dryas is characterized by both an abrupt appearance and demise of long-chain alkenones indicative for haptophyte algae. Based on algal and bacterial biomarker distribution, the Younger Dryas can be divided into three stages, each characterized by the dominance of a microorganism group. The first phase was dominated by nC$_{17}$ alkanes and hopanoids indicative of cyanophytes and heterotrophic bacteria. The second phase shows a proliferation of cold-adapted haptophyte algae, while in the latest phase highly-branched isoprenoids (HBI) reveal an aquatic community shift towards diatoms. Heterocyte glycolipids document a moderate change in N_2-fixing cyanobacterial community structure over the Allerød/Younger Dryas transition but show a marked collapse of the cyanobacteria association at the Younger Dryas/Preboreal climate recovery. Terrigenic wax lipids indicate significant changes in vegetation between the Allerød, Younger Dryas and Preboreal chronozones but remain homogeneous within the Younger Dryas.

3.1 Introduction

The Holocene has witnessed several periods of rapid climate change of different intensity, duration and spatial extent, including amongst others the little ice age, or the 4.2 ka and the 8.2 ka event (Johnsen et al., 2001; Wick et al., 2003; Mayewski et al., 2004). One of the most severe climate perturbations occurred during the Younger Dryas (YD) chronozone (12,680 – 11,590 yr BP), when mean annual air temperatures dropped by about 3-4°C in NW-Europe and 14°C in Greenland (Brauer et al., 1999; Lotter et al., 2000; Grachev and Severinghaus, 2005; Heiri et al., 2007). This cold event is well documented in Greenland ice cores and also recorded in many lacustrine and marine archives (Fairbanks, 1990; Johnsen et al., 1992; Bond

et al., 1993; Brauer et al., 2001; Schwark et al., 2002; Stansell et al., 2010; Słowiński et al., 2017). A peculiarity of the Younger Dryas is that its onset as well as its termination seem to have occurred over a short time span of only a few years or decades (Alley, 2000). This very rapid response to a climatic trigger has been explained by an instantaneous outburst of proglacial lake meltwater on the Laurentian ice shield in North America (Lowell et al., 2005). When the huge freshwater masses flowed into the North Atlantic, the Atlantic Meridional Overturning Circulation (AMOC) was reduced, shifting the Gulf Stream southward and thus leading to a massive cooling of NW-Europe after the comparatively warm climate of the Allerød (13,560 – 12,680 yr BP) (Broecker, 2006; Carlson et al., 2007; Condron and Winsor, 2012). The sudden onset of the Younger Dryas is in perfect agreement with such a scenario and its duration of about 1,000 years. The re-establishment of the AMOC and the climatic amelioration in NW-Europe also seems to have occurred over only a few decades and not in a slow transient mode (Sirocko, 2009).

Previous studies recognized that climatic conditions during the Younger Dryas were not uniformly stable (Baldini et al., 2015; Lane et al., 2013; Neugebauer et al., 2012; Schlolaut et al., 2017). Moreover, von Grafenstein et al. (1999) identified a short relapse of warmer continental climate measuring the $\delta^{18}O$ of ostracods shells in the sediments of Lake Ammersee (Germany) and termed this anomaly “Mid-Younger Dryas Event”. A bi-partition of the YD with still warm to moderate summer temperatures in the first interval and a second phase with colder summers is expressed in the sediments of Lake Rehwiese, Germany (Neugebauer et al., 2012). The same phenomenon of a two-phase Younger Dryas has also been reported from Lake Kråkenes (Norway), Meerfelder Maar (Germany) and Lake Suigetsu (Japan) with a slightly different timing due to an interaction of the North Atlantic sea surface temperature and an eastwards moisture transport (Bakke et al., 2009; Lane et al., 2013; Schlolaut et al., 2017). Besides the outburst theory other potential causes of the Younger Dryas cooling event have been proposed, e.g. an extra-terrestrial impact accompanied with massive biomass burning or the sulfur-rich Laacher See volcanic eruption (Firestone et al., 2007; Baldini et al., 2018; Wolbach et al., 2018a, 2018b).

In contrast to vegetation dynamics manifested in pollen distributions, the effect of the Younger Dryas climate event on limnic ecosystems has not been studied to a comparable degree. In order to investigate the environmental response to the Younger Dryas cold event on aquatic ecosystems, we performed a high-resolution biomarker and stable isotope study of a sediment record from Lake Steisslingen (SW-Germany). Our results indicate a multiphased climate and ecosystem perturbation in Lake Steisslingen during the late Pleistocene and early Holocene.

3.2 Site description

Lake Steisslingen (47°47’54”N, 8°54’57”E) is a small kettle lake located 20 km west of Lake Constance (SW-Germany) (Fig. 3.1). It formed at the end of the Würm glaciation with the retreat of the alpine ice sheets (Schreiner, 1973a, 1973b). The local geology in the lake’s catchment is dominated by glauconitic sandstones from the “Obere Meeres Molasse” and marls and sandstones from the “Untere Süsswasser Molasse” deposited within the Alpine Tertiary Molasse Basin (Eusterhues et al., 2005). Current Lake Steisslingen (446 m a.s.l.) covers an area of about 0.11 km^2, has a length of 600 m (NW-SE) and a width of about 250 m (NE-SW) (Mayer and Schwark, 1999). The maximum water depth of about 20.5 m is located in the south-eastern part of the lake (Eusterhues et al., 2002). The lake is fed by several submerged springs in 8 to 10 m water depth and drained by an artificial outflow that was built in the 15th century to operate a mill located on the SE-shore (Mayer and Schwark, 1999; Eusterhues et al., 2005). Prior, the lake drained to the NW into a wetland area (Mayer and Schwark, 1999). Modern Lake Steisslingen is mesotrophic with a chemocline situated in a water depth of about 11 to 15 m (Barnikol-Schlamm, 1994). The mean annual water temperature is about 11.5°C and varies between 22°C in summer and 4°C in winter (LUBW, 2016).

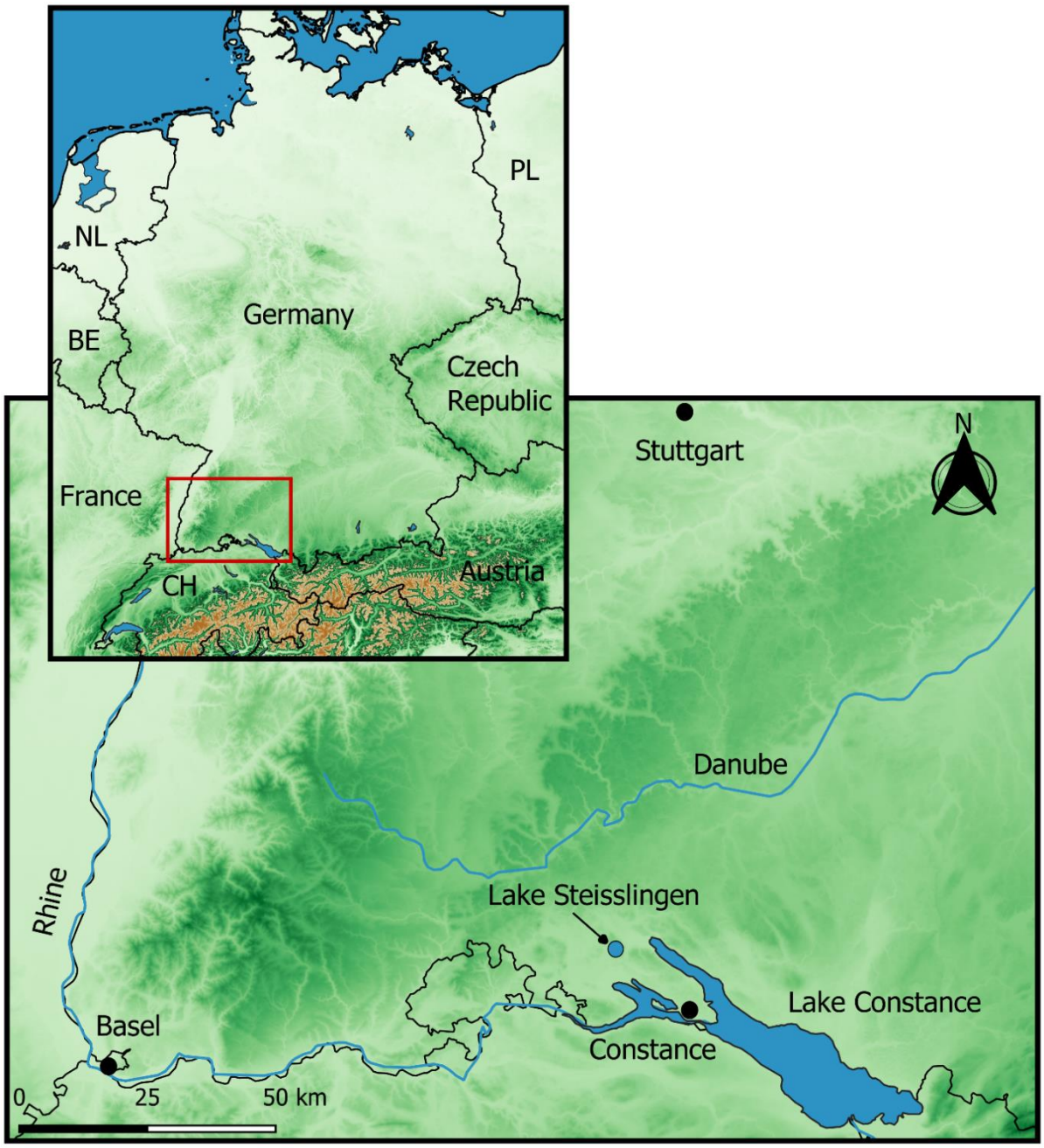

Figure 3.1: Map showing the location of Lake Steisslingen in SW-Germany.

3.3 Geochemical background

In this paleoenvironmental study, we applied a variety of geochemical proxies and provide a short overview on how these tools are commonly applied.

Stable oxygen isotopes of carbonates

The oxygen isotopic composition ($\delta^{18}O$) of biogenic or abiogenic authigenic carbonates can be used to determine paleo-lake temperatures at the time of carbonate precipitation (Leng and Marshall, 2004). Determination of absolute temperatures is not straightforward, since a variety

of factors such as atmospheric precipitation, evaporation and in- and outflow in the hydrological regime can influence the $\delta^{18}O$ of the ambient water (Talbot, 1990). Since there is no evidences for a significant input of carbonate-rich detrital input in the sediments of Lake Steisslingen, the majority of the $CaCO_3$ content is formed by autochthonous precipitation of discrete carbonate crystals (micrite) in the surface waters (Mayer and Schwark, 1999). Therefore, $\delta^{18}O_{carbonate}$ values are directly related to the lake surface temperature, or at least to the temperature during highest productivity of the photic zone of Lake Steisslingen (Zink et al., 2001).

Stable carbon isotopes of organic matter

Stable carbon isotope ($\delta^{13}C_{TOC}$) values in general allow to distinguish between marine and terrestrial plants and to identify the photosynthesis pathways (C_3 vs. C_4) (Meyers, 2003). Additionally, $\delta^{13}C_{TOC}$ values compared with TOC/TN-ratio can be used to differentiate between terrestrial plant and algae debris, since the former synthesize woody tissue that is rich in structural carbon (Ertel and Hedges, 1985; Talbot and Johannessen, 1992; Meyers, 1994). In contrast, algae and bacteria are a plentiful source of nitrogen containing compounds (such as amino acids and proteins). As such, they generally have TOC/TN ratios ranging between 6-10 (Meyers, 1994).

Stable nitrogen isotopes

Stable nitrogen isotopes of organic matter ($\delta^{15}N$) are commonly used to characterize the paleoproductivity and for examining sources of organic matter (Ohlendieck et al., 2000; Meyers, 2003). Various factors can affect the interpretation of $\delta^{15}N$ including remineralization, shifts in phytoplankton assemblage and input of terrestrial plant sources or soils (Castañeda and Schouten, 2011).

Long-chain alkenones

Long-chain alkenones (LCAs) are a class of C_{35} – C_{42} di-, tri- and tetra-unsaturated methyl (Me) and ethyl (Et) ketones found in lacustrine and marine sediments. The relative degree of unsaturation expressed as the U^K_{37} correlates with marine and lake surface water temperatures (Brassell et al., 1986; Prahl and Wakeham, 1987; Zink et al., 2001; Castañeda and Schouten, 2011; Longo et al., 2016). In marine environments the main producers of LCAs are the haptophyte algae *Emiliania huxleyi* and *Gephyrocapsa oceanica*, which are phylogenetically classified as Group III haptophytes. The producer(s) in lacustrine environments is/are not entirely clarified due to a higher genetic diversity of LCA-producing species (Volkman et al., 1980, 1995; Zink et al., 2001; D'Andrea and Huang, 2005; Theroux et al., 2010; Randlett et al., 2014; Longo et al., 2018). Based on the relative distribution of C_{37}-

and C_{38}-alkenones, it is possible to classify lacustrine LCA-producers. The Group I or Greenland phylotype shows an even C_{37}/C_{38} ratio and the Group II yields a ratio >2 (Theroux et al., 2010; Longo et al., 2018)

Highly branched isoprenoids

Highly branched isoprenoids (HBIs) with varying chain length ranging from C_{20} - C_{30} are specific biomarkers for diatoms and have been detected in several species (Belt et al., 2000, 2017; Brown et al., 2014; He et al., 2016). HBI-20 compounds are mainly found in marine sediments but also occur in lacustrine sediments. In addition to diatoms, HBI-20 was found in the green macroalgae *Enteromorpha prolifera*. (Rowland et al., 1985). On the other hand, saturated and unsaturated HBI-25 analogues are exclusively known from diatom species such as *Haslea ostrearia* and *Rhizosolenia setigera* (Volkman et al., 1994; Sinninghe Damsté et al., 2004; He et al., 2016).

Glycerol dialkyl glycerol tetraethers

Isoprenoidal and branched glycerol dialkyl glycerol tetraethers (GDGTs) are membrane lipids produced by Archaea and Bacteria, respectively. Branched GDGTs are most dominant in soils and lacustrine sediments (Schouten et al., 2013a). The methylation of the 5-methyl isomers of brGDGTs expressed in the MBT'_{5ME} ratio is primary correlated with the mean annual air temperature (MAAT) and thus used to reconstruct paleoclimate variabilities (De Jonge et al., 2014; Russell et al., 2018). In lakes, the ratio of GDGT-0 to crenarchaeol can be used to trace methanogenesis due to the fact that methanogenic Euryarchaeota produce GDGT-0 but lack crenarchaeol (Blaga et al., 2009).

Hopanoids

Hopanoids are biomarkers for bacteria, as these compounds are generally thought to mainly originate from bacteriohopanepolyols occurring in cell membranes of prokaryotic organisms. Dehydration and reduction of bacteriohopanepolyols during diagenesis forms hopenes and hopanes as degradation products (Ourisson and Albrecht, 1992; Ourisson and Rohmer, 1992). Some of these pentacyclic triterpenoids with a wide range of structural variety, e.g. number and position of functional groups, can be related to typical bacteria or bacteria populations (Talbot and Farrimond, 2007; Cooke et al., 2008).

Heterocyte glycolipids

Heterocyte glycolipids (HGs) are a unique product synthesized exclusively by N_2-fixing heterocytous cyanobacteria. These components consist of even-numbered diol, triol, keto-ol, keto-diol or diketone structures with 26 to 32 carbon atoms that are glycosidically bound to a

polar sugar headgroup (Gambacorta et al., 1998; Bauersachs et al., 2009b). Culture experiments have demonstrated that HG distribution patterns vary between heterocytous cyanobacteria of different families and orders (Gambacorta et al., 1999; Bauersachs et al., 2009a; 2019). This allows for investigating the community assemblages of cyanobacteria in fossil ecosystems, as done previously in the Holocene Baltic Sea (Sollai et al., 2017). A specific feature of these components is that the relative proportions of HG diols and their corresponding keto-ols changes as a function of temperature (Bauersachs et al., 2014). Very similar changes in HG composition have also been observed in surface waters of a temperate lake in northern Germany and quantified using the heterocyte diol index of 26 carbon atoms (HDI_{26}; Bauersachs et al. 2015). In addition, changes in the relative abundance of structural isomers of a given HG have been observed with temperature and may represent an additional means to provide a microaerobic environments to the heterocyte at varying temperatures (Bauersachs et al., 2013). For the two isomers of HG_{28} diol commonly found in lacustrine sequences, temperature changes can be recorded using the heterocyte isomer ratio of diols with 28 carbon atoms (HIR_{28D}; Fig. S3.1).

n-Alkanes

Long chain *n*-alkanes (nC_{27}-nC_{35}) derive from the epicuticular leaf waxes of higher plants (Eglinton and Hamilton, 1967; Meyers, 2003). In sediment sequences, the distribution of these components provides information about vegetation types in a lake's catchment such as woody, herbaceous or grassy plant types or in some instances it can also be related to specific genera (Schwark et al., 2002; Bush and McInerney, 2013; Aichner et al., 2018). However, it has been shown, that certain algae species, e.g. *Botryococcus braunii*, can be a potential source of long-chain *n*-alkanes in sediments where they result from the diagenetic reduction of alkadienes (Lichtfouse et al., 1994). In contrast, short chain *n*-alkanes (nC_{15}, nC_{17} and nC_{19}) are mainly synthesized by phytoplankton. The most dominant short chain *n*-alkane in aquatic environments is nC_{17}, which is synthesized predominantly by algae and cyanobacteria and is a potential indicator for lacustrine paleoproductivity rates (Giger et al., 1980; Cranwell et al., 1987; Meyers, 2003; Zhang et al., 2018).

3.4 Materials and Methods

3.4.1 Sediment

Sediment core STK-9 comprises a 6.97 m-thick sediment sequence obtained from the profundal of Lake Steisslingen in 1997. Cores were stored at 4°C in non-transparent plastic liners to minimize alteration/oxidation of sedimentary organic matter. At a core depth between 570.55 – 618.75 cm, the Younger Dryas sediments present a 48.2 cm-thick interval characterized by finely laminated organic varves. Sediments from this interval as well as from

the adjacent Allerød and Preboreal chronozones were sampled at high resolution as 2-3 mm thick sediment slices. A total of 80 samples were taken, which were lyophilized for 24 h and ground to a homogenous powder using an agate mortar and pestle. Subsequently, all sediments were stored frozen until further processing.

3.4.2 Core chronology

Sediment core STK-9 investigated here was taken parallel to cores STK-2, 7 and 8 for which a detailed age model and sedimentation rates have been established previously (Wolf, 1994; Mayer and Schwark, 1999; Eusterhues et al., 2002, 2005). Sedimentological characteristics of STK-9 are similar to those of STK-2, 7 and 8. The Laacher See Tephra (LST) with an age of 12,880 yr BP, found at a depth of 621.4 cm as a 5 mm-thick discrete layer, is used as an age-anchor point. The age-model for core STK-9 is based on the bulk element distribution and lithological changes compared with parallel core STK-2 and other cores collected previously from Lake Steisslingen (Mayer and Schwark, 1999; Zink et al., 2001; Eusterhues et al., 2002).

3.4.3 Bulk geochemistry

The total carbon (TC), total nitrogen (TN) and total sulfur (TS) content of the sediments were determined by an Elementar Vario EL-III CNS analyser. Total organic carbon (TOC) was measured on decalcified samples using an Eltra Helios system. For this, sediments were treated with excess 10% and 25% hydrochloric acid (HCl) until reaction ceased. Subsequently, all sediments were dried at 100 °C overnight before analysis. The total inorganic carbon content (TIC) was calculated as the difference between TC and TOC. The calcium carbonate ($CaCO_3$) content was calculated by multiplying the TIC by 8.33 (stoichiometry of carbon in $CaCO_3$). Sedimentary TOC/TN ratios were calculated on a molar basis.

3.4.4 Stable isotope measurements

$\delta^{18}O$ analyses of carbonates were performed at the isotope laboratory of the GeoZentrum Nordbayern (Erlangen, Germany) using a Kiel III carbonate preparation line coupled with a ThermoFinnigan 252 mass spectrometer. Reproducibility and quality of the measurements were determined by analysing every 10^{th} sample in duplicate, yielding a standard deviation of <0.1‰ for $\delta^{18}O$.

The carbon isotopic composition of the bulk organic matter ($\delta^{13}C_{TOC}$) was determined on decalcified and neutralized sediment samples using a Flash EA ConFlow III interface elemental analyzer coupled to a Delta V isotope ratio mass spectrometer (Thermo Scientific, US). Bulk nitrogen isotopes ($\delta^{15}N$) were measured on the same instrument set-up on non-decalcified sediments. All isotope ratios are given in conventional δ-notation with respect to

the VPDB (Vienna Pee Dee Belemnite) standard for $\delta^{13}C_{TOC}$ and atmospheric dinitrogen gas for $\delta^{15}N$.

3.4.5 Lipid extraction

An aliquot of the homogenized sediments (0.5-1.1 g) was extracted following a modified Bligh and Dyer procedure (Bligh and Dyer, 1959; Rütters et al., 2002). The sediments were ultrasonically extracted for ~10 min with a solvent mixture of methanol (MeOH), dichloromethane (DCM) and phosphate buffer at pH 7-8 (2:1:0.8, *v/v/v*). After centrifugation (3000 rpm; 4 min), the supernatant was collected and the residuum extracted as described above. This procedure was repeated until the extract was colourless (between 5 to 7 times). DCM and phosphate buffer were added to the pooled extracts in order to yield a solvent ratio of 1:1:0.9 (MeOH:DCM:phosphate buffer, *v/v/v*), which induced a phase separation. After centrifugation (3000 rpm; 4 min), the DCM bottom layer, containing the organic fraction, was transferred to a round-bottomed flask and the remaining MeOH/phosphate buffer phase was extracted twice with DCM. Subsequently, the Bligh and Dyer extract (BDE) was rotary evaporated to near dryness and transferred to pre-weighted glass vials with DCM:MeOH (9:1, *v/v*). The BDE was then dried under N_2 and stored at -18°C until further processing.

An aliquot (4-8 mg) of each BDE was separated into an aliphatic, a ketone and a polar fraction using a Freestyle SPE-system (LC-Tech, Germany). Activated silica gel (SiO_2; 2.5 cm) underlain by aluminium oxide (Al_2O_3; 3.5 cm) was used as stationary phase. The aliphatic fractions were eluted with 8 ml *n*-hexane, the ketone fractions with 8 ml *n*-hexane:ethylacetate (7:3, *v/v*) and the polar fractions with 16 ml DCM:MeOH (1:1, *v/v*) as mobile phases.

3.4.6 Gas chromatography-mass spectrometry (GC-MS)

Aliphatic hydrocarbons

The aliphatic fraction was subjected to gas chromatography-mass spectrometry (GC-MS) using an Agilent 7890A GC equipped with a Phenomenex Zebron ZB-5 column (60m × 0.25mm i.d.; 0.25 µm film thickness) and coupled to an Agilent 5975B mass chromatograph. Prior to analysis, the aliphatic fractions were dissolved in *n*-hexane to a concentration of 1 mg/ml and 1 µg deuterated tetracosane (D50) was added as internal standard. The injection temperature was held at 60°C for 4 min, after which the oven temperature was raised to 140°C at 10°C/min and subsequently to 320 °C at 3°C/min, at which it was held for 8 min. The MS was operated at an electron energy of 70 eV and an ion source temperature of 250°C.

The average chain-length (ACL) of *n*-alkanes with 23 to 33 carbon atoms was calculated according to Poynter and Eglinton (1990):

$$ACL = (23 \times nC_{23} + 25 \times nC_{25} + 27 \times nC_{27} + 29 \times nC_{29} + 31 \times nC_{31} + 33 \times nC_{33}) / (nC_{23} + nC_{25} + nC_{27} + nC_{29} + nC_{31} + nC_{33}) \quad (1)$$

with C_n as relative abundance of *n*-alkanes with the chain length *n*.

Ketone fraction

The ketone fraction, containing long-chain alkenones, was analysed on the GC-MS system described above using a Zebron ZB-1 column (60 m × 250 µm i.d.; 0.25 µm film thickness). Prior to analysis, 4 to 10 µl squalane with a concentration of 10 µg/µl was added as internal standard. The oven temperature was held at 60°C for 2 min, increased with a rate of 20°C/min to 260°C and then to 340°C at 1.5°C/min with 5 min isotherm. The MS was operated at an electron energy of 70 eV and an ion source temperature of 250°C. Di-, tri- and tetraunsaturated alkenones were identified by retention time and published mass spectra (de Leeuw et al., 1980). The U^K_{37} was calculated according to Brassell et al. (1986):

$$U^K_{37} = [C_{37:2} - C_{37:4}] / [C_{37:2} + C_{37:3} + C_{37:4}] \quad (2)$$

3.4.7 Analysis of GDGTs

The polar fractions were dried under a gentle stream of nitrogen, dissolved in *n*-hexane:2-propanol (99:1, *v/v*) to a concentration of 1 mg/ml and passed through a 0.45 µm polytetrafluoroethylene (PTFE) filter (Macherey-Nagel, Germany) prior to analysis. GDGTs were analysed using a Waters Alliance 2695 HPLC system following the analytical protocol described by Hopmans et al. (2016), which allows the separation of 5- and 6-methyl branched GDGTs.

The MBT'_{5ME} was calculated according to de Jonge et al. (2014) and transferred to mean annual air temperature (MAAT) using the lacustrine temperature calibration of Russel et al. (2018):

$$MBT'_{5ME} = (Ia + Ib + Ic) / (Ia + Ib + Ic + IIa + IIb + IIc + IIIa) \quad (3)$$

$$MAAT = -1.21 + 32.42 \times MBT'_{5ME} \quad (4)$$

The BIT index was calculated as detailed in Hopmans et al. (2004) using the combined peak areas of the 5- and 6-methyl isomers of branched GDGTs:

$$BIT\ Index = (Ia + IIa + IIa' + IIIa + IIIa') / (Ia + IIa + IIa' + IIIa + IIIa' + IV) \quad (5)$$

3.4.8 Analysis of HGs

For the analysis of heterocyte glycolipids (HGs), a second aliquot of the BDE was dissolved in a mixture of hexane:2-propanol:H_2O (72:27:1, *v/v/v*) and filtered through a 0.45 µm regenerated cellulose filter. Concentrations ranged from 7 to 10 mg/ml depending on the abundance of the target analyte in the sample. HGs were analysed using a Waters Alliance 2690 HPLC system coupled to Micromass Quattro LC triple quadrupole mass spectrometer as described in Bauersachs et al. (2017).

In Lake Steisslingen, the HG_{28} diol occurred in form of two closely eluting structural isomers. The relative abundance of both isomers was used to calculate the heterocyte isomer ratio of diols with 28 carbon atoms (HIR_{28D}), which is defined as the abundance of the early eluting isomer (HG_{28} diol [I]) divided by the sum of both isomers (HG_{28} diol [I] and HG_{28} diol [II]). See supplementary figure S3.1 for definition of HG_{28} diol isomers.

3.5 Results

3.5.1 Bulk composition and stable isotopes

$CaCO_3$

The average $CaCO_3$ content of the Lake Steisslingen sediment sequence was 21.0±12.5%. The concentration of $CaCO_3$ decreased from a maximum of 35.6% at 13,465 yr BP to 4.3% at the end of the Allerød (12,752 yr BP) with a minimum of 1.2% at 13,126 yr BP (Fig. 3.2). In sediments deposited during the Younger Dryas, the $CaCO_3$ content increased and ranged from 13.9% to 39.4% (average 28.6±6.8%) with maximum values observed during the mid-Younger Dryas. The onset of the Preboreal is marked by a rapid decline in the $CaCO_3$ content to average values of 3.7±3.4%.

$\delta^{18}O_{carbonate}$

The oxygen isotopic composition of sedimentary carbonates ($\delta^{18}O_{carbonate}$) varied between -9.3‰ and -5.6‰ (average -8.1±0.8‰; Fig. 3.2). Decreasing $\delta^{18}O_{carbonate}$ values from -5.7 to -8.0‰ indicated a gradual cooling during the Allerød, interrupted by a more negative $\delta^{18}O_{carbonate}$ value of -8.2‰ at 13,126 yr BP. During the Younger Dryas, $\delta^{18}O_{carbonate}$ values varied only moderately and averaged -8.4±0.3‰, indicating relatively cold but stable climatic conditions. At the end of the Younger Dryas, $\delta^{18}O_{carbonate}$ values increased by 3‰ indicating a period of rapid warming. A second excursion to lower temperatures with $\delta^{18}O_{carbonate}$ values varying from -8.7‰ to -9.3‰ occurred during the Preboreal Oscillation (11,300 – 11,150 yr BP).

TOC

The TOC contents showed an average of 11.4±4.3% across the interval investigated. During the early Allerød, TOC values increased from 11.7% at 13,465 yr BP to a maximum of 22.0% at 13,054 yr BP (Fig. 3.2). Thereafter, the TOC decreased steadily to 14.6% until the end of the Allerød and showed a sudden drop of about 10% to an average of 8.7±2.0% at the onset of the Younger Dryas, after which it increased again slowly. During the Preboreal, TOC values revealed an increasing trend with a maximum of 23.3% at 11,198 yr BP but then declined rapidly after the Preboreal Oscillation to values of 15.5% or less.

TOC/TN

Total organic carbon to total nitrogen (TOC/TN) ratios were generally low and varied from 10.4 to 13.3 (average 11.7±0.6). Lowest TOC/TN ratios were observed in the Allerød and Preboreal warm phases with 11.3±0.3 and 11.0±0.4, respectively (Fig. 3.2). During the Younger Dryas, molar TOC/TN ratios were slightly higher and gave an average of 12.0±0.5.

$\delta^{13}C_{TOC}$

The stable carbon isotope composition of the bulk organic matter ($\delta^{13}C_{TOC}$) varied between -27.8 and -34.9‰ (average -32.4±1.6‰). During the Allerød, $\delta^{13}C_{TOC}$ values decreased gradually from -30.4‰ to -33.2±0.8‰ during the Younger Dryas (Fig. 3.2). A shift to more positive $\delta^{13}C_{TOC}$ values was observed at the onset of the Preboreal, during which $\delta^{13}C_{TOC}$ values averaged -30.8±2.0‰. At 11,409 yr BP, $\delta^{13}C_{TOC}$ started to decline again, resulting in comparatively light stable carbon isotopes of -32.3±0.5‰ for the remainder of the record.

$\delta^{15}N$

The stable nitrogen isotope composition of the bulk sediment ($\delta^{15}N$) varied between -1.8‰ and +2.9‰ (average +1.6±1.3‰). Low values of on average -1.4±0.5‰ occurred during the Allerød except for one sample preceding the LST (12,880 yr BP) (Fig. 3.2). At the onset of the Younger Dryas, $\delta^{15}N$ values rapidly increased by 4‰, resulting in $\delta^{15}N$ values ranging from +1.0‰ to +2.9‰ (average +2.3±0.4‰). At the YD/PB boundary, $\delta^{15}N$ values declined rapidly and ranged from -0.1‰ to 1.6‰ between 11,589 and 11,300 yr BP. With the onset of the PBO, $\delta^{15}N$ values increase again and average at +2.3±0.1‰.

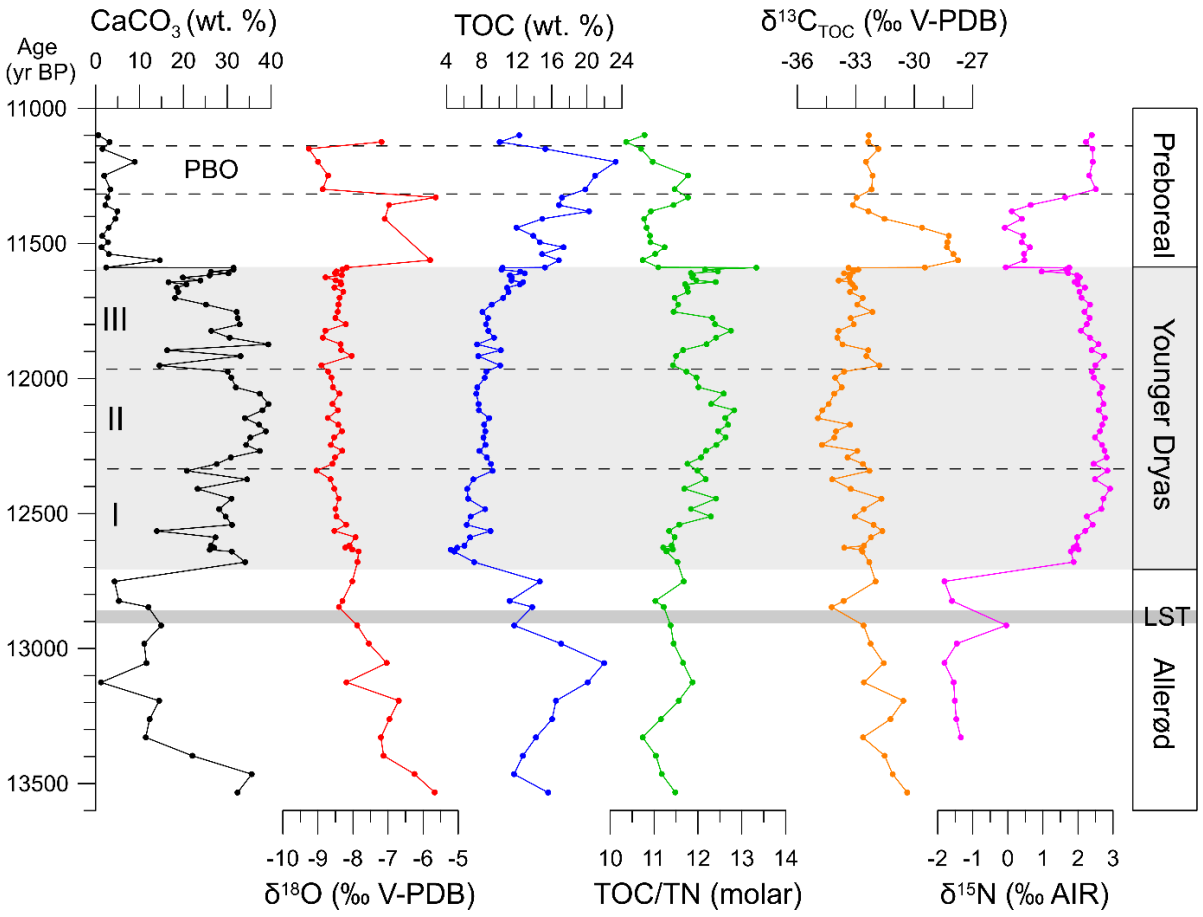

Figure 3.2: Overview of the bulk results from STK-9 of Lake Steisslingen with concentration of total calcium carbonate ($CaCO_3$), oxygen isotopes of calcium carbonate ($\delta^{18}O$), total organic carbon (TOC), molar organic carbon to nitrogen ratio (TOC/TN), bulk carbon isotopes of organic matter ($\delta^{13}C_{TOC}$) and bulk nitrogen isotopes of organic matter ($\delta^{15}N$) vs. time and chronozones. Roman numerals denote the three stages of the Younger Dryas. PBO = Preboreal oscillation; LST = Laacher See Tephra (12,880 yr BP).

3.5.2 Lipid biomarkers

A variety of different lipid classes were detected in the extractable organic matter, including *n*-alkanes, *n*-alkenes, hopanoids, highly branched isoprenoids (HBIs), plant triterpenoids, long-chain alkenones, glycerol dialkyl glycerol tetraethers (GDGTs) and heterocyte glycolipids (HGs), which are described and discussed below.

Aliphatic hydrocarbons

The aliphatic lipid fraction was dominated by *n*-alkanes, highly branched isoprenoids (HBIs) and hopanoids (Fig. S3.2). Of these, *n*-alkanes were most abundant showing a strong odd over even carbon number preference. They varied from nC_{15} to nC_{33} and displayed a pronounced dominance of mid- to long-chain homologues (nC_{23} to nC_{33}).

Amongst the short-chain *n*-alkanes nC_{17} was the most abundant. During the Allerød, the concentration of the nC_{17} was low and varied between 0.3 and 1.7 µg/g TOC (average 1.3±1.0 µg/g TOC) with an exception of 3.3 µg/g TOC at 13,054 yr BP (Fig. 3.3). In the first phase of the Younger Dryas highest average nC_{17} concentrations occurred, yielding a maximum value of 7.1 µg/g TOC at 12,588 yr BP. Over the next ~300 years, comprising a second stage of the Younger Dryas, the concentrations decreased constantly and then increased abruptly to a maximum of 4.3 µg/g TOC at 11,952 yr BP. During the last stage of the Younger Dryas and the following Preboreal concentrations were generally low and ranged from 0.0 to 1.4 µg/g TOC.

During the Allerød, ACL values ranged from 25.8 to 27.2 with a minimum of 25.8 at 13,126 yr BP. With the onset of the Younger Dryas, the ACL increased to a maximum of 27.5 at 12,680 yr BP. Subsequently, the ACL decreased to an average value of 26.8±0.3 for the remainder of the Younger Dryas. In the early Preboreal, ACL values were similar to those observed during the late Younger Dryas (26.9±0.2) and declined slightly during the PBO with values averaging 26.3±0.2.

n-Alkane concentrations of a land plant origin (nC_{27}, nC_{29}, nC_{31}) were generally high in contrast to aquatic biomarkers (HBI-20, nC_{17}) with an average of 160.9±84.5 µg/g TOC (n = 51). The *n*-alkane concentration reached 131.4±65.1 µg/g TOC during the Allerød (Fig. 3.3) but increased to 187.8±88.1 µg/g TOC with a maximum of about 500 µg/g TOC at the onset of the Younger Dryas (Fig. 3.3). During the mid- and late-Younger Dryas, *n*-alkane concentrations decreased again and usually were below 200 µg/g TOC. With the beginning of the Preboreal, plant-derived *n*-alkane concentrations declined to an average of 126.0±72.4 µg/g TOC and simultaneously showed a shift in distribution pattern from a dominance of nC_{27} to the nC_{29} homologue.

HBI-20 was detected over most of the sediment sequence except for the late Preboreal (Fig. 3.3). During the Allerød, the HBI-20 occurred only in low concentrations, ranging from 0.5 to 5.4 µg/g TOC (average 2.2±1.5 µg/g TOC). At the beginning of the Younger Dryas, the concentration rose to values from 0.6 to 7.6 µg/g TOC and maximized in the mid Younger Dryas with 13.7 µg/g TOC at 12,056 yr BP. The late Younger Dryas was characterized by highest average HBI-20 concentrations of 11.5±4.3 µg/g TOC with a maximum of 23.3 µg/g TOC at 11,754 yr BP. At the YD/PB transition, HBI-20 concentrations declined rapidly, resulting in the almost absence of this component in the later Preboreal.

In the sediment record of Lake Steisslingen a diverse suite of hopanes and hopenes was identified (Fig. S3.3). Typical hopanes included 17β-trisnorhopane, 17β,21β-30-norhopane, 17α,21β-homohopane(22R), 17β,21β-hopane, 17β,21β-homohopane and 17β,21β-

bishomohopane. Hopenes included hop(17,21)ene, hop(22,29)ene (diploptene) and 17β,21β-homohop(29/30)ene.

Hopane concentrations decreased from 99.1 µg/g TOC at 13,261 yr BP to 9.3 µg/g TOC at the Allerød/Younger Dryas-transition, while hopene concentrations simultaneously decreased from 30.0 µg/g TOC to 5.1 µg/g TOC (Fig. 3.3). During the Allerød, the average hopene/hopane ratio was 0.35±0.11. With the onset of the Younger Dryas, both hopanes and hopenes increased rapidly, resulting in average concentrations of 46.1±21.1 µg/g TOC and 28.7±14.4 µg/g TOC, respectively. During the mid- and late-Younger Dryas, hopane and hopene concentrations diminished concomitantly and yielded an average ratio of 0.62±0.1. At the Younger Dryas/Preboreal transition hopanoid concentrations increased to maximum values of 106.0 µg/g TOC for hopanes and 56.9 µg/g TOC for hopenes but thereafter, throughout the Preboreal declined again to minimum values of 17.0 and 10.7, respectively, at 11,150 yr BP. During the Preboreal, the average hopene/hopane ratio with 0.56±0.15 declined only slightly compared to the Younger Dryas.

Long-chain alkenones (LCA)

Alkenones were absent during the Allerød and the Preboreal (Fig. 3.4). During the Younger Dryas, di-, tri-, and tetraunsaturated ketones with carbon chain lengths from C_{37}-C_{39} were detected. The highest alkenone concentration (>7000 µg/g TOC) occurred at the onset of the Younger Dryas, after which it decreased rapidly during the early Younger Dryas (<500 µg/g TOC). C_{37} alkenones were most dominant at the start of the Younger Dryas, while C_{38} alkenones showed a pronounced maximum during the mid-Younger Dryas. At the termination of the Younger Dryas the C_{37}/C_{38} ratio shifted back to values >1.

The absence of alkenones in the Allerød and Preboreal prevented determining U^K_{37} values for both chronozones. In the early- and mid-Younger Dryas, however, a general increase in U^K_{37} values from -0.48 to -0.31 was observed. In the late Younger Dryas, U^K_{37} values first stayed constantly around -0.40. Thereafter, they showed a brief excursion to values as low as -0.52 before a strong increase to more positive values of -0.27 was observed at the termination of the Younger Dryas.

Glycerol dialkyl glycerol tetraethers (GDGTs)

Isoprenoidal and branched GDGTs were detected throughout the entire sediment succession investigated (Fig. 3.4). BrGDGTs were the dominating analogues ranging from 70.3 to 87.4% (average 78.9±4.2%), whilst isoGDGTs occurred in minor relative abundances only, varying from 12.6 to 29.7% (average 21.1±4.2%). GDGT-0 (caldarchaeol) was predominant among the isoGDGTs and constituted 20.4±4.1% to the total GDGT pool. Other isoGDGTs (GDGT-1, GDGT-2, GDGT-3, GDGT-4, crenarchaeol) were present in minor amounts only (together

<1.5% of all GDGTs). The crenarchaeol regioisomer could not be detected in any of the samples. The pool of brGDGTs was dominated by the 5-methyl and 6-methyl isomers of GDGT-IIIa (5ME: 12.3±1.6%, 6ME: 10.2±1.3%), followed by GDGT-IIa (5ME: 11.9±0.8%, 6ME: 13.6±1.6%) and GDGT-Ia (14.6±1.2%). The remaining brGDGTs represented 16.4±3.1% of all GDGTs. The BIT ratio (Schouten et al., 2013) was consistently high and averaged 1.

The GDGT-0/crenarchaeol ratio was generally high with values averaging 561.7±271.0 but showed distinct variations along the profile (Fig. 3.3). During the Allerød, GDGT-0/crenarchaeol ratios varied between 442.7 and 894.9 (average 672.7±153.0) and declined rapidly at the onset of the Younger Dryas, after which they ranged between 299.6 and 508.5 (average 412.2±59.3). At the beginning of the Preboreal, a maximum value of 978.8 was observed. Subsequently, GDGT-0/crenarchaeol ratios varied between 398.3 and 1753.4 (average 768.4±432.5) throughout the Preboreal with the lowest value of 398.3 found during the PBO.

MBT'_{5ME}-based MAAT estimates varied from 10.1 to 13.4°C throughout the studied interval. MAATs averaged 11.3±0.7°C during the Allerød and with the onset of the Younger Dryas increased by 1.6°C to yield an absolute temperature of 12.9°C. Thereafter, MAATs decreased gradually to result in a temperature of 10.4°C at the end of the Younger Dryas. At the transition to the Preboreal, MAAT increased by 1.7°C and in the following shows a general warming trend with two brief excursions to lower MAATs observed shortly prior and during the PBO. Highest temperatures were observed during the late PBO, during which MBT'_{5ME}-MAATs showed a maximum of 13.4°C at 11,150 yr BP.

Heterocyte glycolipids (HGs)

A total of 14 different HG structures was detected in the lacustrine sediments in variable relative abundances (Fig. 3.5). The heterocyte glycolipids HG_{26} diol, HG_{28} diol, HG_{28} triol and HG_{30} triol together constituted the majority of all HGs (>90%). Principal component analysis demonstrates that the relative abundance of HGs showed significant variation between the Allerød, Younger Dryas and Preboreal (Fig. S3.4).

The HIR_{28D} showed a rapid decrease from ~0.18±0.02 during the late Allerød to 0.09 at the onset of the Younger Dryas. During the lower and middle part of the cold event, the HIR_{28D} stayed rather constant at 0.12±0.02 but increased gradually during the late Younger Dryas from 0.13 to a maximum of 0.24 at 11,618 yr BP. This trend was interrupted by a short cooling at the Younger Dryas/Preboreal transition, after which the HIR_{28D} first increased to 0.21 and thereafter declined to a value 0.16 at the top of the sediment succession investigated.

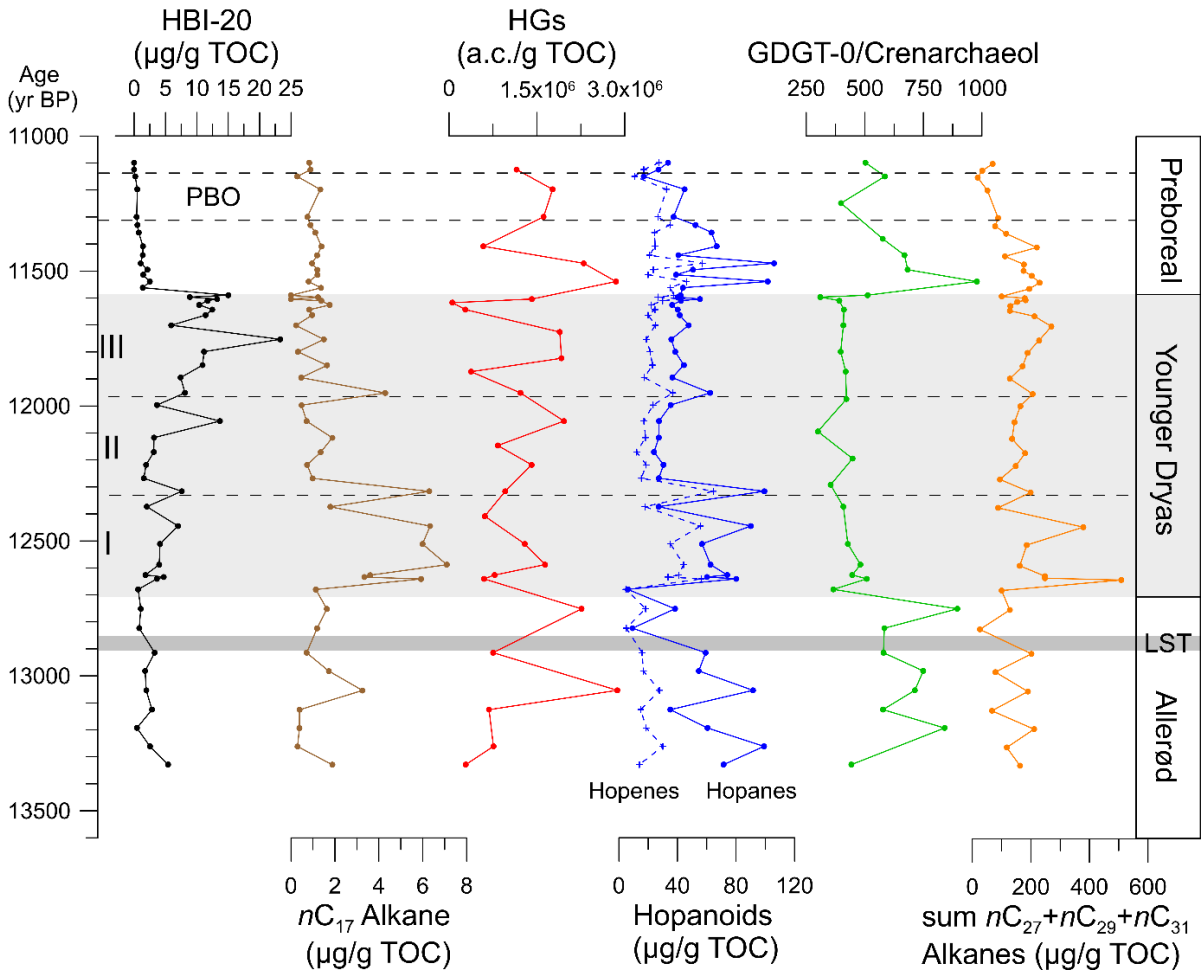

Figure 3.3: Concentration of C20-highly branched isoprenoids (HBI-20), nC$_{17}$-alkanes, HGs, hopanoids and plant-derived n-alkanes (sum nC$_{27}$, nC$_{29}$, nC$_{31}$) in the sediments of Lake Steisslingen vs. time and chronozones. Roman numerals denote the three stages of the Younger Dryas. PBO = Preboreal oscillation; LST = Laacher See Tephra (12,880 yr BP).

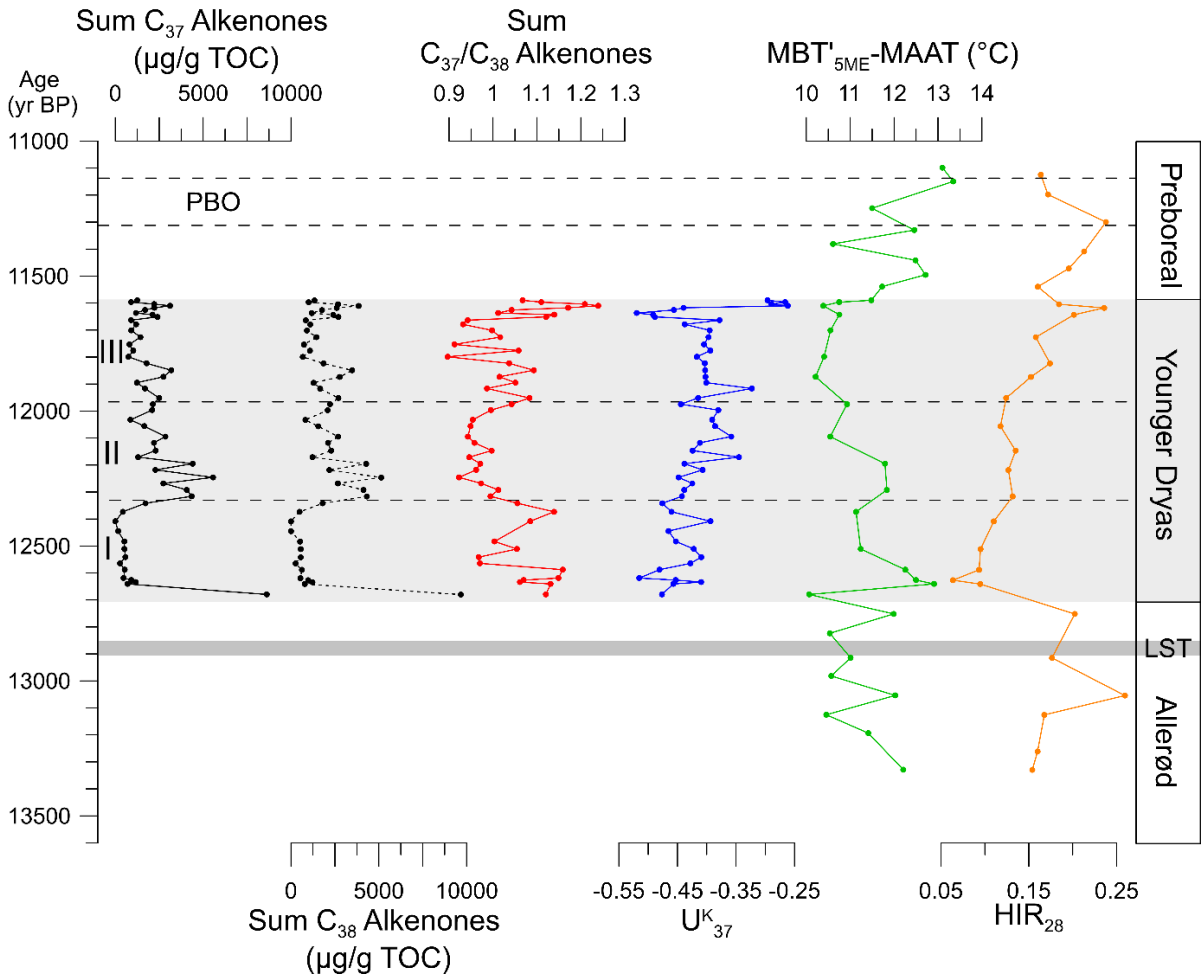

Figure 3.4: Long-chain alkenone concentrations and ratios, MBT'$_{5ME}$-inferred temperature and heterocyte glycolipids-inferred temperature trend in the sediments of Lake Steisslingen vs. time and chronozones. Roman numerals denote the three stages of the Younger Dryas. PBO = Preboreal oscillation; LST = Laacher See Tephra (12,880 yr BP).

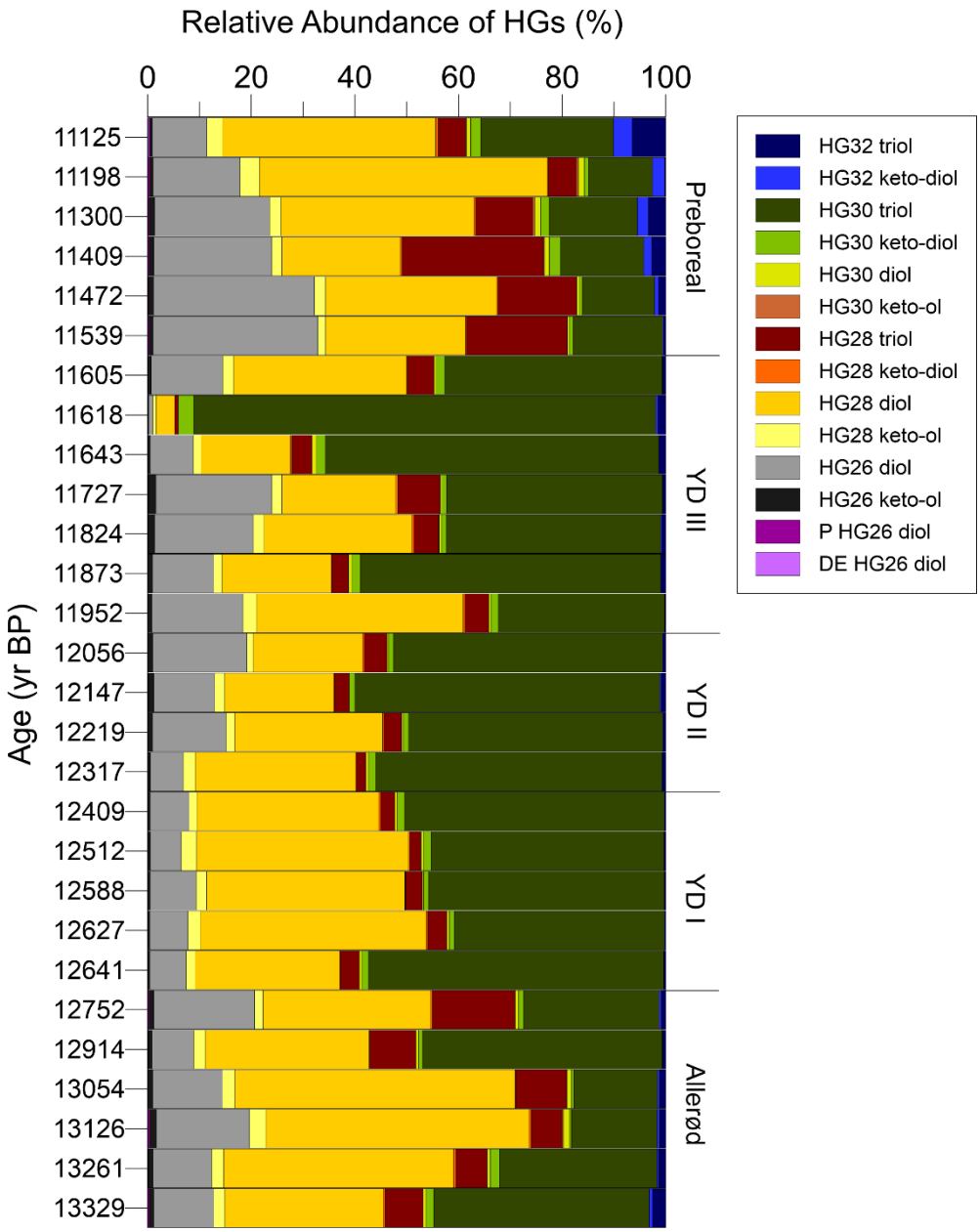

Figure 3.5: Relative abundance heterocyte glycolipids (HGs) in the sediments of Lake Steisslingen.

3.6 Discussion

Chronology

Bulk-geochemical properties, stable isotopes and biomarkers indicated major changes in the lake's productivity and phytoplankton community during the Allerød, Younger Dryas and Preboreal times. Moreover, they pointed to significant changes in the productivity and composition of primary producers that allow separating the Younger Dryas into three distinct sub-chronozones. These paleoenvironmental changes are discussed below:

3.6.1 Allerød (13,560 – 12,680 yr BP)

The Allerød is a time period characterized by a warmer and more humid climate, which followed the cool and arid conditions of the last glacial maximum in central Europe (Leroy et al., 2013). Sediments deposited in Lake Steisslingen during the Allerød are finely laminated and do not bear any signs of bioturbation. This, together with a high TOC content (15.2±3.2%), this indicates a high primary productivity and conditions favouring the preservation of organic matter (i.e. bottom water anoxia). Indeed, the establishment of a permanent stratification and reducing conditions at the monimolimnion has previously been suggested for Lake Steisslingen based on well described seasonal lamination in a parallel core of STK-9 (Eusterhues et al., 2002). Mean GDGT-0/crenarchaeol ratios of 672±153 support this finding as they suggest that methanogenesis, a process that requires anoxic conditions, played a major role in the carbon cycling of Lake Steisslingen during the Allerød. This is also in line with sedimentary $\delta^{13}C_{TOC}$ values ranging from -30.6 to -34.2‰ (-32.0±1.0‰). These values suggest a significant contribution of isotopically light carbon to the lake's carbon pool. One such source may have been methane produced by methanogenic archaea, which is known to be strongly depleted in ^{13}C (Whiticar, 1999). The lake's high organic matter export flux and anoxic bottom waters may have constituted ideal growth conditions for methanogens.

It is generally accepted that the start of the Younger Dryas was characterized by a sudden cooling in central Europe (Brauer et al., 2001), North America (Yu and Eicher, 1998) and elsewhere (Stansell et al., 2010). This is explained by a slowdown of the AMOC due to a rapid outflow of massive proglacial lake water (Lowell et al., 2005). In Lake Steisslingen, however, a gradual decline in $\delta^{18}O_{carbonate}$ values during the relatively warm latest Allerød period by about -2.5‰ may indicate a long-term cooling that cumulated in the Younger Dryas cold period. Comparable $\delta^{18}O_{carbonate}$ trends have been reported for the Meerfelder Maar sediments (Brauer et al., 2008) pointing to a more widespread gradual change in lake carbonate oxygen isotope signatures. This gradual decrease in $\delta^{18}O_{carbonate}$ values was interrupted after the LST and the $\delta^{18}O_{carbonate}$ values increased slightly for the next ~200 years (Fig. 3.2), indicative of a minor warming. An earlier cooling, coincident with the Laacher See Tephra at 12,880 yr BP and prior to the Younger Dryas cooling event, was potentially initiated by the sulfur-rich volcanic eruption itself via a solar irradiation decline due to stratospheric sulfate aerosol emission (Baldini et al., 2018). A pre-Younger Dryas cooling was furtherly inferred from aquatic and wax lipid hydrogen isotope ratios determined on sediments from Meerfelder Maar (Rach et al., 2014).

Prior to the LST, an excursion to significantly more negative $\delta^{18}O_{carbonate}$ values, indicating colder conditions, was observed for the time around 13,100 yr BP. The magnitude of this excursion was similar to the one observed during the Younger Dryas and provided evidence for a brief period of cooling. A short cold spell during the late Allerød, known as the Gerzensee Oscillation, has been reported previously from other European lakes as well as from

Greenland ice cores (GRIP) (Goslar et al., 1995; Björck et al., 1996, 1998; Schwander et al., 2000)(Goslar et al., 1995; Björck et al., 1996, 1998; Schwander et al., 2000)(Goslar et al., 1995; Björck et al., 1996, 1998; Schwander et al., 2000)(Goslar et al., 1995; Björck et al., 1996, 1998; Schwander et al., 2000). The Gerzensee Oscillation is characterized by a 1-2°C decrease in summer temperature in the Swiss Alps based on pollen and Cladoceran assemblages (Lotter et al., 2000). This momentary relapse to glacial temperatures was also noted in the MBT'_{5ME} record of Lake Steisslingen, which showed a 0.9°C decline in MAAT. A short cooler phase before the onset of the Younger Dryas could also be identified in the $\delta^{18}O_{carbonate}$ curve from the previous study on Lake Steisslingen (Mayer and Schwark, 1999). This study, however, was conducted at lower resolution thus not reflect the Gerzensee oscillation in detail.

An alternative means for the reconstruction of lake surface water temperatures has recently been introduced by the analysis of cyanophyte heterocyte glycolipids (HGs) (Bauersachs et al., 2015). These components are exclusively found in the heterocyte of diazotrophic (N_2-fixing) cyanobacteria, where their relative abundances changes as a function of growth temperature (Bauersachs et al., 2014b). In lakes, the relative distribution of HGs in surface waters has been shown to track surface water temperatures with the signal of highest productivity being transferred to the sediment record (Bauersachs et al., 2015). Similar to changes in the HG alcohol to ketone ratio, the relative abundance of structural isomers of HG_{32} triol has been demonstrated to vary with temperature in culture experiments of the thermophilic cyanobacterium *Mastigocladus laminosus* (Bauersachs et al., 2013). In Lake Steisslingen sediments two HG_{28} diol isomers were identified, the relative proportions of which were termed HIR_{28D} and used to detect relative temperature. Here, HIR_{28D} decreased from 0.18 to 0.09 during the Allerød indicative for a rapid relative temperature decrease.

Low $\delta^{15}N$ values (-1.4±0.5‰) during the Allerød are in line with cyanobacterial N_2 fixation (Wada and Hattori, 1991) and suggest that diazotrophic cyanobacteria may have constituted an abundant part of the phytoplankton community of Lake Steisslingen. This is corroborated by enhanced HG abundances in Lake Steisslingen sediments during the Allerød (Fig. 3.3). The HG distributions were dominated by HG_{28} diols (40.6%), HG_{30} triols (29.5%) and HG_{26} diols (13.6%), which together constituted >80% of all HGs. The HG_{28} and HG_{26} diols are commonly found in nostocalean cyanobacteria of the family Nostocaceae, including e.g. *Anabaenopsis*, *Aphanizomenon,* and *Dolichospermum* (previously *Anabaena*) (Gambacorta et al., 1998; Bauersachs et al., 2009a, 2017). Cyanobacteria of the genus *Dolichospermum* have indeed been report from the phytoplankton community of modern Lake Steisslingen and are known to become particularly abundant during the warm summer month (LUBW, 2016), suggesting that they may constitute one biological source of the HGs in the lake. HG_{30} triols on the contrary have been described exclusively from Scytonemataceae (Gambacorta et al.,

1999; Bauersachs et al., 2019). These cyanobacteria are common in benthic microbial mats (Castenholz, 2015), which may also have formed in the littoral of Lake Steisslingen. Additional evidence for the occurrence of cyanobacteria during the Allerød comes from the presence of 7-methylheptadecane (7Me-C_{17}). This component has been observed in cyanobacteria before, for which it is thought to be highly diagnostic (Gelpi et al., 1970; Bauersachs et al., 2017). In contrast to HGs, however, 7Me-C_{17} is not exclusively synthesized by heterocytous cyanobacteria and can also be derived from unicellular or filamentous non-heterocytous cyanobacteria (Gelpi et al., 1970; Coates et al., 2014) thriving in Lake Steisslingen. Such cyanobacteria may include the unicellular species *Aphanocapsa* sp. or the filamentous non-heterocytous forms *Planktothrix* sp. and *Pseudanbaena limnetica*, which have previously been reported from the lake's phytoplankton (LUBW, 2016).

Aliphatic biomarker distributions (e.g. *n*$C_{17,}$ HBI-20, hopanoids) indicate that a diverse community of aquatic and microbial primary producers persisted in Lake Steisslingen. This includes cyanobacteria (*n*C_{17}), diatoms (HBI-20), and heterotrophic bacteria (hopanoids). Our data thus suggests that Lake Steisslingen received a majority of its organic matter content during the Allerød from aquatic sources, which is in line with the generally low TOC/TN ratios (i.e., 10.7-11.9) of this interval. The high variety of microbial primary producers matches the composition of today's Lake Steisslingen (LUBW, 2016). Freshwater algae like Chlorophyta, Chrysophyceae, Cryptophyceae but also dinoflagellates of the class Dinophyceae and diatoms form a large part of the recent phytoplankton community (LUBW, 2016). High concentrations of hopanoid hydrocarbons suggest an enhanced microbial activity of bacteria in the early Allerød (Fig. 3.3). Significant amounts of hopenes in sediments from the entire chronozone indicated a certain but not to extensive degree of diagenetic alteration of organic matter.

Besides aquatic organic matter, the lake also received input of organic matter from terrigenic sources growing in the lake's surroundings. Epicuticular leaf wax-derived long-chain alkanes and alkenes ranged from *n*C_{25} to *n*C_{33} with a predominance of *n*C_{27} and only minor abundances of *n*C_{31}. This can be attributed to an increase in *Betula* sp. and a decrease in *Juniperus* sp. as well as *Artemisia sp*., which point to a dominance of woody plants over bushes and shrubs during the Allerød (Schwark et al., 2002). Pollen data from Lake Steisslingen suggested a mixed pine/birch forest with still sparely forested areas due to the presence of grass and heliophilous herb/shrub pollen (Eusterhues et al., 2002). *Betula* and *Pinus sp*. have also been reported to dominate in the catchment of paleolake Trzechowskie, northern Poland (Aichner et al., 2018), possibly suggesting the spread of a mixed birch-pine forest vegetation in central and eastern Europe during the Allerød.

3.6.2 Younger Dryas (12,680 – 11, 590 yr BP)

With the onset and termination of the Younger Dryas major shifts in the bulk and isotope signal were recorded in the lake, whereas throughout the Younger Dryas the bulk composition of organic matter and its isotopes remained rather monotonous (Fig. 3.2). In contrast, the biomarker composition and/or concentration changed substantially (Fig. 3.3, 3.4), which revealed different responses of aquatic and terrestrial primary producers to varying environmental conditions. The latter scenario seems more in accordance with a climatically stressed paleoenvironment whereas 1000 years of environmental quiescence throughout the Younger Dryas seems less probable. The fluctuations in organic matter composition favour a differentiation into 3 sub stages (Fig. 3.6) rather than 2 phases of the Younger Dryas as previously suggested (von Grafenstein et al., 1999; Schwark et al., 2002; Bakke et al., 2009; Neugebauer et al., 2012; Lane et al., 2013; Schlolaut et al., 2017).

Younger Dryas Stage I (12,680 – 12,342 yr BP)

The onset of the Younger Dryas was marked by an abrupt increase in $CaCO_3$ and a concomitant decrease in TOC content (Fig. 3.2), which was also manifested in the generally brighter sediment colour of this interval. A -2‰ shift in $\delta^{18}O_{carbonate}$ values was considered to reflect a decline in water temperatures by about 3-5°C and possibly also a change in the water balance of the lake, due to precipitation or a change in the subsurface in-/outflow budget (Mayer and Schwark, 1999). The decrease in $\delta^{18}O_{carbonate}$ was in good agreement with other records from Central Europe which also suggested a decline in MAAT between 3 and 5°C (Lotter et al., 2000; Heiri et al., 2007). MBT'_{5ME}-reconstructed MAATs decreased by 1.8°C at the Allerød/Younger Dryas boundary followed by an increase to a maximum temperature during the Younger Dryas of about 12.9°C. Such a temperature maximum was neither reflected in $\delta^{18}O_{carbonate}$ nor HIR_{28D}, which both generally indicated cool conditions during the Younger Dryas. The inaccuracy of the brGDGT based temperature at the Allerød/Younger Dryas boundary could be explained by a shift in the microbial community. This might be caused by soil erosion due to decreased forest density and therefore an enhanced soil inwash into the lake leading to higher MBT'_{5ME}.

The onset of the Younger Dryas was marked by the first appearance of LCAs, which was already stated in an earlier study of Lake Steisslingen by Zink et al. (2001). Of these, C_{37} and C_{38} alkenones were generally present with high relative abundances of the tetraunsaturated C_{37} alkenone ($C_{37:4}$). Such a distribution has previously been reported as a distinct characteristic of lake environments (D'Andrea and Huang, 2005; Theroux et al., 2010; Sun et al., 2018). In contrast to the open ocean where *Emiliana huxleyi* and *Geophyocapsa oceania* are the main sources of alkenones, the producers in lake systems are more diverse (Theroux et al., 2010). The sudden occurrence of LCAs at the onset of the Younger Dryas may be

attributed to the development of blooms of cold-adapted haptophyte algae, which were less competitive during the preceding warmer climate conditions of the Allerød (Zink et al., 2001). Exceptionally high concentration of C_{37} and C_{38} alkenones (C_{37}+C_{38}) with 16,000 µg/g TOC were observed at the base of the Younger Dryas, suggesting that haptophytes algae were the dominant contributors of aquatic origin to the Lake Steisslingen organic matter pool at this time (Fig. 3.6) and supporting the thesis of a spontaneous mass bloom. Since alkenones were resistant to degradation the variations in alkenone concentrations during the ~1100 year of Younger Dryas represented a biotic response of alkenones producers to the environmental condition prevailing and not a change in preservation rate (Goñi et al., 2001; Prahl et al., 2001). The C_{37}/C_{38}-alkenone ratio of ~1 and the high amount of the $C_{37:4}$ homologue (35.4 to 54.5% of all C_{37} alkenones) suggest that the haptophytes in Lake Steisslingen were closely related to the cold-adapted Greenland I phylotype (Group I) (Longo et al., 2018). The simultaneous presence of methyl-C_{38} and ethyl-C_{38}-alkenone, which are common in northern hemispheric lakes, like Alaska and Greenland dominated by the Greenland I phylotype, is in agreement with this hypothesis (D'Andrea and Huang, 2005; D'Andrea et al., 2011; Longo et al., 2016).

Due to the large number of different primary producers in lakes and the difference in seasonal productivity many contrasting alkenones temperature calibration have been reported (e.g. Chu et al., 2005; Longo et al., 2016; Sun et al., 2007; Zink et al., 2001). Lowest average U^K_{37} values of about -0.45 occurred in the lower Younger Dryas (YD-I) representing coldest temperatures. This was in line with coldest GDGT-inferred temperatures of about 10°C and coldest HIR_{28D} relative temperatures. Reconstructed summer temperatures for Central Europe of about 10-15°C based on pollen, macro fossils and chironomids are slightly higher than our predicted temperatures (Isarin and Bohncke, 1999; van Asch et al., 2012; Pawłowski et al., 2015). However, this can be explained by the fact that temperatures reported here do not reflect the probably warmest temperatures in summer, but rather the average annual air temperature or water temperature. It has to be taken into account that the abundance of the $C_{37:4}$ alkenone might have been effected by environmental factors other than temperature, such as salinity (Liu et al., 2008, 2011).

In response to the changing climate, significant changes in the phytoplankton community occurred in Lake Steisslingen (Fig. 3.6). The onset of the Younger Dryas was marked by high concentrations of *n*C_{17} and only low concentrations of HBI-20 (Fig. 3.3). The former is a common component of many algae (Meyers et al., 2003) but particularly abundant in cyanobacteria (Bauersachs et al., 2017). Abundances of diatom-derived saturated HBI-20 as well as saturated and unsaturated HBI-25, previously observed in other freshwater systems (Muschitiello et al., 2015; Zhang et al., 2018), remained low during the YD-I phase. In lacustrine sediments from south-eastern Sweden covering the Late Glacial/early Holocene periods it was demonstrated that HBI-20 originated from the epiphytic diatom *Gomphonema*

acuminatum (Muschitiello et al., 2015). Since other HBIs, such as HBI-25, and the unsaturated HBI-25:1 and HBI-25:2, were also present in Lake Steisslingen other freshwater diatoms cannot be excluded as potential producers, e.g. the *Navicula* genus or *Enteromorpha sp*. (Rowland et al., 1985; Belt et al., 2001).

Compared to the Allerød, the Younger Dryas was marked by a shift in $\delta^{15}N$ values from -1.5‰ to +2.5‰ suggesting that the phytoplankton community changed from a dominance of N_2-fixing, possibly heterocytous cyanobacterial association to a community dominated by nitrate-utilizing algae (Meyers, 2003). However, HGs of heterocytous cyanobacteria origin still were present in the basal Younger Dryas. In contrast to the Allerød, the HG content changed significantly with a gradual increase in the relative abundance of HG_{30} triols (Fig. 3.5). The latter have been described from heterocytous cyanobacteria of the Scytonemataceae, including e.g. *Scytonema* sp. and *Tolypothrix tenuis* (Gambacorta et al., 1999) and as a constituent of the HG inventory of the stigonematalean cyanobacterium *Stigonema ocellatum* (Bauersachs et al., 2019). Heterocytous cyanobacteria of both families are known to form benthic microbial mats in the shallow littoral zone (Smith et al., 2011; Stal, 2012). The increase in the relative abundance of HG_{30} triols with the onset of the Younger Dryas may thus have been associated with a decline in water level and an increase in the habitable zone suitable for the growth of benthic microbial mats. This lowstand may have been caused by more arid conditions with the start of the Younger Dryas that have also been postulated for other lacustrine environments (Brauer et al., 1999; Rach et al., 2014).

After a rapid decrease in the GDGT-0/crenarchaeol ratio to values of >800 to <400 at the Allerød/Younger Dryas boundary, the GDGT-0/crenarchaeol ratio remained almost constant during the Younger Dryas. Although these values are still indicative for methanogenesis and in turn anoxic bottom waters in Lake Steisslingen during the Younger Dryas, the strong decline likely indicated a less strong stratification and perhaps periodically mixing of the water column, which was also reflected in less well-developed sediment lamination. Furthermore, a change in the archaeal community from anaerobic methanogen species (synthesizing GDGT-0) to aerobic Thaumarchaeota (source of crenarchaeol) might also have occurred and as such will have affected the ratio (Leininger et al., 2006; Blaga et al., 2009; Naeher et al., 2014).

In central Europe, with the beginning of the Younger Dryas the terrestrial vegetation changed from a dense forested landscape to an open tundra dominated by shrubs (Starkel et al., 2012). An increase in non-arboreal pollen (NAP) has been observed previously in parallel core STK-2 from Lake Steisslingen (Eusterhues et al., 2002). Here, in STK-9, an increase in long-chain alkane concentration coupled with a decline in relative abundance of nC_{27}- and higher amount of nC_{29}- and nC_{31}-alkanes at the Allerød /Younger Dryas transition implied a shift in vegetation. However, nC_{27} still remained the most abundant *n*-alkane in the sediments of Lake Steisslingen. Leaf waxes of recent *Betula* and *Pinus* species contain high relative abundances

of nC_{27}-alkanes, but absolute concentration vary by factor >10, with higher absolute concentration in *Betula* leaves (Diefendorf et al., 2011). Thus, *Pinus* contributes to a minor extent only to the inventory of *n*-alkanes in the sedimentary record (Ali et al., 2005; Dove and Mayes, 2006). The increase in absolute concentration of long-chain *n*-alkanes in the sediments of Lake Steisslingen therefore more likely was due to the expansion of *Betula* species rather than Pinus as inferred from palynological data of earlier investigations on Lake Steisslingen (Eusterhues et al., 2002; Schwark et al., 2002). This previously reported increase in *Pinus sp.* pollen could be explained by a high airborne transport of *Pinus* pollen overestimating the actual presence of pine trees around the study site (Szczepanek et al., 2017). Intensified wind strength in course with the climate perturbation of the Younger Dryas (Brauer et al., 2008) may have favoured pollen dispersal.

Neugebauer et al. (2012) divided the Younger Dryas in two stages, whereby they characterized the early Younger Dryas expressed in the sediments of Paleolake Rehwiese (NE-Germany) with still warm to moderate summer temperatures. Thus, the high concentrations of plant-derived alkanes (Fig. 3.6) could be explained by still warmer summer temperatures since the main growth phase of plant leaves occurs during the summer months. Recent studies postulated a large episode of biomass burning triggered by a bolide impact at the onset of the Younger Dryas (Wolbach et al., 2018a, 2018b). Since the concentrations of terrestrial wax lipids did not decrease markedly and complementary pollen data also did not indicate a decline in the tree population, there are no indications of massive wildfires in SW-Germany (Schwark et al., 2002).

Younger Dryas Stage II (12,342 – 11,975 yr BP)

The start of the Younger Dryas Stage II (YD-II) was characterized by significant changes in biomarker distributions (Fig. 3.6). The most prominent change was associated with an increase in the abundance of C_{37} and C_{38} alkenones, a shift to lower C_{37}/C_{38} ratios and slightly higher U^{K}_{37} values (Fig. 3.4). Together these observations suggest that haptophyte algae, likely related to the Greenland Phylotype I, proliferated in the lake after temperatures started to recover from the substantial decline at the start of the Younger Dryas. Although most biological sources of alkenones in freshwater environments remain enigmatic, haptophyte blooms via photosynthetic drawdown of dissolved CO_2 in surface lake water may have contributed to the high carbonate content observed during the Younger Dryas (Fig. 3.2). Concomitantly, concentrations of the diatom-specific HBI-20 started to increase, while the previously abundant nC_{17} and hopanoids significantly declined in abundance (Fig. 3.6) after peaking at the base of YD-II. This was thought to reflect a higher production of freshwater diatoms over algae and bacteria (Cranwell et al., 1987; Zhang et al., 2017). Similar to the short-chain *n*-alkanes, the concentrations of long-chain *n*-alkanes decreased, corroborating a

decline in the productivity in the watershed of Lake Steisslingen. Indeed, a change in the terrestrial vegetation pattern with a shift from deciduous trees to shrubs has been documented previously based on pollen (Schwark et al., 2002).

Compared to YD-I, the distribution of HGs was characterized by slightly higher abundances of HG_{30} triols (57.8±4.4%) and HG_{26} diols (13.9±5.1%) and markedly lower abundances of HG_{28} diols (26.6±5.4%; Fig. 3.5). HG_{30} triols and keto-diols have been reported in cyanobacteria of the family Scytonemataceae (Gambacorta et al., 1999; Bauersachs et al., 2019), which are known to form epilithic colonies attached to a hard substrate. This may suggest that water level variations within in the lake remained low, providing the basis for the proliferation of the benthic microbial mats that previously established in lake´s littoral during the onset of the Younger Dryas. Low TOC and concomitantly high $\delta^{15}N$ values throughout the Younger Dryas, however, suggest a lower in-lake productivity and a decline in the contribution of organic matter derived from the biologically fixation of N_2 (Fig. 3.2).

A prior study identified a short relapse to a warmer climate around 12,080 yr BP in the sediments of Lake Ammersee, which is situated ca. 160 km to the east of Lake Steisslingen (von Grafenstein et al., 1999). Such a relapse was not discernible in sediments of Lake Steisslingen. In fact, comparatively cold temperatures were deduced for the mid-Younger Dryas based on strongly depleted $\delta^{18}O_{carbonate}$. In contrast, increasing U^{K}_{37} values indicated a warming trend, similar to the HG-derived HIR_{28D}, which stands in contrast to the brGDGT-reconstructed MAAT. Therefore, uncertainties between the proxies could be caused by seasonally differing production maxima of the biological lipid sources. To this end, brGDGTs preferentially reflect the mean annual air temperature (Russell et al., 2018), whereas alkenones represent water temperatures during growing season when the lake is ice-free (Chu et al., 2012) or summer temperature (Zink et al., 2001).

Younger Dryas Stage III (11,975 – 11,590 yr BP)

The last stage of the Younger Dryas (YD-III) was marked by a decrease in alkenone concentrations towards the Younger Dryas/Preboreal boundary and their absence thereafter. This was accompanied by a relative increase of the C_{37}/C_{38} alkenone ratio, potentially due to a change in alkenones producers or increasing temperature reflected in rising U^{K}_{37} value. Interestingly, alkenone derived temperatures showed high fluctuations not observed in other proxies or previous studies in Lake Steisslingen at the termination of the Younger Dryas (Zink et al., 2001). A significant decrease in U^{K}_{37} at 11,637 yr BP occurred after a period of constant temperature followed by a rapid warming trend around 11,618 yr BP at the Younger Dryas/Preboreal boundary. This temperature increase was also expressed in $\delta^{18}O_{carbonate}$ and HIR_{28D} and was in a good agreement with previous studies, which postulated a relapse to more moderate climate within 10-30 years at the Pleistocene/Holocene-transition (Dansgaard

et al., 1989; Gulliksen et al., 1998). An increase in GDGTs-MAAT occurred with a delay of about 100 years during the early Preboreal.

Peak concentration of HBI-20 producing freshwater diatoms were present in the latest stage of the Younger Dryas suggesting a massive proliferation of diatoms during this period (Fig. 3.3). At the same time, other biomarkers like nC_{17} (algae), hopanoids (bacteria) and long-chain *n*-alkanes (terrestrial vegetation) showed no significant change compared to the YD-II phase (Fig. 3.6). The change in algal/diatom population dynamics may have been an adaption to slightly warmer temperatures only reflected by HG-inferred relative temperatures but suppressed in the response of other aquatic organism in Lake Steisslingen. Although more variable in the YD-II phase, the trend to increasing relative abundances of HG_{30} triols and keto-diols continued and maximized in the late stage of the YD-III phase, during which HG_{30} triols constituted >90% of all HGs (Fig. 3.5). The massive increase in the abundance of HG_{30} triols might have been related to a further increase in shallow lake areas suitable for microbial mats growth and in turn might suggest a low water level of Lake Steisslingen during YD-III, which was also reported from inorganic geochemical proxies (Eusterhues et al., 2002).

3.6.3 Preboreal (11,590 – 10,300 yr BP)

The onset of the Preboreal was initiated by a change from lighter to darker coloured sediment, which was caused by a higher amount of organic matter and a simultaneous decrease in calcium carbonate content. This rapid decrease was accompanied by an increase in $\delta^{18}O_{carbonate}$ of about 3‰ (Fig. 3.2). HIR_{28D} and brGDGT-based temperature estimates showed a delayed temperature increase but average temperature trends during Preboreal were in consensus with those previously described from other lacustrine and terrestrial settings (Heiri et al., 2007). Discrepancy between the different temperature proxies ($\delta^{18}O_{carbonate}$, alkenones, brGDGTs, HGs) may have been caused by a different response of the biological sources to the newly established environmental conditions. For example, increased erosion rates due to warmer and more humid climate together with a rising water level could have qualitatively and quantitatively affected the brGDGT pool. However, BIT values remained constant at a value near 1. Our analyses have found evidence for a brief colder period during the Preboreal (11,300 – 11,150 yr BP) expressed in more negative $\delta^{18}O_{carbonate}$ values similar in magnitude to the Younger Dryas cold period. These relapse to colder temperatures, known as the Preboreal Oscillation, was caused by an increased freshwater forcing that hampered the North Atlantic heat conveyor and was previously reported from other records in Central Europe (Björck et al., 1996; Bos et al., 2007; Magny et al., 2007a). In contrast to the Allerød or Younger Dryas, however, the biotic responses, expressed in e.g. the aliphatic hydrocarbons and the occurrence of alkenones, could not be observed during the Preboreal Oscillation.

Higher TOC concentrations indicated enhanced input of organic matter with the onset of the Preboreal. This was also reflected in a rapid increase of about +5‰ in $\delta^{13}C_{TOC}$ potentially due to a higher growth rate of phytoplankton or alternatively a change in the isotopic composition of dissolved inorganic carbon. A decline in $\delta^{15}N$ to values close to 0‰, suggested a new proliferation of N_2-fixing cyanobacteria in Lake Steisslingen (Fig. 3.6). In accordance with this perception, relative HG abundances started to increase again with the onset of the Preboreal and profound changes in HG distribution patterns occurred. In contrast to the dominance of HG_{30} triols previously observed during the Younger Dryas, HG_{26} diols, HG_{28} diols, and HG_{28} triols significantly increased in abundance (Fig. 3.5). These HGs are commonly reported in pelagic cyanobacteria, such as *Aphanizomenon* sp., *Anabaenopsis* sp. and *Dolichopsermum* sp. (Gambacorta et al., 1999; Bauersachs et al., 2009; 2017; 2019; Wörmer et al. 2012), freshwater phytoplankton (Bauersachs et al., 2015) and lake sediments (Bauersachs et al., 2015; Bale et al., 2016) and may indicate an increased share of non-benthic cyanobacteria in aquatic primary productivity. A unique characteristic of the Preboreal was the presence of HG_{32} triol and keto-diol, which together constituted between 0.6 to 10% of all HGs. Both HGs exclusively occur in true-branching cyanobacteria (Gambacorta et al., 1998; Bauersachs et al., 2014a, 2019), which may occur as part of the phytoplankton community but are particularly widespread as subaerophytes. Although it could not be excluded that some HG_{32} triols and keto-diols may have originated from in-lake production, the increased abundance of both HGs may have been caused by an increased run-off and transport to the lake under more humid conditions. Wetter conditions with the onset of the Preboreal have been reported from Lake Meerfelder Maar (W-Germany) (Rach et al., 2014).

An increased activity of cyanobacteria with the start of the Preboreal might have been triggered by the higher lake water temperature as indicated by heavier $\delta^{18}O_{carbonate}$ and increased HIR_{28D} values and was also supported by higher concentrations of hopanoids and heavier $\delta^{13}C_{TOC}$ values (Figs. 3.2 and 3.3). With the onset of the Preboreal Oscillation at 11,300 yr BP, however, $\delta^{15}N$ values increased again to an average of +2.5‰, indicating a shift in the nitrogen utilization metabolism and to a declining contribution of cyanobacteria to the organic matter content. This was also expressed in a significant decrease in HG abundance and the concomitant shift in $\delta^{13}C_{TOC}$ to more depleted values.

The absence of alkenones during the entire Preboreal, including the Preboreal Oscillation, reflected a shift in aquatic community and supported the assumption of a haptophyte algae community only viable in Lake Steisslingen upon a colder climate (Fig. 3.6). HBI producing freshwater diatoms population decreased constantly with the new climate conditions at the beginning of the Preboreal until they disappeared exhaustively from 11,125 yr BP on. We infer that this freshwater diatom required colder temperatures, whereas its occurrence during

moderate Allerød does not suggest this hypothesis unless the HBIs where produced by different precursors.

With the onset of the Preboreal a response in vegetation to the new environmental conditions was visible in decreasing nC_{27}-alkanes and increasing relative abundances of nC_{29}- and nC_{31}-alkanes, respectively. This observation would predict a spread of conifers and grasses with only moderate contribution of birches to the plant lipid pool (Schwark et al., 2002). Palynological data of Lake Steisslingen, on the contrary, reveal a clear increase in birch pollen, which could also be identified in the *n*-alkane and pollen distribution in the sediments of the Polish Lake Trzechowskie at the Pleistocene/Holocene-transition (Eusterhues et al., 2002; Aichner et al., 2018). The increase of in particular the nC_{29}-alkanes at this time may have reflected the input of other non-birch broadleaf trees.

3.7 Conclusion

Sediments deposited in Lake Steisslingen provide high-resolution archives (Fig. 3.6) for the reconstruction of climate and environmental change during the cold event of the Younger Dryas. Our data demonstrated that significant perturbations in the productivity and composition of the aquatic and terrestrial community in and around the lake occurred during the chronozones of the Allerød, Younger Dryas and Preboreal. These were likely driven by a decline of temperature with the onset of the Younger Dryas. The Younger Dryas cold spell did not evolve monotonous but could be separated in three sub-zones YD-I, YD-II, YD-III, each showing a differential response in preferentially aquatic biomass composition to environmental change, which is not or much less reflected in the bulk parameters (Fig. 3.6). The YD-I is characterized by high in-lake production of phytoplankton and bacteria. High average abundance of alkenones, which are indicative for a sufficient adaption of freshwater haptophyte algae to ongoing cold condition, marked the YD-II phase (Fig. 3.6). The terminal YD-III phase (Fig. 3.6) was characterized by a high productivity of HBI producing freshwater diatoms.

In addition to the frequently used molecular temperature proxies U^{K}_{37} and MBT'_{5ME}, we first applied the new HG-based HIR_{28D} proxy to a paleo-lake sediment to determine continental relative temperature shifts. The HIR_{28D} was in a good agreement with estimated temperature trends for the Pleistocene/Holocene transition and demonstrated the potential of HGs in paleoclimate und paleoenvironmental reconstruction although a temperature calibration to convert proxy values to absolute temperatures is still pending.

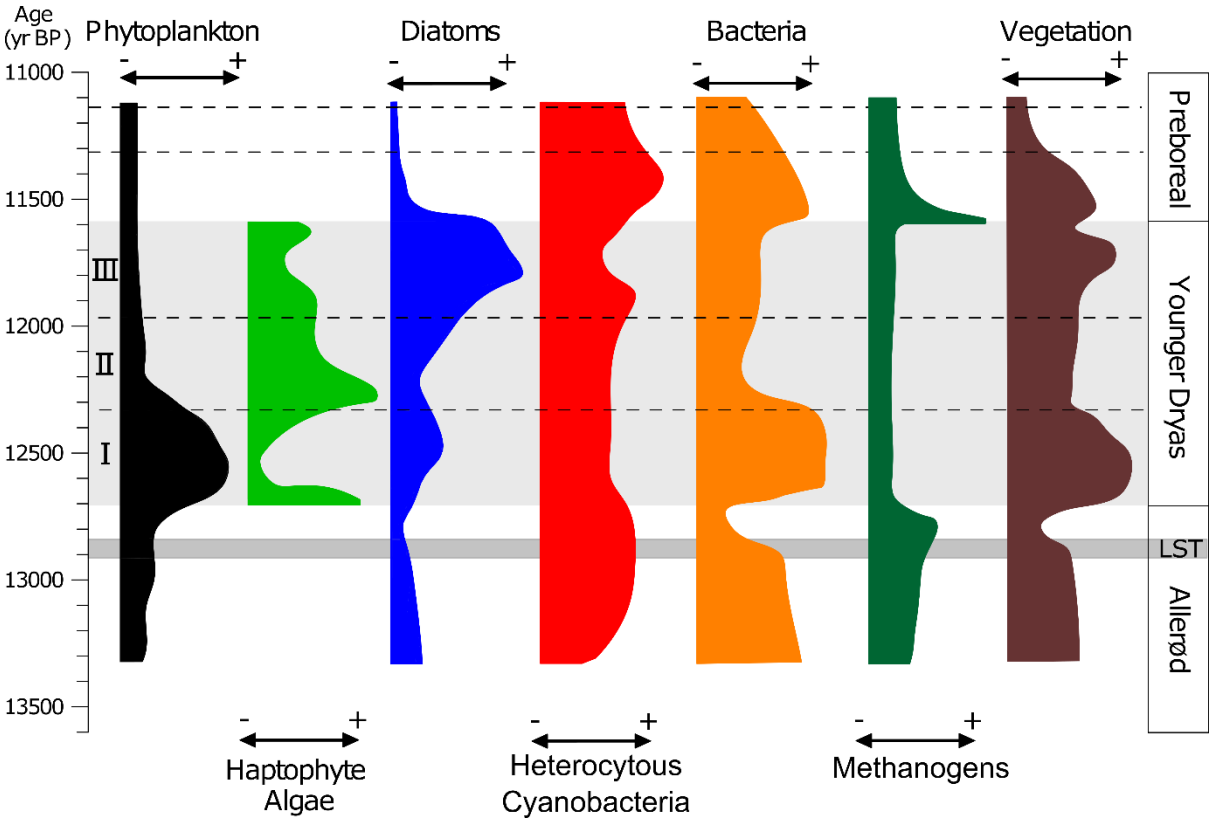

Figure 3.6: Schematic overview of aquatic and terrestrial organisms contribute to the organic matter in Lake Steisslingen.

Acknowledgments

N. Häuser and V. Grote are thanked during core sampling and for excellent laboratory assistance.

3.8 Supplementary material

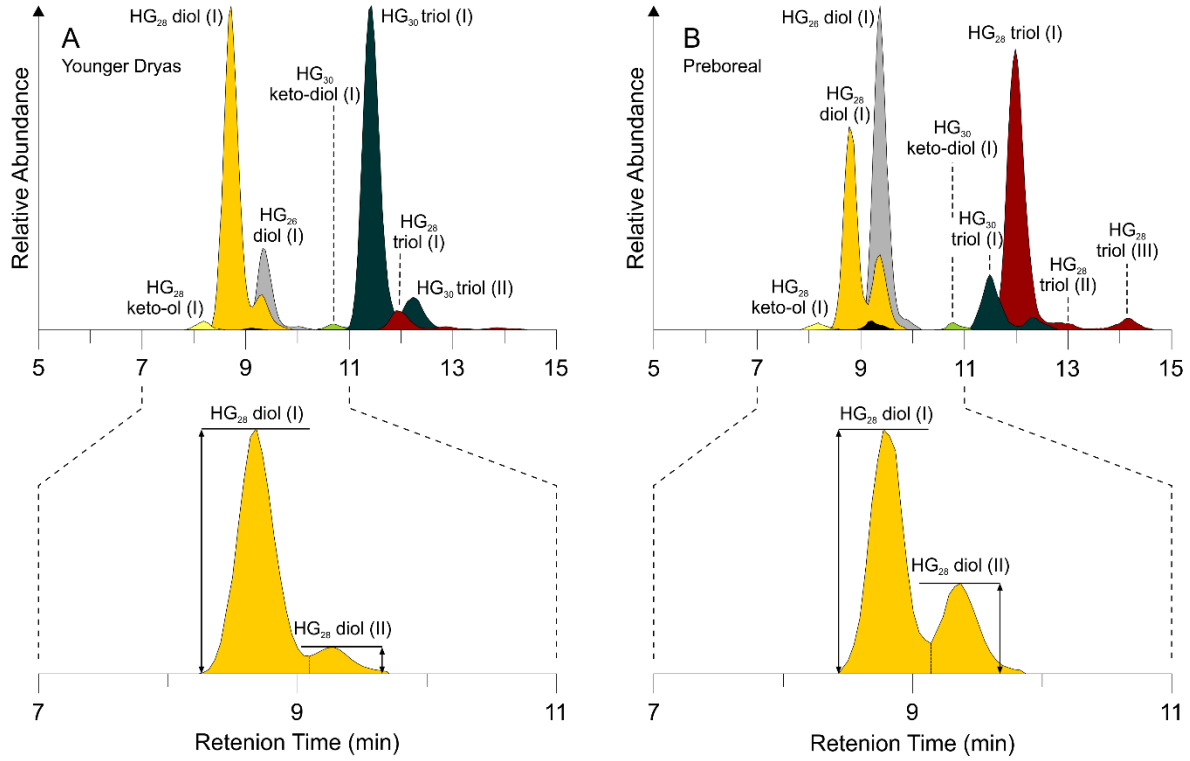

Figure S3.1: Distribution of heterocyte glycolipids, showing temperature effects on HG_{28}-isomers.

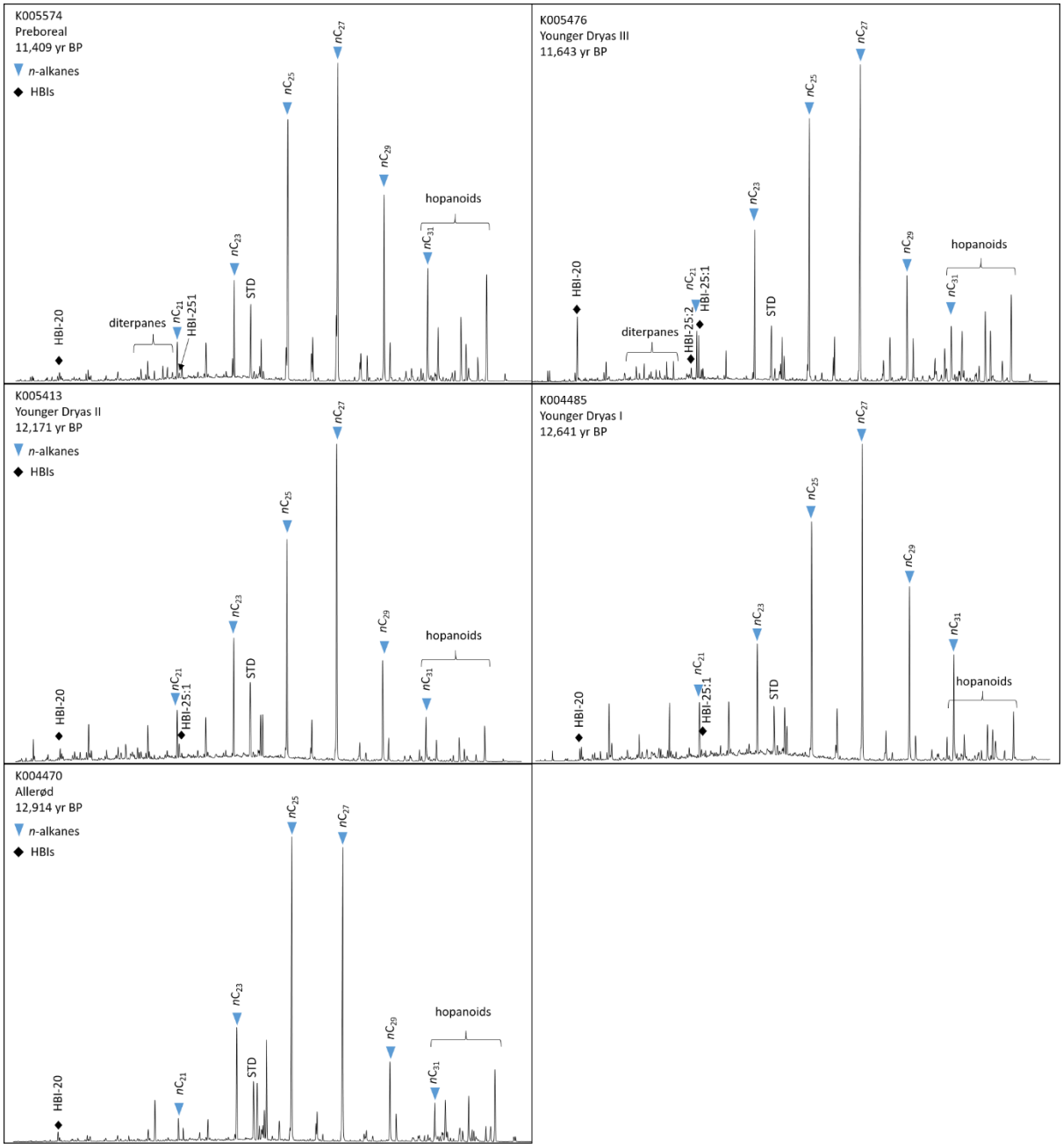

Figure S3.2: Chromatograms of the aliphatic fractions of each chronozone Allerød, Preboreal and the subdivided Younger Dryas (YD-I, YD-II, YD-III)

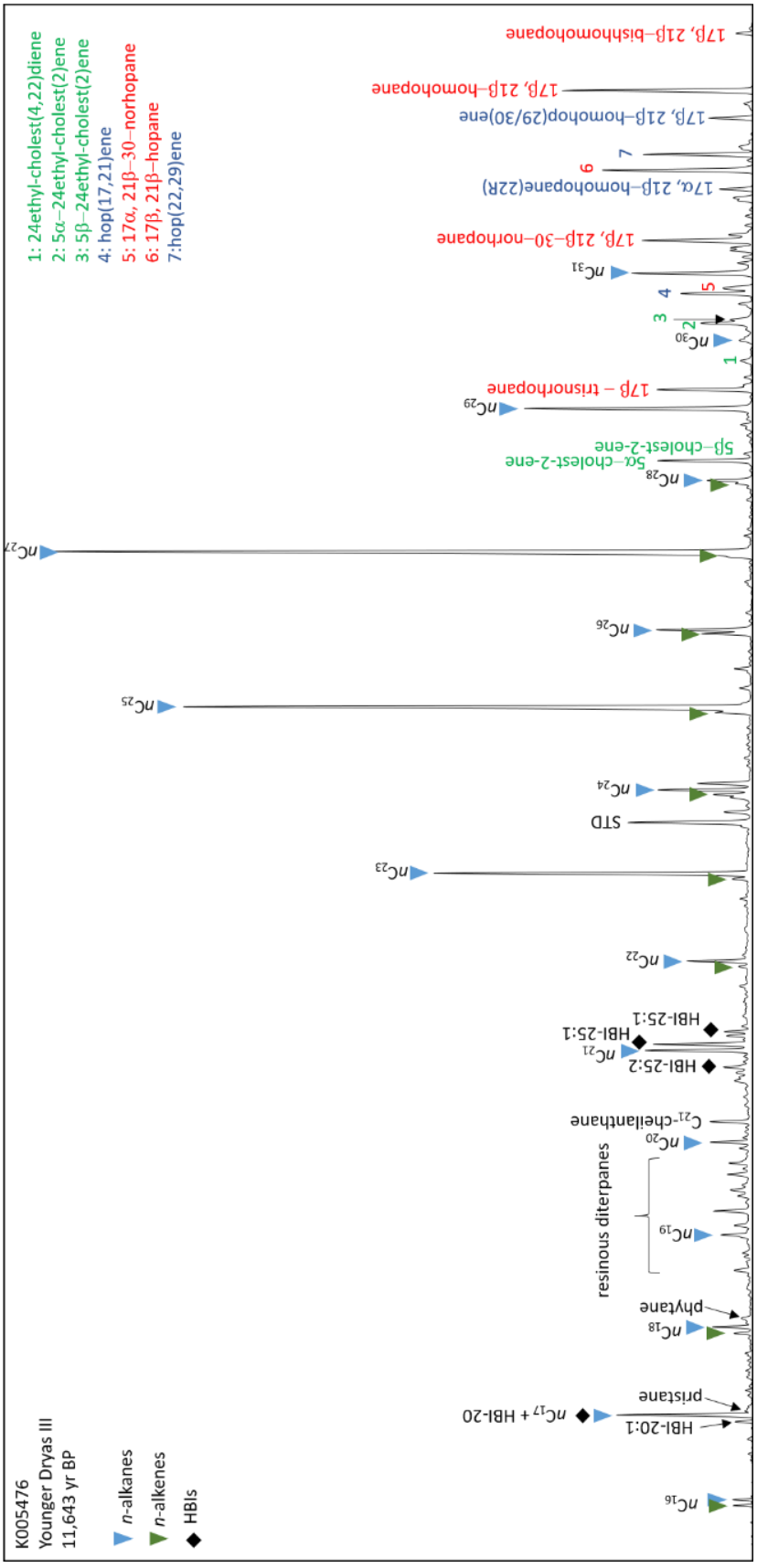

Figure S3.3: Chromatogram of the aliphatic fraction of a sample from the Younger Dryas, showing distribution of saturated and unsaturated hopanoids and steroids.

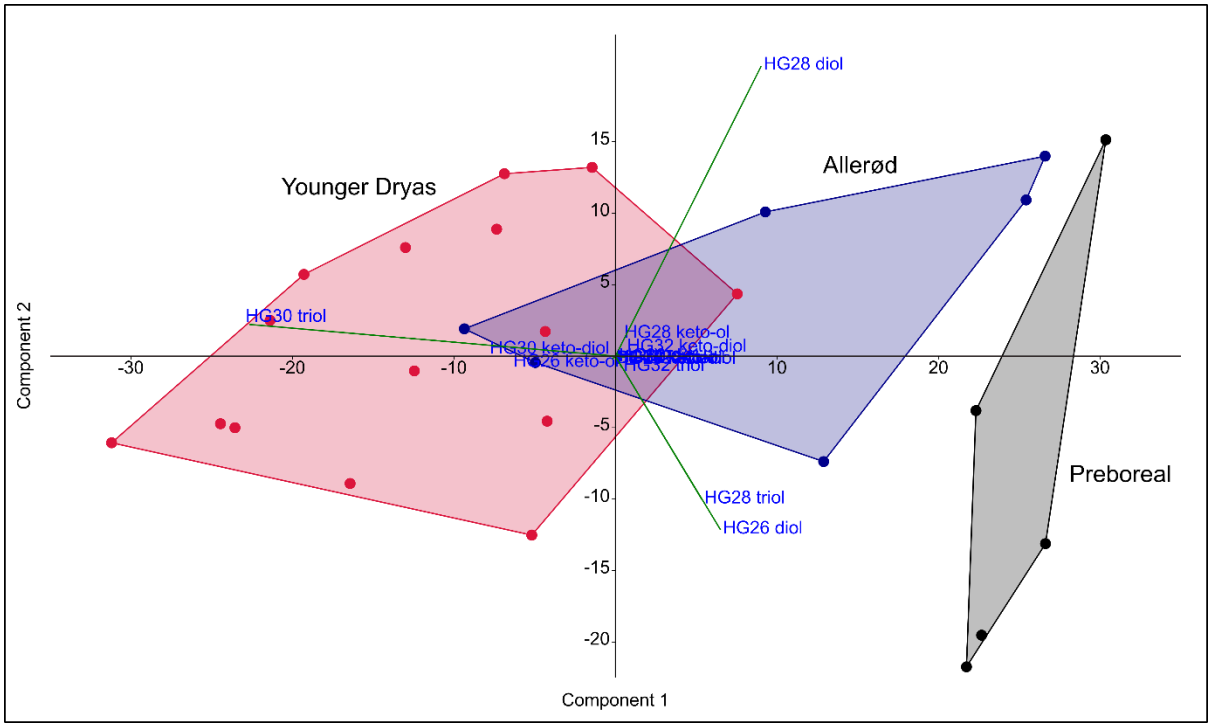

Figure S3.4: Principle component analysis (PCA) of HG data.

4. Holocene and late Pleistocene vegetation and environmental history of Lake Stymphalia (Peloponnese/Greece)

4.1 Introduction

The Mediterranean region is of great interest for paleoclimate-/paleoenvironmental reconstruction since the region is highly sensitive to climate change due to its unique position between the mid-latitude (European climate) and subtropical (northern African climate) atmospheric regimes (Lionello, 2012). Several studies have been conducted across the Mediterranean Basin to reconstruct both regional and temporal differences in the environmental and climate evolution (Bar-Matthews et al., 1999; Kim et al., 2004; Magny et al., 2007b; Roberts et al., 2012; Martrat et al., 2014). In order to improve understanding the individual regional climate forcing mechanisms, it is necessary to enhance the spatial coverage and the quality of paleorecords. The eastern Mediterranean Sea region and the Peloponnese peninsula are particularly vulnerable to climate change as they are influenced by multiple atmospheric circulation patterns, which create strong west-east rainfall and temperature gradients (Katrantsiotis et al., 2019). In addition, the region is characterized by the early presence of humans and the development of ancient Greek societies to advanced civilisations, from early farmers to the Greek city-states (Weiberg et al., 2016). Thus, the Peloponnese peninsula in the southern region of Greece has become the focus of numerous studies investigating climate and environmental change (Kontopoulos and Avramidis, 2003; Fuchs, 2007; Unkel et al., 2014; Katrantsiotis et al., 2016, 2018; Emmanouilidis et al., 2018; Norström et al., 2018) as well as human-environmental interactions during the late and mid Holocene (Weiberg et al., 2016; Seguin et al., 2019). Paleoclimate and paleoenvironmental studies from terrestrial and/or lacustrine archives, however, are scarce in southern Greece and in particular from the central Peloponnese. The limited information available derived mainly from studies focusing on lagoons (Lazarova et al., 2012; Avramidis et al., 2013; Emmanouilidis et al., 2018), speleothems (Finné et al., 2014, 2017) and coastal paleolakes (Norström et al., 2017; Katrantsiotis et al., 2019). Moreover, most records only cover the most recent climate history of Greece and usually do not exceed more than the last 7,000 years (Fig. 4.1). Thus, here is a pressing need for sediment records that date back to the early Holocene and late Pleistocene to put the climate and environmental evolution of the Peloponnese into a larger climate context. The only continuous long-term lacustrine record from the Peloponnese is preserved in Lake Stymphalia, which is the only remaining natural lake located in the north-eastern region of the peninsula. Previous studies on Lake Stymphalia have focused on either studying the most recent lake history (e.g. the last 2,500 years) using X-ray fluorescence (XRF) measurements (Seguin et al., 2019) or the late Glacial to mid-

Holocene period (Heymann et al., 2013) and identified several local environmental/climatic variation, but also regional climatic changes. Additionally, a short period from the Roman to Early Byzantine time (~100-700 AD) has been studied using glycerol dialkyl glycerol tetraethers (GDGTs) to reconstruct mean annual air temperatures (MAATs) (Seguin et al., 2019). Previous pollen analysis for a short interval of ca. 250 years during the middle Holocene period have demonstrated that the vegetation was dominated by oak *Quercus* trees and herbs of the subfamily *Lactucoideae* (Walsh et al., 2017a), despite the generally poor pollen preservation at this site (Seguin et al., 2019).

The Lake Stymphalia record thus constitutes a highly valuable archive of climate and environmental change of the south-eastern Mediterranean that up until now has not yet been comprehensively investigated. In this study, we investigated the late Pleistocene to Holocene sediment sequence of Lake Stymphalia to reconstruct the paleoclimate of the Peloponnese and associated changes in the terrestrial vegetation cover as well as aquatic community structure by application of organic-geochemical methods.

4.2 Study area

Lake Stymphalia (37°51'14"N, 22°27'49"E) is located in a karst polje on the south side of Mt. Kyllini (also known as Mt. Ziria) in the north-eastern Peloponnese, Greece (Fig. 4.1). The polje stretches east-west and is bordered in the south by the 1,900 m high Mt. Oligirtos. The western end of the polje is formed by the ~1,700 m high mountain ridge of Mt. Mavrovouni (Morfis and Zojer, 1986). The shallow holomictic lake is situated at 600 meters above sea level (masl). It is fed by several karst springs and minor torrential river systems (Morfis and Zojer, 1986). At present, Lake Stymphalia is the largest natural lake of the Peloponnese with an average surface area of ~3.5 km^2. During high water in spring, the lake size can increase up to 5 km^2. In arid years, however, the lake can also desiccate completely (Morfis & Zojer, 1986). Lake Stymphalia is a shallow lake with an average water depth of 0.8 m and a maximum depth of 1.2 m (Papastergiadou et al., 2007). The lake experiences a Mediterranean climate with warm, dry summers and colder but humid winters. The mean annual air temperature (MAAT) in the Stymphalia polje is about 14°C (2017/2018), while the annual precipitation is 618 mm (Seguin et al., 2019). Today's pH value is 8.5 (Heymann et al., 2013).

The periodically wet meadow areas of the lake's catchment are characterised by Molinio-Holoschoenion and Magnocaricetea marshland plant communities, while reed beds are dominated by Phragmitetalia (Papastergiadou et al., 2007). The regularly flooded areas allow growth of the white willow *Salix alba* and the poplar *Populus alba*, while the forested areas are characterised by *Abies cephalonica, Quercus coccifera, Pistacia lentiscus* and *Cistus spp.* (Papastergiadou et al., 2007).

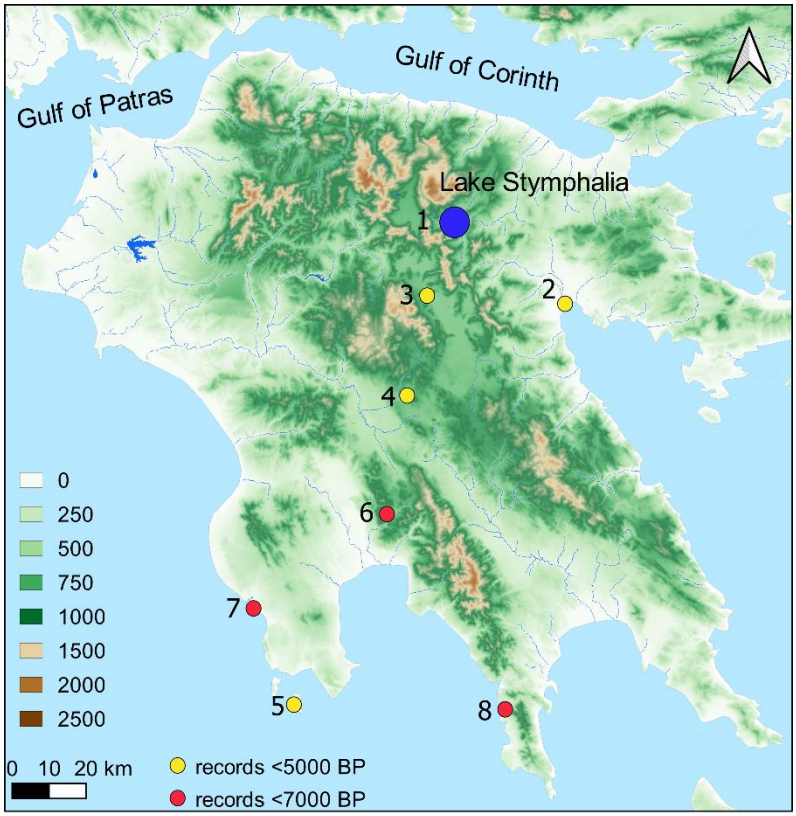

Figure 4.1: Map of study area showing the Peloponnese peninsula in south Greece. Numbers represent important paleoclimate achieves on the Peloponnese: 1. Lake Stymphalia (this study, Seguin et al., 2019), 2. Lake Lerna (Jahns, 1993; Katrantsiotis et al., 2019), 3. Kapsia Cave (Finné et al., 2014), 4. Asea Valley (Unkel et al., 2014), 5. Mavry Trypa Cave (Finné et al., 2017), 6. Agios Floros (Katrantsiotis et al., 2016; Norström et al., 2017, 2018), 7. Gialova Lagoon (Emmanouilidis et al., 2018; Katrantsiotis et al., 2018), 8. Alepotrypa Cave (Boyd, 2015). The colour code marks the maximum time range of the records.

4.3 Methods

4.3.1 Coring and sampling

The field and coring campaigns were conducted in March 2010 and March/April 2011 as detailed in Heymann et al. (2013). Briefly, the 16 m-long sediment core STY-1A and a 5.6 m-long parallel core STY-1B were obtained using a Usinger piston corer employed from a floating platform. The collected sediment core was sliced immediately in 1 m-long sections and stored in plastic liners at 4°C at Kiel University. In addition, a lake surface sediment sample and soils surrounding the lake were taken in autumn 2018 and 2019.

The lithostratigraphy of the core mainly consists of clay to silty clay with sparse sand/gravel clastic fragments and gastropod shells/shell fragments (Heymann et al., 2013; Seguin et al., 2019).

In order to recover Holocene and late Pleistocene sediments, 5-10 mm-thick samples were collected between 152 to 431 cm from core STY-1A. A total of 97 samples were taken, lyophilized for 24 h and ground to a homogenous powder using solvent-cleaned pestle and mortar. Subsequently, all sediments were stored frozen until further processing.

4.3.2 Age-depth model

For dating purposes, 21 bulk sediment samples from the Lake Stymphalia record were collected between 72 and 430.5 cm and radiocarbon-dated using accelerator mass spectrometry (AMS; Table 1). For the age-depth-model (ADM) we included dating results of the humic acid fractions published previously by Heymann et al. (2013) and Seguin et al. (2019) from the Leibniz-Laboratory for Radiometric Dating and Isotope Research at Kiel University (KIA) and new dates from the National Laboratory for Age Determination at NTNU University Museum Trondheim (TRa) for the lower part of the sediment core (Fig. 4.2). The humic acid fraction was selected for dating as it compositionally fits best with the lipid organic material studied. In addition, lake sediment received substantial influx of older, recalcitrant soil and sediment organic matter from adjacent slopes that would compromise the chronology. All dates are reported as calibrated years BP (cal yr BP; 1950 AD = 0 BP). Age-depth-modelling was conducted using the R package Rbacon v.2.3.8 (Blaauw and Christen, 2011) with the InCal13 calibration curve (Reimer et al., 2013).

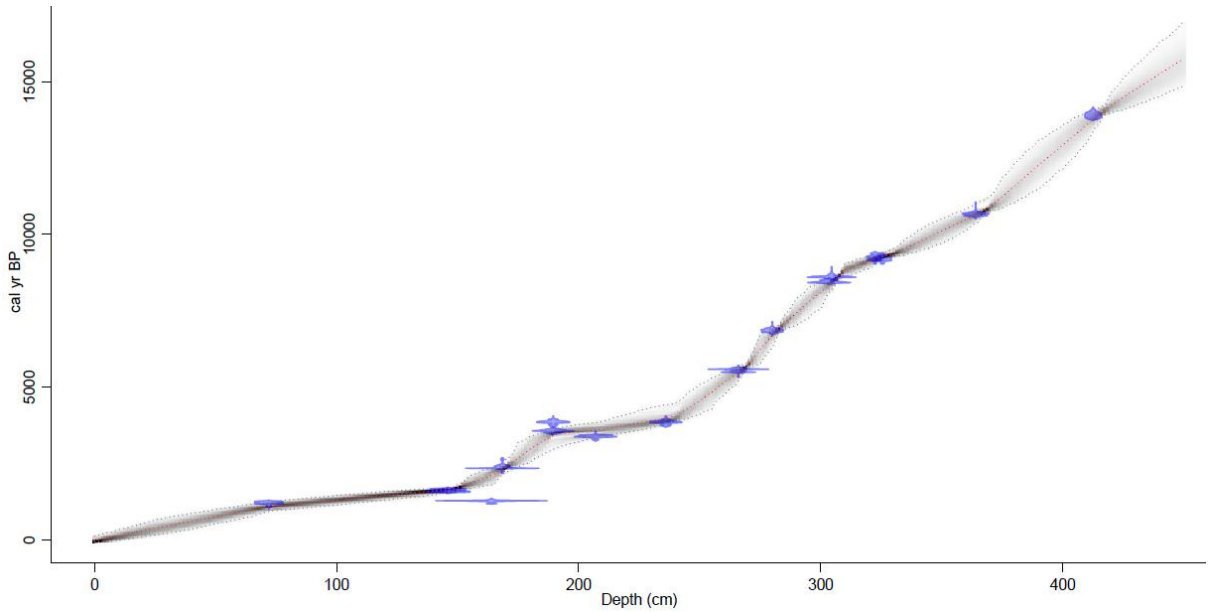

Figure 4.2: Age-depth model of Lake Stymphalia.

Table 4.1: Results of ADM dates of bulk sediments. Calibrated ages are shown in 1σ range. Median probabilities are shown in brackets.

Sample ID	Depth (cm)	^{14}C Age (yr BP)	Calibrated Ages (yr BP)
KIA-47446	72	1285±35	1184-1275 (1232)
KIA-47450	146	1731±17	1609-1694 (1652)
KIA-47450	146	1690±18	1562-1608 (1588)
KIA-42912	164	1355±22	1280-1299 (1289)
KIA-47447	168.5	2355±26	2338-2420 (2357)
KIA-47451	189.5	3336±22	3515-3612 (3576)
KIA-47451	189.5	3567±26	3833-3895 (3863)
KIA-47448	207	3168±27	3365-3443 (3394)
KIA-44005	236	3563±27	3833-3895 (3863)
KIA-44006	266	4837±32	5486-5607 (5587)
KIA-45955	280	6023±33	6797-6910 (6865)
TRa-13962	303.5	7656±30	8404-8506 (8438)
TRa-13956	304.5	7836±24	8591-8633 (8610)
TRa-13963	322.5	8261±32	9138-9301 (9248)
TRa-13957	325.5	8235±27	9135-9263 (9202)
KIA-45956	345	10,673±51	12,601-12,690 (12,643)[a]
TRa-13964	364	9433±27	10,595-10,708 (10,665)
TRa-13958	365.5	15,305±80	18,486-18,681 (18,578) [a]
TRa-13959	378.5	15,320±73	18,511-18,691 (18,596) [a]
TRa-13960	412.5	12,046±45	13,797-13,960 (13,890)
TRa-13961	430.5	15,714±68	18,866-19,033 (18,955) [a]

[a] Dates excluded from age-depth modelling.

4.3.3 Bulk organic-geochemical and stable carbon isotope analyses

The total carbon (TC), total nitrogen (TN) and total sulphur (TS) content of the sediment samples were determined with an Elementar Vario EL-III CNS analyzer. The amount of total organic carbon (TOC) was measured on an Eltra Helios system after decalcification using 10% and 25% hydrochloric acid (HCl) until no reaction occurred. The total inorganic carbon content (TIC) was calculated as the difference between TC and TOC. The calcium carbonate ($CaCO_3$) content was calculated by multiplying the TIC by 8.33 (stoichiometry of carbon in $CaCO_3$). Sedimentary TOC/TN ratios were calculated on a molar basis.

The carbon isotopic composition of the bulk organic matter ($\delta^{13}C_{TOC}$) was determined on decalcified and neutralized sediment samples using a Flash EA elemental analyzer interfaced via a ConFlow III to a Delta V isotope ratio mass spectrometer (Thermo Scientific, US). Results were expressed in conventional delta (δ) notation with reference to the Vienna PeeDee Belemnite standard (V-PDB). Reproducibility of duplicate analysis was <0.1‰.

4.3.4 Lipid extraction

Sediment samples were extracted using an accelerated solvent extraction (ASE 200) method or a modified Bligh and Dyer procedure (Bligh and Dyer, 1959; Rütters et al., 2002). For sample extraction by ASE, 5 to 8 g of sediment were extracted with a mixture of DCM:methanol (MeOH) (9:1, *v:v*), at a temperature of 75°C and 5.0×10^6 Pa to obtain a TLE. Sediment samples, which were extracted using the Bligh and Dyer procedure were ultrasonically extracted for 10 min with a solvent mixture of MeOH:DCM:phosphate buffer at pH 7-8 (2:1:0.8, *v/v/v*). After centrifugation (1690 g, 4 min), the supernatant was collected and the remaining residue extracted twice more as described above. In the following, DCM and phosphate puffer were added to the extract to yield a solvent ratio of 1:1:0.9 (MeOH:DCM:phosphate buffer, *v/v/v*), which induced phase separation. The bottom layer, containing the organic fraction, was transferred into a round-bottom flask and the remaining solution was extracted twice with DCM. The Bligh and Dyer extracts (BDE) were rotary evaporated and stored at -18°C until further processing.

4.3.5 *n*-Alkane analysis and proxy calculation

Aliquots of all extracts were analysed using an Agilent 7890A (GC) equipped with an Agilent DB-5 column (30m × 0.25mm × 0.25µm) coupled to an Agilent 5975 B (MS). Samples were injected splitless with the injector temperature set to 320°C. The oven program started at 60°C for 4 min, followed by a ramp to 140°C at 10°C/min and subsequently to 325°C at 3°C, followed by an isothermal period of 45 min. The MS operated with a scanning mass range of *m/z* 50-850 Da and an ionization energy of 70 eV. Alkanes were identified by comparison with an *n*-alkane standard mixture containing $n\mathrm{C}_{20}$ to $n\mathrm{C}_{40}$ (Supelco).

The average chain lengths (ACL) of *n*-alkanes was calculated as

$$\mathrm{ACL} = \Sigma(n \times \mathrm{C}_n)/\ \Sigma\mathrm{C}_n) \quad (1)$$

where C_n is the relative abundance of an *n*-alkane and *n* indicating the number of carbon atoms (Poynter and Eglinton, 1990). The P_{aq} index was calculated using the relative abundance of *n*-alkanes as described by (Ficken et al., 2000):

$$\mathrm{P}_{aq} = (\mathrm{C}_{23} + \mathrm{C}_{25})/(\mathrm{C}_{23} + \mathrm{C}_{25} + \mathrm{C}_{29} + \mathrm{C}_{31}) \quad (2)$$

4.3.6 GDGT analysis and proxy calculation

An aliquot of each extract was separated into an apolar and a polar fraction using column chromatography. A small Pasteur pipette filled with activated aluminium oxide was used as stationary phase. The aliphatic fraction was eluted with 4 ml hexane:DCM (9:1, *v/v*) and the polar fraction with 4 ml DCM:MeOH (1:1, *v/v*), respectively. The polar fractions were dried under a gentle stream of nitrogen, re-dissolved in *n*-hexane:2-propanol (99:1, *v/v*) to a

concentration of 2 mg/ml and passed through a 0.45 µm polytetrafluoroethylene (PTFE) filter (Macherey-Nagel, Germany) prior to analysis. GDGTs were analysed using a Waters Alliance 2695 HPLC system coupled to a Micromass Quattro LC triple quadrupole mass spectrometer (HPLC-MS) following the analytical protocol described of Hopmans et al. (2016). This protocol allows the separation of 5- and 6-methyl branched GDGTs (brGDGTs).

Mean annual air temperatures were reconstructed using the Index 1 (De Jonge et al., 2014) and applying the lake calibration of Russell et al. (2018):

$$\text{Index 1} = \log((\text{Ia} + \text{Ib} + \text{Ic} + \text{IIa'} + \text{IIIa'})/(\text{Ic} + \text{IIa} + \text{IIc} + \text{IIIa} + \text{IIIa'})) \quad (3)$$

$$\text{MAAT} = 12.22 + 18.79 \times \text{Index 1} \quad (4)$$

The pH was calculated using the CBT' index for the cyclisation of brGDGTs defined by De Jonge et al. (2014) and using the surface water calibration of Russell et al. (2018):

$$\text{CBT'} = \log(\text{Ic} + \text{IIa'} + \text{IIb'} + \text{IIc'} + \text{IIIa'} + \text{IIIb'} + \text{IIIc'})/(\text{Ia} + \text{IIa} + \text{IIIa}) \quad (5)$$

$$\text{pH} = 8.95 + 2.65 \times \text{CBT'} \quad (6)$$

The BIT index was determined as detailed in Hopmans et al. (2004) using the combined peak areas of the 5- and 6-methyl isomers of brGDGTs:

$$\text{BIT Index} = (\text{Ia} + \text{IIa} + \text{IIa'} + \text{IIIa} + \text{IIIa'}) / (\text{Ia} + \text{IIa} + \text{IIa'} + \text{IIIa} + \text{IIIa'} + \text{crenarchaeol}) \quad (7)$$

The relative abundance of 6-methyl over 5-methyl brGDGTs is expressed as IR ratio (De Jonge et al., 2014):

$$\text{IR} = (\text{IIa'} + \text{IIb'} + \text{IIc'} + \text{IIIa'} + \text{IIIb'} + \text{IIIc'})/ (\text{IIa} + \text{IIa'} + \text{IIb} + \text{IIb'} + \text{IIc} + \text{IIc'} + \text{IIIa} + \text{IIIa'} + \text{IIIb} + \text{IIIb'} + \text{IIIc} + \text{IIIc'}) \quad (8)$$

To trace for the process of methanogenesis in lake systems the %GDGT-0 ratio has been used and is defined by Blaga et al. (2009) as

$$\%\text{GDGT-0} = \text{GDGT-0}/(\text{Crenarchaeol} + \text{GDGT-0}) \quad (9)$$

The %crenarchaeol isomer ratio has been defined by (Sinninghe Damsté et al., 2012a) as

$$\%\text{crenarchaeol isomer} = \text{crenarchaeol regioisomer}/(\text{cren.} + \text{cren. regioisomer}) \quad (10)$$

4.3.7 HG analysis and proxy calculation

For the analysis of heterocyte glycolipids (HGs), an aliquot of the BDE was dissolved in a mixture of hexane:2-propanol:H_2O (72:27:1, *v/v/v*) and filtered through a 0.45 µm regenerated cellulose filter. Concentrations ranged from 7 to 10 mg/ml depending on the abundance of the target analyte in the sample. HGs were analysed using high-performance liquid

chromatography coupled to electrospray ionization tandem mass spectrometry (HPLC-ESI/MS^2) as described by Bauersachs et al. (2017, 2009b).

A number of different indices based on the ratio of HG alcohols and hydroxyketones has been postulated, which all correlate with either grow temperate in cultures of heterocystous cyanobacteria (Bauersachs et al., 2009; 2014) (Bauersachs et al., 2009a, 2014b) or surface water temperature (SWT) in lake environments (Bauersachs et al., 2015). Here, we used the heterocyte diol index of 26 carbon atoms (HDI_{26}) to investigate SWT changes in Lake Stymphalia over time. The HDI_{26} was calculated and transferred to SWT as described by Bauersachs et al. (2015):

$HDI_{26} = HG_{26}\,diol / (HG_{26}\,keto\text{-}ol + HG_{26}\,diol)$ (11)

$HDI_{26} = 0.0405 \times SWT + 0.0401$ (12)

4.3.8 Statistical analysis for phase separation

Principal components analysis (PCA) was performed after normalisation of the relative abundances of GDGT abundances using the statistical software Past 3.17 (Hammer et al., 2001). The PCA results demonstrate significant differences in geochemical characteristics of GDGT data over time (Fig. S4.1). Therefore, the lipid record was divided into five main phases as discussed below.

4.4 Results

4.4.1 Bulk composition and stable carbon isotopes in Lake Stymphalia sediments

The TOC content varies between 0.2 and 4.6%, with an average of 1.1±0.7% (Fig. 4.3). Lowest values of 0.2% occured at the base of the sediment sequence, after which the TOC content increased gradually towards the youngest samples. Around 3,600 yr BP, a maximum in TOC with a value of 4.6% was observed. The average TIC content in the sediments of Lake Stymphalia was 4.5±1.5%. High TIC values varying between 4.3 and 6.8 from 14,720 to 10,288 yr BP were replaced by low values of around 3.7±0.9 around 10,000 yr BP. Thereafter, a period with maximum average values of 6.5±1.3 occurred from 9,447 to 7,457 yr BP, while the TIC values varied between 2.4 and 5.5% for the next 3,500 years. At 3,332 yr BP, the TIC dropped by about 3% to 1.7% and remained on a low level until 2,120 yr BP, when the TIC value raised to 5.3%. The TOC/TN ratio showed an average value of ca. 20±5.4 between 14,720 and 13,200 yr BP. Thereafter, values varied between 19 and 44 until 10,730 yr BP, followed by a decrease to average values around 20 for the next 800 years. Subsequently, the TOC/TN ratio increased to 28.9 at 8,648 yr BP and then declined to an average of 20 until 6,750 yr BP. The period from 6,750 to 2,000 yr BP was characterized by comparatively low TOC/TN ratios that average 13.0±3.8%. The $\delta^{13}C_{TOC}$ values ranged from -23.4 to -27.7‰ (average -26.1±0.8‰) and showed a shift to more enriched values towards the core top. A

shift from -25.7 to -23.4‰ occurred at 8,290 yr BP. The most depleted values of -27.7‰ occurred around 3,700 yr BP.

4.4.2 Aliphatic hydrocarbons in Lake Stymphalia

n-Alkane distributions in Lake Stymphalia sediments ranged from nC_{17} to nC_{33} and usually showed a unimodal distribution pattern maximizing at nC_{29} or nC_{31}. The mid- and long-carbon number homologues ($\geq nC_{23}$) comprised more than 90% of the total *n*-alkane pool. During the late Pleistocene the ACL was comparatively high with values >29.5 (Fig. 4.3). In the following 2,350 years, the ACL decreased gradually to a minimum of 28.5 at 11,645 yr BP. With the onset of the Holocene, the proportion of long-chain *n*-alkanes increased continuously. This trend was interrupted around 8,600 and 3,600 yr BP, where short oscillations to lower values were observed.

The nC_{31}/nC_{27}-alkane ratio (Fig. 4.3) used for the differentiation of vegetation sources (grass *vs.* trees) reached its maximum of 4.9 at 14,003 yr BP. Thereafter, the ratio declined to 0.6 at 10,398 yr BP, followed by a new increase to 2.4 within 1,000 years. In the following 5,500 years the vegetation remained relatively constant with nC_{31}/nC_{27} values around 1.4±0.4. At 3,584 yr BP a minimum of 0.4 was observed, followed by an increase to 2.3 at 2,885 yr BP.

During the late Pleistocene, the P_{aq} values of about 0.13 remained relatively low at 14,003 yr BP (Fig. 4.3). In the following 2,350 years the P_{aq} increased to a maximum of 0.56, followed by a decline to 0.25 at 9,268 yr BP. The period from about 9,000 to 3,800 yr BP was characterized by P_{aq} values between 0.27 and 0.47, with a short spell of 0.53 at 8,290 yr BP. Subsequently, the P_{aq} increased to 0.56 at 3,584 yr BP, followed by a minimum of 0.12 at 2,885 yr BP.

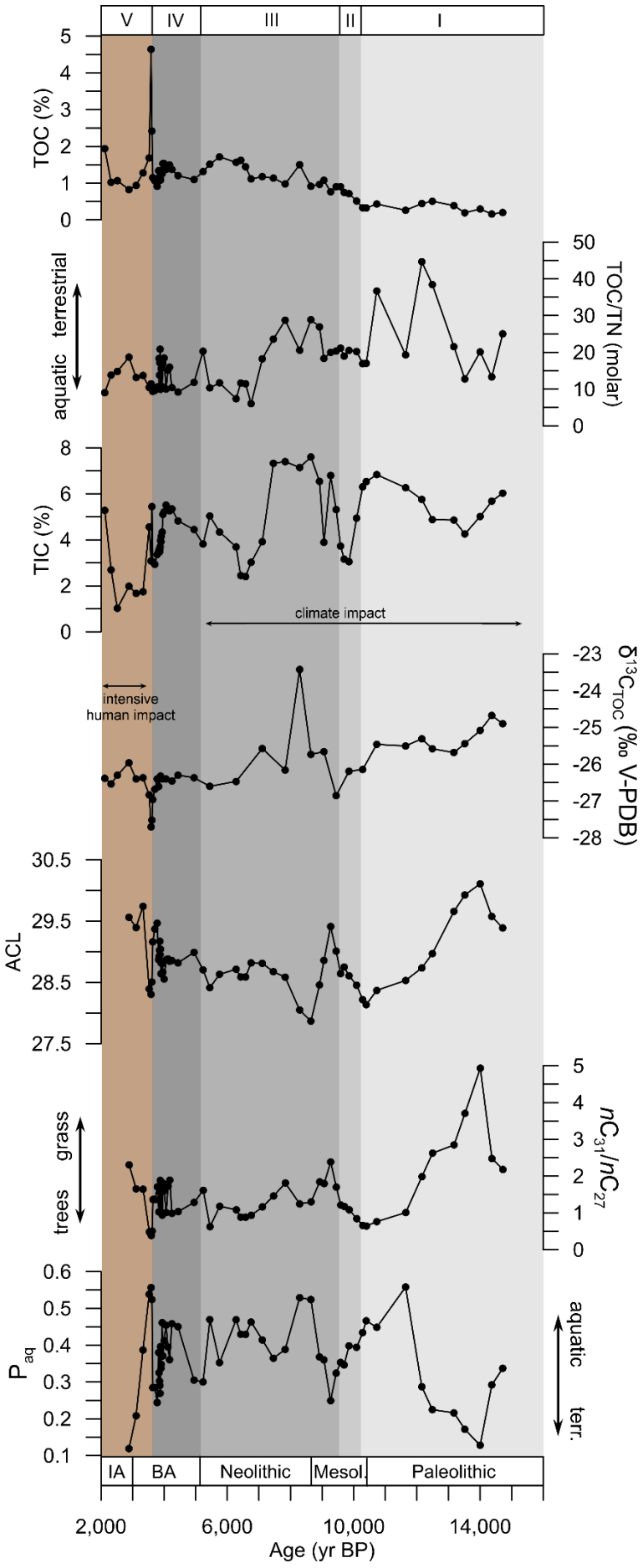
V
IV
III
II
I
TOC (%)
aquatic
terrestrial
TOC/TN (molar)
TIC (%)
climate impact
intensive
human impact
δ13CTOC (‰ V-PDB)
ACL
grass
trees
nC31/nC27
Paq
aquatic
terr.
IA
BA
Neolithic
Mesol.
Paleolithic
2,000
6,000
10,000
14,000
Age (yr BP)

Figure 4.3: Downcore bulk-geochemical, isotope and lipid data from Lake Stymphalia with concentration of total organic carbon (TOC), molar total organic carbon to total nitrogen ratio (TOC/TN), total inorganic carbon (TIC), bulk isotopes of organic carbon ($\delta^{13}C_{TOC}$), average chain lengths (ACL) of n-alkanes, nC_{31}/nC_{27} alkane ratio and a proxy for the proportion aquatic macrophytes (P_{aq}).

4.4.3 Glycerol dialkyl glycerol tetraethers (GDGTs) in Lake Stymphalia

In the modern lake surface sediment, brGDGTs dominated over isoGDGTs and constitute 92.3% of all GDGTs (Fig. 4.4) as expressed in a BIT index of 0.98. The corresponding GDGT-reconstructed MAAT is 12.6°C and the GDGT-reconstructed pH is 8.9. Catchment soils (n=4) exhibited a GDGT composition similar to those of the lake surface sediment with brGDGTs constituting on average 87.3±6.1% of all GDGTs (Fig. 4.4). The BIT index values were about 0.93±0.05, while the GDGT-derived MAATs were 14.5±1.6°C and the reconstructed pH values averaged 9.2±0.5.

Both iso- and brGDGTs were detected throughout the entire sediment sequence. Amongst these, brGDGTs dominated, ranging from 85 to 98% of all GDGTs during the Holocene but comprising only ~65% during the late Pleistocene. GDGT-0 predominated among the isoGDGTs, except between 10,093 and 12,158 yr BP, when crenarchaeol contributed most to the isoGDGT pool. The brGDGTs consisted of GDGT-Ia (16.09±3.81), GDGT-Ib (13.68±3.24%), GDGT-IIb (10.49±3.4%), GDGT-IIa (9,60±2.66%), GDGT-IIa' (9,32±1.29%) and GDGT-IIb' (6.11±2.28%; Fig. 4.4).

Branched GDGT-reconstructed MAATs varied between 14.7 and 20.8°C (Fig. 4.5). From the base of the record to 9,854 yr BP, MAAT increased from 16.6 to 20.8°C. Thereafter, MAAT remained relatively constant at about 17.9±0.9°C until 4,000 yr BP and was only interrupted by a short but strong cooling to 14.7 °C at 8,290 yr BP. Between 4,000 and 2,000 yr BP, MAAT fluctuated but showed a cooling trend from 20.0°C to 15.6°C (Fig. 4.5).

BIT and %Cren exhibited an inverse trend between 14,720 and 10,288 yr BP, followed by a period of relative constancy until 3,854 yr BP, when BIT values remained around 0.9 and %Cren at 0.15, respectively. Thereafter, the BIT index increased and showed highest values of >0.95. %Cren values were lowest in this interval and remained below 0.1 mostly.

GDGT-reconstructed pH values ranged from 8.4 to 9.8 (average 8.8±0.3) with highest pH values occurring during the late Pleistocene. In the following, pH values decreased substantially reaching a minimum at 9,700 yr BP with pH values of 8.4. From 9,268 until 3,936 yr BP, pH values varied between 8.8 and 9.2, followed by a decline to a pH of 8.4. Thereafter, the pH value ranged from 8.4 to 8.8 until 2,000 yr BP.

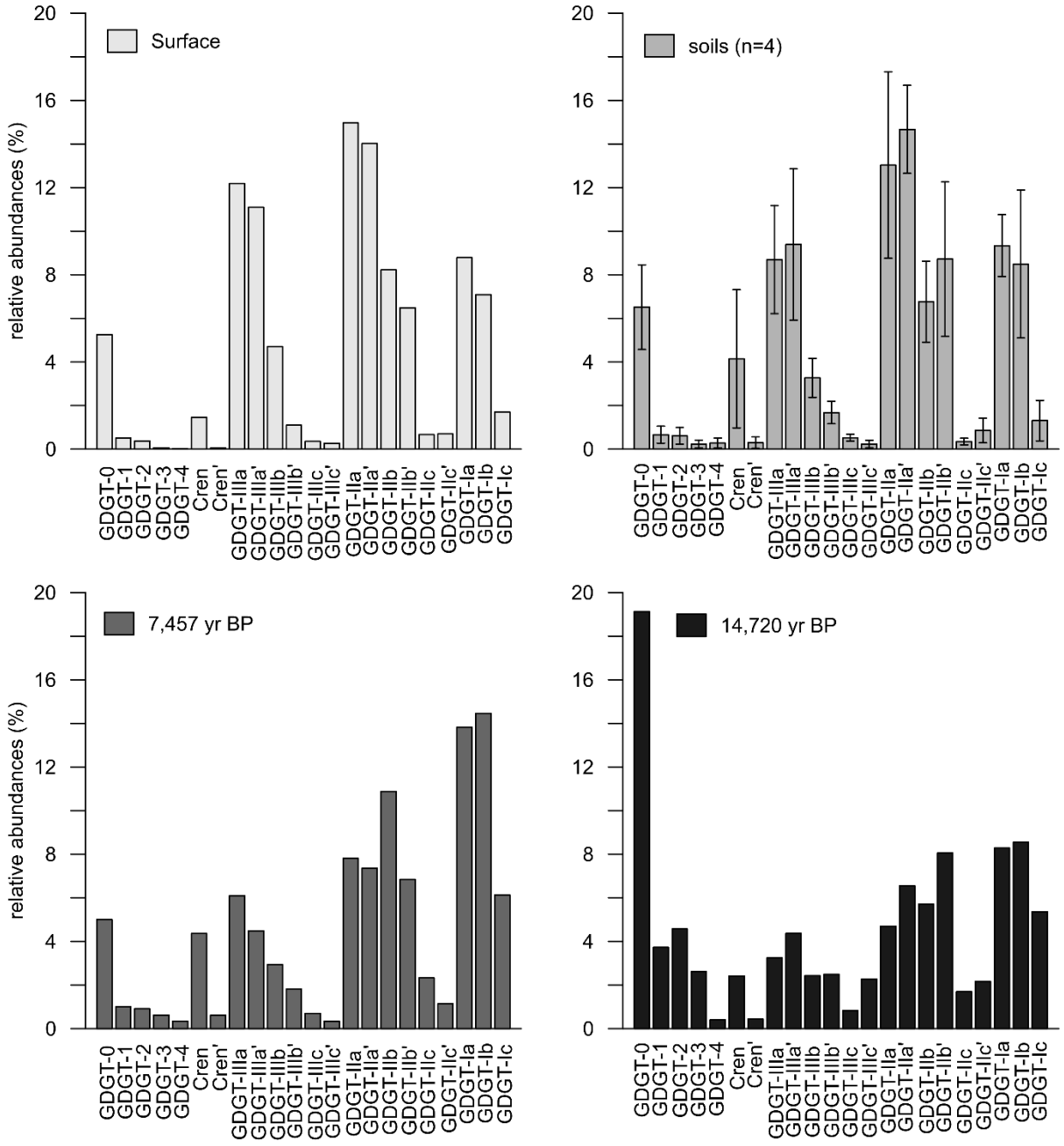

Figure 4.4: Relative abundances of individual GDGTs in the lake surface sediment, catchment soils and selected intervals of the sediment core.

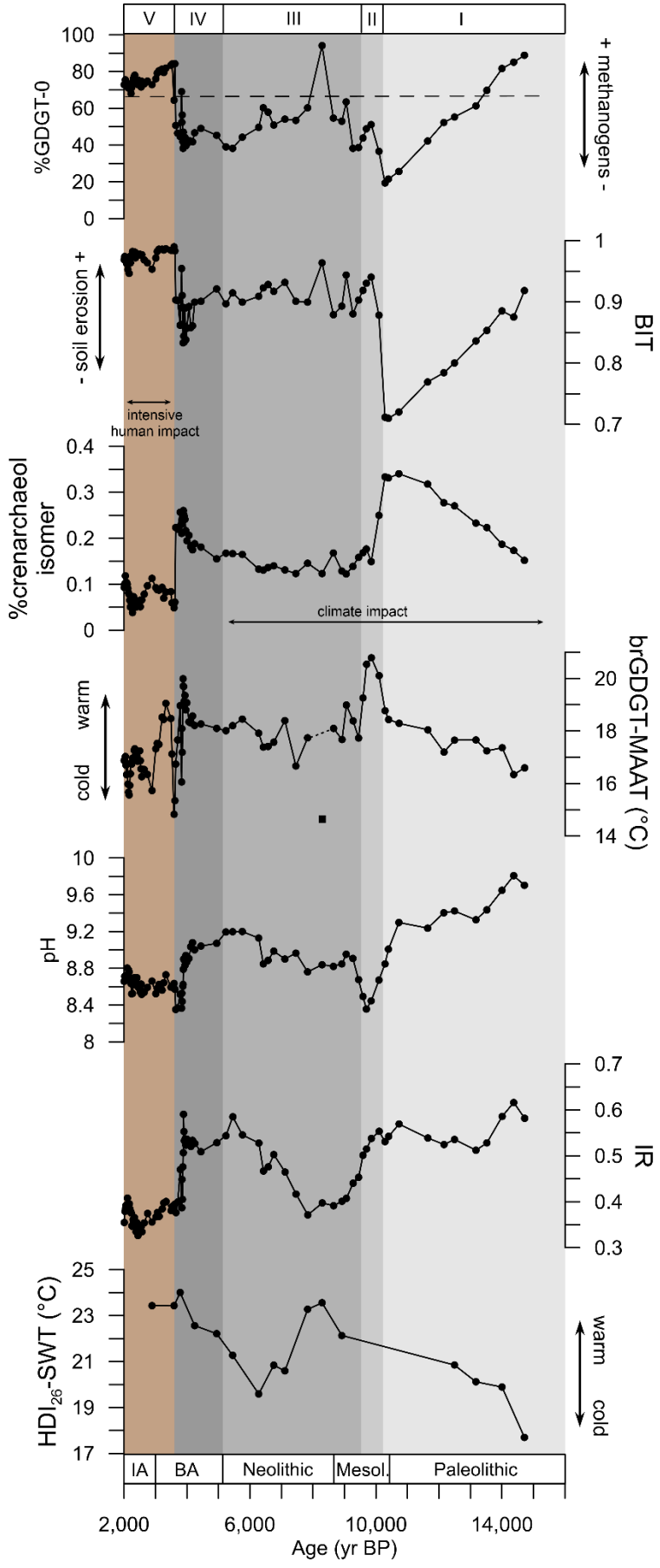

Figure 4.5: Downcore variation in GDGT- and HG-based proxies for Lake Stymphalia.

4.4.4 Heterocyte glycolipids in Lake Stymphalia

The lake surface sediment contained abundant HG_{26} diols (23.8%), HG_{28} diols (17.3%) and HG_{30} triols (26.7%) together with their corresponding keto-ol and keto-diol structures. Minor relative abundances of HG_{28} diol with a pentose headgroup (P HG_{28} diol) were detected as well. The HDI_{26}-inferred lake surface water temperature (SWT) was 16.3 °C, which is close to, but somewhat higher than the mean SWT of 14.6°C of modern Lake Stymphalia (Morfis and Zojer, 1986).

Fourteen different HG structures were detected in variable proportions in the fossil sediments (Fig. 4.6). HG_{26} diols, HG_{28} diols and HG_{30} triols constituted the most dominant HG homologues contributing >80% to all HGs. In addition to these three dominant components, the four oldest samples (12,493 - 14,720 yr BP) also contained comparatively large proportions of the HG_{28} diol (7.7±3.9%). From 8,917 to 7,830 yr BP the amount of HG_{28} diols increased substantially contributing to more than half of the total HG pool. Thereafter, the relative abundance of HG_{26} diols and HG_{28} triols increased gradually with a relapse to a dominance of HG_{28} diols at 3,584 yr BP. HG_{32} triols (2.6±1.5%) and keto-diols (0.5±0.4%) exhibited subordinate abundances only and were absent in the youngest fossil sample and the lake surface sediment.

HDI_{26}-inferred SWT varied from 17.7 to 24.0°C (Fig. 4.5). The SWT with 17.7°C was lowest in the basal sediment sample but increased to 20.9°C during the late Pleistocene. With the transition to the Holocene, reconstructed SWTs increased pointing to a climate optimum with a maximum temperature of 23.6°C at 8,290 yr BP. In the following 2,000 years, HDI_{26}-based temperatures declined and yielded a minimum of 19.6°C at 6,276 yr BP, while subsequently increasing to 24.0°C at 3,782 yr BP. During the late Holocene, the SWT showed only little variation and averaged 23.5°C.

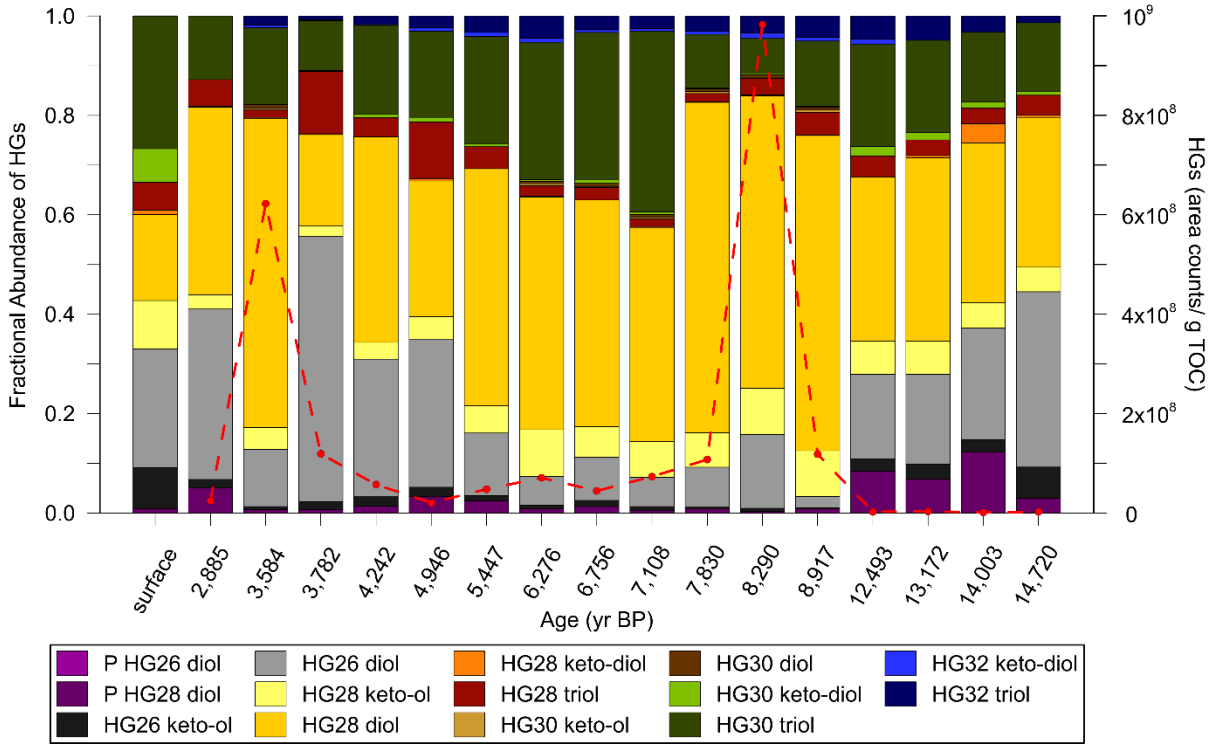

Figure 4.6: Fractional abundances and semi-concentrations (stippled red line) of heterocyte glycolipids in Lake Stymphalia.

4.5 Discussion

4.5.1 Modern lipid distributions in Lake Stymphalia surface sediments

4.5.1.1 Modern GDGT distributions

In the surface sediment of Lake Stymphalia, brGDGTs were most abundant and constitute 92.3% of all GDGTs (Fig. 4.4). These components were most likely synthesized by soil living *Acidobacteria* but possibly also other bacteria (Sinninghe Damsté et al., 2018b) and transported to lakes by means of run-off. In meromictic lakes with anoxic bottom water they may also derive from an in situ source (Blaga et al., 2009; Sinninghe Damsté et al., 2012a; Zink et al., 2016). IsoGDGTs, derived from Archaea, contributed only subordinate (7.7%) to the total GDGT pool. This was expressed in a BIT value of 0.98 in the surface sediment, which suggested a high organic matter input to the lake from surrounding soils. GDGT-0, the predominant isoGDGT in the surface sediment of Lake Stymphalia, is primarily found in Euryarchaeota and considered diagnostic for methanogens (Blaga et al., 2009; Bauersachs et al., 2015b). In lake environments, high %GDGT-0 values (>67%) have been advocated as a tool to trace for methanogenesis, a process exclusively carried out under anaerobic conditions (Sinninghe Damsté et al., 2012a). In Lake Stymphalia, the %GDGT-0 ratio was 78 in the surface sediment and ranged from 47 to 89 in the soils adjacent to the shore, which indicated the activity of methanogens in the modern lake. The ratio of crenarchaeol to its regioisomer (%Cren) has been proposed as an indicator to trace for a *thaumarchaeotal* input

from soils to lake environments (Pitcher et al., 2011; Sinninghe Damsté et al., 2012a). The lake surface sediment had low to intermediate %Cren values ranging from 0.05 to 0.09, which may suggests that aquatic Thaumarcheota were the main source of crenarchaeol and its regioisomer in the surface sediments and that the loading of a soil-derived organic matter was moderate. This was also suggested by the dominance of pentamethylated brGDGTs in the surface sediment (Fig. S4.2), which are also abundant in other lake systems (Russell et al., 2018). Tetramethylated brGDGTs, which are common in soils and peats (De Jonge et al., 2014; Naafs et al., 2017b), on the contrary were only present in minor abundances.

As the majority of brGDGTs seemed to be lake derived, we here used the East African lake calibration of Russell et al. (2018) to infer past MAAT. The surface sediment yielded a brGDGT-reconstructed MAAT of 12.6°C, which was 2°C lower than average SWT of 14.6°C of modern Lake Stymphalia (Morfis and Zojer, 1986) and the MAAT of 14°C recorded by single temperature logging in 2016/17 (Seguin et al., 2019).

4.5.1.2 Modern heterocyte glycolipid (HG) distributions

Heterocyte glycolipids are biological markers unique to N_2-fixing heterocytous cyanobacteria (Gambacorta et al., 1999; Bauersachs et al., 2009b). The distribution of HGs in cultured cyanobacteria has been shown to vary on an order and family level (Bauersachs et al., 2009a, 2017, 2019), which has been used to study the community composition of heterocytous cyanobacteria in freshwater and brackish environments (Bauersachs et al., 2015a; Sollai et al., 2017). In Lake Stymphalia, the surface sediment was dominated by HG_{26} diols and keto-ols as well as HG_{28} diols and keto-ols (Fig. 4.6). These components are common in aquatic cyanobacteria of the family Nostocaceae (Gambacorta et al., 1998; Bauersachs et al., 2009a, 2017) and have been reported previously from European (Wörmer et al., 2012; Bauersachs et al., 2015a) and North American lakes (Bale et al., 2016). Although the phytoplankton community of Lake Stymphalia has not been studied phycologically, our data suggests that cyanobacteria such as *Dolichospermum* (previously *Anabaena*), *Anabaenopsis*, *Aphanizomenon* and/or *Nodularia* may occur as part of the phytoplankton community in Lake Stymphalia. In contrast, HG_{30} triols and keto-diols have only been reported from mat-forming heterocytous cyanobacteria belonging to the Scytonemataceae (Gambacorta et al., 1999; Bauersachs et al., 2019). Their presence in Lake Styphalia surface sediment suggested a potential origin from benthic microbial mats developed along the fringes of the lake. The absence of HGs with a longer carbon chain (e.g. HG_{32} triol and HG_{32} keto-diol) suggested that true-branching heterocyte cyanobacteria of the order *Stigonematales* (Gambacorta et al., 1999; Bauersachs et al., 2013, 2014a) were not endemic to modern Lake Stymphalia.

The HDI_{26}-reconstructed temperature for the lakes surface sediment sample was 16.4°C and was considered to reflect summer SWT (Bauersachs et al., 2015a). As, however, the summer

air temperature varied between 20°C and 23°C between June and September in the Stymphalia polje (Seguin et al., 2019), the calculated HDI_{26}-temperatures rather seemed to reflect spring or autumn temperatures.

4.5.2 Paleoclimate and paleoenvironmental reconstruction of Lake Stymphalia

Changes in the elemental, isotope and biomarker composition reflected the evolution of Lake Stymphalia from the late Pleistocene to ~2000 yr BP and allowed the definition of five distinct lake stages that are discussed below.

.

4.5.2.1 Late Pleistocene/early Holocene – Stage I (14,720 – 10,288 yr BP)

The early stage of Lake Stymphalia was characterized by low sedimentary TOC (<1%) and comparatively high $CaCO_3$ (4-7%) contents indicative of a low primary productivity and/or poor preservation conditions of organic matter in a well oxygenated limestone-rich karst environment. Oxic conditions in the water column usually promote the degradation of organic matter prior to its incorporation into sediments (Meyers, 2003), which may explain the low organic matter content observed for stage I. The TOC/TN ratios initially varied between 10 and 20, suggesting a mixed contribution of algal and terrestrial/pedogenic organic matter to the lake at this stage. However, from about ~12,300 yr BP to the top of stage I, the TOC/TN ratio increased and ranged from 17 to 45. This may indicate a period of increased input of land plants or emergent macrophytes, both of which have been shown previously to express TOC/TN ratios >20 (Tyson, 1995; Mayr et al., 2009). The P_{aq}, an indicator for the loading of macrophyte organic matter to lake environments (Ficken et al., 2000), followed the TOC/TN profile and increased in parallel with the TOC/TN ratio. P_{aq} values in this interval range from 0.22 to 0.56 and thus were well in line with an input of organic matter from emergent macrophytes (Ficken et al., 2000). Emergent macrophytes, such as the reed *Phragmites australis*, form dense stands in the littoral zone of modern Lake Stymphalia and today cover more than 60% of the open water areas (Papastergiadou et al., 2007). Lake level lowstand is generally considered to promote the expansion of reed vegetation. The simultaneous increase in TOC/TN ratios and P_{aq} values from 12,300 yr BP to ~10,500 yr BP may thus suggest a decline in algal productivity (Fig. 4.3).

Epicuticular leaf wax-derived *n*-alkanes were dominated by nC_{29} and nC_{31} resulting in ACL values indicative for evergreen or deciduous angiosperms or phrygana plants (Norström et al., 2017). The input of long-chain *n*-alkanes, diagnostic for gymnosperms, may be under-represented, since gymnosperms generally produce low *n*-alkanes concentrations in their epicuticular waxes (Diefendorf et al., 2011; Bush and McInerney, 2013; Norström et al., 2017). The most common gymnosperms in Greece are *Pinus* species, which then due to their low

wax *n*-alkane content (Diefendorf et al., 2015) should not affect the sedimentary *n*-alkane pool of Lake Stymphalia. Between 14,700 and 13,000 yr BP a substantial part of sedimentary *n*-alkanes may have originated from phrygana bushes and shrubs (Norström et al., 2017) or grasses as indicated by the predominance of nC_{31} over nC_{27} (Maffei, 1996; Marseille et al., 1999). In this period at the end of the Late Glacial, the vegetation cover in the catchment may have been rather sparse due to adverse climatic conditions. After this phase, the ACL decreased steadily and the amount of predominantly tree-derived nC_{27} increased, indicative of a forest extension due to warmer conditions. From about 11,600 yr BP, the proportion of mid-chain *n*-alkanes (nC_{23} and nC_{25}) increased, expressed in an elevated P_{aq} index and lower ACL, which refers to an enhanced proportion of submerged or floating macrophytes to the total organic matter (Ficken et al., 2000). The growth of macrophytes may have been favoured by a lake expansion, leading to a decline of the BIT index indicative of diminished terrestrial influx during the same period (Fig.4. 5). Another explanation for low BIT values could be the in-situ production of brGDGTs in the water column, which has been previously reported from other lakes (Blaga et al., 2009; Tierney and Russell, 2009; Naeher et al., 2014; Weber et al., 2015; Zhang et al., 2016; Zink et al., 2016).

During the early lake stage methanogens likely constituted a significant proportion of the archaea thriving in the lake. A strong correlation between %GDGT-0 and BIT index is observed when the sediment record is divided into two phases (Fig. S4.3). A comparable correlation has been found for GDGTs in sediments from Lake Chala (Kenya/Tanzania) and was interpreted to derive from in-situ production of brGDGTs in the lake's anoxic bottom waters (Sinninghe Damsté et al., 2012a). Lake Stymphalia as a very shallow lake with a modern average water depth of about 0.8 m, is unlikely to develop anoxic bottom waters, where production of GDGT-0 might occur. However, the lake's historic water-level might have been higher until later reduced due to water withdrawal via an aqueduct built in the 2nd century AD that transported water from Lake Stymphalia to the city of Corinth situated ca. 40 km to the north (Walsh et al., 2017a). Both ratios, however, the %GDGT-0 and BIT, were affected by the amount of crenarchaeol, which was highly variable in sediments from Lake Stymphalia (Fig. 4.5). High contribution of pedogenic thaumarchaeal GDGTs characterized the period between 13,500 and 10,100 yr BP, when BIT values were minimal.

The brGDGT-based reconstruction of MAAT showed a temperature increase from 16 to 18°C in the period from 14,700 to 10,500 yr BP. The HDI_{26} indicated lowest SWTs in the oldest samples and a rapid increase in SWT to 21 °C thereafter. Although showing a similar temperature trend during stage I, absolute temperature estimates between both proxies differed by 1.1 to 8.6 °C for the entire record. This offset may be explained by (1) the environmental compartments reflected by the proxies (water vs. air temperature) and/or (2) a different seasonality captured by both proxies as the HDI_{26} is considered to indicate summer

SWT (Bauersachs et al., 2015a). The overall trend seen in both proxies reflected increasing temperatures from the cold Late Glacial period to the warmer early Holocene. A distinctive Younger Dryas cold event cannot be identified, which is compatible with a previous study on Lake Stymphalia (Heymann et al., 2013). In the marine record though, a Younger Dryas cooling was noted for the wider Aegean region (Rohling et al., 2002; Kotthoff et al., 2008, 2011; Kuhnt et al., 2008). At Lake Stymphalia a minor cooling event of about 0.5°C between 12,500 and 11,600 yr BP coincided with the time of the Younger Dryas cold event. This moderate local cooling might be explained by the isolated position of the Stymphalia polje in an elevated mountain valley.

The dominance of both HG diols with 26 and 28 carbon atoms, respectively, is indicative for cyanobacteria of the family *Nostocaceae* including *Anabaenopsis*, *Aphanizomenon and Dolichospermum* (Gambacorta et al., 1998; Bauersachs et al., 2009a, 2017), whereas the HG_{30} triol has been reported from benthic Scytonemataceae (Gambacorta et al., 1999; Bauersachs et al., 2019). The presence of a HG_{28} diol with a pentose (C_5) sugar headgroup instead of a hexose (C_6) is unusual for a lacustrine sediment. Such HGs have been found as nC_{30} and nC_{32} triols or tetraols in marine sediments or strains of endosymbiotic heterocytous cyanobacteria (Schouten et al., 2013b; Bale et al., 2015, 2019). The only evidence for a freshwater cyanobacterium synthesizing a pentose headgroup is provided by a cultivation experiment employing an *Aphanizomenon ovalisporum* strain found in three Spanish freshwater reservoirs (Wörmer et al., 2012). Thus, a freshwater HG-producer may have been present in early Lake Stymphalia.

4.5.2.2 Early Holocene - Stage II (10,093 – 9,585 yr BP)

The second stage of Lake Stymphalia was initiated by an abrupt increase in temperature of about 3°C around 10,000 yr BP that has not been reported in literature before. This dramatic change could have been triggered by a sinking lake level resulting in heliothermic heating of the shallow water and thus presumably was a local phenomenon. Increasing input of soil derived brGDGTs and less methanogens indicated a stronger allochthonous influence, leading to a community shift in archaea as expressed in a decreased Cren'/cren ratio. A concomitant pH shift to more acidic conditions (pH: <7), which could have been promoted by a water low-stand and a diminished calcium carbonate ($CaCO_3$) influx, can be deduced from low TIC values. The temperature increase may have led to an increase in lake productivity (TOC) and was inferred from the composition of terrigenic wax lipids, which suggested a more grass-derived input.

4.5.2.3 Mid Holocene - Stage III (9,447 – 5,234 yr BP)

During phase III the productivity increased constantly, while TOC/TN values of around 20 suggested a mixed signal of aquatic and terrestrial derived organic matter. For the interval between 7,500 and 8,900 yr BP, TOC/TN values >20 indicated a predominance of terrestrial input (Meyers, 2003). The ACL values suggested a constant input of deciduous/evergreen angiosperms during the middle Holocene. This is supported by enhanced *Quercus sp.* and subordinate *Pinus sp.* pollen in Lake Stymphalia and Lake Lerna (NE Peloponnese) (Jahns, 1993; Walsh et al., 2017a). In the aquatic community, the cyanobacteria population changed to a dominance of *Dolichospermum sp.* (former *Anabaena sp.*) as indicated by the predominance of the HG_{28} diol, while the corresponding pentose homologue decreased to a minimum.

At 8,290 yr BP an environmental perturbation may have affected Lake Stymphalia. The amount of GDGT-0 over crenarchaeol increased drastically and was accompanied by a heavy $\delta^{13}C_{org}$ signature of almost -23‰. Less negative $\delta^{13}C_{org}$ values in lake sediments have been associated with phases of elevated algae productivity (Meyers, 2003), which would be in accordance with an increase in aquatic macrophytes and heterocyte cyanobacteria in Lake Stymphalia. Simultaneously, the GDGT-reconstructed MAAT dropped by more than 3°C. In parallel, the different GDGT composition for this interval may indicate a massive change in the microbial association. The environmental disturbance in the Lake Stymphalia record coincides with the 8.2 ka event (Alley et al., 1997), which has been identified previously in records from Tenaghi Philippon (NE Greece) and the Aegean Sea (Kotthoff et al., 2008; Peyron et al., 2011). Despite of the coevolution of the environmental perturbation at Lake Stymphalia with the 8.2 ka event, the increase in lake level and the warmer temperatures stand in opposition to the cold and dry character of the 8.2 ka event (Alley et al., 1997; Robinson et al., 2006). Previous studies of the lake based on element distribution determined by XRF-scanning failed to detect a 8.2 ka event (Heymann et al., 2013). Following the 8.2 ka anomaly, the HDI_{26}-derived SWT decreased to about 20°C around 6,100 yr BP though this was not matched by GDGT-derived MAAT. Potentially, the mean annual temperatures remained constant, while the summer temperatures during maxima of heterocyte cyanobacteria production were constantly higher. In the second half of phase III the predominant brGDGT isomer switched from a 5-methyl to a 6-methyl predominance, which might be associated with a community shift in soil-derived bacteria. A positive relation between 6-methyl abundance and soil/lake pH (De Jonge et al., 2014; Dang et al., 2016) was not recognized in the Lake Stymphalia record.

4.5.2.4 Late Holocene – Stage IV (4,946 – 3,584 yr BP)

During phase IV, comprising the Early Bronze Age, the landscape around Lake Stymphalia was forested, while the TOC/TN ratio suggested that the organic matter derived from both

allochthonous land plant and autochthonous aquatic sources. In comparison with the low SWT values of the Neolithic, the HG-derived temperature increased by almost 5°C with the onset of the Bronze Age. Just before the end of the second phase between 4,000 and 3,900 yr BP, a short spell in the GDGT-reconstructed MAAT was noted, accompanied by a maximum SWT of about 27°C. This warmer spell coincided with a dry period reported for ancient Lake Lerna (Katrantsiotis et al., 2019). A short warm, arid period around 4,000 yr BP is also known from the Western Mediterranean, Eastern Mediterranean and Arabian Sea (Finné et al., 2011; Bini et al., 2019). Subsequently, a short decrease in BIT values and enhanced %GDGT-0 values suggested a reduced soil input accompanied with a higher proportion of methanogens, compatible with a deeper lake.

4.5.2.5 Late Holocene – Stage V (3,527 – 2,000 yr BP)

An increase in sedimentary %GDGT-0, BIT and TOC values characterized the onset of the Greek Late Bronze Age. Indications of enhanced methanogenesis and soil erosion reflect an intensification of anthropogenic impact onto the lake. Methanogenesis could have been associated with first agriculturalism and fertilization in the surrounding catchment area. Nowadays, methanogenesis is mainly found in episodically subaquatic paddy soils, which differ by a strongly elevated GDGT-0/crenarchaeol ratio from subaeric soils (Mueller-Niggemann et al., 2016). Opposite to the Neolithic, the Greek Bronze Age on the Peloponnese was characterized by intensive land use (Weiberg et al., 2016), corroborated by archaeological findings from the ancient city Stymphalos, dated to the early 3rd millennium BC., and from the Mycenaean period, suggesting human presence at the lake during the Bronze Age (Walsh et al., 2017a). Low P_{aq}, TIC and high BIT indicated a dry period corresponding with a low-stand of the lake, which may have affected the brGDGT-reconstructed temperature due to microbial community shifts. This was supported by a general change in GDGT proxies with the onset of phase III. The relative abundance of the crenarchaeol regioisomer dropped to almost <0.1, which is considered an intermediate value between aquatic (group 1.1a) and soil (group 1.1b) *Thaumarcheota*. (Pitcher et al., 2011; Sinninghe Damsté et al., 2012b). Furthermore, a change in the IR ratio from a predominance of the 6-methyl isomer during phase II to a predominance of the 5-methyl isomer in phase III occurred. The heterocyte cyanobacteria population changed to a predominance of species of the order Nostocales including *Dolichospermum sp.* (HG_{28} diol) and *Nodularia sp., Aphanizomenon sp.* and *Nostoc sp*. (HG_{26} diol) (Bauersachs et al., 2009a). The absence of longer-chain HGs with more than 30 carbon atoms from 2,800 years BP onwards indicates the lack of species of the order *Stigonematales* (Gambacorta et al., 1999; Bauersachs et al., 2013, 2014a).

Between 3,900 and 3,000 yr BP a period of great instability with two significant cold spells at 3,827 and 3,584 yr BP, accompanied by a decrease in carbonate content occurred in Lake Stymphalia. Coeval environmental changes were reported from Lake Dojran (northern Greece) for the same interval, with low productivity caused by lower temperatures (Francke et al., 2013). In the following ~1000 years Neugebauer et al. (2015) found two dry period from 3,500 to 3,300 yr BP and 3,000 to 2,400 yr BP in the Dead Sea region, while Finné et al. (2017) recognised generally wetter conditions around 3,200 yr BP in southern Peloponnese. For Lake Stymphalia, lipid temperature proxies indicate a warming trend from 3,580 to 3,330 yr BP, followed by an inverted temperature trend for the following 250 years. The HG-inferred SWT remained at warm 26°C, while the brGDGTs-based MAAT decreased to about 18°C. The discrepancy could be induced either by seasonality in bioproduction of the microbial organisms or by greater cyanophyte species diversity. The MAAT cooling at 3,580 to 3,330 yr BP occured contemporaneous with a time of high perturbation in Greek societies. At the end of the Greek Bronze Age (13th cent. BC), the Palatial Civilization collapsed and the Greek Dark Ages (13th to 8th cent. BC) began. In contrast to our colder GDGT-inferred MAAT, however, arid conditions were postulated as potential trigger for this phase (Drake, 2012). Aridity was reflected in enhanced δD values of terrigenic *n*-alkanes in sediments from Lake Lerna (Katrantsiotis et al., 2019). Due to the potentially intensive human impact on the Lake Stymphalia ecosystem, the reconstructed MAAT anomalies should be interpreted with caution when compared with other climate records.

4.6 Conclusion

Organic-geochemical analysis of Lake Stymphalia sediments revealed significant changes in environmental and climatic evolution during the Late Glacial to the late Holocene period. Local climate deterioration often did not comply with other records from the Peleponnese region. The lake's history could be divided in five phases based on GDGT distributions. The low TOC content of the sediments suggested a low productivity and poor preservation of organic matter due to mostly oxic conditions associated potentially with dry phases and corresponding low lake level. Terrigenic *n*-alkane distributions indicated vegetation shifts in the catchment of Lake Stymphalia. During the late Pleistocene, dense forests were replaced by open grasslands, accompanied by colder temperatures. With the onset of the warmer Holocene, forestation with deciduous trees began as expressed in enhanced nC_{27} alkane proportions. For the Bronze Age (~4,000 yr BP), an intensive human impact on the ecosystem was recognised by enhanced soil erosion, methanogenesis and shifts in microbial community structure. Paleotemperature reconstruction using the established brGDGTs-based MBT'_{5ME} proxy, complied with the heterocyte cyanobacteria-derived HDI_{26} proxy, which was applied for the first time to a lacustrine paleorecord.

Acknowledgments:

The research was conducted and financed in context of the Collaborative Research Centre 1266 “Scales of Transformation – Human –environmental interaction in prehistoric and archaic societies” of the German Research foundation (DFG, German Research Foundation – project number 2901391021 – SFB 1266).

Supplement material:

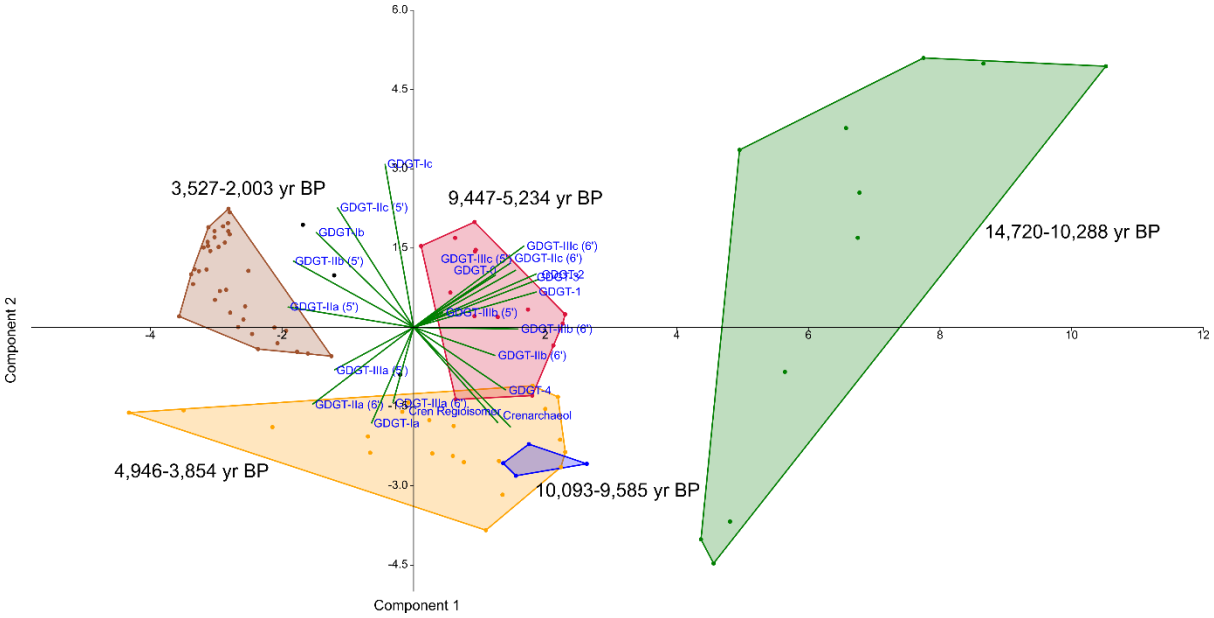

Figure S4.1: Principle component analysis (PCA) of GDGT for separation of the sediment core into 5 phases. Three samples (2,885; 8,290; 9,059 yr BP) were defined as outliers, due to deviant GDGT distribution.

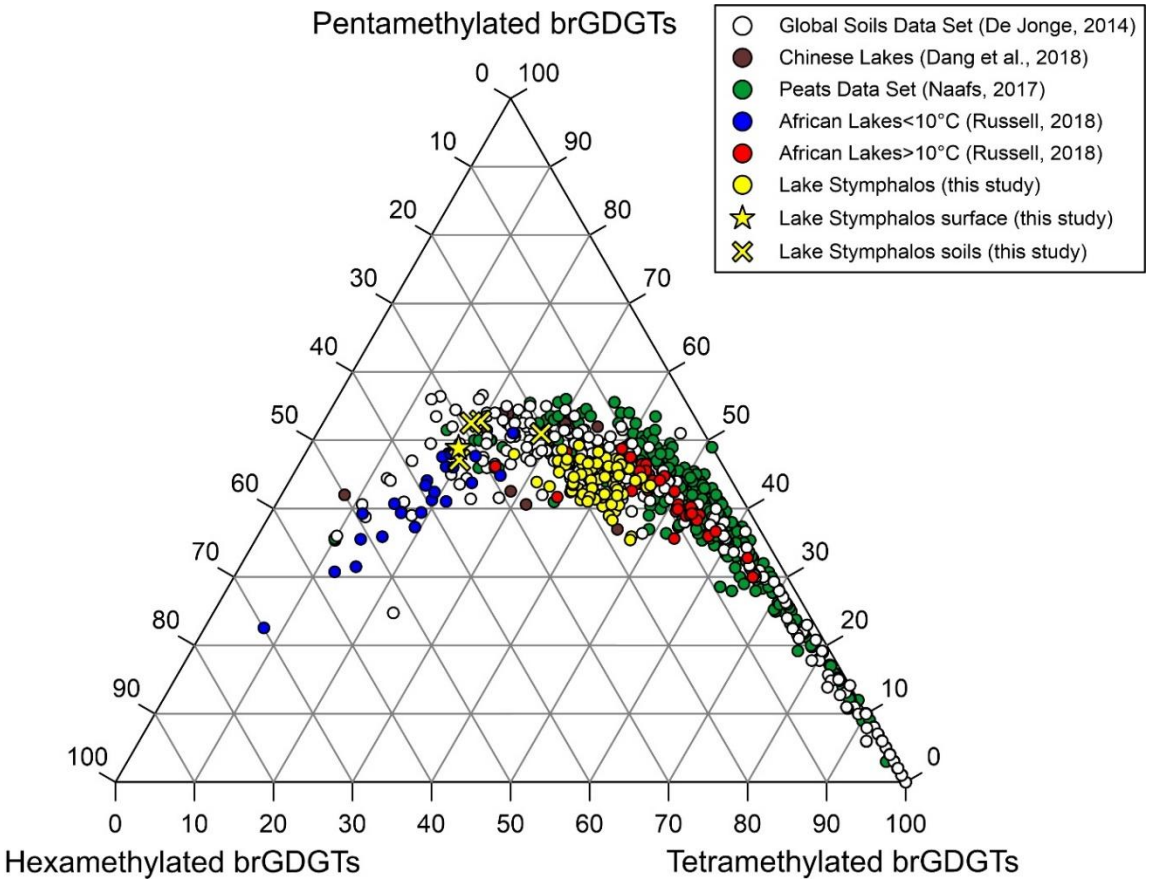

Figure S4.2: brGDGT data from Lake Stymphalia (yellow) in comparison with global data.

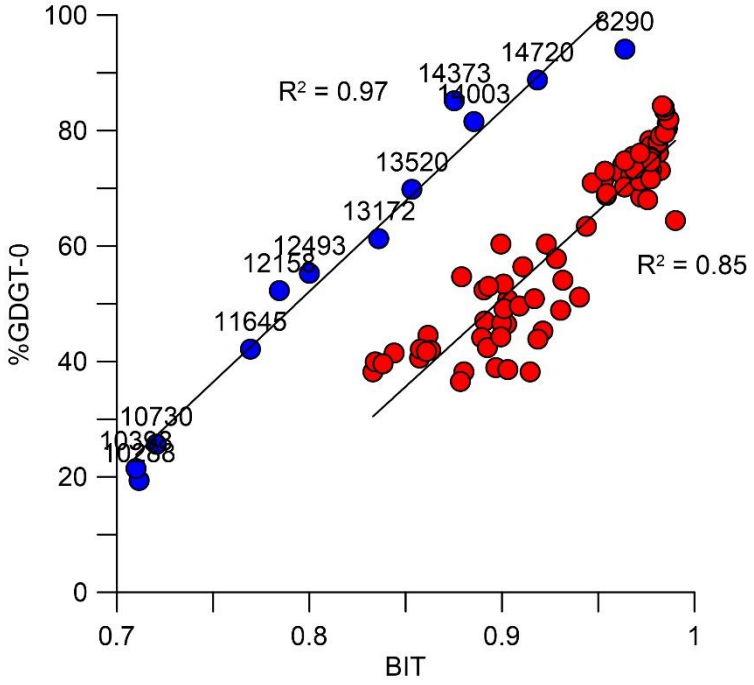

Figure S4.3: Correlation between %GDGT-0 and BIT index identifies two lake stages.

5. Organic residue analysis on ceramic vessels from Cucuteni-Trypillia sites in Ukraine and Moldova

5.1 Introduction

Chemical and isotopic analysis of organic residues from archaeological pottery vessels provide direct information about the dietary habits of ancient cultures and the function of different types of ceramic vessels (Evershed, 1993; Craig et al., 2011). Unfortunately, most biomolecules do not survive completely intact over archaeological periods, which is why the lipid composition in modern animal fats is not the same as in archaeological samples (Dudd and Evershed, 1998). For example, modern animal fats from sheep, goat, pig, cattle or dairy fats can be distinguished by their carbon atom number of triacyclglycerols (TAGs), but these lipids decompose over time and free fatty acids, mainly $C_{16:0}$ and $C_{18:0}$, are released (Mukherjee et al., 2007). Therefore, these fatty acids are diagnostic for degraded animal fat and have been documented by several archaeological studies on organic residues from pottery vessels (Evershed et al., 1990; Copley et al., 2005a; Spangenberg et al., 2006). Recent studies have used these free fatty acids to measure their specific carbon isotope ($\delta^{13}C$) values to distinguish their origin as their relative distribution is rather undiagnostic and influenced by numerous factors (Dudd and Evershed, 1998; Spangenberg et al., 2006; Gregg et al., 2009). These studies include the differentiation of animal products of ruminant and non-ruminant adipose fats, but also dairy and aquatic fats based on recording the $\delta^{13}C$ values of the two major fatty acids (Copley et al., 2003; Cramp et al., 2019). The major variations in $\delta^{13}C$ values of modern animal fats are interpreted as differences in the metabolism and physiology of the animals and the biosynthetic pathway of fats (Copley et al., 2003; Mukherjee et al., 2007; Roffet-Salque et al., 2017). Nevertheless, the $\delta^{13}C$ values can also be affected by the consumption of forage plants of different photosynthetic pathways (C_3 vs. C_4) and other environmental factors (Dunne et al., 2012; Roffet-Salque et al., 2017). Since the aim of this study is the characterization of lipid residues from archaeological ceramics from Cucuteni-Trypillia settlements in Ukraine and Moldova and no previous studies have been carried out in this region so far, we analysed modern reference fats from Ukraine to establish a local calibration.

The Neolithic/Eneolithic Cucuteni-Trypillia culture occurred between 5,400 and 2,700 BC in southwestern Europe, in the territory presently occupied by modern Ukraine, Moldova and Romania (Fig. 1.4) (Shukurov et al., 2015). The culture is characterised by their giant settlements or “mega-sites” with concentric rings of up to thousands of houses arranged around a central unbuild place, which at that time were probably the largest settlements in the

world (Chapman et al., 2019; Hofmann et al., 2019). Due to the enormous dimensions of the settlements, numerous inhabitants had to be supplied with food and natural resources by pastoralism and subsistence economy. Archaeozoological data revealed that the early Trypillia phase A was dominated by consumption of wild animals like red deer (*Cerus elaphus*) and wild boar (*Sus scrofa ferus*) and minor contributions of horses (*Equus caballus*), while domesticated animals were only consumed in minor amounts, though this portion increased in later phases (Kirleis and Dal Corso, 2016). Domesticated animals were dominated by cattle and pigs, while small livestock like sheep and goats were only found as supplements (Kirleis and Dal Corso, 2016). Phytolith analyses and macro remain analyses also evidence that numerous cereals and other plants were devoured (Kirleis and Dal Corso, 2016; Dal Corso et al., 2018).

5.2 Material and methods

5.2.1 Collection and extraction of modern reference fats

Dairy and adipose fats from cattle, sheep, goats and pigs were collected on local markets within rural villages in Ukraine during a field trip in 2018. All animals were raised on pure C_3 plant diet. Samples were kept refrigerated at 6°C during storage and transport. At Kiel University, the meat samples were lyophilized and a few milligrams of fat were extracted with a mixture of 5 ml dichloromethane:methanol (DCM:MeOH) (2:1 *v/v*, 2 × 10 min) by sonification. The solvent was evaporated to dryness under a gentle stream of nitrogen to obtain a total lipid extract (TLE). TLEs were then re-dissolved in DCM and derivatized by using *N*,*O*-bis(trimethylsilyl)trifluoroacetamide and pyridine (70°C, 60 min) for HTGC-MS analysis.

An aliquot of each sample was extracted using a direct-acidification-methanol extraction method to obtain fatty acid methyl esters (FAME) (Correa-Ascencio and Evershed, 2014). Briefly, animal fats were treated with 5ml H_2SO_4-methanol (4%, *v/v*) and heated for 4 hours at 70°C. Subsequently, 2 ml water (HPLC-grade) was added and lipids were extracted three times with 3 ml *n*-hexane and transferred into a clean vial. Combined *n*-hexane extracts were taken to dryness under a gentle stream of N_2. FAME derivatives were then re-dissolved in *n*-hexane for GC-MS and GC-C-IRMS analysis.

All carbon isotope values were corrected for the addition of one methyl carbon derived from methanol (-23.0‰) during transesterification of FAMES and corrected by +1.3‰ due to contribution of post-industrial carbon (Friedli et al., 1986).

5.2.2 Extraction of pottery vessels

Organic residue analysis were conducted on 28 pottery vessels excavated from five Cucuteni-Trypillia sites (Stolniceni, Volodymyrovka, Vesely Kut, Chyzhivka, Dobrovody) in Ukraine and Moldova following previously published extraction protocols (Copley et al., 2003). Briefly, sub-

samples were taken from intact pots and sherds were abraded with a Dremel tool to remove any exogenous contaminations from handling and soil. Subsequently, the samples were crushed with a solvent washed mortar and pestle. 3-4 g crushed potsherds were extracted by ultrasonication with DCM:MeOH (2:1 *v/v*, 3 × 5 ml). All supernatants were combined and filtered through $NaSO_4$ to remove any water and clay particles. Solvents were removed by evaporation to dryness under a gentle steam of nitrogen (N_2) to obtain a total lipid extract (TLE). An aliquot of each sample was trimethylsilylated by adding 30 µl of *N*,*O*-Bis(trimethylsilyl)trifluoroacetamide and pyridine (70°C, 60 min), and analysed by high-temperature gas chromatography-mass spectrometry (HTGC-MS).

An aliquot (~2g) of surface-cleaned sherd was extracted again using a direct acidified methanol extraction to obtain FAME as described above for the reference fats. An aliquot of the FAME extract was separated over aluminium oxide with *n*-hexane:DCM (95:5, *v/v*) yielding *n*-alkanes and *n*-hexane:DCM (1:2, *v/v*) affording FAMEs.

5.2.3 GC-MS and GC-C-IRMS analysis

High-temperature gas chromatography-mass spectrometry (HTGC-MS)

HTGC-MS for TLE measurements were performed using an Agilent 7890A GC equipped with a Phenomenex ZB-1HT (10m × 0.25mm × 0.25µm) column connected to a Phenomenex ZB-5HT Inferno (5m × 0.25mm × 0.25µm) column coupled to an Agilent 5975B mass spectrometer. 1 µl of dissolved TLE was inject splitless at an injector temperature of 350°C. The oven temperature was held at 80°C for 2 min, after which the temperature was raised to 400°C at 8°C/min and held for 1 min. Transfer line temperatrure was 350°C and the MS was operated at an electron energy of 70 eV, scanning the range of m/z 50-750 Dalton.

GC-MS analysis on FAMEs were performed using an Agilent 7890A GC equipped with an Agilent DB-5 (30m x 0.25mm) column coupled to an Agilent 5975B mass spectrometer. 1 µl of dissolved TLE was inject splitless at an injector temperature of 320°C. GC oven temperature was set to 40°C, held for 2 min and then ramped to 240°C at 15°C/min and held isothermal for 15 min. Transfer line temperatrure was 320°C and the he MS was operated at an electron energy of 70 eV scanning the range of m/z 50-750 Dalton. Peak identifications were performed using NIST14 mass spectral database, published mass spectra and retention time.

Gas Chromatography-Combustion-Isotope Ratio Mass Spectrometry for $\delta^{13}C$ Analysis (GC-C-IRMS)

GC-C-IRMS analyses was performed using a Thermo Delta V Plus isotope ratio mass spectrometer coupled to a Thermo Fisher Trace 1310 GC. Samples were diluted in *n*-hexane and 1 µl was injected onto an Agilent DB-5 (30m × 0.25mm) column in split mode with a split

ratio of 50:1. The temperature program was 2 min isothermal at 40°C followed by an increase of 12°C/min to 250°C and 7°C min at 250°C isothermal. The combustion reactor consisted of a NiO tube filled with CuO, NiO and Pt wires and was maintained at 850°C. The ion intensities of m/z 44, 45, and 46 were monitored and the $^{13}C/^{12}C$ ratios of each sample peak were automatically computed by comparison with a standard reference of known isotopic composition. Each sample was run in duplicate. External standards were run every 8 samples. Instrument precision and accuracy of FAME isotope standard analyses were better than 0.5‰. $\delta^{13}C$ values of samples were corrected for the carbon atom addition derived from methanol (-23.0‰) during methylation using mass balance equations.

5.3 Results

5.3.1 Lipid and isotopic composition of modern reference fats

$\delta^{13}C$ values of 19 modern reference fats are shown in figure 5.1. The species have been grouped using a *p*= 0.683 (1σ) confidence ellipse drawn around them. Since the cattle and sheep adipose fats show similar values and both contribute to the ruminant animals, they are grouped in one confidence ellipse. The mean $\delta^{13}C_{16:0}$ values of dairy fats from cow milk and goat milk are -26.67 and -23.43‰, respectively, while the mean $\delta^{13}C_{18:0}$ values are -33.16 and – 29.39‰ (Fig. 5.1). The mean $\delta^{13}C_{16}$ values of ruminant adipose fats of cattle and sheep are -25.18 and -24.1‰, respectively, while the corresponding $\delta^{13}C_{18}$ values are more depleted in ^{13}C resulting in lower values of -27.8 and -27.47‰, respectively. Porcine adipose fats obtain mean $\delta^{13}C_{16:0}$ and $\delta^{13}C_{18:0}$ values of -22.17 and -22.37‰.

$\Delta^{13}C$ (= $\delta^{13}C_{18:0}$ - $\delta^{13}C_{16:0}$) values of dairy fats from cattle range between -8.4 and -5.6‰, while goat milk fats range from -6.68 to -4.92‰ (Fig. 5.2). Ruminant fats from cattle and sheep are significantly different with mean values of -2.62 and -3.37‰, respectively. Non-ruminant fats from porcine range between -1.15 and 1.27 ‰ (mean -0.2‰).

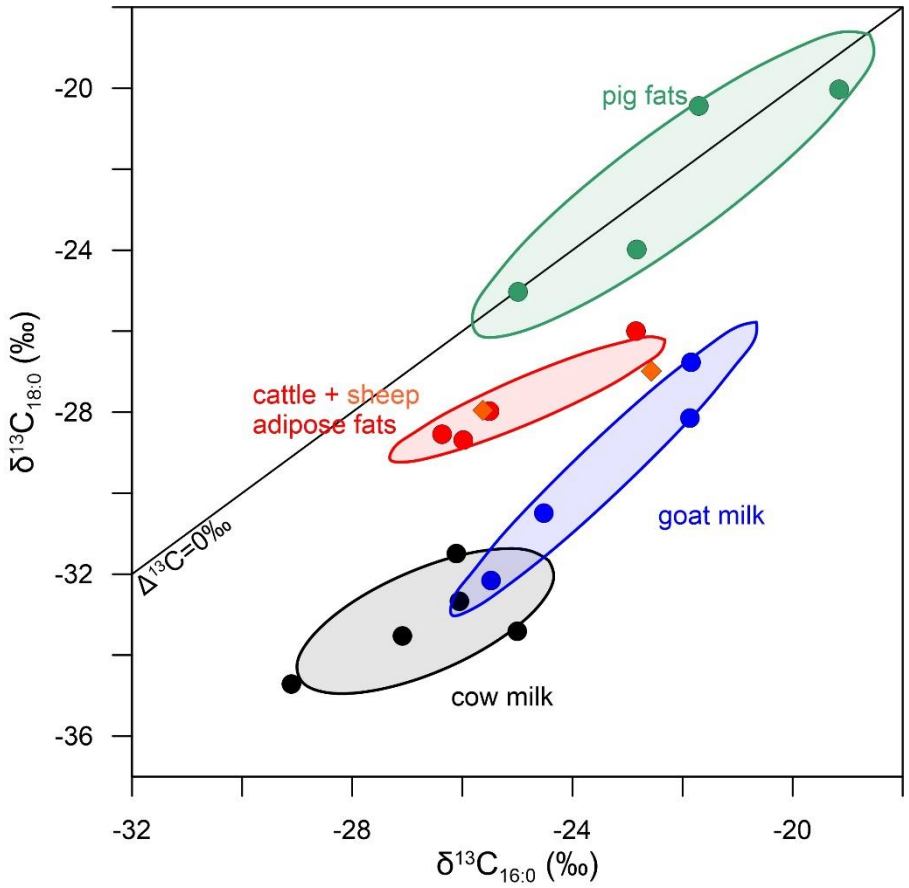

Figure 5.1: Plot of the $\delta^{13}C$ values of individual saturated fatty acids $C_{16:0}$ and $C_{18:0}$ obtained from modern reference fats from the Ukraine. Values of cattle and sheep adipose fats are combined to one reference field. The fields designated correspond to 1σ confidence ellipses calculated from the $\delta^{13}C$ values of fatty acids.

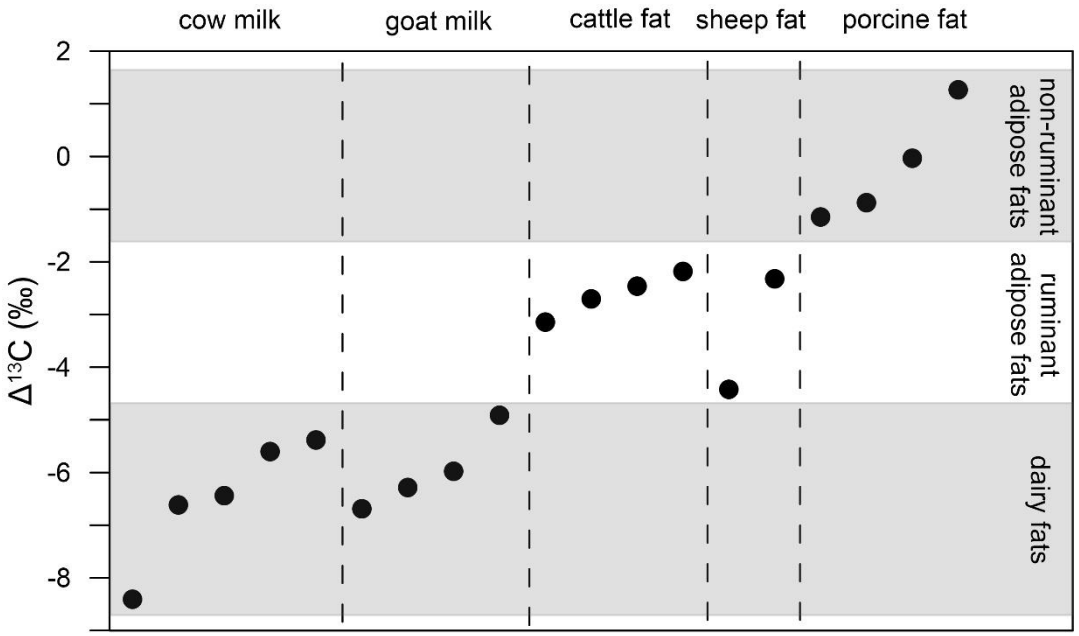

Figure 5.2: Plot of the $\Delta^{13}C$ (= $\delta^{13}C_{18:0}$ - $\delta^{13}C_{16:0}$) values of modern reference fats from the Ukraine.

5.3.2 Lipid and isotopic composition of pottery vessels

25 of 28 pottery vessels (89%) yielded sufficient amounts of lipids for further interpretation (Table 5.1 and 5.2). GC-MS analysis revealed that the majority of sherds were dominated by palmitic ($C_{16:0}$) and stearic ($C_{18:0}$) fatty acids (Fig. 5.3) with a P/S ratio ranging between 0.41 and 2.53 typical for degraded animal fats (Evershed et al., 2002). Approximately 64% of all samples contain monoacylglycerols (MAGs), while di- and triacylglycerols (DAGs/TAGs) are only present in minor contributions. In two sherds (Ves-1017, Chy-1011-2) alkyl monoesters (C_{40}-C_{50}), long-chain *n*-alkanes (nC_{25}-nC_{31}) and long-chain *n*-alcohols (nC_{24}-nC_{32}) were present. In addition, hydroxyl fatty acyl monoesters were also detected in Ves-1017 (Fig. 5.4). These in combination with the previously mentioned lipids, are typical for beeswax (Roffet-Salque et al., 2015).

$\Delta^{13}C$ and $\delta^{13}C$ values of $C_{16:0}$ and $C_{18:0}$ fatty acids were measured from 22 pottery vessel samples and plotted in a discrimination diagram containg reference values (ellipses) of modern fats from Ukraine and from Kazakhstan (Outram et al., 2009) (Fig. 5.5 and 5.6). $\delta^{13}C_{16}$ values range between -30.25 and -25.23‰, while the $\delta^{13}C_{18}$ values vary from -36.25 to -26.25‰. The $\Delta^{13}C$ values obtained from potsherds range from -6.0 to 1.28‰ and thus cover all three reference fields (Fig. 5.6). Most samples plot close to the $\Delta^{13}C$ = 0‰ line in the $\delta^{13}C_{16}$ vs $\delta^{13}C_{18}$ graph. However, they do not fall within a reference ellipse for modern non-ruminant, ruminant or dairy fats from Ukraine. It is suggested that an appreciable number of residues from especially Stolniceni and Volodymyrovka are derived from equine products. In the $\Delta^{13}C$ vs $\delta^{13}C_{16}$ plot, which excludes environmental factors, the predominant values are characteristic for non-ruminant fats (porcine or equine?) (59%), followed by ruminant (32%) and dairy products (9%).

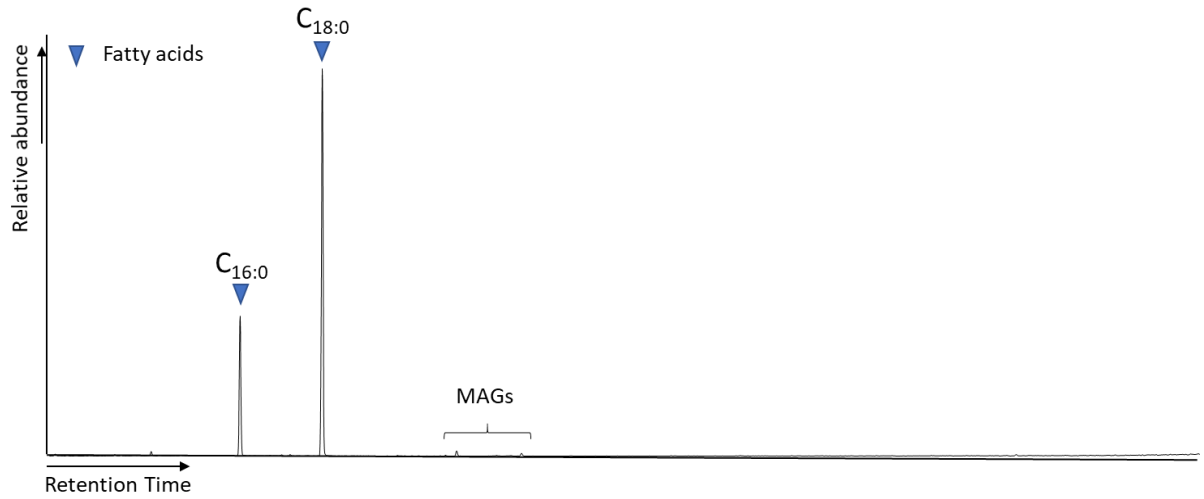

Figure 5.3: Chromatogram of sherd Vol-1078-2 from Volodymyrovka indicative for degraded animal fats. MAGs = monoacylglycerols.

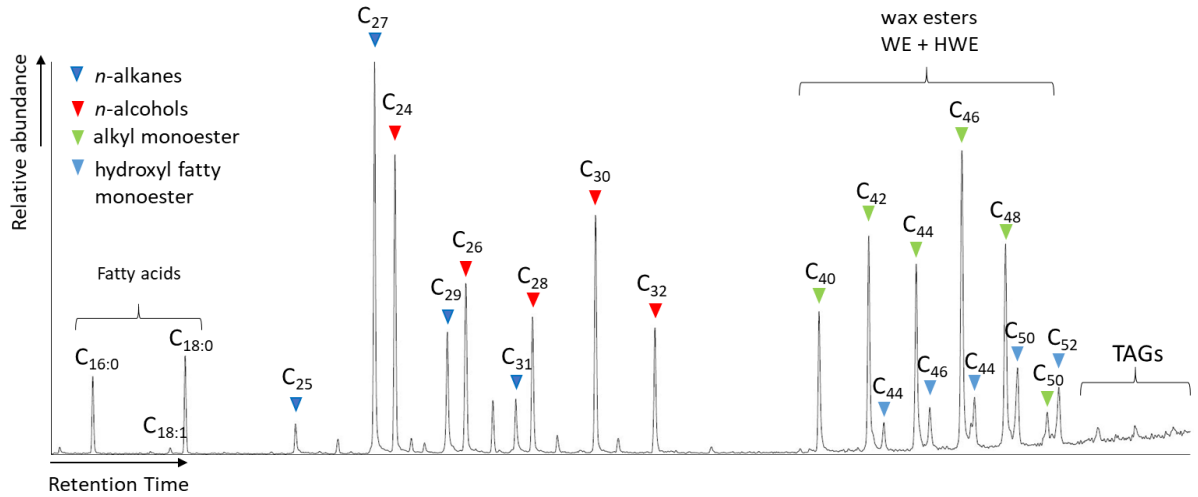

Figure 5.4: Chromatogram of sherd Ves-1017 from Vesely Kut indicative of beeswax and minor contributions of animal fats. Blue = *n*-alkanes, red = *n*-alcohols, green = *n*-alkyl monoester (WE), blue = *n*-hydroxyl fatty monoesters (HWE), TAGs = triacylglycerols.

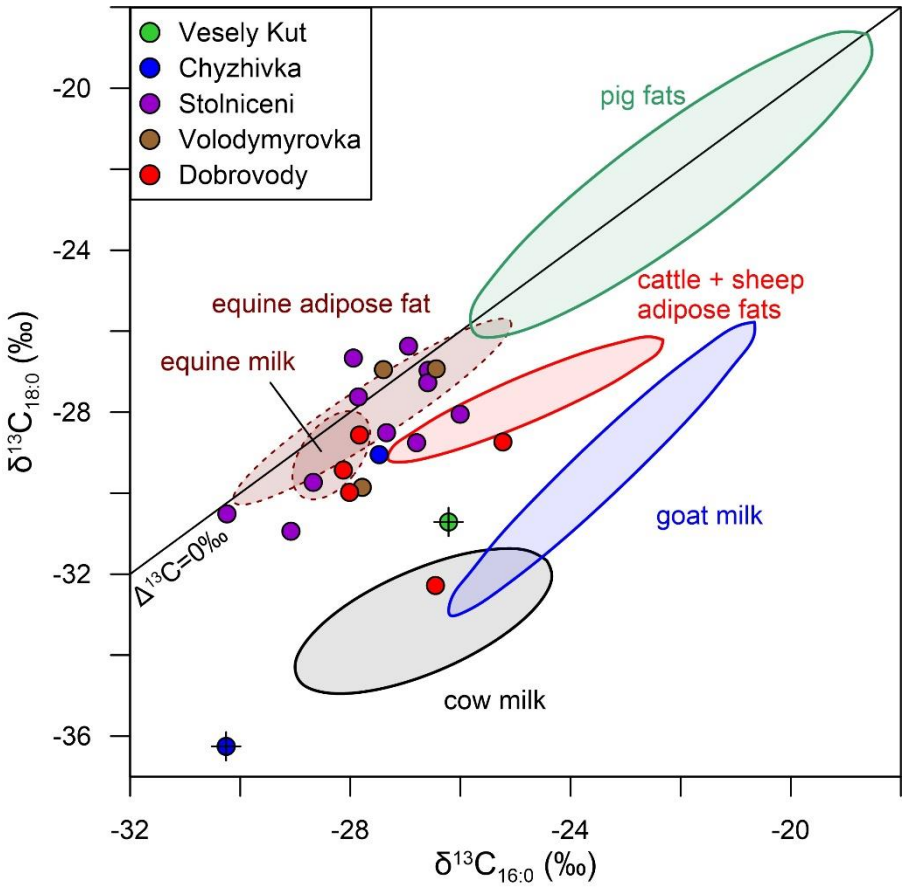

Figure 5.5: Scatter plot of the $\delta^{13}C$ values of the $C_{16:0}$ and $C_{18:0}$ fatty acids from residues of Cucuteni-Trypillia pottery vessels. All confidence ellipses correspond to modern to reference fats from the Ukraine (this study) and a previous study on equine fats from Kazakhstan (Outram et al., 2009). Both samples marked with a cross contain large amounts of lipids indicative for beeswax.

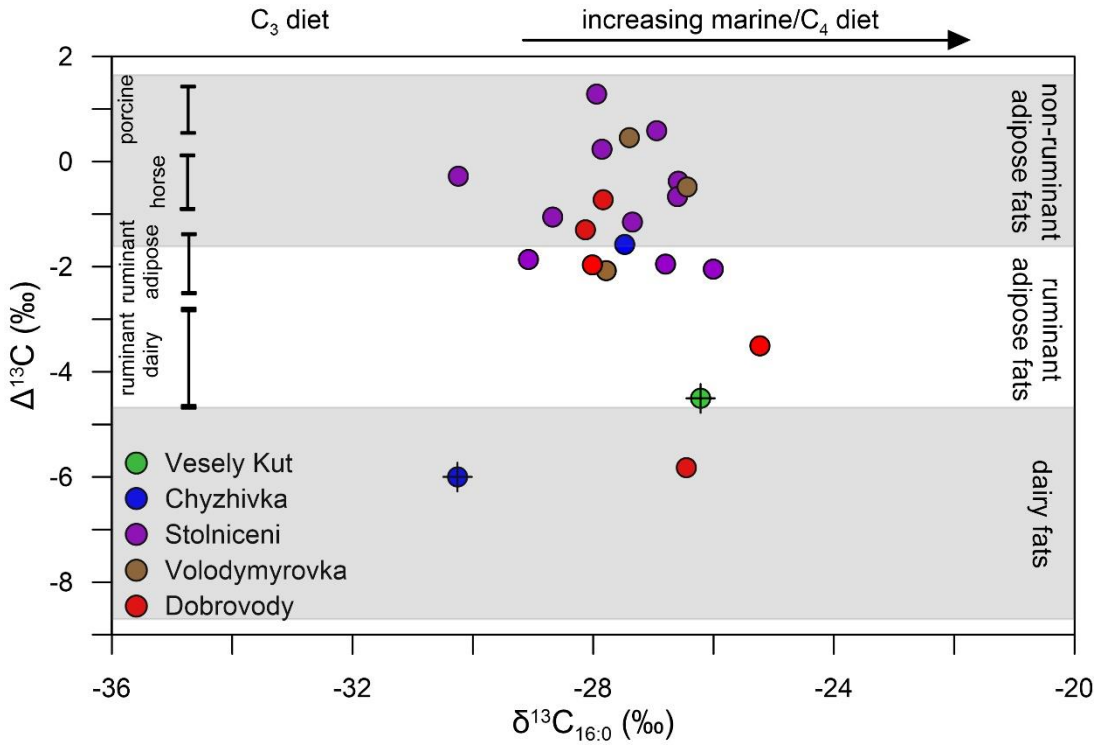

Figure 5.6: Plot of the $\Delta^{13}C$ and $C_{16:0}$ values from residues of Cucuteni-Trypillia pottery vessels. Reference ranges were obtained from modern reference fats from Kazakhstan (left, Outram et al., 2009) and Ukraine (right, this study). Both samples marked with a cross contain large amounts of lipids indicative for beeswax.

5.4 Discussion

5.4.1 Modern reference fats

The ruminant dairy fats from goat and cattle plot below the 1:1 line in the $\delta^{13}C_{16}$ vs. $\delta^{13}C_{18}$ diagram and have lower $\delta^{13}C$ values as the corresponding adipose fats from sheep and cattle, compatible with previous studies (Copley et al., 2003; Outram et al., 2009; Craig et al., 2011). In contrast, porcine fats plot close to the 1:1 line, which can be explained by the different metabolism of ruminant and non-ruminant animals (Dudd and Evershed, 1998). However, some $\delta^{13}C$ values, in particular from porcine adipose fats and goat dairy fats, isotopically are slightly heavier than shown in previous studies which may indicate a contribution of isotopically heavier forage like C_4 plants (Roffet-Salque et al., 2017).

It has been postulated that ruminant dairy fats can be distinguished from adipose fats by having lighter $\Delta^{13}C$ values offset by > -3.1 or -3.3‰ (Copley et al., 2003; Dunne et al., 2012). Our data confirms the global applicability of a threshold around $\Delta^{13}C$ = -3‰, except for one sheep sample, which shows an exceptionally light $C_{16:0}$ value resulting in a low $\Delta^{13}C$ value of -4.42 (Fig. 5.6). Similarly, the separation between ruminants and non-ruminant adipose fats is shifted to slightly lighter $\Delta^{13}C$ values than previously stated (Copley et al., 2003). Our set of modern fats did not contain equine meat/milk refernces. Since it is under discussion whether

the Cucuteni-Trypillia culture has also kept or even consumed horses, we have adopted the carbon isotope values of horse adipose and dairy fats from a previous study including modern reference fats from Kazakhstan (Outram et al., 2009).

5.4.2 Archaeological context

Stable isotope analysis on human bone collagen from the Neolithic and Eneolithic in Romania, roughly coeval to the Cucuteni-Trypillia culture, suggested that humans utilised primary terrestrial resources from ruminant animals like cattle and goat/sheep (Honch et al., 2006). This is in good agreement with an archaeological record spanning the Neolithic to the Copper Age in Eastern Hungary, which indicates that predominantly animal meat from domesticated animals was devoured, while dairy products did not play a major dietary role (Hoekman-Sites and Giblin, 2012).

However, so far little is known about the diet and animal husbandry of the Cucuteni-Trypillia culture. Although there is archaeological evidence on the type of the animals used, either for people's diet or as draught animals, this is the first direct evidence indicating that animals were used as staple food. Bone assemblages from Cucuteni-Trypillia sites indicated that preferential domestic animals like cattle, pigs and a minor proportion of sheep/goats were consumed rather than wild animals like deer and wild boar (Shukurov et al., 2015). In addition, the proportion of wild animals decreased from the Early Trypillia A to Late Trypillia C (Shukurov et al., 2015). The carbon isotopic values of the potsherds from the five sites indicate a predominant non-ruminant adipose origin, especially in comparison with modern reference fats from Kazakhstan having an equine adipose and/or dairy origin (Fig. 5.5). This is very striking, since horse bones have been found only to a small amount and were primarily interpreted as draught animals (Shukurov et al., 2015). Since one sample each from Stolniceni and Dobrovody fell into the reference ellipse for horse milk, this could be an indication for utilization of domesticated horses. However, most samples that fell into the equine adipose fat ellipse may derive from game animals. Earlier evidence of horse domestication, both for nutrition and in a mortuary rite, was reported for Eneolithic and Bronze Age cultures from Kazakhstan (Outram et al., 2009, 2011). Since, however, the $\Delta^{13}C$ values fell into the field of pig fats from Ukraine, which overlap with the equine fats field, a porcine origin cannot be excluded completely.

Fats from ruminant animals like cattle, sheep and goats are the second abundant class found in the residue analysis. Since red deer and roe deer bones were also found in large quantities atTrypillia sites, their corresponding fats were probably also processed in the pots (Shukurov et al., 2015). However, since deer fats have $\Delta^{13}C$ values lighther than -3.3‰ and thus similar to dairy products, only two samples can be considered to be of deer origin (Craig et al., 2012). One of these samples, however, is very rich in beeswax, with the result that the isotopic signal

should be interpreted with caution since a portion of $C_{16:0}$ and $C_{18:0}$ fatty acids will have been released upon hydrolyses of wax esters in beeswax. Pure ruminant dairy products were observed just in one sample indicating that animals were primary utilized for their meat. The two findings of beeswax in the pottery vessels from Vesely Kut and Chyzhivka indicate that prehistoric humans exploited the honeybee. Beeswax was an important commodity used for sealing of pots, as ingredient in medicine and cosmetics or probably later as fuel for illumination (Mayyas et al., 2012). The findings of beeswax also imply the use of honey as sweetener or as source of fermented beverages (Heron et al., 1994). In a synthesis publication on beeswax findings in pottery vessels, the Eurasian Steppe region north of the Black Sea lacked any evidence of beeswax residues. This has been explained by the ecological limit of the honeybee (*Apis mellifera*) during this time (Roffet-Salque et al., 2015). Our results though manifest that the honeybee either already existed in the region north of the Black Sea or beeswax/honey was imported through trade from Anatolia, where it had been used since the 7^{th} millennium BC (Evershed, 2008; Roffet-Salque et al., 2015).

Specific compounds like ω-(o-alkylphenyl) alkanoic fatty acids (APAAs), isoprenoid fatty acids and dihydroxy fatty acids have been established as diagnostic biomarker for aquatic resources (Hansel et al., 2011; Cramp and Evershed, 2014). As aquatic biomarkers are absent in the ceramic samples, a major diet based on fish or other aquatic animals can be excluded and a subsistence economy based on terrestrial animals is more likely.

Sample	Site	Period	lipid conc. (µg/g)	$C_{16:0}FA/C_{18:0}FA$	MAGs	DAGs	TAGs	Wax ester	Hydroxyl fatty acyl monoesters	*n*-Alcohols	*n*-Alkanes	$\delta^{13}C_{16}FA$ (‰)	$\delta^{13}C_{18}FA$ (‰)	$\Delta^{13}C$	Interpretation
Ves-1017	Vesely Kut	Trypillia BI/BII (4100-4000 BCE)	13.09	0.74				C_{40}-C_{50}	C_{44}-C_{52}	C_{24}-C_{32}	C_{25}-C_{31}	-26.21	-30.71	-4.50	beeswax
Ves-1012	Vesely Kut		0.00												empty
Ves-1011	Vesely Kut		7.12	0.75		C_{32}-C_{36}	C_{46}-C_{54}					n. d.	n. d.	n. d.	animal fat
Chy-1010	Chyzhivka	Trypillia BI/BII (4100-4000 BCE)	3.21	0.72	C_{16}, C_{18}							-27.47	-29.05	-1.58	ruminant/non-ruminant adipose
Chy-1011-1	Chyzhivka		14.35	0.92	C_{16}, C_{18}							n. d.	n. d.	n. d.	animal fat
Chy-1011-2	Chyzhivka		45.30	1.64	C_{16}, C_{18}		C_{46}-C_{54}	C_{40}-C_{48}		C_{24}-C_{32}	C_{25}-C_{31}	-30.25	-36.25	-6.00	beeswax + ruminant dairy
Sto-7003	Stolniceni	Trypillia BII (3950-3850 BCE)	10.69	1.45	C_{16}, C_{18}	C_{32}-C_{36}	C_{48}-C_{54}					-29.08	-30.94	-1.86	ruminant adipose
Sto-7981	Stolniceni		13.78	1.56	C_{16}, C_{18}	tr	tr					-26.59	-26.97	-0.38	equine?
Sto-70075	Stolniceni		24.20	0.74	C_{16}, C_{18}	C_{32}, C_{34}	C_{46}-C_{50}					-26.01	-28.05	-2.04	ruminant adipose
Sto-11046	Stolniceni		8.52	1.35								-27.85	-27.62	0.24	equine?
Sto-13092	Stolniceni		27.97	1.27								-26.60	-27.27	-0.67	equine?
Sto-13093	Stolniceni		2.16	0.42	C_{16}, C_{18}							-26.95	-26.37	0.58	equine?
Sto-13094	Stolniceni		18.70	2.27	C_{16}, C_{18}	tr	C_{50}-C_{52}					n. d.	n. d.	n. d.	
Sto-13106	Stolniceni		1.29	0.44								-30.24	-30.52	-0.28	equine?
Sto-13108	Stolniceni		656.49	1.06								-28.67	-29.73	-1.06	equine?
Sto-13109	Stolniceni		27.84	1.70			C_{48}-C_{54}					-27.35	-28.50	-1.15	equine?
Sto-13113	Stolniceni		12.21	0.71	C_{16}, C_{18}							-26.80	-28.75	-1.95	ruminant adipose
Sto-7300	Stolniceni		35.52	1.13	C_{16}, C_{18}							-27.94	-26.66	1.28	equine? porcine?

Table 5.1: Summary of the results from biomolecular analyses and carbon isotope analyses of individual fatty acids from Cucuteni-Trypillia sites in Ukraine and Moldova. tr = traces.

Sample	Site	Period	lipid conc. (µg/g)	$C_{16:0}FA/C_{18:0}FA$	MAGs	DAGs	TAGs	Wax ester	Hydroxyl fatty acyl monoesters	*n*-Alcohols	*n*-Alkanes	$\delta^{13}C_{16}FA$ (‰)	$\delta^{13}C_{18}FA$ (‰)	$\Delta^{13}C$	Interpretation
Vol-1035	Volodymyrovka		0.00												empty
Vol-1047	Volodymyrovka	Trypillia BII (3950-3850 BCE)	0.00												empty
Vol-1062	Volodymyrovka		7.45	2.17	C_{16}, C_{18}							-27.78	-29.86	-2.08	ruminant adipose
Vol-1078-1	Volodymyrovka		1.72	2.53	C_{16}, C_{18}							-27.40	-26.94	0.46	equine?
Vol-1078-2	Volodymyrovka		1.82	0.41	C_{16}, C_{18}							-26.44	-26.92	-0.48	equine?
Dob-1	Dobrovody		1.11	1.56	C_{16}, C_{18}	tr						-27.83	-28.56	-0.73	equine?
Dob-2	Dobrovody	Trypillia C1 (3800-3680 BCE)	4.31	2.24								-28.02	-29.98	-1.97	ruminant adipose
Dob-3	Dobrovody		0.92	0.67	C_{16}, C_{18}					tr	tr	-26.45	-32.28	-5.83	dairy
Dob-4	Dobrovody		2.56	1.58								-28.13	-29.43	-1.30	equine?
Dob-5	Dobrovody		3.03	1.11	C_{16}, C_{18}							-25.23	-28.73	-3.50	ruminant adipose

Table 5.2: Summary of the results from biomolecular analyses and carbon isotope analyses of individual fatty acids from Cucuteni-Trypillia sites in Ukraine and Moldova. tr = traces, n. d. = no data

6. Grave gifts manifest the ritual status of cattle in Neolithic societies of northern Germany

Abstract

The Neolithic period in NW-Europe marks a time of major transformation in human lifestyle including sedentism, farming, agropastoralism with early animal husbandry and the use of ornamented pottery by “Funnelbeaker” societies. Domestic animals, in particular cattle, served for traction, plowing, and manuring to support agricultural production but also supplied a variety of dietary products including meat, fat, and milk as well as wool. The impact of animal husbandry on improved living conditions in Neolithic societies and in a religious context has been inferred throughout NW-Europe and even earlier in African and Arabian regions by ritual cattle deposits. However, a potential spiritual/religious role of cattle in Neolithic societies is difficult to assess further due to the lack of interpretable Neolithic illustrations. Here, we demonstrate the ritual role of cattle in Neolithic societies from burial gifts preserved in Megalith tombs (3640 – 2900 BC) of Wangels, NW-Germany, where storage vessels for afterlife alimentary provision of the deceased contained cattle meat and milk products identified by their characteristic lipids but no common aquatic food sources or cereals. Pottery from the latest burial phase only yielded fatty acids which may derive from essential plant oils of Sea Buckthorn (*Hippophae rhamnoides*) that may have served as precious burial gift for medical or for alimentary purposes. The status of cattle as an object of veneration in Neolithic societies is represented by its dominating contribution to grave gifts underlining the esteem cattle received not only in agroeconomical but even further in ritual and religious respect.

6.1 Introduction

The Neolithic in Europe and the Middle East comprised a period of innovations in farming practices based on emmer or einkorn crops and agropastoralism with early animal husbandry. The domestication of cattle started during the 9th millennium BC in the Fertile Crescent region in the Middle East, while cattle domestication reached Central Europe only about 3000 years later (Scheu et al., 2015). Domesticated cattle were not only employed in more efficient farming activities like plowing and manuring to increase fertility and agricultural production but also supplied a variety of everyday alimentary products including meat, fats, and milk but also other commodities, e.g. horn and wool (Sherratt, 1983; Bogaard et al., 2013). Lipid analysis on pottery vessels indicate that ruminant milk processing took place since the 6th millennium in Eastern and the 5th millennium in Western and Northern Europe (Copley et al., 2005a; Craig et al., 2005; Isaksson and Hallgren, 2012).

In addition to the use of cattle as livestock and nutritional source, cattle held an important position in the religious and/or ritual context of Neolithic cultures, which is manifested by ubiquitous cattle deposits in Central Europe (Pollex, 1999; Kolodziej, 2011). Cattle burials are either connected to human graves or found individually, whereby cattle are usually laid down intact, but also in pieces, and a fire was lit on the cattle bodies. This procedure has been observed in the context of the early Bernburg culture society around 3100 BC (Müller and Schunke, 2014) or the western Globular Amphora culture (GAC) societies (Johannsen and Laursen, 2010; Woidich, 2014). Thus, it has been thought that cattle burials served to worship deceased animals, or cattle were sacrificed to e.g. humans or natural forces (Pollex, 1999; Kolodziej, 2011). The outstanding role of cattle in a ritual context is reported further from other cultures and regions, including archaeological sites from Arabia (McCorriston et al., 2012) and the Sahara (di Lernia, 2006) region of the 7th millennium or from the Viking Age on Iceland (Lucas and McGovern, 2007). Even today, the cow serves an important religious role in Hinduism, where it is sacred and worshipped.

In contrast, information on the relevance of deposition of cattle in Megalith tombs of the Funnel Beaker culture societies (FBC) in Northern Germany and Southern Scandinavia, except the stone heap graves from northwest Jutland between 3100 and 2800 BC (Johannsen and Laursen, 2010), is very scarce. However, the high significance of cattle in the subsistence economy in this period is characterised by high ratios of cattle versus other bones in domestic sites (Benecke, 1994; Steffens, 2005; Brozio, 2016). The Megalith tombs in Northern Germany, with a boom in construction around 3400 BC, which declined until 3100 BC and ended around 2800 BC, are mainly characterised byvaluable grave goods such as axes, amber objects or highly decorated ceramics (Brozio et al., 2019). The original contents of the ceramic vessels, however, remain mostly unknown. Pottery vessels found in graves and tombs from later periods indicate that luxury and extraordinary goods were added, e.g. wine in amphorae of the Egyptian burial chamber of Tutankhamun (14th cent. BC) (Guasch-Jané et al., 2006), Bronze Age and Iron Age drinking bowls (Sweden) (Isaksson et al., 2010) and frankincense in Medieval pottery vessels from Belgium (Baeten et al., 2014). Thus, grave goods indicate, which resources were highly esteemed in the respective cultures.

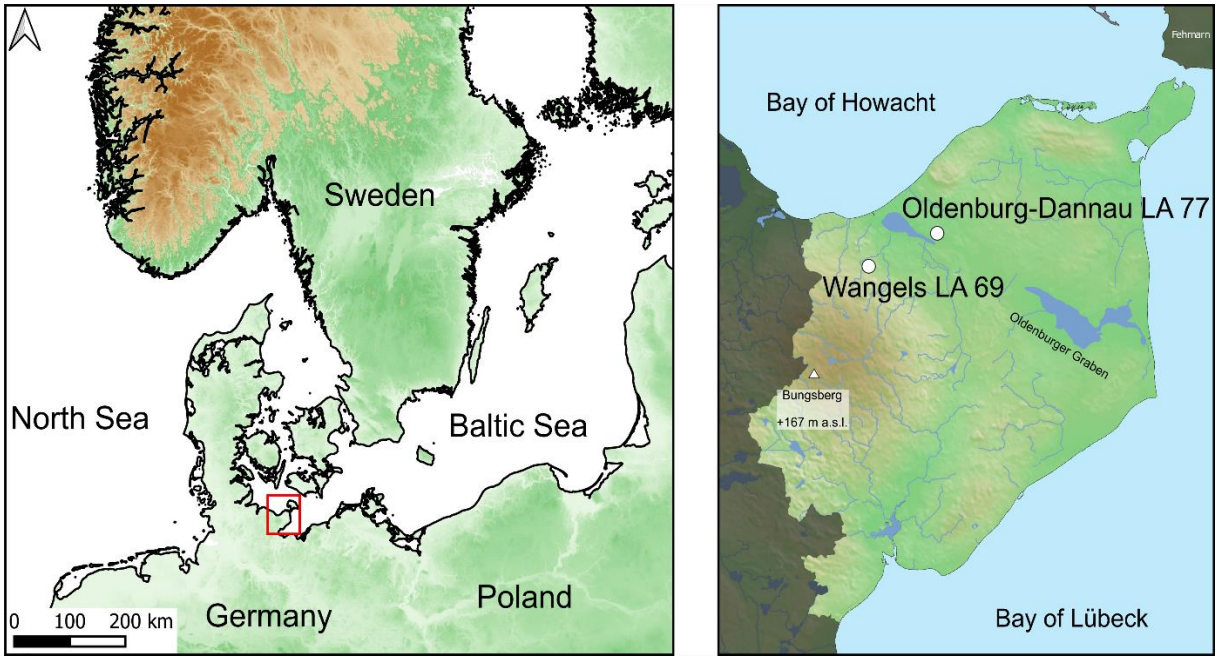

Figure 6.1: Map of study area in Northern Europe and location of archaeological sites Wangels LA 69 and Oldenburg-Dannau LA 77 in the Western Oldenburg Graben area on the Baltic coast of Northern Germany.

6.2 Archaeological field work and chronology

The investigation area of the Western Oldenburger Graben is located on the Wagrian Peninsula in Northeast Holstein, NW Germany. The relief comprises terrain elevations, depressions, lowlands and wetlands formed by glacial-geological processes during the Weichselian glacial period. Geomorphology is defined by the Oldenburger Graben, a lowland area 23 km long and up to 3 km wide (Fig. 6.1). After the formation of two fjords during the Holocene sea-level rise, coastline stabilised by a sequential arrangement of cliffs and beach ridges during the Late Mesolithic. The former bays and fjords were cut off from the sea during the Neolithic by sand barriers, promoting the development of inland lagoons (Brozio, 2016, 2019), with Mesolithic and Neolithic settlement activity concentrated along their shores. The settlement site Oldenburg-Dannau LA 77 is located on a WNW – ESE oriented terrain elevation, measuring approximately 280 m long and 125 m wide (Brozio, 2016, 2019).

Except for the western part, the archaeological site is covered with a settlement layer of variable conservation status. Organic materials such as botanical macroremains (Kirleis and Klooß, 2014) and bones were identified on the former prehistoric riparian zone and the terrain elevation. Settlement features occur as pits and postholes, well structures and rows of stakes, serving to enclose the settlement area between 3087 – 2927 BC (Brozio, 2016, 2019). Burials within the settlement date to 3960 – 3806 BC, 3489 – 3363 BC, and in the riparian zone to the Late Neolithic, 2897 – 2872 BC. The find material primarily comprises stone artefacts and the

ceramic material is mainly composed of highly-fragmented pieces. Overall, only 25 % of the vessels exhibit decoration, whereby ornamented vessels tend to be of a finer design (Brozio, 2016, 2019).

The compilation of the findings makes it possible to identify several huts and houses of the Funnel Beaker (FBC) or “Mossby” type (Artursson et al., 2003; Müller, 2013). Based on ^{14}C dates in combination with a seriation of ceramic patterns, a chronological subdivision has been established for the settlement Oldenburg LA 77 (Fig. S6.1): phase 1, 3270 – 3110 cal BC; phase 2, 3110 – 3020 cal BC; phase 3A, 3020 – 2990 cal BC; and phase 3B, 2990 – 2920 cal BC (Brozio, 2016, 2019). During the Late Neolithic after 2920 cal BC, the terrain elevation was only used with low intensity. Oldenburg-Dannau is one of the few larger Middle Neolithic settlements of the FBC society in the area that was continuously used over a long period of time.

Megalithic tombs separated spatially from the settlements were also located in the hinterland of the Baltic coast. Up to 15,000 megaliths, characterised by their uprights and capstones, were constructed in northern Germany and southern Scandinavia mainly during the early and middle Neolithic (~3500 – 3000 a BC) (Müller, 2011). These monumental collective burials are associated not only with the increasing population size, but also with the appearance of social differentiation and symbolizing a status marker (Furholt and Müller, 2011). The megalithic grave Wangels LA 69 is located in the southern moraine tracts bordering the lowland of the Oldenburger Graben on a natural terrain elevation at ca. +22 m a. s. l. The grave chamber is sub-divided into three areas by stone paving and covered by a mound, which was extended to a tumulus in Neolithic time. In addition to stone artefacts and 69 amber objects such as beads shaped like bobbins or double-edged axes, an extensive ceramic inventory – including 57 vessels of the FBC and the Globular Amphora Culture (GAC) was recovered (Fig. S6.2). The inventory mainly comprises intricately-decorated pieces, some of which are preserved in a completely intact and non-fragmented state (Brozio, 2016, 2019).

A fine chronological differentiation of the structure was achieved by a ^{14}C model with 40 out of a total of 51 ^{14}C datings. As a result, seven individual construction and burial phases can be differentiated and classified by absolute chronology (Fig. S6.3) between 3360 – 1900 cal BC for Wangels: phase 1: Start of use (3640 – 3360 BC), phase 2: Construction of grave chamber and mound (3360 – 3280 BC), phase 3: Aggradation of long barrow and establishment of stone circle (3280 – 3120 BC), phase 4: Burial of a body (3120 – 3100 BC), phase 5: Burial phase (3120 – 3000 BC), phase 6/ 7: Secondary burial phase (3000 – 1900 BC).

Seriation of the ceramics in combination with scientific dating and stratigraphic information enable the distinction of three ceramic phases integrated in the absolute-chronological phase model. A differentiation of the burials in two Funnel Beaker utilisation phases and a Globular

Amphora secondary burial phase (phase 7) is feasible. A unique phenomenon is the deposition of a vessel under one of the orthostats before the construction of the chamber, interpreted as a votive or a building sacrifice.

In conclusion, the beginning of the site´s use is placed between 3640 – 3360 BC, followed by the period from 3360 – 3280 BC, when the construction of the grave chamber and the first mound in the form of a round mound took place. The enlargement of the round mound of the passage grave to a long barrow with a surrounding stone kerb dates between 3280 – 3120 cal BC. A more than 400-year frequentation span of the feature lasting to within the outgoing Late Neolithic around 1900 BC is verified by the ^{14}C model.

6.3 Material and Methods

6.3.1 Lipid analysis

Organic residue analysis were conducted on 33 pottery vessels excavated from two Neolithic sites Wangels LA 69 and Oldenburg-Dannau LA 77 in Northern Germany following previously published extraction protocols (Evershed et al., 2008). Briefly, from intact pots a 4 cm^2 piece was cut and from sherds an equivalent sample size was obtained. Before further crushing and grinding, surfaces were carefully abraded to remove exogenous contaminations. 3-4 g of crushed potsherds were extracted by ultrasonication with dichloromethane:methanol (2:1 *v/v*, 3 × 5 ml). All supernatants were combined and filtered through $NaSO_4$ to remove water and clay particles. Solvents were evaporated to dryness under a gentle steam of nitrogen (N_2) to obtain total lipid extracts (TLE). An aliquot of each sample was derivatized by using *N*,*O*-bis(trimethylsilyl)trifluoroacetamide and pyridine (70°C, 60 min) and analysed by high-temperature gas chromatography-mass spectrometry (HTGC-MS).

A second aliquot (~2g) of surface-cleaned and powdered sherd was extracted using direct-acidification-methanol extraction to obtain fatty acids methyl esters (FAME) for GC-combustion-isotope ratio mass spectrometry (GC-C-IRMS) analysis (Correa-Ascencio and Evershed, 2014). Briefly, powdered sherds were treated with 5ml H_2SO_4-methanol (4% *v/v*) and heated for 4 hours at 70°C. Subsequently, 2 ml water (HPLC-grade) was added and lipids were extracted thrice with 3 ml *n*-hexane and transferred into a clean vial. Combined *n*-hexane extracts were blown down under a gentle stream of N_2. An aliquot of the extract was separated over aluminium oxide with *n*-hexane:dichloromethane (95:5, *v/v*) to recover the neutral fraction and *n*-hexane:dichloromethane (1:2, *v/v*) to obtain FAMEs.

6.3.2 High-temperature gas chromatography-mass spectrometry (HTGC-MS)

HTGC-MS for TLE measurements were performed using an Agilent 7890A GC equipped with a Phenomenex ZB-1HT (10m × 0.25mm × 0.25µm) column connected to a Phenomenex ZB-

5HT Inferno (5m × 0.25mm × 0.25µm) column coupled to an Agilent 5975B mass spectrometer. The oven temperature was held at 80°C for 2 min, after which the temperature was raised to 400°C at 8°C/min and held for 1 min. The MS was operated at an electron energy of 70 eV, scanning at a rate of 1 scan per second for the range of *m/z* 50-750 Dalton in full scan mode.

GC-MS analysis on FAMEs were performed using an Agilent 7890A GC equipped with an Agilent DB-5 (30m x 0.25mm) column coupled to an Agilent 5975B mass spectrometer. GC oven temperature was set to 40°C and held for 2 min then ramped to 240°C at 15°C/min and held isothermal for 15 min. The MS was operated at an electron energy of 70 eV scanning at a rate of 1 scan per second for the range of m/z 50-750 Dalton in full scan mode. In a second run, the samples were run in SIM mode, scanning the ions *m/z* 105, 262, 290, 318, 346 to detect APAAs. Peak identifications were performed using NIST14 mass spectral database, published mass spectra and retention time.

6.3.3 Gas Chromatography-Combustion-Isotope Ratio Mass Spectrometry for $\delta^{13}C$ Analysis (GC-C-IRMS)

GC-C-IRMS analyses was performed using a Thermo Delta V Plus isotope ratio mass spectrometer coupled to a Thermo Fisher Trace 1310 GC. Samples were diluted in *n*-hexane and 1 µl was injected onto an Agilent DB-5 (30m × 0.25mm × 0.25µm) column in split mode with a split ratio of 50:1. The temperature program was 2 min isothermal at 40°C followed by an increase of 12°C/min to 250°C and 7°C min at 250°C isothermal. The combustion reactor consisted of a NiO tube filled with CuO, NiO and Pt wires and was maintained at 850°C. The ion intensities of m/z 44, 45, and 46 were monitored and the $^{13}C/^{12}C$ ratios of each sample peak were automatically computed by comparison with a standard reference of known isotopic composition. Each sample was run in duplicate. External standards were run every 8 samples. Instrument precision and accuracy of FAME isotope standard analyses were better than 0.5‰. $\delta^{13}C$ values of samples were corrected for carbon atom addition during methylation using mass balance equations.

6.4 Results and Discussion

Here, we present evidence of cattle employed in ritual context based on organic remains detected in Neolithic pottery vessels from Northern Germany. A total of 33 pottery sherds from the Megalith tomb Wangels LA 69 (n=15) and the adjacent domestic dwelling site Oldenburg LA 77 (n=18) in Northern Germany (Fig. 6.1) were solvent extracted and analysed by gas chromatography-mass spectrometry (GC-MS) and gas chromatography combustion isotope ratio mass spectrometry (GC-C-IRMS). Both sites are located in a nearshore landscape characterized by fjords and lagoons in the Oldenburger Graben (Fig. 6.1) (Brozio et al., 2014).

For the Megalith grave Wangels seven individual construction and burial phases have been defined (see SI Appendix) dating from 3640 – 1900 BC, which comprised partially intact and highly decorated ceramic artefacts of the Funnel Beaker Culture (FBC) and the Globular Amphora Culture (GAC). In contrast, in the adjacent settlement Oldenburg (3270 to 2920 BC) strongly fragmented and undecorated ceramics were found, which were interpreted as daily consumers goods (Filipović et al., 2019).

Of the 33 potsherds, 28 (84%) yielded sufficient (>5 µg/g) lipid concentration in the range from 5.9 to 9661.5 µg/g sherd with mean value of 600.8 µg/g (Table S1 and S2), which is concentration considered appropriate for further interpretation (Evershed, 2008). The sherds with concentrations <5 µg/g should be interpreted with caution as they may contain substantial proportions of contaminants. However, no modern contaminants such as squalene from human skin have been detected. Analysis of ceramic-bound organic residues by GC-MS allows subdivision of specimens into two broad categories (Fig. 6.2). The first category is dominated by palmitic ($C_{16:0}$) and stearic ($C_{18:0}$) acids combined with abundant triacylglycerols (C_{42} to C_{54}), which derive from degraded animal fat (Fig. 6.2a). The ratio of both fatty acids expressed as P/S ratio has been used to distinguish between animal fats and plant origin, since plant oils produce up to 3 to 4 times greater amounts of palmitic acid and animal fats more stearic acid (Copley et al., 2005b). Most samples have low P/S values <2. In addition, we identified branched pentadecanoic and heptadecanoic fatty acid, occurring as iso- and anteiso-isomers, which derive from bacteria living in the rumen of the milk-producing species cattle, goat and sheep (Dudd and Evershed, 1998). The second category shows a dominance of C_{16} over C_{18} fatty acids with a P/S ratio of up to 3.3, combined with a higher proportion of unsaturated fatty acids ($C_{16:1}$ and $C_{18:1}$) and high relative abundance of $C_{12:0}$ and $C_{14:0}$ homologues, a distribution diagnostic for plant oils (Copley et al., 2001) (Fig. 6.2b). Most fresh plant oils from e.g. poppy, safflower, hemp and wheat germ are dominated by unsaturated fatty acids such as $C_{18:1}$, $C_{18:2}$ or even $C_{18:3}$ (Bozan and Temelli, 2008; Orsavova et al., 2015). Under common conditions of preservation, polyunsaturated compounds get destroyed or survive in just minor quantities in archaeological samples due to oxidation and microbial mineralization. Therefore, enhanced amounts of the $C_{16:1}$ fatty acid as detected here are rarely found in archaeological vessel.

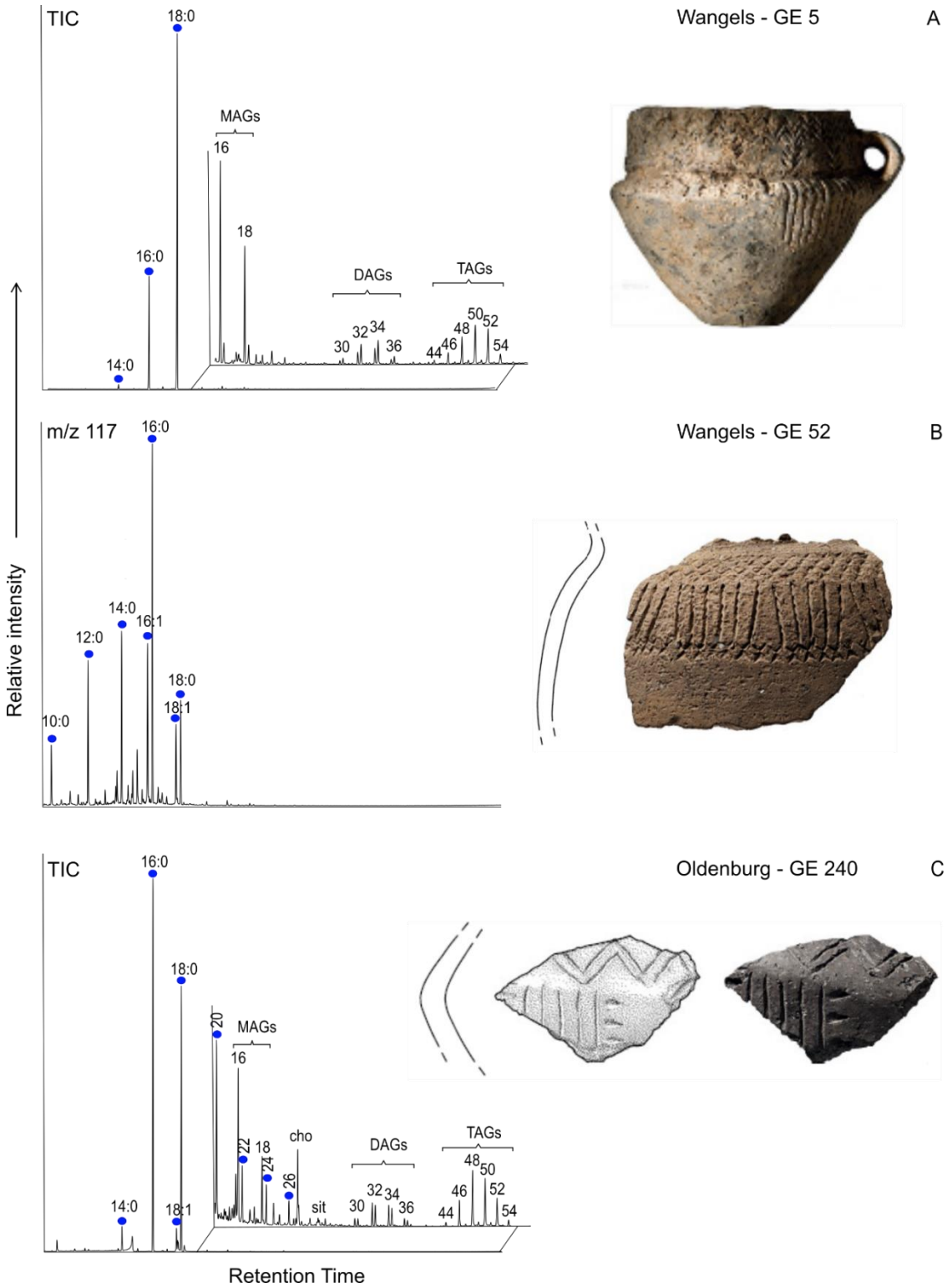

Figure 6.2: Partial ion chromatograms of lipid extracts from three representative pottery vessels. **A**: Pottery vessel from burial site Wangels showing a molecular distribution indicative for degraded animal fats. **B**: Pottery sherd from Wangels containing plant oils as revealed by abundant unsaturated fatty acids. **C**: Ceramic fragment from domestic site Oldenburg containing degraded animal fat with minor amounts of the plant/vegetable biomarkers phytosterols and C_{20} to C_{26} long-chain fatty acids. Blue circle with x:y: free fatty acids with x carbon atoms and y degrees of unsaturation; MAGs: monoacylglycerols; DAGs: diacylglycerols, TAGs: triacylglycerols; cho: cholesterol; sit: sitosterol.

Exceptionally high proportions of palmitic ($C_{16:0}$) and palmitoleic acid ($C_{16:1}^{cis\Delta 9}$) occur in sea buckthorn (*Hippophae rhamnoides*) berry and pulp oils, contributing 50% to 80% of the total fatty acids (Yang and Kallio, 2001; Dulf, 2012; Fatima et al., 2012). These compounds are known as major constituent of human skin fat, leading to application of pulp oil for cosmetic and healing purposes (Yang and Kallio, 2001; Zeb, 2004; Fatima et al., 2012). Rare reports of abundant C_{16} fatty acids in tropical to subtropical plants include macadamia nuts with $C_{16:0}$ and $C_{16:1}$ contributing between 20 to 40% of total fatty acids (Maguire et al., 2004; Aquino-Bolaños et al., 2017) or durian fruit with $C_{16:0}$ and $C_{16:1}$ contributing between 30 to 40% of total fatty acids (Berry, 1981; Amid et al., 2012; Ho and Bhat, 2015). Amongst Zanthoxylium species, only *Zanthoxylum armatum* contain up to 20% C_{16} fatty acids, whereas *Zanthoxylum bungeanum* C_{16} fatty acid proportions did not exceed 10% (Hou et al., 2019). All of these C_{16} fatty acid enriched plants were reported from warmer climates and can be excluded to have inhabit the coastal regions along the Baltic Sea.

A variety of C_{16} fatty acids is further known to occur in non-plant sources, e.g. fish liver oils and in seal bone (Ackman, 1967; Özogul and Özogul, 2007; Heron et al., 2015; Keinänen et al., 2017), where they comprise between 15 to 25% of total fatty acids. The latter two aquatic sources can be excluded as potential origin as firstly, the diagnostic aquatic biomarkers (Hansel et al., 2004, 2011; Evershed et al., 2008a) isoprenoidal, long-chain unsaturated,ω-(o-alkylphenyl) alkanoic fatty acids (APAA), or dihydroxy fatty acids were lacking, secondly, the carbon isotope signatures of the $C_{16:0}$ fatty acid did not correspond with a marine source, although both locations are close to the sea (Fig. 6.3), and thirdly the relative proportions of C_{16} fatty acids are too low.

Sea buckthorn, on the other hand, is nowadays a common widespread growing plant at the coast of northern Germany and is used as healing agent and cosmetic thus explaining their use as precious grave gift. Further source-specific lipids such as animal sterols and phytosterols and their derivates (cholesterol, 7-ketocholesterol, β-sitosterol, stigmasterol) occurred in subordinate amount or traces, which can be explained by the rapid degradation due to oxidation during deposition and/or firing of the vessels (Hammann et al., 2018). In potsherds (n=33) of the burial site Wangels, 73% revealed an origin from animal fats, whereas in contrast the domestic site Oldenburg yielded 61% samples derived from plant sources.

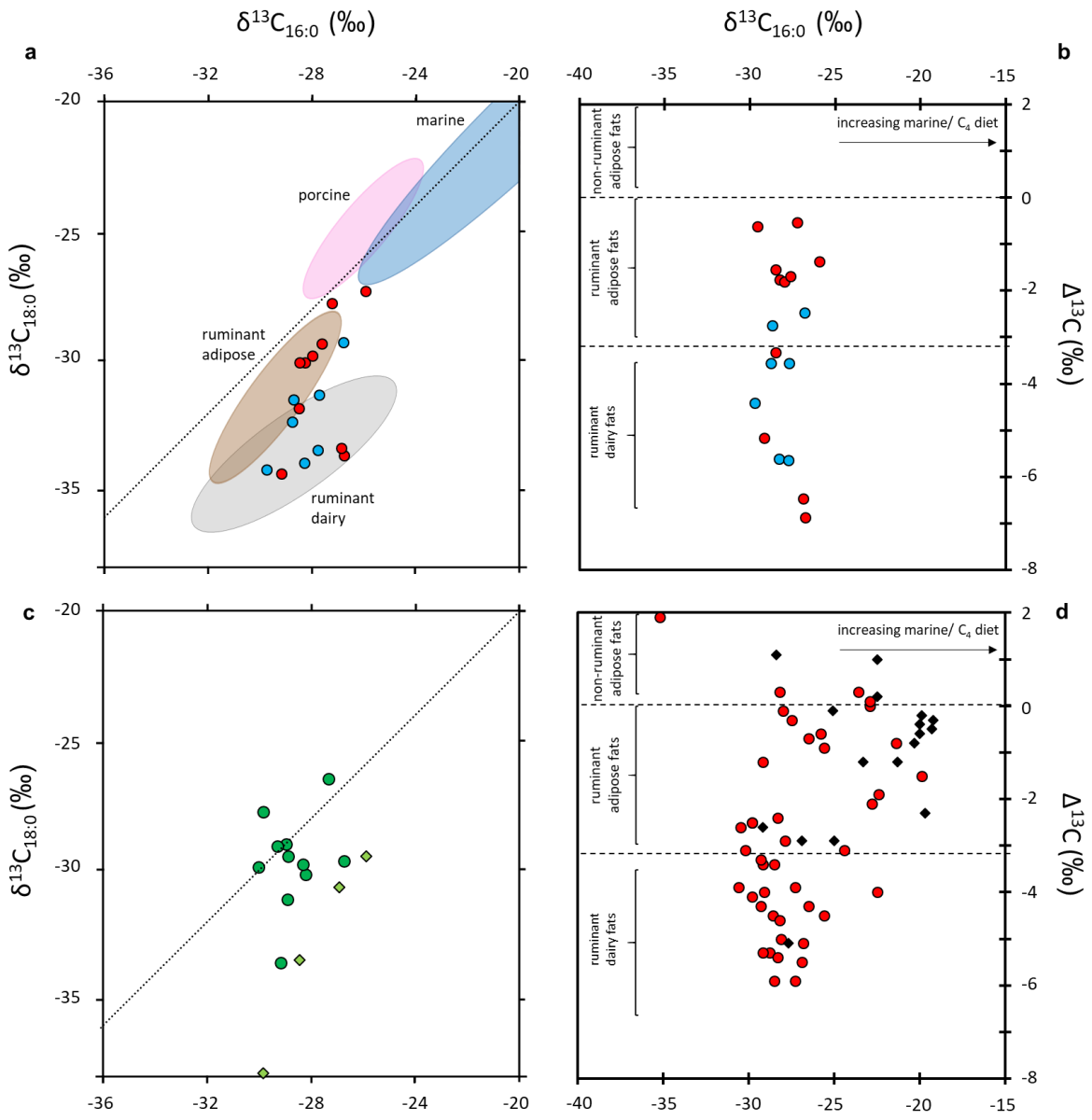

Figure 6.3: Stable carbon isotope composition of individual fatty acids in lipid residues of animal origin from Neolithic pottery vessels of the Megalith tomb Wangels (red) and domestic site Oldenburg (blue) (**a**, **b**). Modern $\delta^{13}C$ reference values in **a** are according to Craig et al., 2011. $\delta^{13}C_{16}$ and $\delta^{13}C_{18}$ values of plant origin from Wangels (green circle) and Oldenburg (green square) (**c**). Distribution of $\delta^{13}C$ values reported for C_{16} and C_{18} fatty acids of Mesolithic age from Northern Germany (Craig et al., 2011) attributed to terrestrial (red dots) and marine (black squares) food sources. A shift from Mesolithic, more marine influenced to fully terrestrial Neolithic diet is evident if compared with **b**. Ranges for $\Delta^{13}C$ values in **b** and **d** are based on a global database comprising modern animal reference fats from the United Kingdom, Switzerland, the Near East, Africa, and Kazakhstan (Dudd and Evershed, 1998; Spangenberg et al., 2006; Gregg et al., 2009; Outram et al., 2009; Dunne et al., 2012).

Further corroboration of animal fat origin in ceramic sherds was achieved by determination of carbon stable isotope ($\delta^{13}C$) values of the two major fatty acid methyl esters derivatives ($C_{16:0}$ and $C_{18:0}$) (Fig. 6.3). Differences in $\delta^{13}C$ values of fatty acids occur due to specific metabolic routes for ruminant and non-ruminant animals (Copley et al., 2003). To diminish local environmental or climatic influence or variation in food source (C_3 *vs*. C_4 plants), a $\Delta^{13}C$ ($=\delta^{13}C_{18:0} - \delta^{13}C_{16:0}$) value is employed to differentiate food source or processing (Copley et al., 2003). For source allocation of animal fats, $\delta^{13}C$ results obtained from archaeological specimens have been compared with those from modern reference fats (Dudd and Evershed, 1998; Copley et al., 2003; Craig et al., 2011). By comparison of the $\Delta^{13}C$ values of the 18 animal fat residues with the modern reference animal fats, a predominance of ruminant fats (73%) over dairy products (27%) is observed for specimens from the Megalith tomb of Wangels (Fig. 6.3). Contrary, pottery sherds from the domestic site Oldenburg contain preferentially dairy fats (71%). The ruminant fats are interpreted as of cattle meat origin, since archaeozoological findings of ruminant species from the coeval Oldenburg site are derived predominantly, about 40%, from cattle (Filipović et al., 2019). The animal bones of the Oldenburg LA 77 site are currently being investigated. A first sample showed 41% cattle, followed by pigs with 33%. Fatty acids derived from porcine meat could not be detected in the burial gift vessels although porcine bone, contributed one third of bones found in the Oldenburg domestic site, the remaining being of cattle origin, this underlining that the spiritual esteem devoted to husbandry animals was selectively placed on cattle. Since decorated beakers were mainly found intact and no evidence for exposure to cooking was observed, they were presumably produced solely for the burial rite and filled with high-quality cattle meat as grave good in a ceremonial ritual. The appreciation of cattle fat as precious burial gift is explained by the fact that slaughter and sacrifice of animals is terminal, whereas sustainable utilization is achieved by milking.

$\delta^{13}C$ values of the archaeological samples with plant origin (Fig. 6.3) to a large extent possess values comparable to modern C_3 vegetable oils (Woodbury et al., 1998; Spangenberg and Ogrinc, 2001; Steele et al., 2010) and plot close to the 1:1 line in the $\delta^{13}C_{16}$ *vs.* $\delta^{13}C_{18}$ discrimination diagram. This parity is characteristic for vegetable oils due to the fatty acids biosynthesis in plant cells (Spangenberg and Ogrinc, 2001). The higher proportion of dairy products and plant oils in the utility vessels from the Oldenburg settlement is in keeping with the common plant spectrum used for subsistence farming based on cereals like barley and einkorn, gathered plants and weeds (Kirleis et al., 2012; Filipović et al., 2019) for this period and contrast sharply with the exclusivity of cattle meat in the burial gifts. However, the presence of cereals in the ceramic is uncertain as no cereal-specific biomarkers like alkylresorcinols or long-chain alkyl lipids have been found. This is ascribed to the substantially lower concentrations of lipids in plants than in animal products (Colonese et al., 2017;

Hammann and Cramp, 2018). The presumed consumption of sea buckthorn, which is widespread on the coast of the Baltic Sea, could have been a healthy dietary supplement due to its active ingredients such as antioxidants, carotenoids, unsaturated fatty acids and vitamin C (Zielińska and Nowak, 2017).

By comparing our results from the coeval Oldenburg domestic site and Wangels ritual burial sites with earlier studies on ceramics from the Baltic Sea region, a transformation in diet over time becomes evident. High proportions of aquatic biomarkers were identified in Late Mesolithic/Early Neolithic potteries from coastal sites in Germany, Denmark and South Sweden, indicating that early farming had not been induced yet (Craig et al., 2011; Papakosta et al., 2019). These studies revealed the utilization of ceramic pots from hunter-gatherer sites in marine or freshwater resource but not terrestrial food (animals and plants) processing. The absence of aquatic biomarkers, despite availability of animal and plant resources in our study of younger Neolithic samples is corroborated by isotope data from human remains suggesting a trend from more aquatic to more terrestrial food consumption in the Mesolithic-Neolithic transition (Fischer et al., 2007; Terberger et al., 2018).

6.5 Conclusion

Food residues recovered from Neolithic (3600 to 2900 BC) delicately designed pottery recovered from a Funnel Beaker Megalith tomb contrasted compositionally from those found in an adjacent domestic dwelling site on the shores of the south-western Baltic, NW-Germany. Burial gift aliments held extraordinary and precious products to serve the buried ancestors during afterlife. Molecular biomarkers and their respective carbon isotope signatures identified a specific plant essential oil and cattle meat or dairy products. Amongst aliments from three different burial phases, the youngest only (3000 to 2900 BC) yielded the plant oil, possibly produced from sea buckthorn (*Hippophae rhamnoides*) and stored in specific vessels of the globular amphora type, exclusively. All remaining grave goods comprised either ruminant meat or milk, consistent with predominant cattle husbandry, corroborated by bone findings in coeval adjacent domestic sites. Here, food residues from pottery used in everyday cooking revealed a mixed composition of dominantly plant and milk origin but only subordinate or no meat. With no porcine burial gifts identified but porcine bone contributing one third of animal bone findings in dwelling sites we note that although pork made up a portion of Middle Neolithic meat diet, it lacks in grave aliments and conclude that domestic pigs possessed no spiritual attribute in the Neolithic spiritual world. Burial gifts of animal origin exclusively consisted of cattle products indicating that these animals not only served as food source but also played an important role in the ritual sphere in Neolithic societies. In particular this underlines the importance of cattle in the spiritual perception of the Globular Amphora Culture, known for its cattle burials. For the Funnel Beaker culture, in which the importance of cattle is also evident

through depositions in settlements and enclosures, we for the first time demonstrate by organic residue analysis that high-quality meat products were used as grave goods and/or sacrifices in the context of megalithic tombs.

Acknowledgements

The research was conducted and financed in context of the Collaborative Research Centre 1266 “Scales of Transformation – Human –environmental interaction in prehistoric and archaic societies” of the German Research foundation (DFG, German Research Foundation – project number 2901391021 – SFB 1266).

6.6 Supplementary material

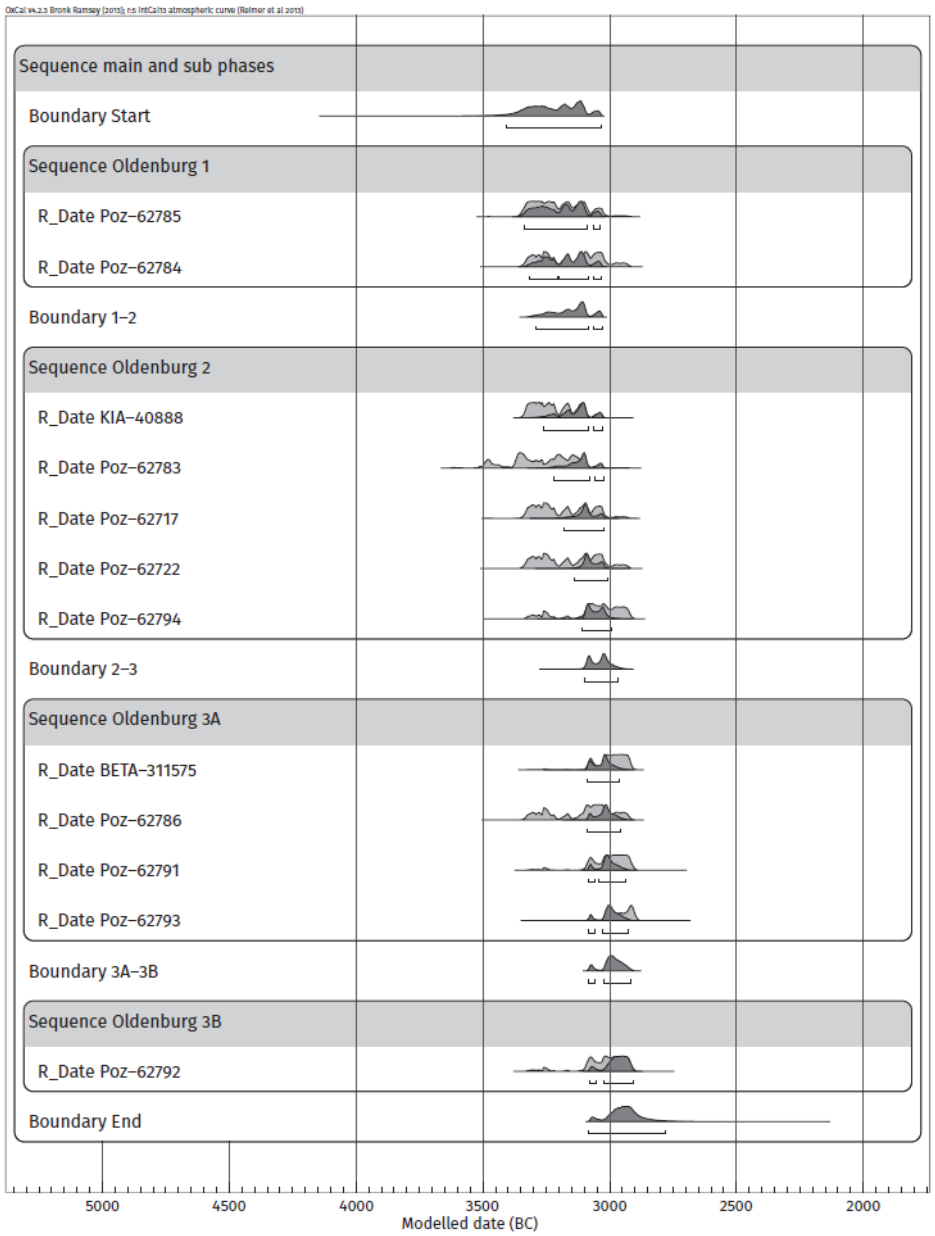

Figure S6.1 Dating of artefacts for establishment of Oldenburg dwelling site chronology

Figure S6.2 Wangels LA 69: Exquisitely ornamented funnel beaker ceramic, globular amphoras and stone artefacts like axes and blades were deposited in the Wangels grave chamber.

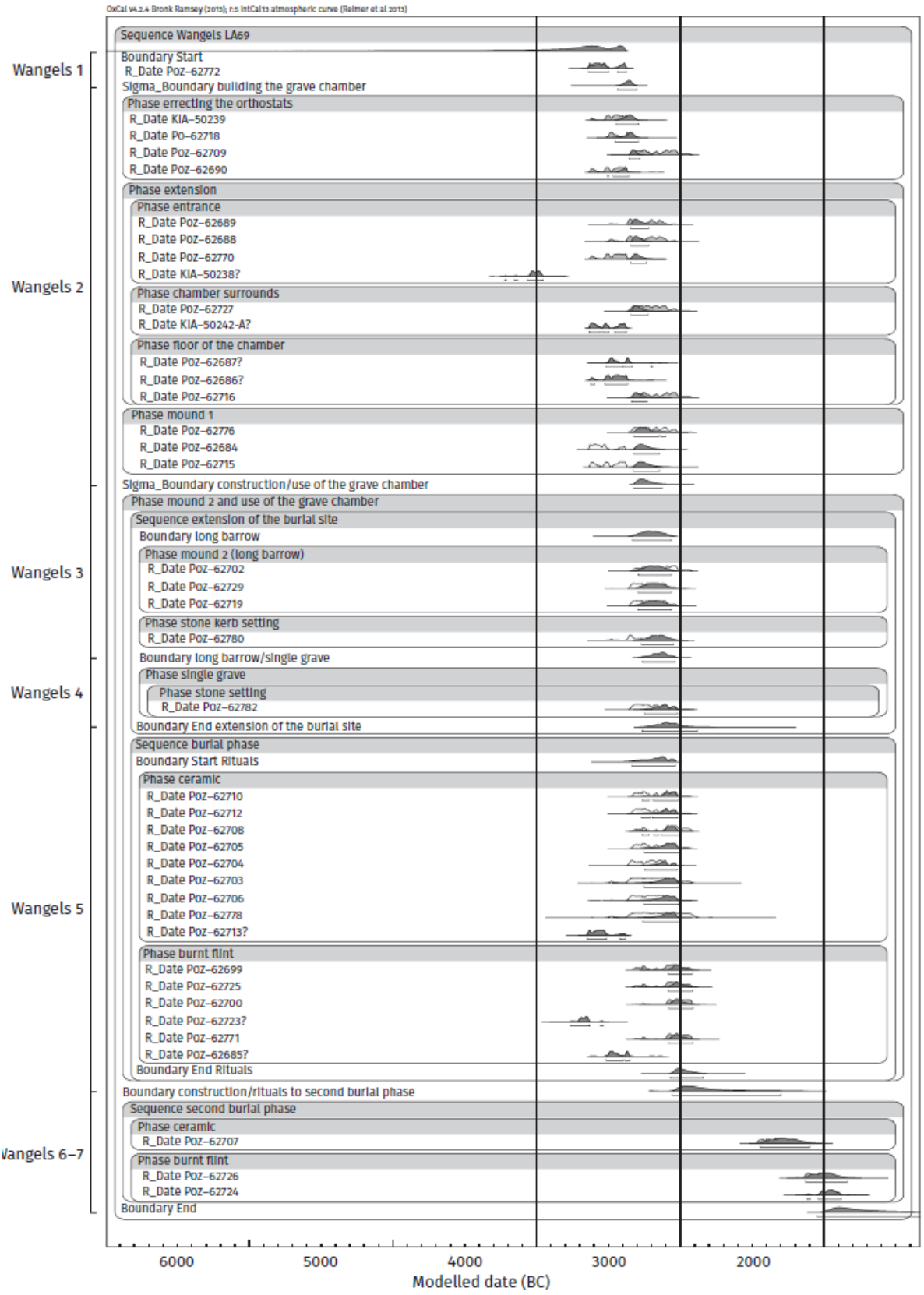

Figure S6.3 Sequential calibration of ^{14}C dates to derive fine chronology of phases 1 to 6-7.

Sample code	Phase	Age (a calBC)	Lipid conc. (µg/g)	$\delta^{13}C_{16}FA$ (‰)	$\delta^{13}C_{18}FA$ (‰)	$\Delta^{13}C$	$C_{16:0}FA/C_{18:0}FA$	unsat. FA	br_{15} FA	br_{17} FA	chole-sterol	phyto-sterol	TAGs	Interpre-tation
Wangels LA 69														
GE 21	Wangels 6	3000-2900	45.3	-25.89	-29.44	-3.55	1.72	x						plant
GE 37	Wangels 6	3000-2900	128.7	-26.90	-30.61	-3.72	1.23							plant
GE 8	Wangels 6	3000-2900	472.2	-29.57	-30.20	-0.62	1.05				tr	tr		meat
GE 16	Wangels 6	3000-2900	5.9	-28.41	-33.41	-4.99	2.52	x			tr	tr		plant
GE 52	Wangels 6	3000-2900	201.9	-29.82	-37.74	-7.92	2.44	x			tr	tr		plant
GE 29	Wangels 6	3000-2900	214.4	-28.28	-30.04	-1.76	0.74						C_{48}-C_{54}	meat
GE 41	Wangels 6	3000-2900	39.1	-26.76	-33.63	-6.87	1.22						C_{46}-C_{54}	milk
GE 1	Wangels 5	3120–3000	1.8	-27.98	-29.79	-1.81	1.16							meat
GE 2	Wangels 5	3120–3000	4.3	-28.49	-30.04	-1.55	0.85							meat
GE 4	Wangels 5	3120–3000	1.4	-27.22	-27.75	-0.53	1.21							meat
GE 5	Wangels 2-5	3360-3000	39.6	-26.87	-33.34	-6.47	0.31			x			C_{42}-C_{54}	milk
GE 7	Wangels 2-3	3360-3120	937.8	-27.63	-29.33	-1.70	2.39							meat
GE 22	Wangels 2-3	3360-3120	1377.2	-25.93	-27.30	-1.37	1.08						tr	meat
GE 27	Wangels 2-3	3360-3120	776.0	-28.50	-31.82	-3.32	0.91		x	x			C_{46}-C_{54}	meat
GE 54	Wangels 1–2	3640-3280	486.1	-29.18	-34.34	-5.16	1.71		x	x			C_{44}-C_{54}	milk

Table S6.1: Summary of the results from biomolecular analyses and carbon isotope analyses of individual fatty acids from Wangels LA 69.

Sample code	Phase	Age (a calBC)	Lipid conc. (µg/g)	$\delta^{13}C_{16}FA$ (‰)	$\delta^{13}C_{18}FA$ (‰)	$\Delta^{13}C$	$C_{16:0}FA/C_{18:0}FA$	unsat. FA	br_{15} FA	br_{17} FA	chole-sterol	phyto-sterol	TAGs	Interpre-tation
Oldenburg-Dannau LA 77														
GE 116	Oldenburg 3A	3020-2990	102.8	-27.32	-26.47	0.85	2.20	x			tr	x		plant
GE 89	Oldenburg 3A	3020-2991	58.2	-28.95	-28.96	-0.01	2.60	x			tr	x		plant
GE 26	Oldenburg 3A	3020-2992	719.2	-27.73	-31.29	-3.56	0.77		x	x	x		C_{48}-C_{54}	milk
GE 168	Oldenburg 3A	3020-2993	0.9	-29.26	-29.04	0.22	2.37	x						plant
GE 248	Oldenburg 3A	3020-2994	3.0	-28.88	-31.09	-2.21	1.51	x						plant
GE 4	Oldenburg 3A	3020-2995	21.2	-26.78	-29.26	-2.47	1.36							meat
GE 74	Oldenburg 2	3110–3020	6.1	-29.98	-29.86	0.12	1.86	x				tr		plant
GE 203	Oldenburg 2	3110–3020	209.7	-29.74	-34.16	-4.42	0.81		x	x	x	x	C_{42}-C_{54}	milk
GE 17	Oldenburg 2	3110–3020	50.9	-29.82	-27.73	2.08	1.92	x						plant
GE 33	Oldenburg 2	3110–3020	38.3	-29.15	-33.52	-4.36	1.82	x						plant
GE 125a	Oldenburg 2	3110-3020	6.0	-28.77	-32.33	-3.56	0.35		x	x			C_{46}-C_{54}	milk
GE 125b	Oldenburg 2	3110-3021	9661.5	-28.71	-31.47	-2.76	0.98		x	x			C_{44}-C_{54}	meat
GE 222	Oldenburg 2	3110-3021	25.4	-28.18	-30.13	-1.95	1.70	x						plant
GE 200	Oldenburg 1-2	3270–3020	338.7	-28.29	-33.91	-5.61	1.36		x	x			C_{44}-C_{54}	milk
GE 118	Oldenburg 1	3270–3110	425.1	-26.72	-29.60	-2.88	3.33	x				x		plant

GE 240	Oldenburg 1	3270–3110	279.4	-27.77	-33.42	-5.65	1.43		x	x	x		C_{42}-C_{54}	milk
GE 248	Oldenburg 1	3280-3110	40.1	-28.30	-29.74	-1.44	1.77	x			tr			plant
GE 39	Oldenburg 1	3280-3111	116.9	-28.86	-29.44	-0.58	2.15	x				x		plant

Table S6.2: Summary of the results from biomolecular analyses and carbon isotope analyses of individual fatty acids from Oldenburg-Dannau LA 77. Lipid conc. = lipid concentration (µg lipids/ g sherd), FA = fatty acid, unsat. FA = unsaturated C_{16} and C_{18} FA, brC_{15}FA = iso-/anteiso-C_{15} FA, brC_{17}FA = iso-/anteiso-C_{17} FA, TAG = triacylglycerol, tr = traces

7. Summary and further perspectives

This PhD project was integrated into the Collaborative Research Center 1266 (CRC 1266) and therefore not only “typical” geological/geochemical questions were addressed. As a result of the interdisciplinary orientation of the CRC 1266, organic-geochemical techniques were applied to related fields including (paleo)botany (chapter 2), paleolimnology (chapter 3 and 4), paleoenvironmental reconstruction (chapter 3 and 4), human-environmental interactions (chapter 4 and appendix B) and archaeology (chapter 5, 6 and appendix A). The main objectives of this thesis were the characterisations of different spheres by biomarkers and stable isotopes, which were implemented by analysing different media including modern plant leaves and animal fats (biosphere), Pleistocene/Holocene lacustrine sediments (geosphere) and ancient pottery vessels (archaeosphere).

The following parameters were collected in at least one of the subprojects that were essential for the work on this PhD project: TOC, TIC, TN and TS content, $\delta^{13}C$ and $\delta^{15}N$ signature of bulk sediment, total and individual lipid distributions as well as $\delta^{13}C$ signature of individual compounds. The results of this thesis indicate that these organic-geochemical techniques used have potential for a wide range of applications. In the following, the main results of each subproject are summarized. As most subprojects opened the door to multiple possibilities for future research work, a future perspective is also given.

The geochemical analyses of leaves from the four European birch species *Betula nana, B. humilis, B. pubescens and B. pendula* grown at the Botanical Garden of Kiel University revealed a distinct differentiation of the four species based on their epicuticular wax composition (*n*-alkanes, *n*-alcohols, *n*-alkanoic acids, *n*-alkyl esters).

For a better understanding of the biosphere-geosphere interaction of leaf wax lipids, a theoretically stepwise degradation of the prior intact *n*-alkyl esters was simulated. The resulting degradation products, *n*-alcohols and *n*-alkanoic acids with varying carbon chain-lengths, were added to the existing free homologues, a procedure simulating continuous alteration expected to occur upon leaf ontogenesis and in soils and sediments after burial. The results indicate that the wax lipid composition changed significantly not only in quantity, but also in quality for all species. Based on the theoretical approach of wax ester decomposition, further research is pending to verify the theoretical values by direct hydrolysis of the wax esters upon extraction and by e.g. saponification.

When comparing the *n*-alkane composition of the *Betula* waxes collected in Kiel with published data, no trend in geographical location or temperature could be observed. Since other studies identified changes in the wax lipid composition dependent on environmental factors like temperature or latitude, further research is encouraged in this field. One possibility to verify a dependence of the wax lipid composition onenvironmental factors would be to expose different

clones of the same tree to different environmental conditions like temperature, water availability, light or CO_2 content.

Further decarboxylation and reduction of *n*-alcohols and *n*-alkanoic acids can affect the *n*-alkane pool, which then is increased in mid-chain homologues mimicking the *n*-alkane fingerprint from mosses or aquatic macrophytes. Since most studies tend to analyse exclusively the *n*-alkane composition in sediments, further studies should also consider other wax lipid compounds and their compound specific carbon/hydrogen isotopic composition as *n*-alkane precursors. Differences in wax composition might yield various secondary or tertiary degradation products of potential devating isotope signature that contribute to the *n*-alkane pool.

Application of biomarkers was carried out on two lacustrine sediment cores from Lake Steisslingen (Germany) and Lake Stymphalia (Greece). The sediment sequence from Lake Steisslingen comprised laminated sediments prior, during and after the Younger Dryas cold event (12,680 – 11,590 yr BP). Several climatic shifts were identified in the sediment core like the Gerzensee Oscillation or Preboreal Oscillation, which correlate with prior studies. However, based on variations in biomarker composition (long-chain alkenones, HBI-20, nC_{17}-alkanes, hopanoids, long-chain *n*-alkanes), a new separation of the Younger Dryas chronozone into three sub-zones I, II, III was implemented, indicating a different response of the aquatic and terrestrial community to environmental change. Surprisingly, well established paleothermometer like U^K_{37} and MBT'_{5ME} did not or only partially show the expected temperature trends during the Late Glacial/ Early Holocene phase in comparison with literature data. Long-chain alkenones (LCA) were only detectable in the Younger Dryas sediments and exhibited a temperature increase only at the end of the cold period. Contrary, the brGDGT based temperature showed both no clear cooling and warming at the onset and the end, respectively, of the Younger Dryas. Consequently, this implies that this proxy is not fully applicable as paleothermometer in the Lake Steisslingen sediment core. A new induced proxy (HIR_{28D}) based on the relation of specific isomers from cyanobacteria-derived heterocyte glycolipids (HGs) was used to determine relative continental temperature shifts and revealeda good agreement with estimated trends. However, further research is needed for understanding paleoenvironment evolution in Lake Steisslingen due to the following reasons. First, lake surface sediments and/or sediment traps should be investigated by lipid analysis and genetic techniques to identify the still unknown producer(s) of LCA in the lake. Second, the same samples could be analysed accompanied by surface sediments from the surrounding soils to understand the origin of brGDGTs in the lake. This could shed light on the brGDGT temperature problems at Lake Steisslingen. Third, based on existing research, a temperature calibration for brGDGTs from African lakes (Russell et al., 2018) has been used

since there is no local or regional calibration existing. This encourages further research on a brGDGTs-temperature calibration on German or other European lakes. Fourth, proposed HG based ratios indicative for a temperature dependency like HDI_{26}, HDI_{28}, HTI_{30} consistently approached the maximum value of 1. This suggests that one homologue is less abundant and potentially preferable degraded over time. In this case, it should be investigated further how resistant the individual HG homologues are against degradation.

For the Lake Stymphalia manuscript, the wax lipid composition the sediment sequence of Lake Stymphalia situated in a karst polje has been investigated to reconstruct paleovegetation changes for the last 15,000 years. As the pollen preservation is poor (Seguin et al., 2019), this is the first attempt to reconstruct the vegetation for the late Pleistocene to early Holocene period in the Peleponnese. As the vegetation reconstruction is based on the *n*-alkane distribution further studies could improve the interpretation by comparing the *n*-alkanes signature of the sediment record with modern local vegetation. Again, the sediments have been analysed by HPLC in respect of HGs and brGDGTs compounds. Based on the latter compounds, a separation of the lake's evolution has been accomplished, with an initial phase of more aquatic influence visible in low BIT values. The following phases are characterised by strong increase in terrigenous soil input and an increase in calculated brGDGTs-MAAT. The youngest phase shows highest BIT values with strong temperature fluctuations, which have not been reported in the literature before. As in this phase a stronger human occupation on the Peloponnese is reported, the lake and its catchment might have been influenced by humans and the lipid composition might be disturbed by human interference.
The HG distribution has been used to firstly describe the heterocyte cyanobacteria community in the ancient lake and secondly to produce a n independentd temperature trend based on the HDI_{28}. In contrast to the brGDGTs-inferred MAAT, this temperature seems to reflect the summer temperatures based on a calibration from a German lake (Bauersachs et al., 2015). However, similar to the Lake Steisslingen problem, further research on both temperature proxies has to be conducted since no local calibrations are existing and the HGs have not been fully applied in (lacustrine) paleo studies.

The second part of this PhD thesis deals with the application of biomarkers and isotopes in archaeology. By analysing the $\delta^{13}C$ values of $C_{16:0}$ and $C_{18:0}$ fatty acid of modern animal reference fats (ruminant and non-ruminant adipose fats, ruminant dairy fats) from Ukraine, a local calibration has been developed for applications to distinguish animal fats from ancient potteries of the same area. Therefore, pottery vessels from Cucuteni-Trypillia sites in modern Ukraine and Moldova haven been analysed to determine their use and content. Some fats originated from ruminant adipose or beeswax. Most of the samples, however, plot outside of

a modern reference fat value regime. By adapting the carbon isotope ranges from modern equine fats from literature (Outram et al., 2009) in our reference dataset, the results indicate that most of these fats originate from equine. However, as these reference samples originate from Kazakhstan, these values should be evaluated with modern samples from Ukraine or Moldova in future research. In addition to archaeozoological remains investigated in previous studies, the results from pottery residue analysis give a direct insight in the feeding behaviour and culinarian practises of Cucuteni-Trypillia culture.

The findings of beeswax in samples from Ukraine as well as in samples from central Germany (Hesse) are highlights from the archaeological point of view. These findings are the first evidence of the use of beeswax in the two study areas. The lipid interpretation of the samples from central Germany of the Neolithic Wartberg Culture could be directly linked to the function of the individual vessels. Biomarkers formed during heating (mid-chain ketones) were found in vessels with heavy temper indicative for fire exposure. Milk fats with beeswax, which may have served as impregnation, were found in vessels with an outwardly directed rim that facilitates pouring.

In samples from Neolithic pottery vessels from two Funnelbeaker and Globular Amphora culture sites in northern Germany, molecular biomarkers and their respective carbon isotope signatures identified a plant oil and ruminant meat or dairy product origin. In the highly decorated pots from the Megalithic tomb Wangels, preferential ruminant adipose fats and plant oils were found, which were interpreted as precious funerary objects like cattle meat and sea buckthorn oil. In contrast, in the non- or only less decorated pots from the adjacent dwelling site Oldenburg-Dannau, less valuable products like plant and dairy products were found. These results demonstrate the exclusive use of valuable grave goods at funeral sites and manifest the important role of cattle in Neolithic societies.

The application of organic residue analysis in archaeology offers a unique opportunity to directly trace human diet in ancient cultures. However, there are some contradictions and unresolved issues. Especially plant material is underrepresented in most studies. Mostly the carbon isotope values of fatty acids after hydrolysation are interpreted as animal fat origin although these compounds may also be produced by plant oils with similar carbon isotope ranges. The argument that animal fats produce more fatty acids than plant oils and therefore the fatty acids found in ceramic vessels derive predominantly from animals is not tenable, if only vegetable material was cooked. More research is needed to identify other typical plant biomarkers such as miliacin for broomcorn millet (Jacob et al., 2005). Additionally, cooking and degradation experiments with mixed ingredients should be performed, to identify how the lipid distribution and isotope ratios behave.

Overall, this study has shown that molecular biomarkers are an essential tool in paleoclimate and (paleo)environmental studies to trace the interaction between biosphere and geosphere.

Additionally, organic compounds can be applied to identify transformation in human-environmental-interaction. In the field of molecular archaeology, biomarkers are a potent tool to identify the use and contents of unglazed pots and help to reconstruct the ancient diet and domestication of certain animals and plants.

Appendix A: Organic residue analysis on pottery vessels from the Wartberg culture in central Germany

In the following chapter, first results of organic residue analysis on pottery vessels from the settlement Wittelsberg (n=5) and the gallery grave Altendorf (n=1) located in central Germany are outlined. The results will be incorporated in a further publication with colleagues from the B2 project “Third millennium transformations of social and economic practices in the German Lower Mountain Range” of the CRC 1266. The extraction and analysis of lipids were performed as described in the manuscripts of chapters 5 and 6.

Results and discussion

Palmitic ($C_{16:0}$) and stearic ($C_{18:0}$) fatty acids were the most dominant compounds in all samples, which is due to their widespread occurrence in both animal fats and plant oils (Fig. A1 and A2). A simple ratio of both fatty acids expressed as palmitic to stearic acid ratio (P:S) has been used to distinguish between animal fats and plant origin, where a plant origin in pottery is interpreted with a predominance of stearic acid (Copley et al., 2005b). However, the ratio should be used with caution, since there are stearic acid lean oil plants like linseed or sesame (Copley et al., 2005). Furthermore, the degradation processes of lipids are complicated and not fully understood (Romanus et al., 2007) and may lead to a preferable removal of either stearic or palmitic acid. As noted for most archaeological samples, the odd carbon numbered fatty acids pentadecanoic ($C_{15:0}$) and heptadecanoic ($C_{17:0}$) were detected as well as their branched iso- and anteiso homologues ($brC_{15:0}$, $brC_{17:0}$). These components preferentially derive from ruminant animal fats like cattle, goat, sheep adipose fats or their dairy products (Baeten et al., 2012). An animal origin is also supported by the presence of monoacylglycerols (MAGs) in four and diacylglycerols (DAGs) in two samples, respectively, which are formed during the hydrolyses of triacyclglycerols (TAGs) the most abundant compounds in modern animal fats (Evershed et al., 2002). Additionally, the presence of mid-chain ketones in the range of C_{29} to $C_{35,}$ which are formed upon pyrolysis (>300°C) of acylglycerols was indicative for heating of the pots (Fig. A1) (Raven et al., 1997). This supports the assumption that the pots (Wit 7 9007 3.86 / 4.47, Wit 7 9003 4.17/1.02) were used as cooking rather than storage utensils, which is in agreement with their medium to heavy tempering that corroborates heat exposure.

One sherd each from Wittelsberg and Altendorf contains large amounts of *n*-alkyl monoesters (wax esters in the range of nC_{40} to nC_{50}), long-chain *n*-alkanes (nC_{25}-nC_{33}), long-chain *n*-alcohols (nC_{24}-nC_{32}) as well as minor amounts of long-chain *n*-fatty acids (Fig. A2). This type of lipid mixture has been interpreted as of beeswax origin (Heron et al., 1994). As modern beeswax does not contain large amounts of $C_{16:0}$ and $C_{18:0}$ fatty acids, these may originate

from the hydrolysis of the wax esters during burial or derive from plant oil storage in the vessels. Beeswax is thought to have been used for sealing of the pots, which served to store oily liquids or medical ingredients and cosmetics inside (Mayyas et al., 2012). As both samples containing beeswax have an outwardly orientated rim that allowed an easy pouring, a use for liquid storage is considered. The presence of branched fatty acids and MAGs in one of these samples (WIT 7- 3D- 2.60/3.60) may indicate the presence of an animal fat such as milk or another dairy product (butter) in the ceramic pot. Evidence for beeswax in pottery was found in several sites from all over Europe with a predominance in south-east Europe/Anatolia, with the oldest samples found in Çatalhöyük (Anatolia, 7,000 cal BC) (Roffet-Salque et al., 2015). In central Europe, beeswax was found in pottery from Altheim and from the Linearbandkeramik culture (Linear Pottery culture, LBK) sites in Austria and southern Germany, which are up to 2,000 years older than the Wartberg culture samples in this study (Heron et al., 1994; Roffet-Salque et al., 2015). However, the two findings are the first evidence for the use of beeswax processing and potentially beekeeping for central Germany.

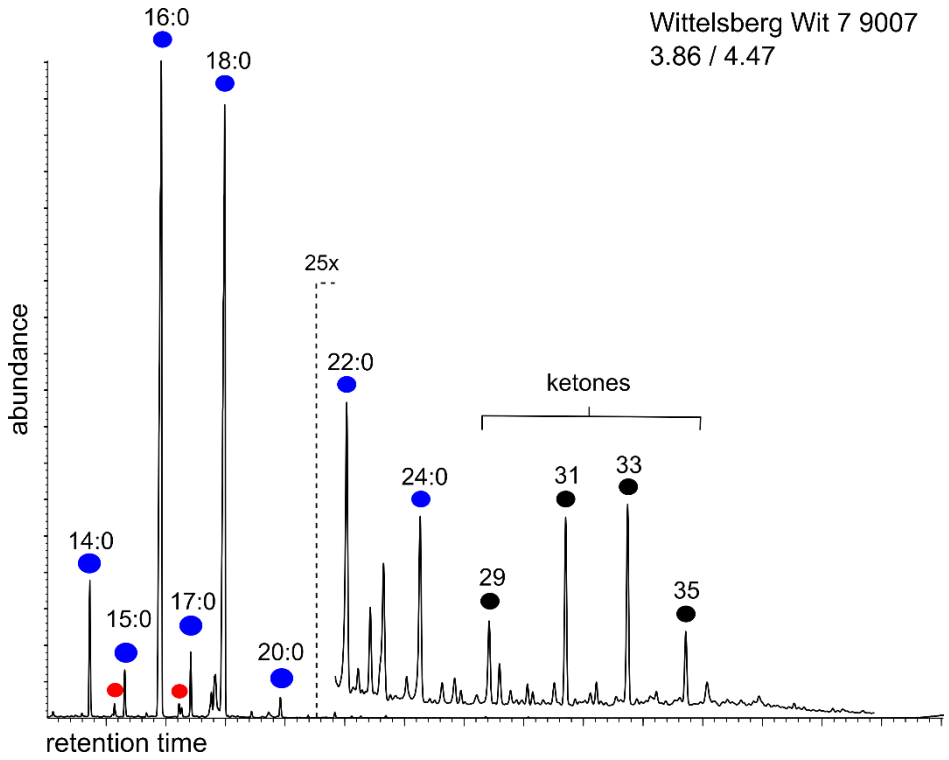

Figure A1: Partial ion chromatogram of derivatized lipid extract (TLE) from sample Wittelsberg Wit 7 9007 3.86/4.47 showing a lipid distribution indicative for cooked ruminant animal fat. Blue circle: *n*-fatty acids, red circle: branched fatty acids (C_{br15}, C_{br17}), black circles: mid-chain ketones.

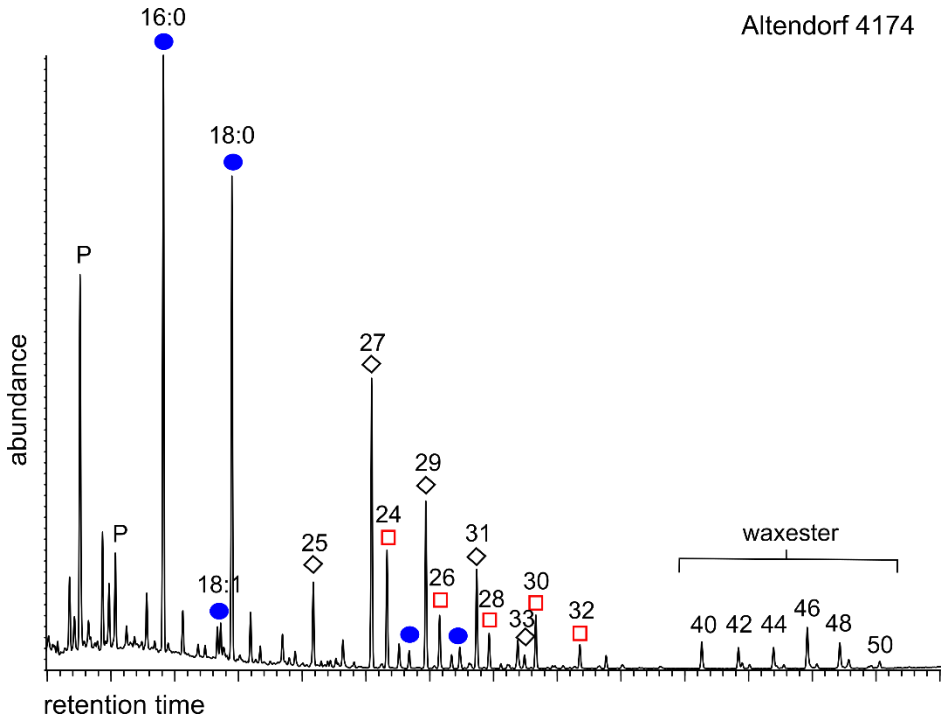

Figure A2: Partial ion chromatogram of derivatized lipid extract (TLE) from sample Altendorf 4174 showing a lipid distribution indicative for beeswax. Blue circle: *n*-fatty acids, black diamonds: *n*-alkanes, red square: *n*-alcohols, P: phthalates (contaminations from plastic bags during storage).

Appendix table 1: Summary of the lipid results from the investigated pottery vessels from central Germany.

		Fatty acids					Acylglycerols		others	Wax compounds			Interpretation
Findnumber	Site	$C_{16:0}/C_{18:0}$	C_{15}	C_{17}	brC_{15}	brC_{17}	MAGs	DAGs	Ketones	Waxester	Alkanes	Alkohols	
WIT 7- 3D- 2.60/3.60	Wittelsberg	0.59	x	x	x	x	C_{16}, C_{18}			C_{42}-C_{50}	C_{25}-C_{31}	C_{24}-C_{32}	Beeswax
Wit 7 9007 3.86 / 4.47	Wittelsberg	1.11	x	x	x	x			C_{29}-C_{35}				Ruminant fats
Wit 7 9003 4.17/1.02	Wittelsberg	1.32	x	x		x	C_{16}, C_{18}	C_{32}, C_{34}	C_{31}				Ruminant fats
Wit 7 9003 1.60/3.00, schn. 4, pl.2 (I)	Wittelsberg	0.41	x	x		x	C_{16}, C_{18}	C_{32}, C_{34}					Ruminant fats
Wit 7b- 7-F-2.65/3.43	Wittelsberg	1.57	x	x		x	C_{16}, C_{18}						Ruminant fats
4174	Altendorf	1.25								C_{40}-C_{50}	C_{25}-C_{33}	C_{24}-C_{32}	Beeswax

Appendix B: 2,500 years of anthropogenic and climatic landscape transformation in the Stymphalia polje, Greece

Joana Seguin[1]*, John L. Bintliff[2], Pieter M. Grootes[1,3,4], Thorsten Bauersachs[5], Walter Dörfler[3,6], Christian Heymann[1,3], Sturt W. Manning[7], Samuel Müller[8], Marie-Josée Nadeau[4], Oliver Nelle[1,3,9], Peter Steier[10], **Jan Weber[5]**, Eva-Maria Wild[10], Eleni Zagana[11], Ingmar Unkel[1,3]

[1]Institute for Ecosystem Research, Christian-Albrechts-University, Olshausenstraße 75, 24118 Kiel, Germany
[2]Department of Archeology, Edinburgh University, Teviot Place, EH8 9AG, United Kingdom
[3]Graduate School, "Human Development in Landscapes", Christian-Albrechts-University, Leibnizstr. 3, 24118 Kiel, Germany
[4]National Laboratory for Age Determination, NTNU Vitenskapsmuseet, 7491 Trondheim, Norway [5]Institute of Geosciences, Department of Organic Geochemistry, Christian-Albrechts-University Kiel, Ludewig-Meyn-Straße 10, 24118 Kiel, Germany
[6]Institute of Pre- and Protohistoric Archaeology, Christian-Albrechts-University, Johanna-Mestorf-Straße 2-6, 24118 Kiel, Germany
[7]Cornell Tree-Ring Laboratory, Department of Classics, Cornell University, Ithaca NY 14853-3201, USA
[8]Insitute of Geosciences, Department of Paleoceanography & Paleoclimate, Christian-Albrechts-University, Ludewig-Meyn-Straße 10, 24118 Kiel, Germany
[9]Tree-ring Lab, Landesamt für Denkmalpflege im Regierungspräsidium Stuttgart, Fischersteig 9, D-78343 Hemmenhofen, Germany
[10]VERA-Laboratorium, Währinger Straße 17, Kavalierstrakt, 1090 Wien, Austria
[11]Department of Geology, University of Patras, Rio 26500 Patras, Greece

Status: manuscript published in *Quaternary Science Reviews*
doi.org/10.1016/j.quascirev.2019.04.028

Keywords: Late Holocene; Palaeoclimatology; Palaeolimnology; Eastern Mediterranean; Greece; Geochemistry; Sedimentology; XRF; GDGT; Late Antique Little Ice Age

Abstract

Lacustrine sediments generally record landscape development in the lake's catchment area controlled by palaeoclimatic and human induced changes. To improve our understanding on the anthropogenic and climatic influences on landscape development in Southern Greece for the last 2,500 years, we report a 2 m-long, continuous high-resolution sedimentary record from shallow Lake Stymphalia (Peloponnese, Greece). Our proxies record climatically as well as anthropogenically induced landscape changes, influencing the lake area and lake depth.

The Classical-Hellenistic era reflects a moderate, stable Mediterranean climate with low sedimentation rates. The parallel existence of the highly populated, major ancient city of Stymphalos, on the contemporary lake edge, doesn't seem to have caused lasting alterations in the record. The construction of the Hadrianic Aqueduct in the Roman era, ca. 130 AD, however causes an influential transformation in the lake development. It has a lasting effect on the lake hydrology as well as the vulnerability of this ecosystem. During Late Roman times, 5th to 6th century cal AD, the abandonment of the aqueduct combined with cooler climate conditions allows lake levels to recover. A phase of very high climatic instability was identified for the subsequent Early Byzantine (EB) period, during the 7th and 8th century cal AD. For this period, the later phase of the Late Antique Little Ice Age (LALIA), our proxies indicate further cooling and highly fluctuating water availability in a rather small lake area. The Middle Byzantine (MB) Period (9th-12th century AD) is characterized by an over fivefold increase in sedimentation rates. Since local population was still well below Classical levels, we explain this singular period through an interaction of modest increase in land use but marked by careless management of deforested areas, warm and wet climatic conditions during the Medieval Warm Period and long-term effects of vulnerability caused by the aqueduct construction. Probably during this phase, the lake level rose through unparalleled sedimentary infill to flood and bury a significant part of the Lower Town of the abandoned ancient city. The Late Byzantine Period (13th and 14th century AD) sees core evidence for erosion of established, non-vegetated soils (high magnetic susceptibility), in a period of almost total depopulation. In the subsequent Ottoman era (late 15th – early 19th centuries AD) local settlement made only slight recovery, the climatic conditions seem less stable during the Little Ice Age (LIA) and the lake seasonally and later periodically starts to dry up, cumulating in a longer dry phase at the end of the 19th century AD, when agricultural activity on the polje floor was possible. The conclusion conforms with recent modelling of environmental change, critical of mono-causation, rather focussing on complex interactions of human and natural factors in the inception of landscape transformation.

1. Introduction

The Late Holocene in southern Greece is shaped by a strong interaction of climatic changes with natural and anthropogenic landscape transformations. Although there is an increasing number of studies demonstrating the complex interrelationship between climate and societies, it often remains challenging to decipher the influence of climatic change versus human activities in environmental records. Palaeoclimatologists have developed reconstructions of climate change in the Mediterranean region during the Holocene, covering cultural periods back to the Neolithic, when humans became sedentary and the interrelationship between climatic fluctuations and human activity grew in importance (Finné et al., 2011; Magny and Magny, 2013; Roberts et al., 2016; Meriam et al., 2017; Palmisano et al., 2017, 2019).

Recent studies have suggested that important climatic shifts in the Late Holocene coincide with major changes in Mediterranean cultural history (Butzer, 2012; Drake, 2012; Kaniewski et al., 2013; Langgut et al., 2013; Staubwasser and Weiss, 2006; Weninger et al., 2009). However, many archaeologists and historians have been critical of naïve use of climate change as a forcing factor in the socio-cultural development of the region due to the lack of both high-resolution terrestrial palaeoclimate data in a solid chronology framework and simple forcing-and-response mechanisms (Haldon et al., 2018). Hence, there is a strong need for closer interdisciplinary collaboration on research questions dealing with human-environmental interaction and societal response to climatic changes (Bintliff, 2002, 2012a; Casana, 2008; Sadori et al., 2008; Izdebski et al., 2016; Knapp and Manning, 2016).

Climate reconstructions from lake sediment archives in the Eastern Mediterranean are still relatively scarce and the climate patterns often seem less well constrained compared to the Western Mediterranean (Gogou et al., 2016; Luterbacher et al., 2012, McCormick et al., 2012). In particular, the last 2,500 years have been studied less frequently or with lower resolution in palaeoenvironmental records although this time period is of major relevance for the development of Greek society (Finné et al., 2011; Sadori et al., 2016; Xoplaki et al., 2016). Recently, Büntgen et al. (2016) identified a cold phase in Eurasia lasting from 536 to 660 AD based on high-resolution tree ring records and named it Late Antique Little Ice Age (LALIA). This overlaps with the latter part of the European Migration Period (4^{th} – 7^{th} century AD; Moschen et al., 2011), an interval of widespread migration movements into the Roman Empire, which saw considerable societal changes, including the collapse of the Western Roman Empire, the transformation of the Eastern Roman Empire into the Byzantine state, the collapse of the Sasanian Empire, the expansion of Slavic-speaking peoples in central and eastern Europe and the Justinian Plague (Moschen et al., 2011). Due to these significant societal changes and its negative impacts on European civilisations, this wider period is also referred to as the "Dark Age[s]" (McCormick et al., 2012; Brooke, 2014; Büntgen et al., 2016; Helama et al., 2017a). While there is considerable archaeological information from the Greek

Mainland, including the Peloponnese Peninsula, for human activities during the last two millennia (Bintliff, 2012b; Izdebski et al., 2016), high resolution palaeoclimate records for this period are rare (Atherden and Hall, 1994; Finné et al., 2011; Izdebski et al., 2016; Jahns, 1993). In a recent review of the currently available climate records from the Mediterranean for the last two millennia, Luterbacher et al. (2012) state that the existing climate proxies often express varying trends, even within the same region. All of this demonstrates the need for further interdisciplinary, high-resolution studies on landscape development in the Eastern Mediterranean.

With the intention of addressing this gap and limited dataset, we here provide a detailed palaeoenvironmental reconstruction of the last 2,500 years from Lake Stymphalia, the only remaining natural perennial lake in the Peloponnese. We discuss the environmental changes in the catchment in relation to the human history known from the area in order to distinguish anthropogenic from climatic developments imprinted into the sedimentary record. The potential expression of the LALIA in Southern Greece is investigated in order to improve our understanding of the societal and environmental history of this area during this period of rapid climate fluctuations. Excavations at Ancient Stymphalos by the Canadian Institute in Greece since 1983 provide the archaeological groundwork to reconstruct human activity in the area (cf. section 0). As a karst polje without surficial outflow represents on the one hand a continuous sediment sink and on the other hand has always been considered as an important location for agriculture and farming in the Mediterranean area (Vött et al., 2009), Lake Stymphalia represents an excellent archive to study a combination of climatically as well as anthropogenically induced environmental changes. The differentiation between human and climate induced factors behind environmental changes, however, is not always trivial and several causes may provoke the same response in the sedimentary record. For example, reduction in the amount of water available in Lake Stymphalia may result from either: (1) a decrease in precipitation; (2) an increase in evaporation; (3) changes in the thawing period and variations in the discharge related to snowmelt; (4) inferred or recorded human channelling of the water from the source; (5) increased water usage of lake water for agricultural purposes. To get a better idea of the complete picture, we take into account several different palaeoenvironmental proxies, traditional and well-established ones as well as new and innovative proxies. As far as available, we included archaeological or historical evidence and when we can still not be certain of the process causing a signal in the record, we provide a selection of possible scenarios.

2. Study area

Lake Stymphalia (Λίμνη Στυμφαλία) (37.85° N, 22.46° E), is a shallow karstic lake located in the north-eastern Peloponnese (Greece; Figure B1 and B3-A). It is described in detail by Heymann et al. (2013). Sediment material is only received from surface runoff and torrential rivers originating from karst springs, which depend on the amount of precipitation that is brought mainly in winter and early spring (Figure B2). On the polje floor, the karstified limestone is covered by argillaceous sediments of up to 160 m thickness (Morfis and Zojer, 1986). Presently, Lake Stymphalia is the largest remaining mountain lake in the Peloponnese, protected by the NATURA 2000 network (Heymann et al., 2013; Morfis and Zojer, 1986, Papastergiadou et al., 2007).

Modern climatic conditions are described in Heymann et al. (2013) and Morfis and Zojer (1986). In a recent publication, Nanou and Zagana (2018) indicate a mean annual precipitation of 850 mm and ranges from 719 to 1656 mm for the time period 1975–2015, confirming high inter-annual variation. Based on daily precipitation data recorded between 1949 and 2011 at the meteorological station Driza-Stymphalia (37.8699° N, 22.4643° E, Greek Special Secretariat for Water, Ministry of Environment and Energy), we calculated the mean annual precipitation at 618±201 mm over the respective period; this occurs mainly from October to February (Figure B2). In April 2017, we installed a small datalogger (Tinytag Plus 2) close to the fountain house of ancient Stymphalos to measure daily temperatures and relative humidity, which provided the monthly temperature values shown in Figure B2.

The lake's surface area may have varied substantially throughout time and there is evidence for seasonal desiccation (Walsh et al., 2017b). Since the 19th century, the lake occasionally dried out completely, which in the mid-20th century allowed it occasionally to function as an aircraft runway (hence the reason for its local nickname "aerodromio" (airport)). In recent times, Lake Stymphalia fell dry during the early 1990s and was used for agricultural purposes (Papastergiadou et al., 2007). For several reasons, we do not assume any extreme lake level rise at Lake Stymphalia, at least not during the last 2,500 years, although local archaeological and historical records indicate significant variation in the height and extent of the lake since Classical times: (1) there is no evidence of rocky, barren beach deposits in Stymphalia comparable to those described by Knauss (1990) from the neighbouring Pheneos polje, where an exceptionally high lake level was artificially induced by Ottoman troops during the Greek liberation battle in the 19th century; (2) Stymphalia has three discharge possibilities, the large natural sinkhole in the Southwest of the polje, a smaller sinkhole in the North (Morfis and Zojer, 1986) and the Hadrianic Aqueduct built around 130 AD; (3) the Cistercian Zaraka Monastery, the best preserved Frankish monastic site in Greece (Campbell, 2018), was built in the first half of the 13th century AD on the relatively flat valley floor, about 2 m above and 1 km distant from the present day lake shore, with no sign of later flooding. However, a major part of the

Lower Town of ancient Stymphalos city has been submerged and silted since the Early Roman era and currently lies under sediments (Williams, 2005), induced by a rise of the lake bottom of only few metres since the founding of that town.

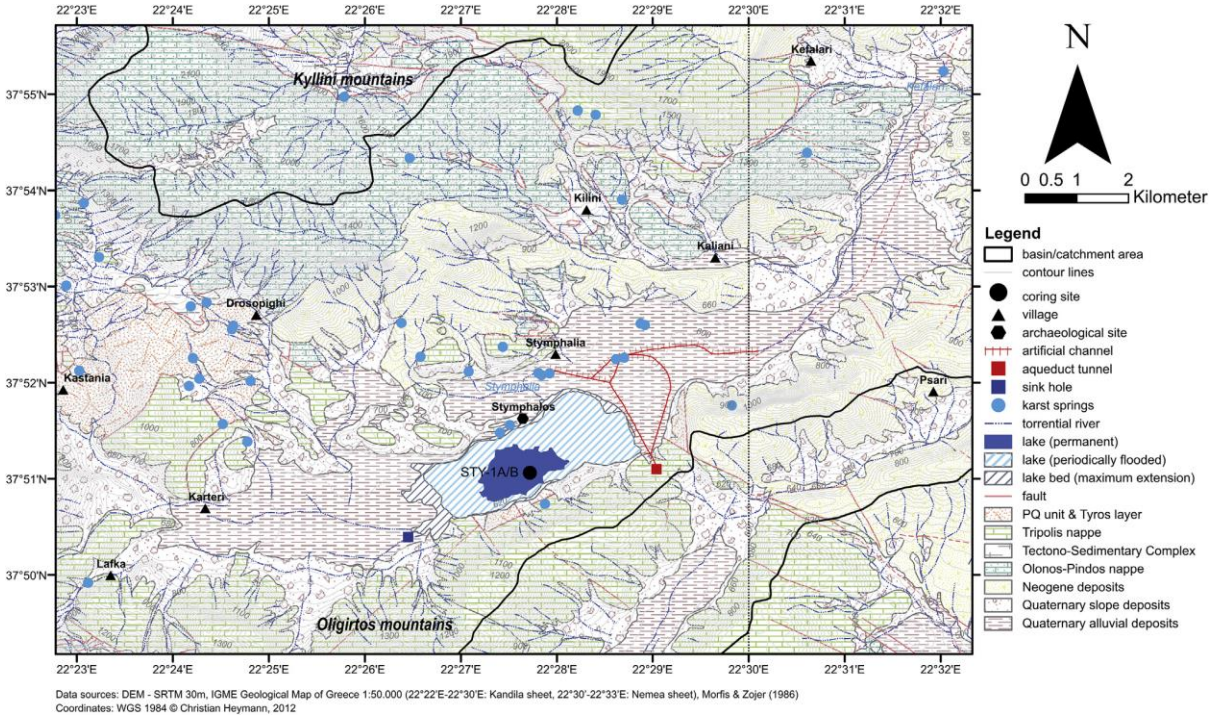

Figure B1. Topographic and geological map. The Stymphalia basin with its drainage system and the approximate catchment area are shown. The map was created using ESRI ArcGIS 10.

3. Materials and Methods

3.1 Sediment cores

Field and initial laboratory work were mostly conducted in 2010 and 2011 and have been described in detail by Heymann et al. (2013). Three overlapping sediment core pairs of different lengths (STY-1, STY-2, and STY-3) were retrieved. The 16-m-long composite core STY-1 is the most complete and here, we discuss the upper 208 cm of it in detail (units 59 – 70b; Table 1), that cover approximately the last 2,500 years based on the updated age-depth-model described below which records both natural and anthropogenic influences. The lower limit was set at the upper sedimentary boundary of unit 58. We use the following proxies measured and described by Heymann et al. (2013): lithology, sediment structure, Munsell color (Munsell, 2000), grain size distribution, total carbon (TC), total inorganic carbon (TIC), total nitrogen (TN), magnetic susceptibility (Nowaczyk et al., 2002; Nowaczyk, 2005), and X-ray fluorescence (XRF) measurement (see section 0 below).

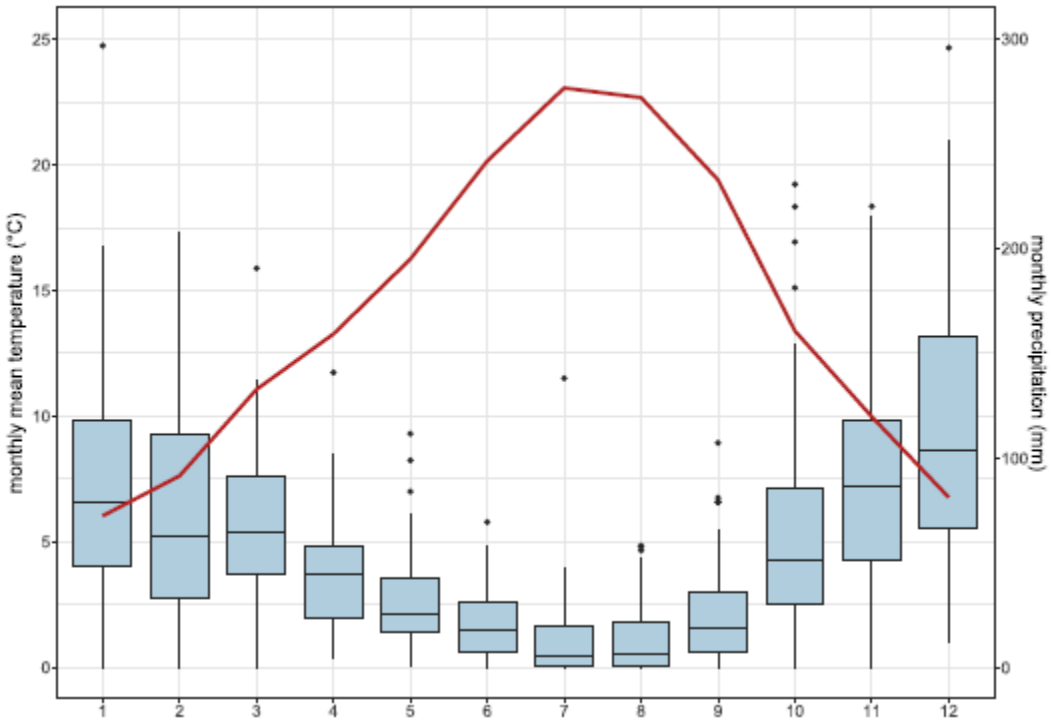

Figure B2. Modern air temperature and precipitation for the Stymphalia basin. The mean monthly temperature for the station Driza-Stymphalia (37.8699 °N, 22.4643 °E, 622 m a.s.l.) for the period 1950 – 2011 (red line) and boxplots for the monthly precipitation are shown from January (1) to December (12).

3.2 Dating technique

The age control of the sediment cores was based on accelerator mass spectrometry (AMS) radiocarbon (^{14}C) measurements performed at four different laboratories. For radiocarbon dating, 24 core samples and 3 surface samples have been taken and, as visible organic remains were almost absent from the core, mainly bulk sediments were used for dating (Table 2). The combined dating results lead to a time scale substantially different from the one published by Heymann et al. (2013). We present the construction of the time scale in detail in the following section 0. Throughout the paper, the year 1950 AD is used as year 0 BP (Mook and Van Der Plicht, 1999).

3.3 Elemental composition: X-ray fluorescence measurements

Non-destructive X-ray fluorescence (XRF) measurements using energy dispersive fluorescence radiation on split core surfaces were performed with an Avaatech XRF Core Scanner, using a Rhodium X-ray source. The scanning parameters are the same as described by Heymann et al. (2013). The scan resolution of the upper 5 m of core STY-1A and overlapping intervals of core STY-1B was 1 mm with an exposure time of 10 s at 10 kV and 15 s at 30 kV, respectively. We selected 13 elements (10 kV: Al, Si, S, Cl, K, Ca, Ti, Mn, Fe;

30 kV: Zn, Rb, Sr, Zr) for a detailed analysis of their presence across the sediment sequence and their palaeo-environmental and -climatic significance (n = 4961). Elements with low intensities (< 300 total counts) which are less reliable (Tjallingii et al., 2007) were excluded. The XRF scanning results represent element intensities in total counts per second (tcps) which mainly depend on element concentration, but also on matrix effects, physical properties, sample geometry, and hardware settings of the scanner (Tjallingii et al., 2007). We chose to plot the XRF scanning results as log-ratios that can be interpreted as changes in relative concentration of an element pair, to avoid statistical analysis of data sensitive to the closed-sum effect and asymmetric element ratios (Weltje and Tjallingii, 2008). As we were applying the R software (R Core Team, 2017) for plotting, natural logarithms with base e (log) were applied by default. To assess the normalized elemental data in a palaeo-environmental and -climatic context, we compare relative changes of one element to another, rather than using absolute changes in element concentration.

3.4 Organic analysis: Lipid extraction and GDGT analysis

The interval 152 – 191 cm has been sampled at an average resolution of 0.5 cm from the sediment core STY-1A. Generally, five mm-thick sediment slices were taken, but for some exceptions, the spacing was varied due to the lithology. The sediments were lyophilized for 24 h and ground to a fine powder using a solvent-cleaned agate pestle and mortar. Subsequently, an aliquot (3.6-8.1 g) of each homogenized sediment was extracted using an ASE 200 (Dionex, USA) at a temperature of 75 °C and a pressure of 5.0×10^6 Pa. Each sample was extracted for 20 min using a solvent mixture of dichloromethane (DMC)/methanol (MeOH) (9:1, v/v). The bulk of solvent was removed by rotary evaporation and the obtained total lipid extract (TLE) dried under a gentle stream of nitrogen. An aliquot (0.7-1.0 mg) of each TLE was separated into an apolar and a polar fraction using a small Pasteur pipette filled with activated aluminum oxide (3.5 cm) as stationary phase. The apolar fractions were eluted with 4 ml *n*-hexane/DCM (9:1, v:v) and the polar fractions with 4 ml DCM:MeOH (1:1, v/v), respectively. The polar fractions (containing isoprenoid and branched glycerol dialkyl glycerol tetraethers (GDGTs)) were dried under nitrogen, re-dissolved in *n*-hexane:2-propanol (99:1, v/v) to a concentration of 2 mg/ml and passed through a 0.45 µm polytetrafluoroethylene (PTFE) filter (Macherey-Nagel, Germany) prior to analysis.

GDGTs were measured using an Alliance 2695 HPLC system (Waters, UK) following the analytical protocol described by Hopmans et al. (2016), which allows the separation of 5- and 6-methyl branched GDGTs. The HPLC system was equipped with two Waters BEH HILIC silica columns (2.1 x 150 mm; 1.7 µm particle size) and a guard column of the same material, which were all maintained at 30 °C. Target compounds were eluted with a flow rate of 0.2 ml/min starting isocratically with 82 % eluent A (*n*-hexane) and 18 % eluent B (*n*-hexane:2-

propanol (9:1, *v/v*)) for 25 min. A linear gradient was set to 65 % eluent A and 35 % eluent B in 25 min, followed by a linear gradient to 0 % eluent A and 100 % eluent B in 30 min. Re-equilibration of the column to initial conditions with 82 % eluent A and 18 % eluent B was within the following 20 min. Detection of isoprenoid and branched GDGTs was achieved using a Micromass ZQ single quadrupole mass spectrometer (MS) equipped with an atmospheric pressure chemical ionization (APCI) interface operated in positive ion mode. MS conditions were as detailed in Weidenbach et al. (2017). The methylation index $MBT'_{5Me,}$ a proxy that was developed to reconstruct absolute temperatures, was calculated using only 5-methyl isomers according to De Jonge et al. (2014) with roman numerals corresponding to GDGT structures displayed in the supplementary online material (BS5).

$$MBT'_{5Me} = (Ia + Ib + Ic) / (Ia + Ib + Ic + IIa + IIb + IIc + IIIa) \quad (1)$$

The branched-over-isoprenoid tetraether (BIT) index, indicating the relative input of terrestrial organic matter, was calculated as given in Hopmans et al. (2004) using the combined peak areas of the 5- and 6-methyl isomers of the branched GDGTs:

$$BIT\ Index = (Ia + IIa + IIa' + IIIa + IIIa') / (Ia + IIa + IIa' + IIIa + IIIa' + IV) \quad (2)$$

3.5 Statistical data processing

We applied statistical approaches such as correlations and multivariate analyses, including principal component analyses (PCA) using the R software (R Version 3.4.2; R Core Team, 2017) to investigate the covariance of the different chemical elements of the sediment core.
For the geochemical data, cleaning of the dataset, i.e. the removal of explicit outliers and filling of missing values by spline interpolation was done manually prior to statistical processing. Correlation coefficients of elemental log-ratios can give an insight into the coupling/decoupling of elements over time. Hence, the relationships between different elemental ratios were explored calculating Pearson correlation coefficients, if normal distribution of the data existed (tested with the Shapiro-Wilk-test), or alternatively, Spearman rank-based correlation was applied. Furthermore, we applied PCA to the original XRF elemental dataset to objectively describe similarities and differences between the elements and to identify the main environmental processes that influence the composition of the lake sediment. The aim of the PCA is to reduce a high dimensional dataset to a very limited amount of meaningful and uncorrelated variables, so called components or factors, that still explain most of the variance in the data set (Filzmoser et al., 2009). Here, the loadings indicate the contribution of each element to the respective principle component (PC). Not all element records in our dataset are normally distributed, and some show a pronounced skewness. As PCA requires a

Gaussian distribution of the data, the dataset was standardized, i.e. z-normalized to a mean of zero (m = 0) and a standard deviation of one (σ = 1) for each parameter. In this way, we also avoid overestimating elements with extremely high counts (mainly calcium and iron) in order to equally weight the different parameters. Subsequently, PCA based on the correlation matrix was applied using the function *prcomp* from the R stats package. This approach also includes an orthogonal rotation of the components, which may facilitate the interpretation of the scores and loadings. We abstained from the application of intensive smoothing of the dataset to avoid any further approximation of the data.

3.6 Archaeological data

Regional surveys in the area started in 1982. From 1983 to 2012, the site of Ancient Stymphalos was excavated under the auspices of the Canadian Institute in Greece, however the publication of the finds has still not been completed. For the present study, no further excavation or archaeological data collection have been conducted, as the focus was on the palaeoenvironmental investigation. Instead, already existing, published data have been gathered (Philippson, 1892; Williams, 1996, 2003, 2005, 1983, 1984a, 1984b; Panagiotopoulos, 1985; Williams and Cronkite Price, 1995; Williams et al., 1997, 1998, 2002; Lolos, 1997; Williams and Gouley, 2005; Bintliff, 2012b; Schaus, 2014; Brown and Walsh, 2017; Walsh et al., 2017b) and consulted for information on human activity in the Stymphalia Polje.

As empirical data collections from archaeological and palaeoenvironmental archives are traditionally very different, juxtaposition of these different kinds of (quantitative) proxies can be challenging (Palmisano et al., 2017) and only a small number of studies try to bring them together (Weiberg et al., 2016; Palmisano et al., 2019). Weiberg et al. (2016) provide continuous quantitative data on settlements from archaeological information during the last 8000 years on the Peloponnese Peninsula. As it is the only quantitative proxy currently available, we use it as indication of settlement intensity, also in the Stymphalia Polje, and refined it from local archaeological information.

4. Results

4.1 Lithology

Building upon the stratigraphy presented by Heymann et al. (2013), the uppermost 208 cm of core STY-1 are subdivided into 20 stratigraphic units (No. 59 – 70b, Table B1, Figure B4) based on sedimentological properties (e.g. colour, texture, macro remains). None of the units is laminated nor are there visual, sedimentological indicators of short-term cyclic beddings. The sediment sequence has a fine texture and is generally composed of a varying mixture of

clay (mean = 27%) and silt (mean = 70%), containing 0 – 4 % sand with the exception of units 63 and 70a, in which 7.5 % and 17 % of sand were recorded (BS3).

Munsell (2000) colours in the upper 161 cm of the core range from olive to greyish brown and are generally brighter than in the lower part, which is also evident in the distance of the respective RGB colours to each other (Figure B4, Table B1). Organic debris and roots are generally small and scarce. Below 164 cm, darker greyish colours dominate and shell fragments of *Bythinia sp.* (Figure B3-D) and *Valvata sp.* gastropods are more frequent. A distinct black layer (unit 62), ranging from 164 – 161 cm, separates the upper brownish units from the lower more greyish units.

TIC values range between 0.8 to 8.0 wt% and correlate well with Ca counts (Figure B4, Figure B2). The TOC content varies from 1.2 to 6.4 wt% and is 3.0 wt% in the black layer (Figure B4, BS2). While TIC values are lower in units 59 and 60 compared to the upper part, the TOC content does not show any obvious differences between these two. The blackish unit 62 exhibits a singularly high magnetic susceptibility (MS) peak (SI = 3000). For the rest of the depicted core sequence, MS constantly fluctuates around a median of 70.27 (mean = 103.68). The upper brownish units 68 and 69 dispose of persistently higher MS values.

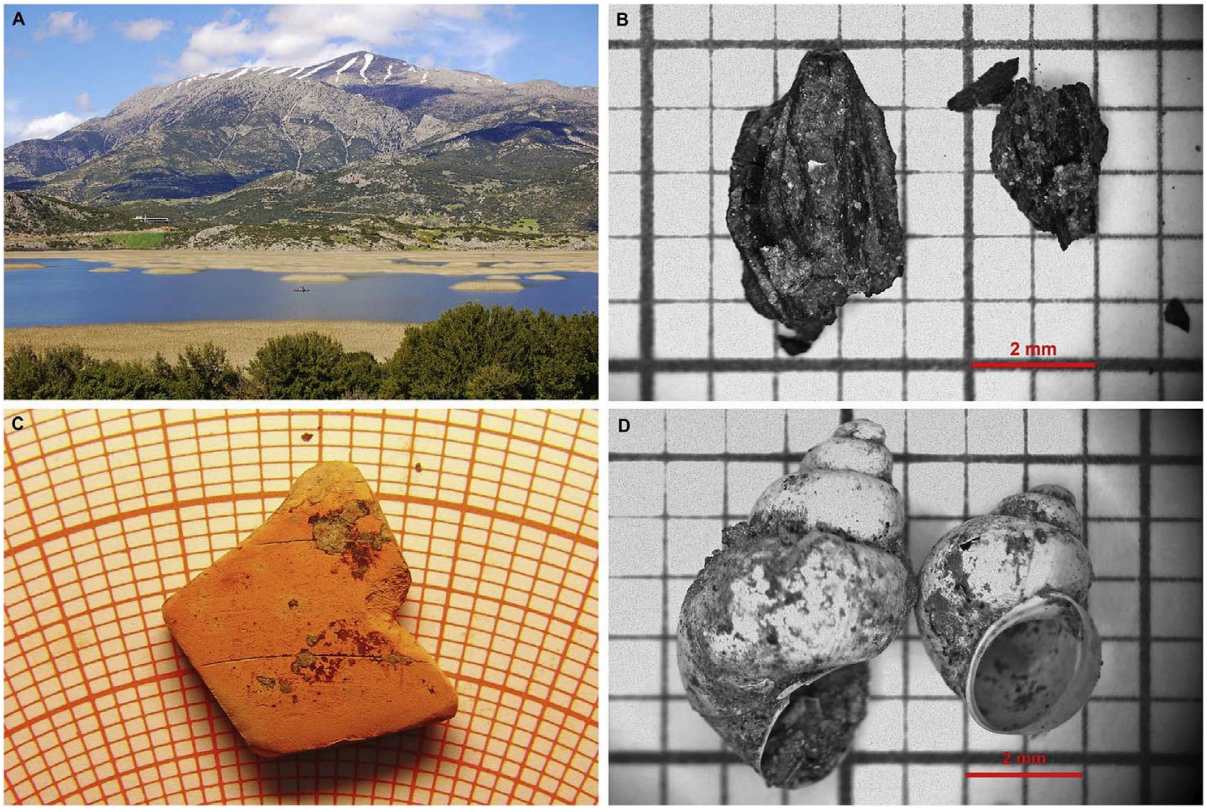

Figure B3: Photos of Lake Stymphalia and sample material. (A) Photo of Lake Stymphalia taken from the southern shore during coring campaign in 2010 with Mt. Ziria in the background (coring platform in the centre for scale). (B) Crataegus seed (VERA-6258) found at 165 cm depth (masterscale) in core

STY-1A. (C) Ceramic shard dated to 5th century BC found at 205 cm depth (masterscale) in core STY-3B. (D) Bythinia sp. shell sample.

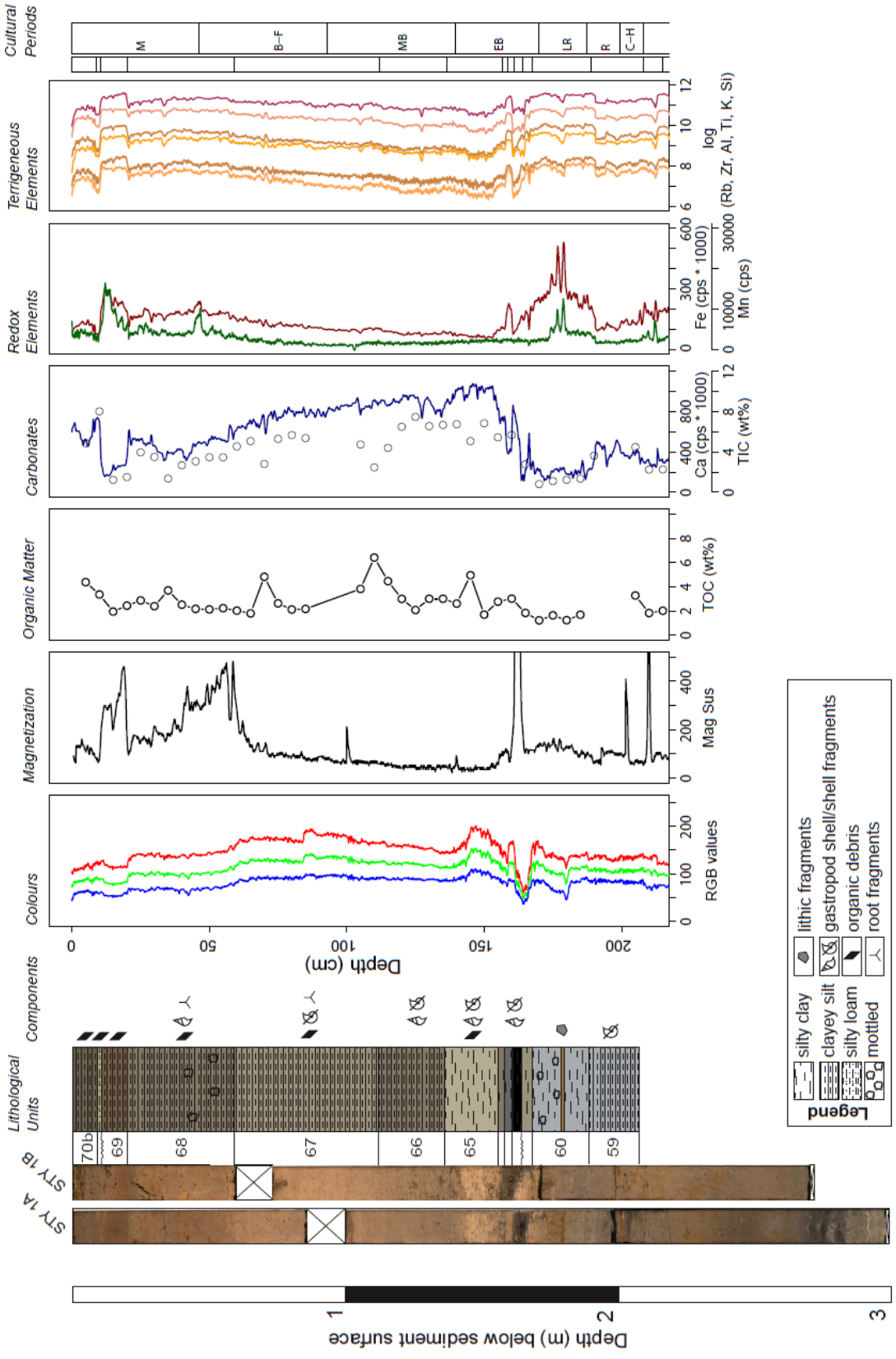

Figure B4: STY-1 composite core log with lithological units for the upper 208 cm (left) and overview of different proxies plotted against depth. Depths where samples for 14C dating were taken from STY-1A are indicated with red arrows. The only sample taken from the parallel core (VERA-6383) at 161 cm is additionally marked on the STY-1B core picture with a red dot. RGB color values (blue, green, red), magnetic susceptibility, TOC, TIC (black) and counts per second of Calcium (darkblue), Iron (darkred) and Manganese (green), as well as log-values of Rubidium, Aluminum, Zirconium, Titanium, Potassium, and Silicon (from left to right) are plotted against depth. For orientation, boxes with cultural periods and ages (BC/AD) at the respective transition boundaries to the right (for abbreviations of cultural periods see Table 3). For interpretation of the references to color, the reader is referred to the web version of this article.

Core Depth [cm]	Sediment Unit	Munsell Color	Soil Type	Description
0–9	70b	5Y 4/2	Ut4	Olive gray clayey silt with organic fragments decreasing to the top
9–10.5	70a	5Y 5/3	Lu	Olive fine sand with silt, medium sand-sized mineral grains, and organic fragments (UB=G)
10.5–20	69	10YR 4/3	Ut4	Very compact brown clayey silt with some organic fragments, irregular down-cutting to 12 cm, (UB=S)
20–59	68	7.5YR 5/4	Ut4	Brown clayey silt with minor silt content, some shells and organic fragments, oxidized root channels (UB=S)
59–112	67	2.5Y 5/2	Ut4	Grayish brown clayey silt with shell fragments (gastropods), becoming lighter towards top, organic fragments, oxidized root channels (UB=G)
112–136.5	66	2.5Y 5/2	Ut4	Grayish brown clayey silt with higher sand content, shells, and shell fragments (gastropods) decreasing to the top, (UB=G)
136.5–156.5	65	2.5Y 6/2	Tu4	Light brownish gray silty clay with higher sand content with shells and shell fragments (gastropods), organic content, organic fragments decrease to the top (UB=G)
156.5–158.5	64	2.5Y 5/2	Tu3	Grayish brown silty clay with some shell fragments, and organic content (UB=S)
158.5–161	63	5Y 4/1	Tu4	Dark gray silty clay with higher sand content, with shells and shell fragments (gastropods) (UB=S)
161–164	62	5Y 2.5/1	Tu4	Black layer of silty clay with shells, and shell fragments (gastropods) (UB=G)
164–167.5	61	5Y 6/2-5Y 5/1	Tu3	Light olive gray silty clay with higher sand content, shell fragments (gastropods), and organic content, intercalated with gray clay, upper boundary irregular (UB=E?); at 167.5 cm and 166 cm: 2 mm-thick fine to medium sand laminae; at 165 cm: 3 mm-thick fine to medium sand laminae
167.5–189	60	10YR 5/1	Tu4	Gray silty clay with coarse sand- to gravel-sized clastic fragments and organic content, both increasing to the top, (UB=S); at 180 cm: thin coarse grained oxidized orange layer, at 183.5 cm, 182 cm, 177 cm and 176.5 cm: carbonatic, coarse sand-sized clastic fragments, oxidized; at 173 cm: carbonatic, gravel-sized clastic fragment, oxidized
189–208	59	10YR 5/1	Ut4	Gray clay with some silt, shell fragments (gastropods), and organic content, shell fragments increase until 201 cm then decrease, organic content increases to the top (UB=G); at 201 cm: layer with partly intact shells

Table B1: Sedimentary units of the uppermost 208 cm of core STY-1. The soil type classification follows the German Arbeitsgruppe Boden (2005). (UB = upper boundary, G = gradational, E = erosional, S = sharp)

4.2 Core chronology

4.2.1 Radiocarbon dates

From the uppermost 324 cm of the parallel cores STY-1A and STY-1B (units 48–70), 24 samples for radiocarbon dating have been taken. Although our focus is on the uppermost 208 cm recording anthropogenic influences, the age model was calculated for a longer interval in order to construct a solid model and avoid boundary effects (Figure B5). The sedimentological analysis of the core sequence gave no indications for any hiatus or erosional discontinuities; hence, a continuous, even if sometimes very low sedimentation is assumed (Figure B6).

To determine the time at which specific layers in a sediment core were deposited, we need to isolate organic material from the time of sedimentation that is either terrestrial or has a known reservoir age. The challenge in dating sediments is that they contain a small fraction of old carbon, eroded and transported with the mineral fraction, in addition to limnic and terrestrial material from the time of deposition. Furthermore, sediments are open systems, so dissolved and colloidal carbon may be introduced at a later point in time. The standard Acid-Alkali-Acid (AAA) chemical pretreatment, commonly used in radiocarbon dating, aims to remove potentially mobile contaminating acid and alkali soluble organic compounds. If no recognizable macrofossils can be found, dating the remaining insoluble fraction (humin fraction) is the best candidate to provide a useful sedimentation age in organic rich sediments (organic content of the residue >1 %) (Grootes et al., 2004). A check on the age inhomogeneity of organic carbon in the sediment can be obtained by dating not only the insoluble residue, but also the organic material removed by alkali extraction. Acidification of this alkali extract precipitates the humic acid fraction. This fraction often dates younger than the insoluble residue since it may contain contaminating younger compounds and is less likely to receive a contribution from recalcitrant reworked carbon compounds. In case of an age difference between the humic acids and the humin, the humins are most likely to indicate the approximate time of sedimentation for organic rich sediments. For organic poor sediments the fraction of old reworked carbon, which is often around 0.1 %, is no longer negligible and can lead to measured humin ages that may be thousands of years too old (Grootes et al., 2004). In the eastern Mediterranean, it has been observed in a number of cases that humic acids extracted from samples appear not to offer appreciably different ^{14}C ages and so likely derive from the sample in question or contemporaneous material (Wild et al., 2013).

In total, 45 radiocarbon measurements were made on these 26 samples (Table 2). Alkali residue, humic acids, shell carbonates, and repeats of some fractions were measured at four different AMS-^{14}C facilities, the Leibniz-Laboratory for Radiometric Dating and Isotope Research at Kiel University (KIA), the Beta Analytic Radiocarbon Dating Laboratory Miami

(BETA), the VERA Laboratory at Vienna University, and the Poznań Radiocarbon Laboratory at Adam Mickiewicz University (POZ).

Due to the limestone rich environment containing a high amount of "old" carbon, a large hard water effect may be expected for limnic organics. Together with an influx of fresh and reworked old terrestrial organics this makes radiocarbon dating of the sediment challenging (Finné et al., 2011).

Table 2 shows sometimes large differences between results from different fractions and laboratories. Carbonate of the *Bythinia* gastropod shells at 141 cm dates at least 700 years older than organic samples above and below it indicating the expected large hard water effect. A *Ranunculus aquatilis* specimen, which grows subaqueously and was sampled live in 2015, provides an apparent age of 657 ± 29 years (PMC 92.15 or $F^{14}C$ 0.92146; VERA-6256, Table 2) that after comparison with the Jungfraujoch atmospheric ^{14}C record (Hammer and Levin, 2017) yields a reservoir age of 810 ± 30 ^{14}C years. This is in good agreement with the carbonate result at 141 cm and slightly higher than the reservoir age of 600±10 years applied by Heymann et al. (2013). The ten KIA results for the alkali residue give, as expected considering the low organic carbon content of 0.19 to 0.83 % of this fraction, unreasonably old ages and should not be used in the time scale construction. Recognizable terrestrial plant remains are largely absent from the core, except for one single *Crataegus* seed, which was found at 165 cm depth (masterscale) in core STY-1A, yielding an age of 1237 ± 35 ^{14}C years (690 – 870 cal AD; VERA-6258; Figure B3-B). The humic acid result for KIA42912 of 1355±23 yr BP at 164 cm is only 118 years older. This small difference indicates that the humic acid fraction is largely of terrestrial origin as opposed to the limnic material with 800-year reservoir effect. Ages obtained on the humic acid fractions may thus better indicate the time of deposition with a reservoir effect in the range 100 to 200 years. This reservoir effect will however vary with the balance between limnic and terrestrial organics supplied to the lake and there is no reason to assume that it was constant in the past. Hence, this is an inherently problematic issue and we can only employ the current situation as a guide and try to estimate the recent reservoir age (as we do below).

4.2.2 Bayesian age model

The *Crataegus* seed and a ceramic fragment (Figure B3-C) – the latter was found at 205 cm depth (masterscale) in core STY-3B and was identified as non-Attic, late or sub-Archaic and dated approximately to 500 BC ± 50 years (ceramic classification: Bernhard Schmaltz, Kiel University, personal communication) –serve as "golden spikes" in the age-depth-model. For the ceramic shard, ca. 500 BC is considered a *terminus post quem*, the earliest possible date when the shard may have found its way into the lake; most likely it continued to exist as part of a decorative bowl for a while before it broke apart and then at some later point in time was

deposited in the lake. A piece of charred organic matter from 324 cm depth, dated at 7708 ± 35 ^{14}C yr BP (KIA42913) and with a combustion yield of 32.5 % carbon, which proves its high organic matter content, sets the lower limit of the age-depth-model (ADM).

Bayesian age-depth-modelling was performed using the R package Rbacon (v.2.3; Blaauw and Christen, 2011) as well as the software OxCal 4.2 (Ramsey, 2008; Bronk Ramsey, 2009; Ramsey and Lee, 2013), both using IntCal13 as the terrestrial calibration curve (Reimer et al., 2013).

The final age-depth-model (STY_25) was constructed with Rbacon in an iterative process based on several key assumptions and offers a best plausible interpretation: (1) The age of the core top is set at 2010 cal AD, the year of coring. The age determinations for the *Crataegus sp.* seed and the ceramic shard serve as reliable, solid anchor points. The charcoal sample at 324 cm likewise gives a reliable result for the bottom of the model. (2) If there are multiple dates for one depth derived from the same carbon fraction, they have been combined to one value using the *R_combine* function in OxCal. Otherwise, the fact of having a higher quantity of datings for a certain depth would have influenced the modelling by assuming a higher credibility for these samples. (3) As the *Bythinia sp*. shell samples (VERA-6381_30, VERA-6381_50) delivered different ages, depending on the degree of etching, they were excluded from the age-model (Figure B5 marked in light blue). (4) Based on the assessment of alkali residue ages versus humic acid ages outlined above, the generally younger humic acid ages were regarded as more plausible and the considerably older KIA alkali residue ages were excluded from modelling (Figure B5 marked in red). (5) As outlined in section 0, the reservoir correction was set to 200 ± 100 years for all bulk sediment samples because of the age difference between the *Crataegus* seed (1237 ± 35 ^{14}C years) and the adjacent KIA42912 humic acid sample (1355 ± 23 ^{14}C years). To take the uncertainty of varying reservoir effects into account, we assigned a relatively high standard deviation of ± 100 years to the reservoir correction (the table can be found in BS1). (6) Finally, the construction of the Hadrianic Aqueduct, a cultural event that took place around 130 AD (Lolos, 1997), indicated in the sediment core among others by a strong and abrupt increase in the Fe content due to oxidation processes (see section 0), was taken into account in the modelling process. In the following, all proxies are plotted against the mean calendar age estimates of model STY_25. Calibrated years are denoted as cal BC/AD, due to the focus of this paper on cultural and climatic aspects of the last 2,500 years (Mook and Van Der Plicht, 1999). The applied cultural chronology (Table 3) is based on Bintliff (2012) and Weiberg et al. (2016).

Based on the age-depth-model, we calculated the sedimentation rate in the lower part to be approx. 0.2 mm/yr. It rises slightly to 0.4 mm/yr at 195 cm and strongly increases to more than 2 mm/yr at 165 cm. For the uppermost 50 cm, a lowering of the sedimentation rate to

0.7 mm/yr was calculated (Figure B6). This pattern of sedimentation largely resembles that of carbonate content and Ca (Figure B4) and hence supports the age-depth-model.

Note that the age-depth-model published by Heymann et al. (2013), which was based on fewer radiocarbon dates for the respective core sequence, is outdated. The discovery of the *Crataegus* seed (VERA-6258) and the improved modelling approach presented here require a substantial shift – to more recent ages – in the dates and associations compared with the published data of Heymann et al. (2013).

sample no.	analysis no.	sample material	sample fraction	C weight[1] [mg]	C content in this fraction[2] [%]	$\delta^{13}C$ [‰]	^{14}C age $\pm 1\sigma$ [BP]	IntCal13 [cal BP][3]	depth [cm]
LSR-01	KIA 42322	Reed	Alkali residue				>1950		0*
STY-1/0	KIA 44002	Green Algae	Alkali residue				280 ± 20	299 – 421	0*
STY-res-03	VERA-6256	*Ranunculus aquatilis*	ABA			-25.2 ± 1.1	657 ± 29	565 – 664	0*
STY-1/32	KIA44003	Bulk sediment	Alkali residue	1.58	0.42	-22.74 ± 0.16	3174 ± 29	3370 – 3443	32*
STY-1A/050	VERA-6380_1	Bulk sediment	TOC			-25.0 ± 0.9	1557 ± 38	1406 – 1521	50
	VERA-6380_2	Bulk sediment	TOC			-23.8 ± 0.8	1568 ± 37	1413 – 1521	50
	VERA-6380HS_2	Bulk sediment	Humic acids			-23.7 ± 0.9	1575 ± 38	1415 – 1522	50
STY-1/52	KIA45954	Bulk sediment	Alkali residue	1.57	0.27	-21.40 ± 0.16	2184 ± 28	2146 – 2302	52*
STY-1A/072	KIA47446	Bulk sediment	Alkali residue	3.12	0.44	-25.25 ± 0.10	2171 ±20	2134 – 2299	72*
	KIA47446	Bulk sediment	Alkali residue	3.12	0.44	-24.50 ± 0.19	2225 ±20	2161 – 2310	72*
	KIA47446	Bulk sediment	Humic acids	1.52	0.07	-25.28 ± 0.23	1285 ±35	1184 – 1273	72
STY-1/92.5	KIA44004	Bulk sediment	Alkali residue	2.55	0.31	-23.77 ± 0.17	2935 ± 25	3045 – 3157	107*
STY-1A/100	VERA-6382_1	Bulk sediment	TOC			-26.2 ± 0.8	1419 ± 36	1298 – 1342	114
	VERA-6382_2	Bulk sediment	TOC			-25.3 ± 0.8	1444 ± 36	1304 – 1357	114
	VERA-6382HS_2	Bulk sediment	Humic acids			-23.9 ± 0.8	1419 ± 37	1297 – 1342	114
STY-1A/127	VERA-6381_30	*Bithynia sp.*	Carbonate		30% etched	-11.7 ± 0.7	2091 ± 34	2005 – 2113	141*
	VERA-6381_50	*Bithynia sp.*	Carbonate		50% etched	-12.1 ± 0.7	2258 ± 35	2183 – 2338	141*
STY-1B/161	VERA-6383_1	Bulk sediment	TOC			-26.4 ± 0.8	1553 ± 35	1403 – 1520	161
	VERA-6383_2	Bulk sediment	TOC			-28.8 ± 0.8	1516 ± 36	1350 – 1515	161
	VERA-6383HS_2	Bulk sediment	Humic acids			-23.4 ± 0.7	1441 ± 35	1304 – 1354	161
STY-1/149.5	KIA42912	Bulk sediment	Alkali Residue	1.62	0.35	-24.94 ± 0.21	3285 ±30	3478 – 3559	164*
	KIA42912	Bulk sediment	Humic acids	2.21	0.69	-27.22 ± 0.19	1355 ±23	1281 – 1298	164
STY-1A/150	VERA-6258	*Crataegus sp.*	ABA			-26.8 ± 0.6	1237 ± 35	1089 – 1258	165
STY-1A/180	VERA-6259	Bulk sediment	TOC			-33.5 ± 2.1	2125 ± 31	2054 – 2148	195
	VERA-6259HS	Bulk sediment	Humic acids			-42.8 ± 6.9	2174 ± 37	2124 – 2303	195
STY-1A/207	KIA47448	Bulk sediment	Alkali Residue				5720 ± 40	6447 – 6560	207*
	KIA47448	Bulk sediment	Humic acids				3170 ± 30	3987 – 4136	207
STY-1A/210	Poz-96329	Bulk sediment	Alkali residue	6.36	4.2	-26.2	2310 ± 35	2316 – 2353	210
STY-1A/220	Poz-96330	Bulk sediment	Alkali residue	2.25	1.8	-26.5	3850 ± 40	4159 – 4395	220
STY-1A/216	VERA-6260	Bulk sediment	TOC			-37.0 ± 1.2	3809 ± 39	4098 – 4280	236
	VERA-6260HS	Bulk sediment	Humic acids			-26.8 ± 0.8	3937 ± 33	4298 – 4434	236
STY-1/216.5	KIA44005	Bulk sediment	Alkali Residue	6.03	0.83	-24.77 ± 0.25	4020 ± 30	4439 – 4521	236*
	KIA44005	Bulk sediment	Humic acids	2.09	0.41	-24.03 ± 0.22	3563 ± 29	3832 – 3899	236
STY-1A/238	Poz-96331	Bulk sediment	Alkali residue	5.46	7.4	-24.8	3335 ± 35	3485 – 3630	238
STY-1A/248	Poz-96325	Bulk sediment	Alkali residue	5.16	2.4	-26.2	4180 ± 40	4630 – 4829	248
STY-1/246.5	KIA44006	Bulk sediment	Alkali Residue	2.89	0.29	-27.00 ± 0.13	6350 ± 40	7185 – 7408	266*
	KIA44006	Bulk sediment	Humic acids	1.95	0.28	-26.22 ± 0.15	4837 ± 34	5486 – 5606	266

STY-1A/247	VERA-6261	Bulk sediment	TOC			-27.2 ± 0.7	4600 ± 35	5295 – 5444	267
	VERA-6261HS	Bulk sediment	Humic acids			-40.7 ± 1.6	4631 ± 36	5312 – 5446	267
STY-1A/250	VERA-6262	Bulk sediment	TOC			-23.1 ± 3.1	4829 ± 38	5485 – 5603	270
	VERA-6262HS	Bulk sediment	Humic acids			-26.6 ± 1.6	4877 ± 29	5590 – 5642	270
STY-1A/253	VERA-6263	Bulk sediment	TOC			-25.9 ± 1.7	4791 ± 31	5481 – 5587	273
	VERA-6263HS	Bulk sediment	Humic acids			-23.7 ± 0.9	4841 ± 36	5486 – 5640	273
STY-1A/280	KIA45955	Bulk sediment	Alkali Residue	1.77	0.19	-25.89 ± 0.19	7178 ± 39	7961 – 8013	280*
	KIA45955	Bulk sediment	Humic acids				6025 ± 35	6798 – 6925	280
STY-1A/300	KIA42913	Charcoal	Alkali Residue	1.76	32.5	-27.6 ± 0.1	7708 ± 35	8450 – 8538	324

Table 1: List of radiocarbon samples taken from Lake Stymphalia parallel cores STY-1A and STY-1B. Lab-Codes: KIA – Kiel; VERA – Vienna; Poz – Poznan; BETA – Beta Analytics. The sample numbers refer to the sampling depth before adjusting the field-based correlations between individual core sections in the laboratory to a master depth scale.

Notes: [1)] calculated from CO_2 pressure

[2)] Fraction of sample material after respective pre-treatment

[3)] calibrated 1σ-age ranges without reservoir correction

* dates excluded from age-depth modelling

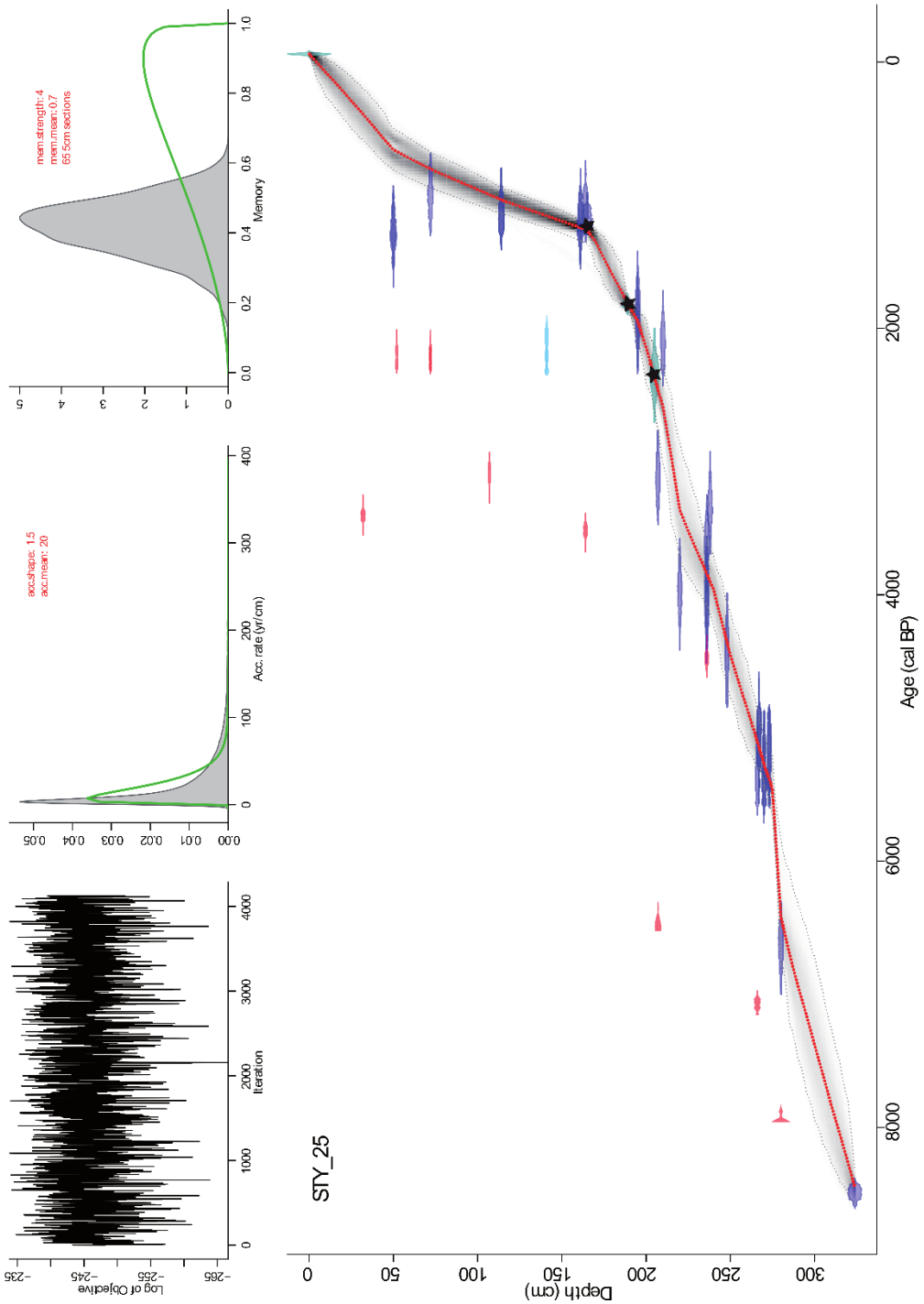

Figure B5: Age-depth model STY_25 from rbacon for 324 cm of STY-1. The red dashed line represents the weighted mean. Black dashed lines represent minimum and maximum ranges (95% confidence interval). The red (Alkali residue) and the light blue (Carbonate shells) dates have been treated as outliers and have been excluded from the modelling processes. The black stars highlight the anchor points ceramic shard, aqueduct, and Crateagus seed (cf. details in section 0). For interpretation of the references to color, the reader is referred to the web version of this article.

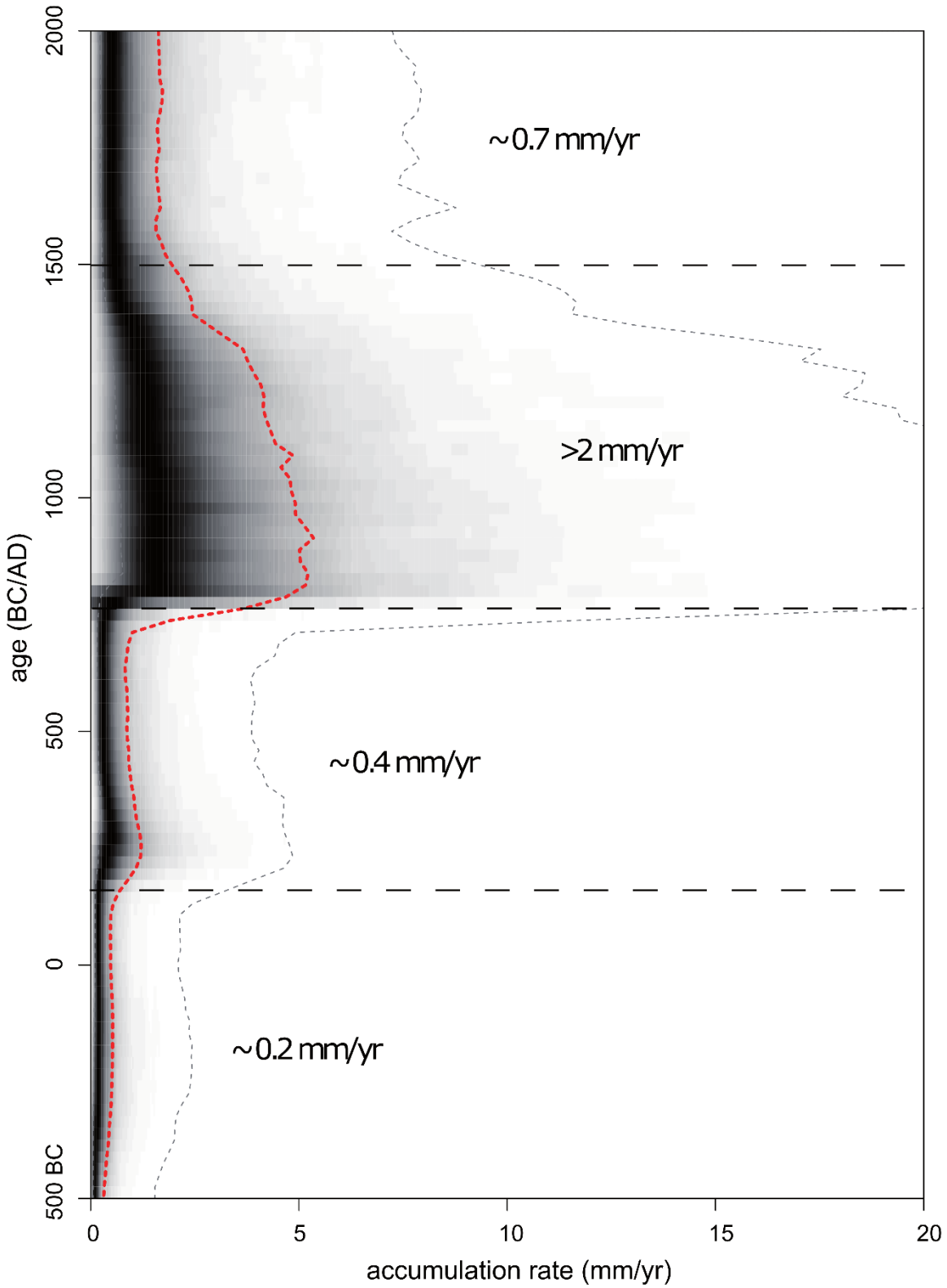

Figure B6: Sediment accumulation rate (mm/yr) over the last 2,500 years. Dashed, horizontal lines broadly indicate 4 phases with differing sedimentation rates and the approximated average sedimentation rate within this phase.

Table 3. Cultural chronology of southern Greece from Early Iron Age to Late Medieval. The chronology is based on Weiberg et al. 2016, Bintliff, 2012, Manning, 2010.

Time (BC/AD)	Period	Event	Abbreviation
AD 1204 – 1460	Byzantine and Frankish/Late Medieval	Start: Frankish conquest of Constantinople.	B-F
AD 900 – 1204	Middle Byzantine/Medieval	Start: Consolidation of the Roman (Byzantine) power in the southern Balkans.	MB
AD 641 – 842	Early Byzantine/Early Medieval	Start: Death of Emperor Heraclius and the collapse of the Late Roman political order.	EB
AD 300 – 641	Late Antiquity/Late Roman	Start: Founding of the city of Constantinople and the parting of ways between the Western and Eastern parts of the Roman Empire.	LR
31 BC – AD 300	Roman	Start: Destruction of Corinth and end of Achaian war.	R
323 – 31 BC	Hellenistic	Start: Death of Alexander	H
479 – 323 BC	Classical	Start: Greek victory over the Persians in the battle of Plataea; Persian invasion of Greece repelled.	C

4.3 Geochemical Proxies

Our palaeoclimate record consists of continuous XRF core-log measurements of 13 chemical elements, augmented with discrete measurements of grain size, TOC, TIC, and TN contents as well as isoprenoid and branched GDGT distributions.

The sediment is dominated by calcium (Ca, 67.3 % of all considered total counts), caused by autochthonous calcium carbonate precipitation in the lake and allochthonous limestone weathering in the catchment. Iron (Fe, 14.7 %) and silicon (Si, 8.6 %) were the elements with the second and third most abundant counts, respectively. The elements Rb, K, Zr, Ti, Si, and Al all show extremely high correlations ($rho_{Sp} > 0.9$) throughout the sequence due to their common allochthonous origin from siliciclastic rocks in the catchment such as schists and breccias (Figure B4).

Gastropod shells in core STY-1B1 in the depth interval 84.4 – 105.4 cm made it difficult to obtain the smooth, planar core surface needed for reliable XRF analysis (Tjallingii, 2006; Tjallingii et al., 2007; Bloemsma et al., 2018). As a result some element counts deviated from those in the other core sections, showing larger oscillation and leading to artefacts at the section boundaries (Figure B7).

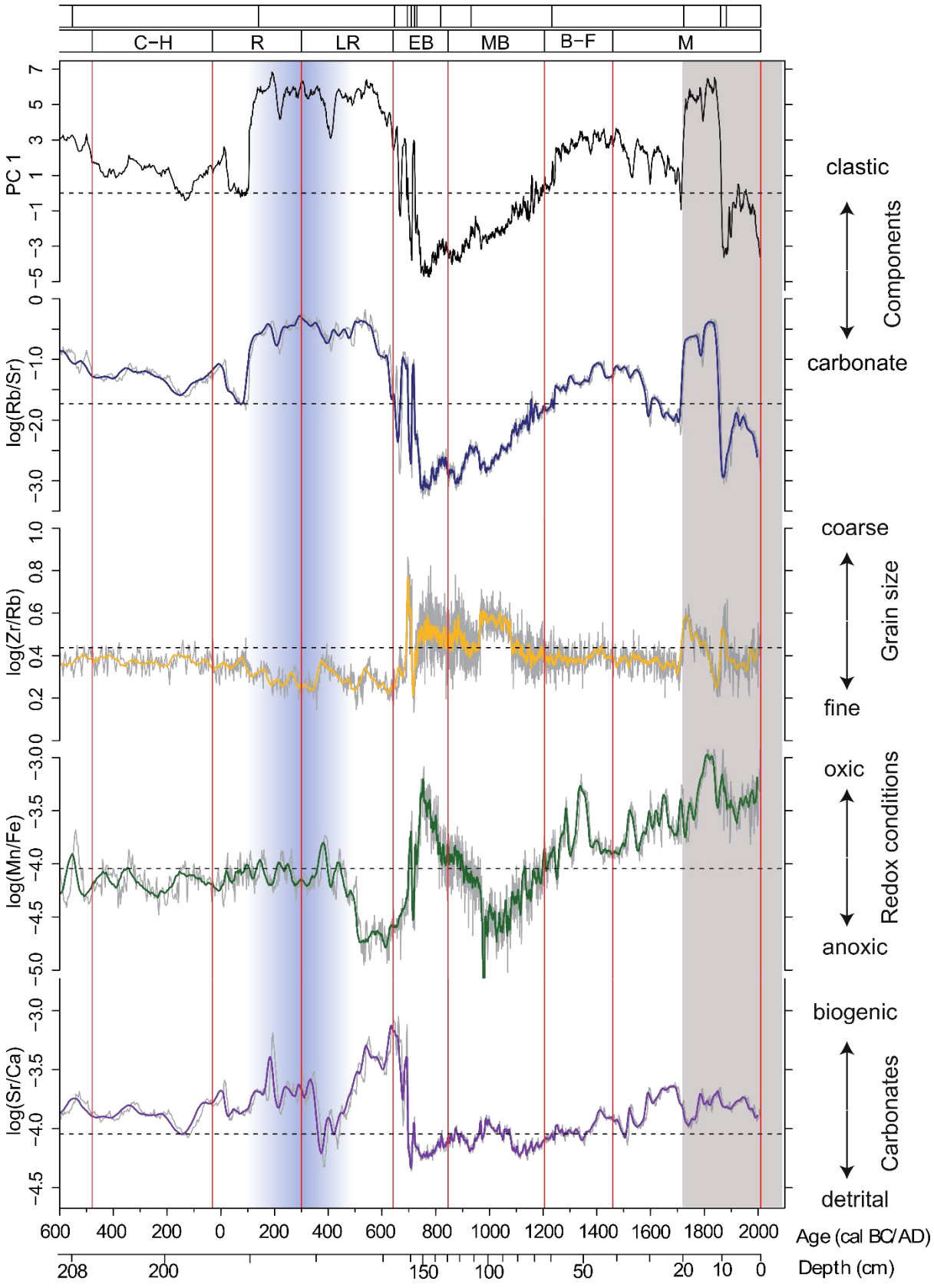
C–H
R
LR
EB
MB
B–F
M
PC 1
clastic
Components
carbonate
log(Rb/Sr)
coarse
log(Zr/Rb)
Grain size
fine
oxic
log(Mn/Fe)
Redox conditions
anoxic
biogenic
log(Sr/Ca)
Carbonates
detrital
600 400 200 0 200 400 600 800 1000 1200 1400 1600 1800 2000
Age (cal BC/AD)
208 200 150 100 50 20 10 0
Depth (cm)

Figure B7. Selected elemental ratios depict paleoenvironmental changes at Lake Stymphalia for the last 2,500 years. The log-normalized ratios plotted in grey are based on the Avaatech XRF counts per second measured on STY-1. Colored lines were calculated with a 5-point moving window. Dashed horizontal lines mark the respective mean values for the whole dataset. PC1 and Rb/Sr indicate changes in the material composition. Zr/Rb is used as a grain size proxy. Mn/Fe hints to redox conditions in the bottom water. Sr/Ca explains the origin of the carbonates. Arrows to the right explain how to read the proxies. All proxies are plotted against age (cal BC/AD). Approximate depth scale (cm) is included for comparison. The upper boxes above the graph show the lithological units. The lower boxes and vertical red lines refer to the transitions between Greek cultural boundaries as specified in Weiberg et al. (2016; cf. Table 3). The blue vertical bar shades the approximate period of the functioning of the Hadrianic Aqueduct (130 – max 500 AD). Values in the grey shaded area (>1720 cal AD) need to be interpreted with caution due to strong anthropogenic alteration. For interpretation of the references to color, the reader is referred to the web version of this article.

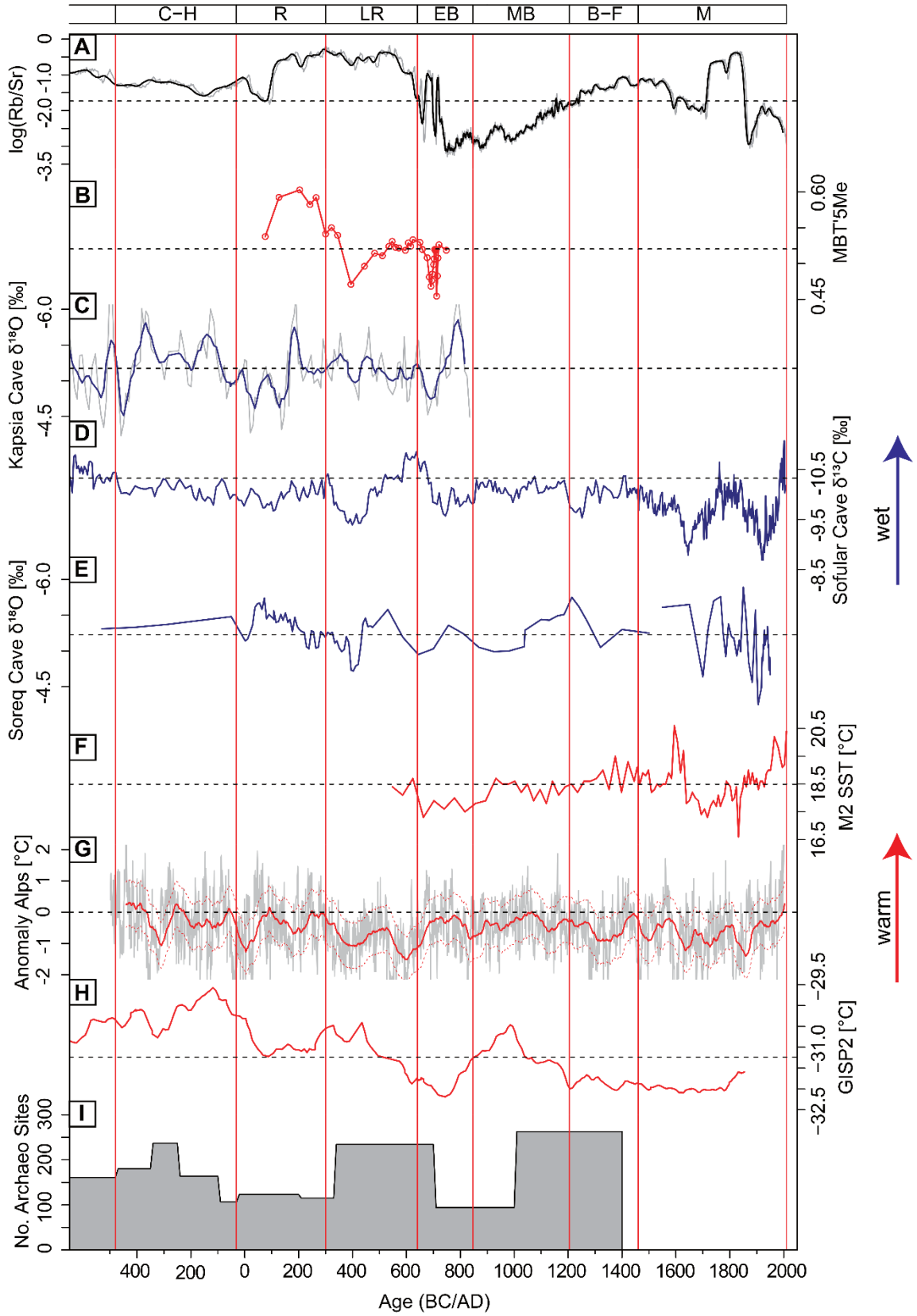
C–H
R
LR
EB
MB
B–F
M
A
B
C
D
E
F
G
H
I
log(Rb/Sr)
-3.5 -2.0 -1.0 0
MBT'5Me
0.45 0.60
Kapsia Cave δ18O [‰]
-6.0 -4.5
Sofular Cave δ13C [‰]
-8.5 -9.5 -10.5
wet
Soreq Cave δ18O [‰]
-6.0 -4.5
M2 SST [°C]
16.5 18.5 20.5
Anomaly Alps [°C]
-2 -1 0 1 2
warm
GISP2 [°C]
−32.5 −31.0 −29.5
No. Archaeo Sites
0 100 200 300
400 200 0 200 400 600 800 1000 1200 1400 1600 1800 2000
Age (BC/AD)

Figure B8: Comparison of Lake Stymphalia climate proxies (log(Rb/Sr), A) and MBT'5Me (B) to other regional (C-F) and supra-regional/global climate archives (G-H) and the number of archaeological sites on the Peloponnese (I) for the last 2,500 years. (C) (Finné et al., 2014) (inverted); (D) Fleitmann et al., 2009 (inverted); (E) Bar-Matthews et al., 1999 (inverted); (F) Gogou et al., 2016; (G) Büntgen et al., 2011; (H) Alley, 2004 (I) Weiberg et al., 2016; Blue proxies reflect precipitation or humidity; higher water availability is plotted towards the top. Red proxies reflect absolute or relative temperature. Warmer temperatures are plotted towards the top. Dashed horizontal lines mark the mean values for the respective dataset. Boxes and vertical red lines represent transitions between Greek cultural boundaries as specified in Weiberg et al. (2016) and Table 3. For interpretation of the references to color, the reader is referred to the web version of this article.

Four element ratios were determined that show trends which can be interpreted as suitable palaeoenvironmental proxies (cf. section 0). The generally negative log(Rb/Sr) ratios (Figure B7) in our record (varying between -0.18 to -3.29) indicate the dominance of carbonates compared to siliciclastic material in the lake's catchment, which is dominated by limestone karst. Relatively higher values of the Rb/Sr ratio occur in units with low carbonate content.

As stated by Heymann et al. (2013), we use the log(Zr/Rb) ratio as a grain size proxy; higher values are linked to the coarser, silt-sized fraction, while low values refer to fine, clayey mineral input. The mean is 0.44 and the median is 0.41. There is a considerable shift in the data around 700 cal AD and afterwards the variability in the ratio is considerably larger than in the first half of the sequence (Figure B7). The log(Mn/Fe) ratio fluctuates between -5.0 to -3.0 and highest variation can be seen for the period 500 to 1000 cal AD. As Fe show a high correlation with other terrestrial elements (rho_{Sp} for Fe and Ti = 0.92), it is mainly related to allochthonous input and hence the potential use of the Fe/Mn ratio as an indicator of redox conditions in the water column needs to be applied with caution. The log(Sr/Ca) ratio (Figure B7) is consistently negative and varies between -4.6 to -2.8. Between 350 to 700 cal AD, we see the highest variation.

We additionally applied a principal component analysis (PCA) to the dataset of the 13 selected geochemical elements in order to reduce the dimensions and summarize the data structure. The scree test suggests using the first three factors, as the first (PC1), second (PC2) and third principal component (PC3) account for about 79 % of the variance in the dataset (BS4). We only apply PC1, taking into account 52.9 % of the variance. The loadings provide information on the influence of the chemical elements on the respective component. While PC1 is tied to Ca and Sr at the negative end and to all the other elements at the positive end, PC2 is negatively related to Zr and Si, while the other elements show positive loadings (BS4). Consequently, PC1 can be interpreted as an axis that spans between carbonate rich samples (Ca, Sr) on the negative end and mineral rich assemblages indicated by positive values. These

divergent elemental compositions are likewise reflected in the Rb/Sr ratio. A Spearman correlation between log(Rb/Sr) and PC1 hence leads to an extremely high correlation (rho_{Sp}= -0.968, $p < 0.05$). This similarity is also apparent in the high degree of alignment between the curve progressions in Figure B7, as they show the same temporal responses. It can thus be concluded that PC1 for the STY-1 XRF dataset represents a suitable summary proxy for chemical weathering. In addition, the results of the PC1 confirm the applicability of Rb/Sr as a palaeoenvironmental proxy, because it covers the most important fluctuations in the complete dataset.

4.4 GDGT distributions

Both isoprenoid and branched GDGTs were ubiquitously present in the investigated interval with the latter dominating the GDGT pool. This is also expressed in generally high BIT values varying between 0.95 and 0.98 (data not shown). Highest MBT'_{5Me} values of about 0.60, reflecting higher mean annual air temperatures (MAATs), are found at 200 cal AD, after which MBT'_{5Me} values decrease by about 0.13 over the next 200 years, yielding a minimum MBT'_{5Me} of 0.47 at 390 cal AD. Subsequently, the MBT'_{5Me} increases over the next 140 years and stays relatively invariant with values between 0.52 and 0.53 in the interval from 535 to 660 cal AD. A second minimum of 0.47 occurred at 690 cal AD followed by an increase in temperature expressed by an increase in the MBT'_{5Me} value of about 0.52 shortly after. The MBT'_{5Me} value decreased to an absolute minimum of about 0.45 at 710 cal AD followed by a rapid increase to 0.53 around 720 cal AD (Figure B8).

5. Discussion

5.1 Geochemical ratios

The geochemical elements obtained from XRF analysis are shown and interpreted as log-ratios to circumvent the closed-sum effect and to obtain a signal that is relatively easy to interpret for palaeoenvironmental variation (Weltje and Tjallingii, 2008; Löwemark et al., 2011). Selected element ratios are explained and discussed in the following.

The rubidium-strontium (Rb/Sr) ratio is commonly applied as a proxy for weathering intensity in the catchment (Chen et al., 1999; Jin et al., 2006; Xu et al., 2010). Rb has an allochthonous source and can replace potassium (K) in the crystal lattice of clay minerals. It enters the lake environment with silicates and K-rich minerals. Sr can have an allochthonous or autochthonous origin and is thus introduced either from carbonate weathering in the catchment or from precipitation of $SrCO_3$, as substitute for Ca, within the lake (Cohen, 2003; Koinig et al., 2003). Precipitation of $SrCO_3$ also increases by evaporative concentration in lakes, a process which often happens during a lowering of the lake level due to dry and warm

climate conditions (Heymann et al., 2013). Hence, high Rb/Sr values in lake sediments may generally be interpreted as enhanced erosion of siliciclastic material under cooler and wetter climatic conditions and enhanced catchment precipitation, while low Rb/Sr values indicate warmer and drier conditions with evaporation-driven carbonate precipitation in the lake (Heymann et al., 2013; Unkel et al., 2014). As the period presented in this paper shows a strong imprint of human activity in the polje, the Rb/Sr ratio cannot unequivocally be linked to climatic variations and firstly reflects the balance between carbonates and clastic components. For the period presented here, the Rb/Sr ratio can instead be interpreted as proxy for water availability and lake size. High Sr and low Rb/Sr values indicate high water availability dissolving carbonates from the limestone bedrock and precipitating in the lake during warm summers, while high Rb and high Rb/Sr values are present in phases with less water availability and thus a smaller lake area, where terrestrial detritus is more easily eroded up to the depocentre of the lake. The proxy does not indicate whether these processes occur naturally or are human induced.

For the strontium-calcium (Sr/Ca) ratio, some authors associate higher values in stalagmites with lower levels of recharge into the karstic aquifer during dry climate conditions (Cruz et al., 2007). Other authors explain higher Sr concentrations with enhanced biogenic carbonate precipitation compared to detrital carbonates, because the Sr partition coefficient (K_{DSr}) for biogenic carbonate is much greater than that for inorganic carbonates (Hodell et al., 2008). We here follow the interpretation of Hodell et al. (2008) and interpret higher Sr/Ca ratios as more biogenic carbonate precipitation in the lake and lower values as more inorganic, detrital carbonate input from the catchment.

Iron (Fe) and manganese (Mn) concentrations correspond among others to oxidation processes within the lake. The Mn/Fe ratio is often interpreted as an indicator for redox conditions (Davison, 1993; Heymann et al., 2013). In the water column, Fe^{2+} is less stable than Mn^{2+} and precipitates earlier. Thus, low (high) Mn/Fe values are considered to indicate anoxic (oxic) conditions, often visible by greyish-blue (brownish-red) sediments (Koinig et al., 2003; Unkel et al., 2014). Besides redox conditions, pH changes affect the ratio, as more Mn is mobilized when pH is decreasing. Hence, low (high) Mn/Fe values may also indicate acidic (alkaline) conditions. In periods of high productivity, intensive degradation of organic matter leads to oxygen depletion and acidic condition and may also be reflected in higher TOC values (Koinig et al., 2003). If the variability of Fe is closely related to allochthonous input, this suggests that Fe mainly originates from terrestrial sources and the use of the Mn/Fe ratio as an indicator of redox conditions in the water column may be limited (Naeher et al., 2013). As Fe and inert Ti show a high correlation (Sp_{rho}: 0.86) at Lake Stymphalia, we assume that Fe mainly originates from terrestrial sources and interpret the Mn/Fe proxy with caution only in phases when both elements show clear signals.

The ratio of allochthonous Rb versus zircon (Zr) is widely used as grain-size proxies, as Rb is associated with clay minerals, while Zr is mainly associated with coarser grain material (Dypvik and Harris, 2001; Koinig et al., 2003; Chen et al., 2006; Cuven et al., 2010; Kylander et al., 2011). In the Stymphalia record, Zr is linked to the silt-sized fraction and Rb is strongly linked to the clay mineral assemblage suggesting no K-feldspar source contribution (Heymann et al., 2013).

5.2 General palaeoenvironmental interpretations

The lack of lamination throughout the entire core sequence indicates that the water level has never been considerably higher than at present over any long time period as would be necessary to allow for water column stratification and repress complete mixing of the water column (Zolitschka et al., 2015). A generally low water level is also supported by the presence of *Bythinia sp.* (Figure B3-D) and *Valvata sp.* shells or shell fragments throughout most of the sediment sequence (Figure B4). Both organisms are gastropods living in well oxygenized, shallow waters and swamps, and are often found, e.g., in the reed belt of shallow lakes in the Balkans (Tom Wilke, pers. comm. 2015; Davies, 2008). Their presence in Lake Stymphalia thus indicates a generally molluscan favourable environment with well-mixed, oxygenized conditions within a small, permanent and constantly shallow freshwater lake even within the blackish units 62 and 63 (Davies, 2008; Mischke et al., 2017).

The different shades of colour in the sediment sequence indicate varying depositional conditions. While the lower part of the core shows signs of low sedimentation under water-logged conditions, the brownish colours of the upper part indicate increased erosion, a higher input of terrigenous material and short periods of desiccation, e.g. during summer (Figure B4). The grain size distribution in lake sediments provides information on the erosion, transport and accumulation mechanisms of material from the source to the lake. The compact, fine-grained silty clay and clayey silt units in this sequence point to a dominance of chemical weathering in the catchment. In a water balance calculated by Morfis and Zojer (1986), more than half of the water discharge volume is ascribed to underground inflow, suggesting the importance of mineral transport in dissolution, mainly concerning the carbonates.

Four main sedimentation phases can be distinguished over the last 2,500 years (Figure B6). During Classical-Hellenistic times, the sedimentation rate is approx. 0.2 mm/yr. It slightly increases to about 0.4 mm/yr during the Roman Period. Interestingly, this is on a comparable scale to the sedimentation rates calculated from colluvia in the neighbouring Phlious basin (Fuchs et al., 2004). Around 800 cal AD, we see a strong increase in the sedimentation to >2 mm/yr lasting for approximately 300 years and then gradually decreasing to the top; and for the last 500 years it is calculated at 0.7 mm/yr (Figure B6). Walsh et al. (2017) report a

mean accumulation rate of 1.7 mm/yr for their Stymphalian sediment cores recovered from the lakeshore.

The MBT'_{5Me} proxy provides a means to quantify temperature variations over time (De Jonge et al., 2014). As no regional lake temperature calibration for the MBT'_{5Me} is currently available and the only other calibrations available for tropical East African lakes (Russel et al., 2018) and alkaline Chinese lakes (Dang et al., 2018) yield temperature estimates for Lake Stymphalia that are much higher than the 20th century data from the meteorological station at Driza-Stymphalia, and are thus highly unrealistic, we prefer to discuss relative temperature trends instead of reporting absolute temperatures (Figure B8). Additionally, we do not address the question of variation between autochthonous and allochthonous sources in the sediment composition, which likely affects the palaeothermometer. As lipid biomarker analysis in Greece is still at an early stage (Gogou et al., 2016; Katrantsiotis et al., 2018; Norström et al., 2018), we assume the full potential of this method is not yet achieved, and only provide a first tentative interpretation. However, we included this dataset with the aim to contribute to the further development of this method.

5.3 The socio-environmental history

5.3.1 Classical-Hellenistic and Early Roman Periods (479 BC – 130 AD; unit 59)

Archaeological investigations and palaeoecological findings postulate agricultural activity in the Stymphalia catchment from the Early Neolithic onwards (Williams, 2005; Walsh et al., 2017b). Thus, variations in the analysed sediment sequence most likely reflect both natural as well as anthropogenic changes in the landscape.

During Archaic to Middle Hellenistic times (600-250 BC), the city of Stymphalos was flourishing, accommodating ca. 2,500 people plus potentially another 500 people in the rural surroundings (Williams, 2005, 2003; Karambinis personal communication). Williams (2005, 2003) describes a large, fortified wealthy city for the 5th to 3rd century BC; the florescence of the city was associated with the maximum regional population and land use unrepeated until the later 20th century AD. Excavations in the Lower Town by Williams, a large part of which lies in the lake flats, have revealed that the archaeology is covered by at least 1 m of fine-grained colluvial sediments deposited into a shallow freshwater environment overlying the abandoned buildings, while the house foundations extend below the modern water level. Clearly, the lake during this urban phase must have been further out into the current lake bed, and at a significantly lower level.

The geochemical records for this urban period (lithological unit 59) are all very stable (Figure B7). The absence of major fluctuations points to a phase of rather stable environmental conditions. Greyish clayey silt with a slightly black mottled appearance and a

high content of shell fragments suggests that the sediments were continuously water-logged at that time.

The finding of a larger ceramic shard at 205 cm in core STY-3B (Figure B3-C) as well as a small amount of tiny ceramic particles in STY-1B prove human presence at this depth, during the 6th to 5th century BC. The shard was embedded in a fine matrix, indicating slow, regular and constant accumulation excluding any extreme event such as a debris flow or strong erosion induced by land-use management which would have required a coarser matrix, whilst the Zr/Rb ratio shows consistently fine sediment. The low sedimentation rate (~ 0.2 mm/yr) for this period further confirms this assumption (Figure B6). On that basis, we assume that the ceramic was deposited under regular, stable sedimentation conditions and it was thus also considered a *terminus post quem* for the surrounding sediment. It is striking, that despite high levels of local population and inferred maximal land use in the surroundings of the lake, unparalleled until the late 19th century AD, no larger disturbances can be found in the sediment core. Clearly, on the one hand, farming and pastoralism were practised in ways that protected the landscape from significant erosion, and on the other hand, reconstructions of contemporary climate in Classical-Hellenistic Greece suggest stable climate conditions unlikely to destabilize the land surface (Finné et al., 2011).

In later Hellenistic into Early Roman times (locally 250 BC – 100 AD) the city shrank and then lost its city status, becoming a far smaller settlement which by Middle Roman times (200-400 AD) may have been little more than a village (Williams, 2003). This demographic decline in Stymphalia is in agreement with decreasing settlement activity from the Peloponnese (cf. Figure B8-I; Weiberg et al., 2016).

Around the beginning of the Roman period, we observe a slight shift in the grain size of the sediment core towards even finer silty clay. This matches the archaeological data indicating that land use was more restricted. During this period, land use will have declined on a massive scale and natural vegetation cover may have spread again, stabilizing the soils, limiting surface weathering, and leading to less detrital input. The sedimentation rate is lowest around 0 – 100 cal AD which suggests a largely abandoned land use and a recolonization of the landscape by stabilizing natural vegetation such as scrub and woodland that hinders the soils from eroding. However, the TOC/TN values for this period are incomplete and pollen is not well-enough preserved in the sediments to support this indication.

It can be considered that during Classical, Hellenistic and the first two centuries of the Early Roman period, inhabitants of the Stymphalia polje practised sustainable agro-pastoralism that didn't cause a lasting imprint in the lake. For this period, the lake seems to have been steady in size and the ecosystem seems to have been resilient and in equilibrium as no large disturbances have been recorded.

5.3.2 Later Early to Late Roman Period (ca. 130 – 641 AD; unit 60)

From approximately the first two centuries of Early Roman times onwards, only a very small settlement is known in the catchment of Stymphalia and the impact on the landscape is assumed to have been small (Williams, 2003). A slight increase in population might be recorded for Late Roman times (400-650 AD), indicated among others by the finding of graves dated to the late 4th and 5th century (Williams et al., 2002; Williams, 2003); but in the former city and in the wider region it will have been a fraction of the population development seen in the climax era of Archaic to Middle Hellenistic times. For the Peloponnese, a higher settlement activity is also reported by Weiberg et al. (2016) for the time span 350 – 700 AD (Figure B8-I).

All geochemical elements measured from the sediment core show an abrupt change in the measured counts at 189 cm (140 cal AD). While the carbonates Ca, Sr as well as the TIC content drop considerably, the terrigenous elements (Rb, Zr, Al, Ti, K, Si) increase sharply and stay constant at higher level for several centuries, with the exception of a small dip at 180 cm (360 cal AD). This very sudden shift at 189 cm, clearly seen in Mn and Fe counts (Figure B4) is interpreted as a direct consequence of the building of the imperial, Hadrianic aqueduct. Around 130 AD the Hadrianic aqueduct was built over a distance of 84 km from the spring of Driza to the ancient city of Corinth in order to extend the latter city's water supply (Lolos, 1997; Unkel et al., 2011). In the natural state, underground discharge from the Stymphalia catchment would drain first into the lake, mainly being fed by two sources, and then by subterranean sinkholes into the Gulf of Argos to the SE (Morfis and Zojer, 1986), but with the help of tunnels and bridges, the engineers of the time redirected the bulk of the water to the NE. Ancient Corinth, as the capital of the Roman province of southern Greece, was flourishing at that time, and although water supply in the city was generally sufficient for the basic needs of the citizens, it is assumed that the Corinthians wanted the additional water source for elaborate water infrastructure features such as fountains and bath complexes (Lolos, 1997). The construction of the aqueduct meant a huge impact for the Stymphalia lake system. As response to the water being diverted directly from the spring of Driza to the aqueduct, the lake area shrank drastically and the lake level became lower. This explains the sudden shift in the geochemical elements at 189 cm (Figures B4 and B7).

The sedimentation rate was at a minimum at the beginning of the aqueduct construction project and reached a small local maximum of approximately 0.5 mm/yr between 200 to 300 cal AD (Figure B6), contemporaneous with the zenith of the aqueduct. We assume that the increase in sedimentation rate can best be explained by the diminishing lake area; the coring spot in the depocentre of the lake would have been closer to the shores and thus more terrigenous material would reach its position. Throughout the existence of the aqueduct during the Roman and Late Roman Period, carbonate content in the system is considerably lower

and we hardly find any gastropod and shell fragments here, while detrital input of terrigenous elements is highest, indicating that material input was dominantly allochthonous.

Additionally, a strong increase in Fe is visible over the running time of the aqueduct, peaking at 178.9 cm and 176.8 cm (ca. 380–440 cal AD). Here, we find a coarser grained, oxidized, orange layer, clearly visible in the high Fe content as well as in the RGB colour together with a peak in Zr/Rb (Figures B4 and B7). Sedimentologically, the orange colour and the high Fe content point towards oxidation and precipitation of Fe-hydroxide. It seems plausible that the lake area continuously shrank over time and by the end of the 4th century AD, the lake seasonally or periodically dried up allowing for oxidation to take place. Several proxies point towards a very small lake, desiccating and oxidizing conditions around 400 cal AD, which can be ascribed to the draw off of water discharges for the aqueduct. When we compare the Stymphalia dataset to other archives for the Eastern Mediterranean, e.g. the $\delta^{18}O$ and $\delta^{13}C$ stable isotope data from Kapsia Cave, Peloponnese (Finné et al., 2014), Soreq Cave, Israel (Orland et al., 2009), and Sofular Cave, Turkey respectively (Fleitmann et al., 2009; Göktürk et al., 2011), we do not see a consistent picture, but rather regionally diverse expressions (Luterbacher et al., 2012; Roberts et al., 2012; Manning, 2013). Around 400 AD however, most proxies tend to indicate slightly drier conditions (Figure B8-C,D,E) and it is thus possible that the dry conditions in Lake Stymphalia at that time may have additionally been influenced by a climatic factor.

Conditions change during the 5th century AD, when relatively more Sr is precipitated within the lake and additionally the Mn/Fe ratio points towards more anoxic conditions suggesting that the lake was continuously waterlogged again. Historical information indicate that during the 3rd to 4th century AD maintenance was carried out to keep the aqueduct working, while during the 5th century AD, the Hadrianic Aqueduct was abandoned and partially collapsed, associated with a significant decline in the size and prosperity of Corinth (Lolos, 1997; Hammond, 2015). The beginning of the long-term abandonment of the aqueduct – which was actually not re-activated until the 1880s (Morfis and Zojer, 1986) – coincides with the changes in the sediment geochemistry. After the collapse of the aqueduct, more water stayed in the basin and the lake was refilling. The Fe content is continuously decreasing again and it seems as if the lake system that had been disturbed and unbalanced by the construction of the aqueduct was trying to retrieve its equilibrium state. The Rb/Sr ratio, which was relatively constant since the construction of the aqueduct, starts to decrease around 540 cal AD, parallel to when Mn/Fe reaches its minimum. Temporally, this coincides with two large volcanic eruptions in 536 AD and probably in 540 AD, which caused atmospheric dimming and contributed to a cold spell in the Northern Hemisphere. A climatic connection, concomitant with cooler conditions at Lake Stymphalia, seems possible and could be consistent with the age-depth-modelling for this phase.

The period 500–650 cal AD, depicting high Sr/Ca values and low Mn/Fe ratios, emphasizes constantly waterlogged conditions. As the Mn/Fe ratio during this period shifts to more anoxic conditions, we conclude that Lake Stymphalia was probably (slightly) deeper and less well ventilated. One possible explanation could be that wind intensity during this phase was lower causing less frequent mixing of the whole water body and the sediment surface. Another scenario would be that the target surface for the wind might have been lower due to protection by vegetation cover, e.g. like a pronounced reed belt as it can be found around the lake today. Sr/Ca shows its highest peak in the record here, pointing to an increased supply of biogenic carbonate material. This is supported by a high amount of shells and shell fragments. The gastropods must have developed under constant water conditions. It can thus be concluded that during the 6th and early 7th century cal AD considerably higher amounts of water reached the Stymphalia polje enabling the extension of the lake area. As the aqueduct was not working anymore and human influence in the area is very low at that time, the water supply can be primarily associated with the reintroduction of water from the lake's main source, the Driza spring. Additional effects of changes in precipitation and temperature may have influenced this turn; reconstructions from the Eastern Mediterranean however do not show a homogeneous pattern. The Sofular Cave proxies show considerable higher precipitation at this time (Fleitmann et al., 2009; Göktürk et al., 2011), while data from Soreq Cave is interpreted as showing a decrease in precipitation for the 2nd to 7th century AD (Göktürk et al., 2011; Luterbacher et al., 2012). In their review of climatic changes during and after the Roman Empire 100 BC – 800 AD, McCormick et al. (2012) state that precipitation in France and central Europe became exceptionally variable between 250 and 650 AD. They see a warming trend in the 4th century AD, while the 6th century is characterized by generally cooler conditions, crop failures and the Justinian Plague (541 AD onwards), a devastating epidemic outbreak in the Mediterranean, as well as droughts and heat events, a high number of famines and cold winters in the Middle East (600–724 AD) (McCormick et al., 2012).

During the Roman Period, we initially see crucial human influence on the lake ecosystem with the building of the aqueduct, followed by a period, when the proxies seem to respond to climatic influences again, however more sensitively than before, which may be ascribed to the unbalancing caused by natural rebound of the hydrographic system once the aqueduct ceased to function.

5.3.3 The Early Byzantine Period (641-842 AD; units 61 – 65)

During the Early Byzantine and the early part of the Middle Byzantine very low population and very limited land use are expected for the Stymphalia basin in the context of generally low settlement activity in the Peloponnese and Greece generally (Bintliff, 2012a; Weiberg et al., 2016; Figure B8-I). The plague in the Eastern Mediterranean began in 541 AD and recurred

several times until ca. 800 AD (Little, 2007; Benovitz, 2014; Izdebski et al., 2016), causing major depopulation for the Stymphalia area. The Migration Period in Greece is most prominent in the 8th century AD, when Slavic colonisation spread to the Peloponnese, taking in some of the land emptied by the lost local population. Although recognition of Slavic sites is highly problematic (just two cemeteries have been excavated in the Peloponnese), and surviving Greek populations in the countryside are hard to detect since much of their material culture continues Late Roman forms, the evidence overall points to a demographic low point in Greek rural landscapes (Bintliff, 2012b). Dated churches confirm the delay in population recovery until the 10th century AD (Sigalos, 2004).

For the 7th and early 8th century cal AD (156.5 – 167.5 cm, unit 61 – 64) we see high variability in the sediment core and all geochemical proxies (Figure B4). As human activity is considered to be low, as outlined above, it can be assumed during this period that fluctuations in the sediment are primarily attributed to natural climatic and environmental changes rather than to anthropogenic influence. Four very thin but lithologically different units (unit 61 – 64) have been identified in this phase. As gastropods are present throughout all phases, we assume the constant existence of a lake, however with varying extent. The short but intense fluctuations indicate that after the vast disruption from building the aqueduct, the lake system had not fully recovered and regained its balance, but was highly vulnerable and new environmental changes led to significant repercussions in the ecosystem.

Unit 61, dating to the second half of the 7th century, contains light olive grey material with a higher amount of coarse material and only few shell fragments (Table 1). It contains a sharp Ca peak, higher than in the units below but lower than in unit 65 and above. High Zr counts indicate coarser grain size most likely due to more intense erosion or strong precipitation events in the lake's catchment. Vegetation cover or a potential reed belt around the lake must have been low or absent, allowing the coarser material to reach the coring spot. Unit 62 again is rather fine grained, has a high amount of terrigenous elements and the lowest Ca counts of the analysed core sequence. The *Crataegus* seed, dated to ca. 780 AD, was found within this unit (modelled to 690 cal AD). The most characteristic features of this unit are its black colour and the high magnetic susceptibility values (>30x higher than the median). The blackish colour may indicate organic matter and anoxic conditions, supported by a very low Mn/Fe ratio. Unit 63, is also black, but consists of considerably coarser material, a high amount of intact shells and shell fragments and shows a strong Fe peak. What can clearly be observed here is a sudden, strong increase in the sedimentation rate to over 2 mm/yr that continues with a slightly decreasing trend for the following centuries. The variable and rapidly changing Zr/Rb proxy, reflecting grain size fluctuations, implies a vulnerable environment with quick changes in water availability. The intensity of variation of the geochemical proxies in units 61–64 is unparalleled

through the entire sequence at Lake Stymphalia, even stronger than during the Pleistocene/Holocene transition (Heymann et al., 2013).

The period between approximately 100 to 750 cal AD was specifically investigated using the distribution of branched GDGTs MBT'_{5Me} to gain information on relative temperature fluctuations, because it is known as a period of significant temperature variations (Büntgen et al., 2016). The relative ΔMAAT variation (Figure B8-B) based on the MBT'_{5Me} lipids suggests relatively warm conditions in Stymphalia during the 2nd to 3rd century cal AD followed by a strong cooling trend at the beginning of the Late Roman period and coldest temperatures around 400 and again later around 700 cal AD. This first cold phase is parallel to the decrease in rainfall described from the Middle East (Orland et al., 2009; Göktürk et al., 2011), and also aligns with $\delta^{18}O$ inferred drier conditions observed in the Kapsia Cave (Finné et al., 2014) and the Soreq Cave (Bar-Matthews et al., 1999). Within the error margin of the age-depth-model, the MBT'_{5Me}-reconstructed relative MAAT variation is also largely in agreement with a previously reported cooling in the 6th and 7th century AD based on dendrochronological data from the French Alps and the Russian Altai described by Büntgen et al. (2016) and referred to as the "Late Antique Little Ice Age" (LALIA, Figure B8-G). As possible triggers, Büntgen et al. (2016) suggest high volcanic activity and low solar forcing. In a recent review paper, Helama et al. (2017) describe a longer period of cold conditions between 400 and 765 AD termed "Dark Ages Cold Period" (DACP). However, we here follow the terminology of Büntgen et al. (2016) and abstain from using the term DACP (Büntgen et al., 2017; Helama et al., 2017b), as the latter is not only culturally pejorative, but it can also easily be confused with the Greek Dark Ages at the Bronze Age/Iron Age transition (Drake, 2012), which for the same cultural reasons are more frequently referred to as the Early Iron Age or (Proto-) Geometric and Archaic Period (Bintliff, 2012b; Weiberg et al., 2016). For the temporal extension of the cold LALIA period as reflected in our Stymphalia record, we would however rather follow Helama et al. (2017), as our brGDGT-inferred relative temperature record shows continuously colder temperatures until the beginning of the 8th century as compared to the 2nd century cal AD. Izdebski et al. (2016) also report colder climate conditions during the Late Antiquity for Anatolia and the Levant and add that the coldest decade most probably covered the time of the devastating pandemic known as the "Justinian plague" (541 AD). Büntgen et al. (2016) also consider the LALIA as one influential factor on "crop failure, famine and plague, as well as a possible trigger for political, societal and economic turmoil". During this period, described as the "rural agrarian system of Antiquity" (Izdebski et al. 2016), the people in the Eastern Mediterranean were strongly depending on cereal cultivation, viticulture and arboriculture, activities that are generally vulnerable to climatic fluctuations. The rapid drop in temperatures may have strongly increased their vulnerability, made them less resilient and more fragile to social crises. More pertinently, as occurred in the early years of the 17th century during the

LIA, closely spaced and even contiguous severe drought years may have caused historically significant unrest/collapse of normal agrarian adaptive systems (White, 2013; Manning, 2018). The situation in the eastern Roman Empire during the 6th and 7th centuries AD is described as showing "signs of hydroclimatic difficulties" and drier conditions that seemed to have prevailed until the 8th century AD (McCormick et al., 2012; Manning, 2013). The onset of the Late Antique cooling in the 7th and 8th century AD is described by McCormick et al. (2012) as a period of "deep transformations". This phase of high climatic instability in the Eastern Mediterranean is contemporaneous to the period of high instability and very varying conditions seen in Lake Stymphalia.

The core sequence reflecting the second half of the Early Byzantine Period, unit 65, comprises bright clayey silt containing some sand and a considerable amount of gastropod shells. Ca content is highest compared to the lower core sequence and the Sr/Ca ratio indicates mainly detrital input due to enhanced limestone weathering intensity. Strong chemical weathering may be explained by episodes of warm and wet climate conditions (Jin et al., 2001). Strong precipitation events may account for the influx of coarser material in unit 62, together with chemical changes. The continuing effects of the LALIA climatic fluctuation may be responsible, given the very low human impact. The notable rise in sedimentation after 780 cal AD and on till the 14th century AD begins in what Büntgen et al. (2011) as well as Bradley et al. (2016) term "Medieval Quiet Period", a period of reduced climate variability between 700 and 1000 AD. With the exception of the Mn/Fe ratio, which points towards decreasing oxic conditions and thus less intense mixing conditions, our proxies also show comparatively few fluctuations within that period, but that may also be explained by low human activity in a more stable land-cover. Although evidence for population changes in the Stymphalos Polje are so far not studied for the entire Early Byzantine period, wider evidence from the Peloponnese and other parts of Greece suggest low population and levels of land use throughout the era. The onset of increased sedimentation seem to mark the earliest phase of the Early Medieval Warm era, but this in itself would not seem sufficient to account for the increased influx of erosion products, which is lacking in the Greco-Roman eras under similar climatic conditions.

5.3.4 Middle Byzantine Period (842 – 1204 AD; units 66 – 67)

In the 9th century AD, southern Greece is re-integrated into the Byzantine Empire (Xoplaki et al., 2016). From Middle Byzantine (MB) times onwards, we see a gradual rise in population and a revival of agricultural use across the study region, reaching its climax after 1150 cal AD (Figure B8-I; Bintliff, 2012b; Williams, 2005; Xoplaki et al., 2016b). Xoplaki et al. (2016) define the 12th century AD as a "most prosperous period for southern Greece, with high agricultural productivity" and a relatively resilient society.

The steady increase in terrigenous elements (Figure B4), consequently an increase in Rb/Sr (Figure B7) and the sustained high sedimentation rate (Figure B6) from the 11th century until approximately 1400 cal AD would fit increasing human impact. While the Zr/Rb ratio showed only minor fluctuations before ca. 700 cal AD, the ratio strongly oscillates within this period starting in the mid-8th century, which could suggest enhanced human activity, land use, and erosion of soils with varying grain sizes. The silt content increases from 63 % in unit 64 to 79 % in unit 68 (BS3). The coarsening of the particles could potentially be linked to more intensified land use, such as herding, agricultural activity or deforestation loosening the soil and destabilizing the slopes, although the archaeologists believe that during this period the area was largely covered by forest (Campbell, 2018). Contrary to the Late Roman period, we do not consider that the lake area was small during the MB time, allowing more coarse-grained material to reach the depocentre, because we see high carbonate content here, which demands chemical weathering due to the presence of water and a rather large lake surface for summer evaporation to be more effective. Additionally, more allogenic organic matter is washed in and preserved, as seen by higher TOC and TOC/TN values at 145 cm (4.9% and 39.6 respectively) or 110-115 cm (6.4% and 43.6 respectively; BS2). For the analysed sequence, TOC/TN ratios usually fluctuate between 10 and 20 (mean = 17.6), which suggests significant mixing of terrestrial and aquatic organic matter (Meyers, 2003). In the MB period, the amount of terrestrial organic matter dominates, while the high sedimentation rates may contribute to the comparatively better preservation of the organic matter as the sediment buries it before it can be completely decomposed. While in unit 66 we still find intact gastropod shells, unit 67 only contains shell fragments and additionally root fragments, suggesting the reworked nature of the material and vegetation growth. The increase in detrital terrestrial material input is likewise visible in PC1 and Rb/Sr (Figure B7). As Ca and Sr still have high values, although decreasing over time, we would expect intensive chemical weathering and high evaporation, thus generally warm and wet conditions. The archaeological and historical evidence for Greece clearly indicate an increasing rate of demographic growth and land intake between the 9th and the 12th centuries (Bintliff, 2012b; Xoplaki et al., 2016). That this took place within a climate phase, which was warm and moist according to current climate reconstructions, was a very positive background to a new political stability in the countryside. Other high resolution climate proxies for this period are still rather sparse (Xoplaki et al., 2016), but SSTs from M2 in the Aegan Sea (Figure B8-F; Gogou et al., 2016) also record increasingly warmer temperatures for this phase starting from 900 AD up to the 14th century.

However since demographic levels are well below those of Classical-Hellenistic times, and by inference the extent of landscape in intensive use, the unparalleled erosion into the lake, seen by the high sedimentation rate, must imply either strong precipitation events, or effective evaporation from a large and shallow water body, or non-investigated more localised and very

destructive deforestation and modes of farming and herding in the immediate catchment of the lake, than prevailed throughout Greco-Roman times.

5.3.5 Late Byzantine-Frankish Period (1204 – 1460 AD; units 67 – 68)

The uppermost part of sedimentary unit 67 and the lower part of 68 cover the era of Crusader occupation and parallel Byzantine control of different parts of the Peloponnese, before the Ottoman conquest of the mid-15th century. Since the 13th to early 14th centuries show dramatic contrasts both in the archaeological and historical record, as in the core evidence, to the period of the late 14th into mid-15th centuries, we shall discuss these separately.

For the 13th century the high sedimentation rate which had commenced already in Middle Byzantine times is maintained, but with a visible slowing down. The continued increase in Rb/Sr points to more terrigenous influence and Mn/Fe suggests that the lake continued to become shallower and/or well mixed, reaching its most oxic state in the first half of the 13th century, which coincides with societal changes in the catchment.

Although we do not expect any major change in regional demography and land use, the Stymphalos lakeside has a truly exceptional history in the 13th century, since it was chosen for the foundation of a Cistercian monastery, located above and slightly inland of the ancient city site (Campbell, 2018). In general, such establishments favoured areas with high agro-pastoral potential but remote from major population centres. They emphasized manual labour by the monks and advanced farming techniques, but the assistance of local labour (lay-brothers) required the existence of nearby settlements. We can expect intensive use of the landscape around the monastery but rather good management of local ecology. That erosion into the lake continued but at a declining rate may indicate new clearance initiatives near the coring site but maybe slightly greater ecological care than in the preceding period of settlement. However, the Zaraka monastery existed for only less than one century and due to the age uncertainties in the sediment core outlined above, it is not possible to draw conclusive links between changes in the sediment sequence and monastery activities. We conclude here that the climatic regime for this century marks the highpoint of the early Medieval Warm period, remaining as favourable to settlement and land use as in previous centuries.

In the second half of the Late Byzantine-Frankish (B-F) era, there is strong societal transformation. The collapse of Frankish power leaves the Peloponnese in Byzantine control, and the monastery at Stymphalos is abandoned. Furthermore, in the mid-14th century, the Black Death produces a massive reduction in European populations, while a period of colder climatic conditions lasting into the 15th century, a first phase of the Little Ice Age, was reconstructed from the Alps (Büntgen et al., 2011). Although this climatic period is associated with increased precipitation in temperate Europe, the effects in the southern parts of Europe may have been temperature and rainfall decline (Magny et al., 2007b).

The latter part of the B-F period is covered by sedimentary unit 68, which shows a more brownish colour and considerably high magnetic susceptibility (MS) values suddenly increasing by a factor of 4 around 1400 cal AD and this continues into the first part of the early Post-Medieval period (Figure B4). High magnetic susceptibility indicates that these sections contain a higher amount of terrigenous material that may be magnetized, especially ferromagnetic elements such as magnetite or maghemite (Lucke and Sprafke, 2015). Fe counts are elevated but not as high as during the Late Roman period (Figure B4). Contrary to the material eroded in early centuries, it seems likely that the sediments eroded at this period were stored locally as colluviums or on terraces before, where processes of soil formation took place before they were finally deposited in the lake. This would likewise explain the strong rise in the magnetic susceptibility followed by a declining trend; upper layers with most intensive development of soil formation and highest MS values eroded first. The loss of soil from abandoned fields following the phase of the Black Death is also described from Macedonia (Gogou et al., 2016).

Throughout Greece, the 14th to early 15th centuries is a period of large-scale depopulation in the countryside, associated with a devastating plague, prolonged episodes of warfare between Franks, Byzantine and the expanding power of the Ottoman Turks, and colder climatic conditions (Finné et al., 2011; Bintliff, 2012b). After the abandonment of the Zaraka monastery in the mid-14th century, we have only minor archaeological traces of human settlement in the region at the ancient city site and the former monastery until archival records from 1700 AD (Williams, 2005; Campbell, 2018). In agreement with better-documented trends elsewhere in Greece (Bintliff, 2012b), we expect very low populations and widespread abandonment of cultivated land in the 14th to early 15th centuries, coinciding with the core trends just discussed. Hence, the highly magnetized sediments eroding into the lake probably mark the erosion of deserted, non-vegetated fields during an unstable and generally colder climate, perhaps with shorter but more powerful precipitation events.

5.3.6 Ottoman to Modern times (1460 – 2010 AD; units 68 – 70)

With the Ottoman conquest of the Peloponnese in mid-15th century, we enter a new phase of local settlement history, so we shall first discuss the relevant evidence up until the end of the 18th century AD, associated with the upper three-quarters of sediment unit 68. The age-depth-model for the uppermost 50 cm of the core has high uncertainties and the calculated ages are probably slightly too old. Thus, we rather combine the geochemical signals with known historical dates.

The Ottoman authorities were proactive in Greece in encouraging the resettlement of abandoned fields and villages (Kiel, 1987, 1997; Bintliff, 2012b), in particular inviting Albanian farmers and pastoralists to recolonise the Greek regions, including the Stymphalos district,

where the modern villages mostly take their origin from this population movement. In Central Greece, repopulation began in the late 14th century and led to settlement growth into the late 16th century. The later inception of repopulation in the Peloponnese occurred within the late 15th into 16th century. This era falls within the generally colder and locally potentially drier Little Ice Age period and posed problems to the population for prosperous land use (White, 2013). The rate of sediment deposition into the lake continues to decrease up to the 16th century and stays at a rather constant level of ca. 0.7 mm/yr until the core top. Throughout unit 68, this is accompanied by a parallel fall-off in magnetized material, indicating that less soil material is eroded. Additionally, a refinement of the material is observed as shown by the Zr/Rb ratio. We suggest this marks stabilisation of an almost empty landscape by vegetation, scrub or emerging young woodland and only minor human impact.

Central Greek populations were to collapse dramatically from the late 16th into the 18th century. The demographic recovery which had begun much later in the Peloponnese, would also have been reversed at this time. The failure of central government, the peak of the Little Ice Age, and devastating warfare between the Ottomans and Venice were the major factors (Bintliff, 2012b). As a result, the first census figures for villages in the Stymphalos district ca. 1700 AD show very low levels, with 50 or less inhabitants per village for almost all settlements in the Stymphalos district (the successor to the ancient city and medieval monastery, the village of Stymphalia, has 52; Panagiotopoulos, 1985).

Brown and Walsh (2017) see a drastic decrease in clastic sedimentation (Cu, Zn, Fe, Ti) and an increase in Ca in the upper 72 cm of their sediment cores taken from the lake shore, which they interpret as a lake level becoming constantly shallower and drying out repeatedly. However, their chronology needs to be regarded with caution, as it is not well anchored in the uppermost part. In contrast to these results, we see the opposite elemental trend in our sediment record, a constant increase in terrigenous elements (Rb, Zr, Al, Ti, K, Si) for the upper 156.5 cm (with the exception of unit 69 – 70) and a decreasing carbonate content (Ca and Sr). TOC and TOC/TN values for this period are low, indicating, as the Mn/Fe ratio implies strongly oxic conditions, that organic matter input in this section was strongly decomposed and not preserved. Unit 68 contains shell fragments of *Bythinia sp.* proving that a lake, however shallow, existed at that time. In addition, the sediment in unit 68 is orange mottled with iron oxides hinting oxygen supply and desiccation. This leads to the conclusion that a small, shallow lake existed for most of the year and periodically dried out in summer. Thus, although the geochemical argumentation is different, we come to a similar conclusion as Brown and Walsh (2017) that the lake bottom became shallower over time and since approximately 1500 AD may have periodically dried out.

The uppermost units 69 and 70, covering the Early Modern era of the 18th to 20th century cal AD, need to be regarded with caution. We see very strong, abrupt changes and we assume

that the material was altered post-hoc; for example, due to desiccation, some material might have been eroded or due to agricultural activity on the lake bottom, it may have been anthropogenically reworked and first soil formation processes may have set in. According to Walsh et al. (2017) the lake dried up completely over several years in the recent and was even used as a landing strip. This is known from historical sources and brought the lake its nickname “aerodromio”, airport (Walsh et al., 2017b). The desiccation, compaction and anthropogenic drainage can also be seen in the sedimentological record; unit 69 (dated to ca. 1720 – 1860 cal AD) is very dense and compact and contains a sudden, abrupt increase in terrigenous elements, especially in Rb and K, typical clay elements; this increase in clay can also be seen in the Mastersizer data. Zr/Rb firstly indicates a shift to coarser material and then a refining within the unit. The TOC content in this section is low, only increasing in unit 70 above, indicating that enough oxygen was present in this section to decompose the organic matter. An increase in Mn, Fe and MS suggests first soil formation processes; gastropods are absent here. All these proxies indicate that in the 19th century the lake has repeatedly fallen dry. Furthermore, there is historical evidence that the authorities in the Corinth region re-activated the aqueduct in the 1880s to irrigate their local farmland (Morfis and Zojer, 1986), giving one explanation why less water reached the lake. Although the sinkhole at the southern shore has been isolated from regular outflow since the 19th century (Walsh et al., 2017b), no larger flooding events are visible in the core apart from the more coarse grained unit 70a (at 9 cm, dated to ca. 1880 cal AD). During the late 19th and early 20th century, agricultural production in the polje strongly expanded. The population of this district, as over the rest of the Peloponnese, grew exponentially; Philippson (1892) lists village sizes in the Stymphalos district that are 10 to 15 times those of the same communities two hundred years earlier (Stymphalos has now 808 inhabitants). This did not simply mean sustainable subsistence and minor commercial agriculture as during Classical-Hellenistic times (cf. section 0), but rather industrialized primary production for the global market with the help of farming machines (Kourelis, 2018), which would also explain the strong compaction of the soil. The shift from the colder LIA climate to a more typical Mediterranean climate over this same period, starting in the 19th century AD based on SSTs in M2 (Figure B8-F; Gogou et al., 2016), was highly positive for the observed agricultural take-off.

The thin unit 70a, characterized by a high amount of sand particles probably indicates a strong precipitation event with surface run-off refilling the lake and feeding in coarser grained material into the centre of the lake that accumulated in the plain during the dry period; reed vegetation holding back the material was probably absent by then.

Unit 70b may be characteristic for today’s conditions; high TOC, average TIC and Ca counts as well as moderate terrigenous input. The lake is perennial, but depending on the season it can vary considerably in size. The polje is intensively used for agricultural purposes. For the

second half of the 20th century, land use has also been analysed by Papastergiadou et al. (2007); wet-meadows and open water areas declined considerably while reed beds and irrigated agricultural land spread out. The use of fertilizers reinforces the reed growth and most likely affects the faunal populations.

6. Conclusion

The geochemical and sedimentological analyses of the Stymphalia lake sequence show a complex interlinking of natural variability and anthropogenic influence on the lake over the last 2,500 years. Water supply to the lake was not constant over time and the land cover in the catchment must have changed substantially in relation to climate fluctuations, intensity of land-use and human occupation phases that influenced the sedimentary conditions. The lake level and particularly the lake area have fluctuated considerably over the last 2,500 years including shorter periods of entire desiccation, more frequently occurring in the younger phase. No evidence for a very high lake level comparable with the neighbouring Pheneos polje has been found in the sediment sequence; we are continuously dealing with a shallow lake system here. Stable climatic conditions and sustainable agro-pastoralism prevailed during Classical Hellenistic times. Major alteration in the lake's hydrological cycle occurred with the construction of the Early Roman Hadrianic Aqueduct around 130 AD, which increased the vulnerability of the ecosystem and, even after its failure, probably had a long-lasting impact on ecosystem reactions to climatic changes during the following centuries. We interpret this event as a trigger for the highly sensitive reaction to climatic variations during the LALIA period in the 6th to 8th century AD. The Lake Stymphalia data indicate that the Late Roman to Early Byzantine Period in southern Greece is associated with a shift to several cold periods of varying durations, strong variation in water availability and a generally more unstable climatic context. Although anthropogenic influence was chronologically limited, it represents a significant element in understanding long-term reactions in the sediment core that were mainly linked to water availability. For the period 9th to 17th century, the age-depth-model implies higher uncertainties; however, we see a phase of higher sedimentation and carbonate precipitation during warm and wet conditions within the Medieval Warm Period roughly until the 15th century and indications for colder conditions during the Little Ice Age. The last 200 years are strongly shaped by desiccation and human activity.

Land use intensity and vegetation cover were in a fluctuating dialectic with temperature and precipitation changes in the degree and nature of surface erosion. These conclusions agree with recent modelling of environmental change, critical of mono-causation, rather focussing on complex interactions of human and natural factors in the inception of landscape transformation (Bintliff, 2002; Casana, 2008). Pollen analysis would lead to an additional

value, supporting our hypotheses or further classifying the land use activities, however pollen preservation in the core sequence was inadequate for any detailed analysis. The close interdisciplinary collaboration between natural scientists and archaeologists in this research field was highly beneficial and offers a more holistic interpretative approach. In the near future, independent sedimentary records from other sedimentary archives in adjacent valleys shall offer additional insights on the reconstruction of climatic changes and associated human impact interaction in the NE Peloponnese.

Supplement Material

Lab_No	14C_age	error	depth	cc	delta.R	delta.STD	Comment
surface	-60	5	0	0	0	0	
VERA-6380HS-combine	1608	20	50	1	200	100	# OxCal
VERA-6380-combine	1537	19	50	1	200	100	# OxCal
KIA47446_HS	1285	35	72	1	200	100	
VERA-6382HS_2	1419	37	114	1	200	100	
VERA-6382-combine	1432	26	114	1	200	100	# OxCal
VERA-6383HS_2	1441	35	161	1	200	100	
VERA-6383-combine	1535	26	161	1	200	100	# OxCal
KIA42912_HS	1355	23	164	1	200	100	
VERA-6258	1237	35	165	1	0	0	# Crataegus
Aqueduct	1820	20	189	0	0	0	# Aqueduct building 130 AD
VERA-6259-combine	2071	20	195	1	200	100	
VERA-6259HS-combine	2206	22	195	1	200	100	
Ceramic	2350	100	205	0	0	0	# 5th century BC
KIA47448_HS	3170	30	207	1	200	100	
Poz-96329	2310	35	210	1	200	100	
Poz-96330	3850	40	220	1	200	100	
VERA-6260	3809	39	236	1	200	100	
VERA-6260HS	3937	33	236	1	200	100	
KIA44005_HS	3563	29	236	1	200	100	
Poz-96331	3335	35	238	1	200	100	
Poz-96325	4180	40	248	1	200	100	
KIA44006_HS	4837	34	266	1	200	100	
VERA-6261	4600	35	267	1	200	100	
VERA-6261HS	4631	36	267	1	200	100	
VERA-6262	4829	38	270	1	200	100	
VERA-6262HS	4877	29	270	1	200	100	
VERA-6263-combine	4674	21	273	1	200	100	# OxCal
VERA-6263HS-combine	4790	22	273	1	200	100	# OxCal
KIA45955_HS	6025	35	280	1	200	100	
KIA42913	7708	35	324	1	0	0	# Charcoal

BS1: Input table as applied for Rbacon modelling of STY_25. Column 2 indicates the uncalibrated C^{14} ages for radiocarbon ages or the calender ages for historical dates. Column 3 mainly shows measurement uncertainties (always ±) or defined errors for historical dates. The depth unit for column 4 is cm. Column 5 indicates the applied calibration curve (cc=0 for none - applied for calender dates or cal BP, cc=1 for northern hemisphere terrestrial material which is calibrated with IntCal13. Column 6 and 7 indicate the mean and error of core-wide age offsets, namely reservoir effects. Comments in the last column were excluded from modelling and only have a documentation purpose to improve the readability.

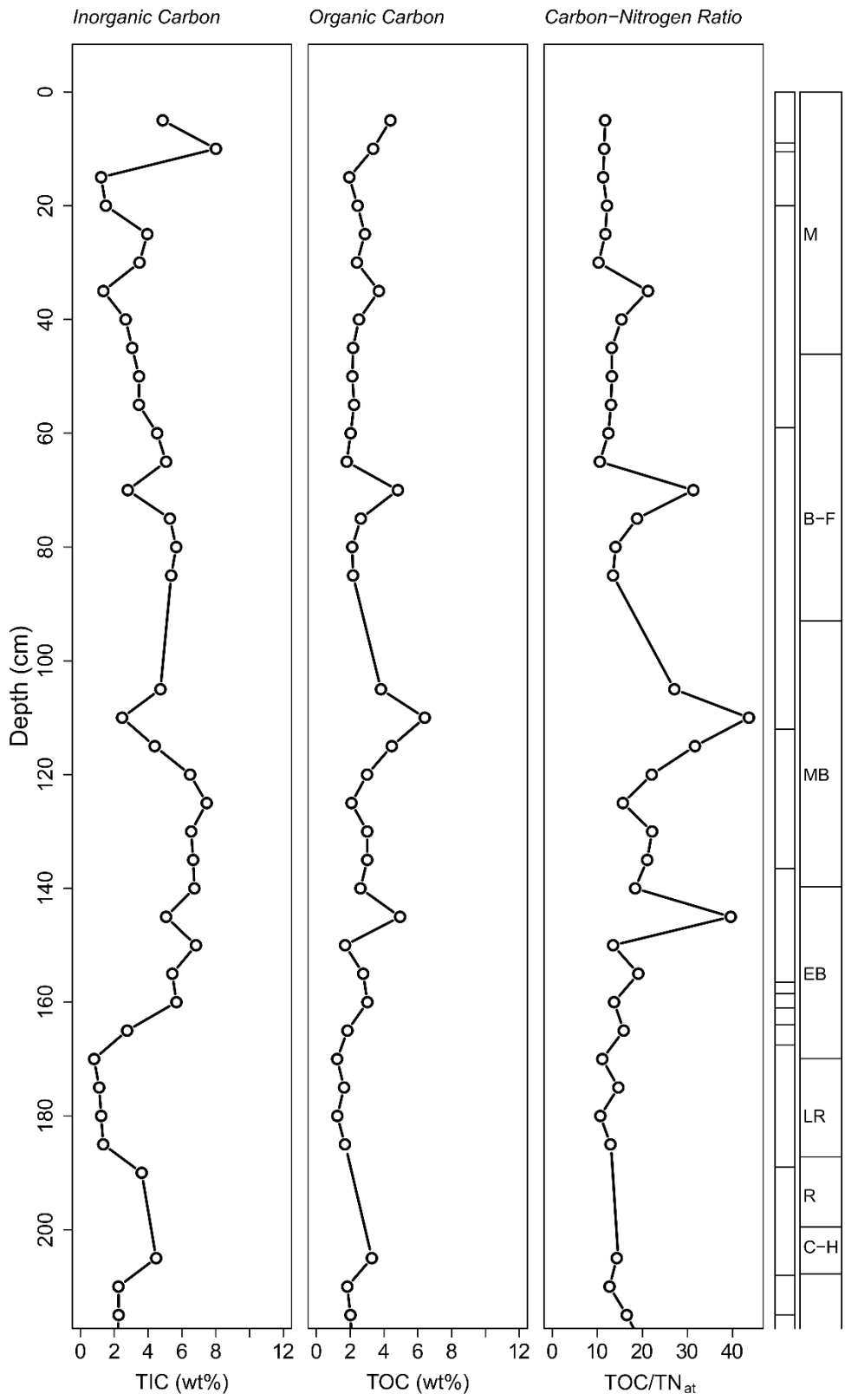

BS2: TIC, TOC and TOC/TN (atomic masses) plotted against depth. The boxes to the right show the lithological units and the Greek cultural phases as specified in Weiberg et al. (2016; cf. Table 3).

BS3: Table of grain size measurements for every sediment unit. The fraction classes and the soil type classification follow the German Arbeitsgruppe Boden (2005).

Depth [cm]	Sediment Unit	Clay [%]	Fine Silt [%]	Medium Silt [%]	Coarse Silt [%]	Fine Sand [%]	Medium Sand [%]	Coarse Sand [%]	Soil Type (AG Boden 2005)
5	70b	22,43	39,47	34,30	3,13	0,66	0,00	0,00	Ut4
10	70a	24,33	28,84	22,71	6,91	6,45	7,67	3,08	Lu
15	69	23,73	35,06	35,72	5,06	0,43	0,00	0,00	Ut4
40	68	20,45	36,02	37,11	6,24	0,18	0,00	0,00	Ut4
65	67	21,87	38,54	35,11	4,41	0,07	0,00	0,00	Ut4
124	66	24,68	35,79	30,72	7,03	1,62	0,14	0,00	Ut4
144	65	27,19	34,29	27,92	7,84	2,73	0,03	0,00	Tu4
158	64	37,33	38,42	20,76	3,43	0,06	0,00	0,00	Tu3
159	63	27,05	30,90	23,53	10,98	4,95	2,58	0,02	Tu4
163	62	31,25	34,34	23,92	7,00	1,69	1,80	0,00	Tu4
165	61	39,57	32,57	19,60	5,43	1,42	1,42	0,00	Tu3
179	60	29,96	42,25	26,06	1,62	0,03	0,06	0,00	Tu4
204	59	24,03	37,54	32,13	5,67	0,46	0,15	0,01	Ut4

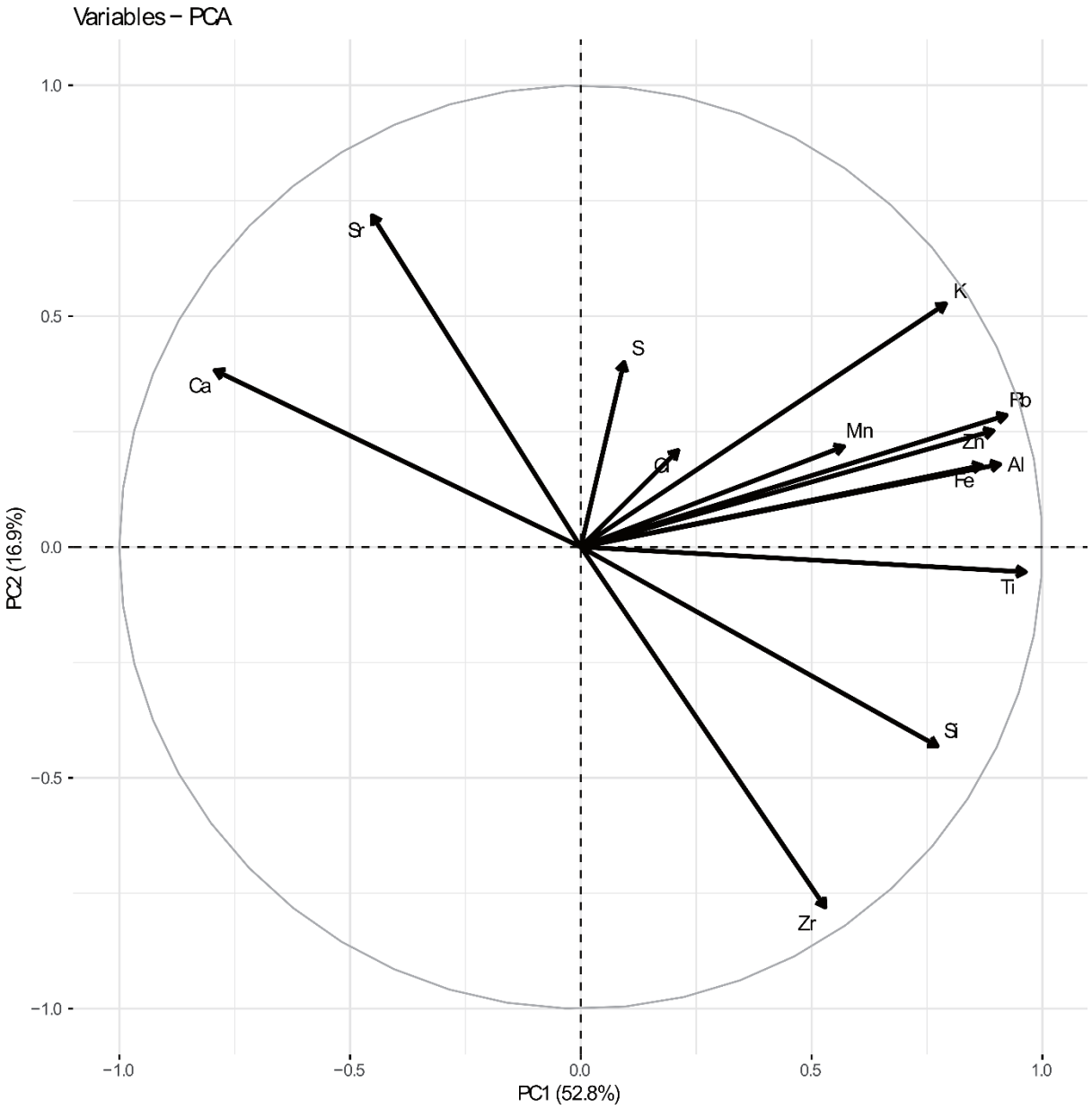

BS4: Principle Components Analysis of XRF data. Plot of the 13 included element variables as defined by the first two principal components of the PCA. The PC1 accounts for 52.8% and PC2 for 16.9% of the observed variability.

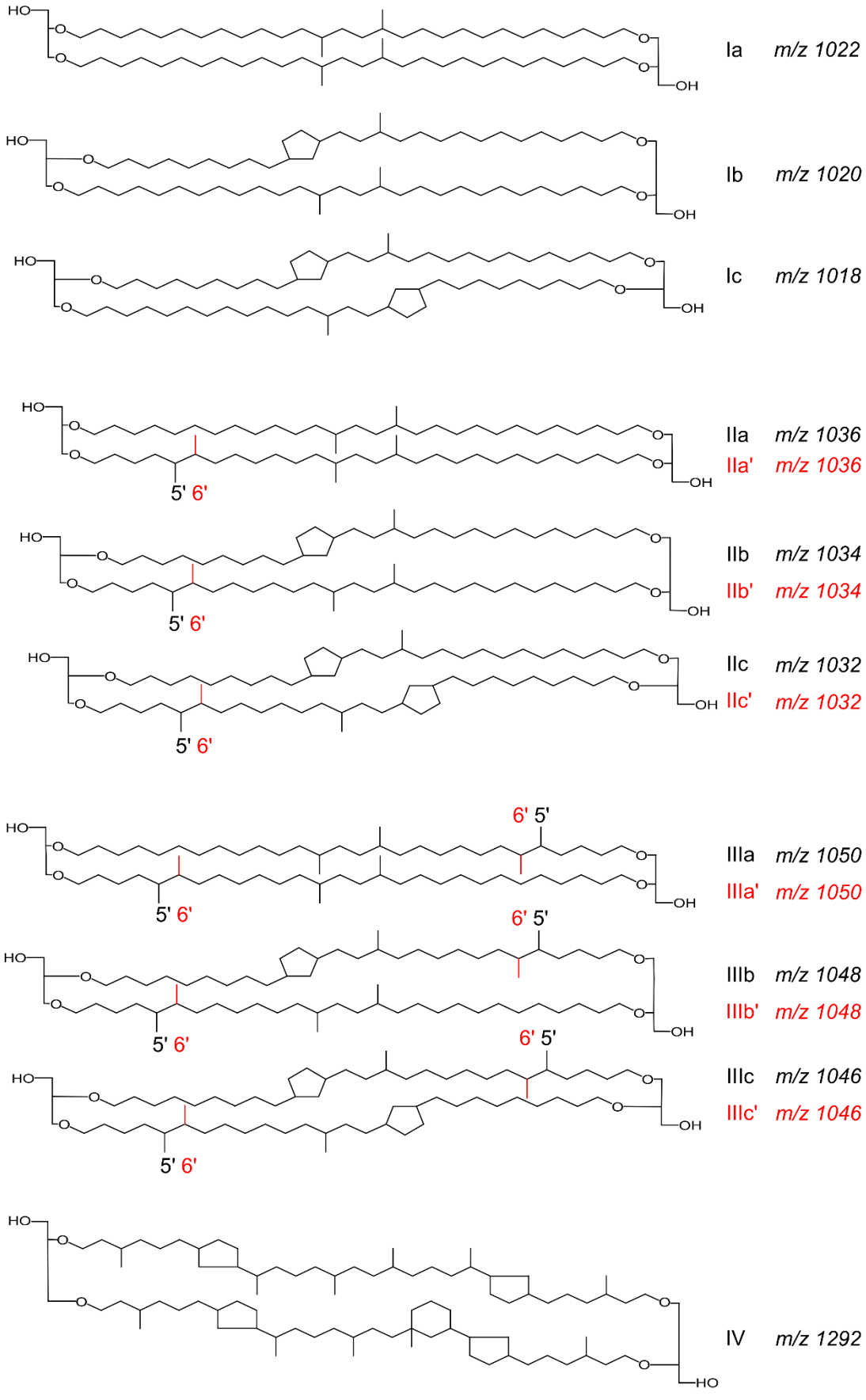

BS5: GDGTs structures.

Acknowledgements

Funded by the Deutsche Forschungsgemeinschaft (DFG, German Research Foundation - Projektnummer 2901391021 – SFB 1266). The positions of Joana Seguin and Jan Weber are funded by the DFG through the Collaborative Research Centre “SFB 1266”. The position of Christian Heymann was funded by the DFG through the Graduate School “Human Development in Landscapes” at Christian-Albrechts-University. The authors acknowledge insights into the archaeology coupled with the history of the lake and the Hadrianic aqueduct from Hector Williams, Malcom Wagstaff, and Iannis Lolos. We kindly thank Tom Wilke (Georg-August-University Göttingen) for the determination of the mollusc species, Jesse Kalwij (Christian-Albrechts-University Kiel) for the determination of the plant species, and Bernhard Schmaltz (Christian-Albrechts-University Kiel) for the classification of the ceramic fragment. In alphabetical order, we kindly thank our following colleagues and students for their invaluable support in the field and in the laboratory: Mathias Bahns, Kimon Christanis, Sophia Dazert, Giorgos Floros, Elke Hänßler, Görkim Oskay, Giorgos Savalas, Marcus Schütz, and Stavros Vrachliotis. We also thank two anonymous reviewers and Neil Roberts as editor for their valuable and constructive comments on the manuscript. The project was carried out with the relevant permits from the Greek Authorities.

Acknowledgments

First of all, I would like to thank my first supervisor Prof. Dr. Lorenz Schwark for giving me the opportunity and the support to work in the lab of the organic geochemistry unit. A special thank you for the discussions, guidance and motivation, which helped me to write this thesis.

Dr. Thorsten Bauersachs is thanked for his co-mentorship and especially the guidance in LC-MS analytic and improving my manuscripts.

I would also thank all of my colleagues of the organic geochemistry unit for assisting in technical and laboratory issues or discussing the results. Special thanks to Dr. Martin Stockhausen, Marieke Muijsers, Ann-Sophie Jonas, Vanessa Grote, Tim Marten, Petra Fiedler, Dr. Wolfgang Rübsam, Fanny Aschmann, Till Malliakas and Dorte Fischer.

Further, I would like to thank all PhD-students and colleagues of the SFB 1266 for the interesting cooperation, motivation and providing helpful background information about especially archaeology and palynology. I am also grateful to the German Research Foundation (DFG) for funding this project.

Last but not least, I am very thankful to my family and Bea for their support and motivation during the last three years. Thank you!

References

Ackman, R.G., 1967. Characteristics of the fatty acid composition and biochemistry of some fresh-water fish oils and lipids in comparison with marine oils and lipids. Comp. Biochem. Physiol. 22, 907–922. https://doi.org/10.1016/0010-406X(67)90781-5

ad-hoc Arbeitsgruppe Boden, 2005. Bodenkundliche Kartieranleitung. E. Schweizerbart'sche Verlagbuchhandlung, Hannover.

Aichner, B., Herzschuh, U., Wilkes, H., 2010. Influence of aquatic macrophytes on the stable carbon isotopic signatures of sedimentary organic matter in lakes on the Tibetan Plateau. Org. Geochem. 41, 706–718. https://doi.org/10.1016/j.orggeochem.2010.02.002

Aichner, B., Feakins, S.J., Lee, J.E., Herzschuh, U., Liu, X., 2015. High-resolution leaf wax carbon and hydrogen isotopic record of the late Holocene paleoclimate in arid Central Asia. Clim. Past 11, 619–633. https://doi.org/10.5194/cp-11-619-2015

Aichner, B., Ott, F., Słowiński, M., Noryśkiewicz, A.M., Brauer, A., Sachse, D., 2018. Leaf wax *n*-alkane distributions record ecological changes during the Younger Dryas at Trzechowskie paleolake (Northern Poland) without temporal delay. Clim. Past Discuss. 1–29. https://doi.org/10.5194/cp-2018-6

Ali, H.A.M., Mayes, R.W., Hector, B.L., Verma, A.K., Ørskov, E.R., 2005. The possible use of *n*-alkanes, long-chain fatty alcohols and long-chain fatty acids as markers in studies of the botanical composition of the diet of free-ranging herbivores. J. Agric. Sci. 143, 85–95. https://doi.org/10.1017/S0021859605004958

Alley, R.B., Mayewski, P.A., Sowers, T., Stuiver, M., Taylor, K.C., Clark, P.U., 1997. Holocene climatic instability: A prominent, widespread event 8200 yr ago. Geology 25, 483–486. https://doi.org/10.1130/0091-7613(1997)025<0483:HCIAPW>2.3.CO;2

Alley, R.B., 2000. The Younger Dryas cold interval as viewed from central Greenland, in: Quaternary Science Reviews. Pergamon, pp. 213–226. https://doi.org/10.1016/S0277-3791(99)00062-1

Alley, R.B., 2004. GISP2 ice core temperature and accumulation data. Boulder CO, USA.

Amid, B.T., Mirhosseini, H., Kostadinović, S., 2012. Chemical composition and molecular structure of polysaccharide-protein biopolymer from Durio zibethinusseed: extraction and purification process. Chem. Cent. J. 6, 117. https://doi.org/10.1186/1752-153X-6-117

Aquino-Bolaños, E.N., Mapel-Velazco, L., Martín-del-Campo, S.T., Chávez-Servia, J.L., Martínez, A.J., Verdalet-Guzmán, I., 2017. Fatty acids profile of oil from nine varieties of Macadamia nut. Int. J. Food Prop. 20, 1262–1269. https://doi.org/10.1080/10942912.2016.1206125

Artursson, M., Linderoth, T., Nilsson, M.L., Svensson, M., 2003. Byggnadskultur i södra och mellersta Skandinavien, in: Det Neolitiska Rummet. Skånska Spår – Arkeologi Längs

Västkustbanan. Stockholm, pp. 40–171.

Ashburner, K., McAllister, H.A., 2013. The Genus Betula: A Taxonomic Revision of Birches.

Atherden, M.A., Hall, J.A., 1994. Holocene Pollen Diagrams from Greece. Hist. Biol. 9, 117–130. https://doi.org/10.1080/10292389409380493

Avramidis, P., Geraga, M., Lazarova, M., Kontopoulos, N., 2013. Holocene record of environmental changes and palaeoclimatic implications in Alykes Lagoon, Zakynthos Island, western Greece, Mediterranean Sea. Quat. Int. 293, 184–195. https://doi.org/10.1016/j.quaint.2012.04.026

Baeten, J., Jervis, B., De Vos, D., Waelkens, M., 2012. Molecular evidence for the mixing of Meat, Fish and Vegetables in Anglo-Saxon coarseware from Hamwic, UK. Archaeometry 55, 1150–1174. https://doi.org/10.1111/j.1475-4754.2012.00731.x

Baeten, J., Deforce, K., Challe, S., De Vos, D., Degryse, P., 2014. Holy Smoke in Medieval Funerary Rites: Chemical Fingerprints of Frankincense in Southern Belgian Incense Burners. PLoS One 9, e113142. https://doi.org/10.1371/journal.pone.0113142

Bakke, J., Lie, O., Heegaard, E., Dokken, T., Haug, G.H., Birks, H.H., Dulski, P., Nilsen, T., 2009. Rapid oceanic and atmospheric changes during the Younger Dryas cold period. Nat. Geosci. 2, 202–205. https://doi.org/10.1038/ngeo439

Balascio, N.L., D'Andrea, W.J., Gjerde, M., Bakke, J., 2018. Hydroclimate variability of High Arctic Svalbard during the Holocene inferred from hydrogen isotopes of leaf waxes. Quat. Sci. Rev. 183, 177–187. https://doi.org/10.1016/j.quascirev.2016.11.036

Baldini, J.U.L., Brown, R.J., Mawdsley, N., 2018. Evaluating the link between the sulfur-rich Laacher See volcanic eruption and the Younger Dryas climate anomaly. Clim. Past 14, 969–990. https://doi.org/10.5194/cp-14-969-2018

Baldini, L.M., McDermott, F., Baldini, J.U.L., Arias, P., Cueto, M., Fairchild, I.J., Hoffmann, D.L., Mattey, D.P., Müller, W., Nita, D.C., Ontañón, R., Garciá-Moncó, C., Richards, D.A., 2015. Regional temperature, atmospheric circulation, and sea-ice variability within the Younger Dryas Event constrained using a speleothem from northern Iberia. Earth Planet. Sci. Lett. 419, 101–110. https://doi.org/10.1016/j.epsl.2015.03.015

Bale, N.J., Hopmans, E.C., Zell, C., Sobrinho, R.L., Kim, J.H., Sinninghe Damsté, J.S., Villareal, T.A., Schouten, S., 2015. Long chain glycolipids with pentose head groups as biomarkers for marine endosymbiotic heterocystous cyanobacteria. Org. Geochem. 81, 1–7. https://doi.org/10.1016/j.orggeochem.2015.01.004

Bale, N.J., Hopmans, E.C., Schoon, P.L., de Kluijver, A., Downing, J.A., Middelburg, J.J., Sinninghe Damsté, J.S., Schouten, S., 2016. Impact of trophic state on the distribution of intact polar lipids in surface waters of lakes. Limnol. Oceanogr. 61, 1065–1077. https://doi.org/10.1002/lno.10274

Bale, N.J., Hennekam, R., Hopmans, E.C., Dorhout, D., Reichart, G.-J., van der Meer, M.,

Villareal, T.A., Sinninghe Damsté, J.S., Schouten, S., 2019. Biomarker evidence for nitrogen-fixing cyanobacterial blooms in a brackish surface layer in the Nile River plume during sapropel deposition. Geology 47, 1088–1092. https://doi.org/10.1130/G46682.1

Bar-Matthews, M., Ayalon, A., Kaufman, A., Wasserburg, G.J., 1999. The Eastern Mediterranean paleoclimate as a reflection of regional events: Soreq cave, Israel. Earth Planet. Sci. Lett. 166, 85–95. https://doi.org/10.1016/S0012-821X(98)00275-1

Barnikol-Schlamm, D., 1994. . Die Sedimente des Steisslinger Sees. Kartierung der Oberflächensedimente und Untersuchung der jüngeren Sedimentationsgeschichte (Bl. 8119 Eigeltingen und 8219 Singen/ Hohentwiel). Universität Göttingen.

Bauersachs, T., Compaoré, J., Hopmans, E.C., Stal, L.J., Schouten, S., Sinninghe Damsté, J.S., 2009a. Distribution of heterocyst glycolipids in cyanobacteria. Phytochemistry 70, 2034–2039. https://doi.org/10.1016/j.phytochem.2009.08.014

Bauersachs, T., Hopmans, E.C., Compaoré, J., Stal, L.J., Schouten, S., Damsté, J.S.S., 2009b. Rapid analysis of long-chain glycolipids in heterocystous cyanobacteria using high-performance liquid chromatography coupled to electrospray ionization tandem mass spectrometry. Rapid Commun. Mass Spectrom. 23, 1387–1394. https://doi.org/10.1002/rcm.4009

Bauersachs, T., Schouten, S., Compaoré, J., Wollenzien, U., Stal, L.J., Sinninghe Damsteé, J.S., 2009c. Nitrogen isotopic fractionation associated with growth on dinitrogen gas and nitrate by cyanobacteria. Limnol. Oceanogr. 54, 1403–1411. https://doi.org/10.4319/lo.2009.54.4.1403

Bauersachs, T., Miller, S.R., van der Meer, M.T.J., Hopmans, E.C., Schouten, S., Sinninghe Damsté, J.S., 2013. Distribution of long chain heterocyst glycolipids in cultures of the thermophilic cyanobacterium Mastigocladus laminosus and a hot spring microbial mat. Org. Geochem. 56, 19–24. https://doi.org/10.1016/j.orggeochem.2012.11.013

Bauersachs, T., Mudimu, O., Schulz, R., Schwark, L., 2014a. Distribution of long chain heterocyst glycolipids in N2-fixing cyanobacteria of the order Stigonematales. Phytochemistry 98, 145–150. https://doi.org/10.1016/j.phytochem.2013.11.007

Bauersachs, T., Stal, L.J., Grego, M., Schwark, L., 2014b. Temperature induced changes in the heterocyst glycolipid composition of N2 fixing heterocystous cyanobacteria. Org. Geochem. 69, 98–105. https://doi.org/10.1016/j.orggeochem.2014.02.006

Bauersachs, T., Rochelmeier, J., Schwark, L., 2015a. Seasonal lake surface water temperature trends reflected by heterocyst glycolipid-based molecular thermometers. Biogeosciences 12, 3741–3751.

Bauersachs, T., Weidenbach, K., Schmitz, R.A., Schwark, L., 2015b. Distribution of glycerol ether lipids in halophilic, methanogenic and hyperthermophilic archaea. Org. Geochem. 83–84, 101–108. https://doi.org/10.1016/j.orggeochem.2015.03.009

Bauersachs, T., Talbot, H.M., Sidgwick, F., Sivonen, K., Schwark, L., 2017. Lipid biomarker signatures as tracers for harmful cyanobacterial blooms in the Baltic Sea. PLoS One 12, 1–25. https://doi.org/10.1371/journal.pone.0186360

Bauersachs, T., Miller, S.R., Gugger, M., Mudimu, O., Friedl, T., Schwark, L., 2019. Heterocyte glycolipids indicate polyphyly of stigonematalean cyanobacteria. Phytochemistry 166, 112059. https://doi.org/10.1016/j.phytochem.2019.112059

Bell, G.H., 1973. Solubilities of normal aliphatic acids, alcohols and alkanes in water. Chem. Phys. Lipids 10, 1–10. https://doi.org/10.1016/0009-3084(73)90036-4

Belt, S.T., Allard, W.G., Massé, G., Robert, J.-M., Rowland, S.J., 2000. Highly branched isoprenoids (HBIs): identification of the most common and abundant sedimentary isomers. Geochim. Cosmochim. Acta 64, 3839–3851. https://doi.org/10.1016/S0016-7037(00)00464-6

Belt, S.T., Massé, G., Allard, W.G., Robert, J.M., Rowland, S.J., 2001. Identification of a C25 highly branched isoprenoid triene in the freshwater diatom Navicula sclesvicensis. Org. Geochem. 32, 1169–1172. https://doi.org/10.1016/S0146-6380(01)00102-4

Belt, S.T., Brown, T.A., Smik, L., Tatarek, A., Wiktor, J., Stowasser, G., Assmy, P., Allen, C.S., Husum, K., 2017. Identification of C25 highly branched isoprenoid (HBI) alkenes in diatoms of the genus Rhizosolenia in polar and sub-polar marine phytoplankton. Org. Geochem. 110, 65–72. https://doi.org/10.1016/j.orggeochem.2017.05.007

Benecke, N., 1994. Archäozoologische Studien zur Entwicklung der Haustierhaltung in Mitteleuropa und Südskandinavien von den Anfängen bis zum ausgehenden Mittelalter. Akademie Verlag, Berlin.

Benovitz, N., 2014. The Justinianic plague: Evidence from the dated Greek epitaphs of Byzantine Palestine and Arabia. J. Rom. Archaeol. 27, 487–498. https://doi.org/10.1017/S1047759414001378

Berke, M.A., Cartagena Sierra, A., Bush, R., Cheah, D., O'Connor, K., 2019. Controls on leaf wax fractionation and δ2H values in tundra vascular plants from western Greenland. Geochim. Cosmochim. Acta 244, 565–583. https://doi.org/10.1016/j.gca.2018.10.020

Berry, S.K., 1981. Fatty acid composition and organoleptic quality of four clones of durian (Durio zibethinus , murr.). J. Am. Oil Chem. Soc. 58, 716–717. https://doi.org/10.1007/BF02899460

Bina, H., Yousefzadeh, H., Ali, S.S., Esmailpour, M., 2016. Phylogenetic relationships, molecular taxonomy, biogeography of Betula, with emphasis on phylogenetic position of Iranian populations. Tree Genet. Genomes 12, 84. https://doi.org/10.1007/s11295-016-1037-4

Bini, M., Zanchetta, G., Perşoiu, A., Cartier, R., Català, A., Cacho, I., Dean, J.R., Di Rita, F., Drysdale, R.N., Finnè, M., Isola, I., Jalali, B., Lirer, F., Magri, D., Masi, A., Marks, L.,

Mercuri, A.M., Peyron, O., Sadori, L., Sicre, M.A., Welc, F., Zielhofer, C., Brisset, E., 2019. The 4.2 ka BP Event in the Mediterranean region: An overview. Clim. Past 15, 555–577. https://doi.org/10.5194/cp-15-555-2019

Bintliff, J.L., 2002. Time, process and catastrophism in the study of Mediterranean alluvial history: A review. World Archaeol. 33, 417–435. https://doi.org/10.1080/00438240120107459

Bintliff, J.L., 2012a. Environmental degradation and the decline of ancient complex societies in the Mediterranean region, in: Bertoncello, F., Braemer, F. (Eds.), Variabilités Environnementales, Mutations Sociales. Nature, Intensités, Échelles et Temporalités Des Changements. XXXIIe Rencontres Internationales d'archéologie et d'histoire d'Antibes. Antibes, pp. 213–220.

Bintliff, J.L., 2012b. The Complete Archaeology of Greece, from Hunter-Gatherers to the Twentieth Century AD. Blackwell-Wiley, Oxford, New York.

Birks, H.J.B., 1968. The Identification of Betula nana Pollen. New Phytol. 67, 309–314. https://doi.org/10.1111/j.1469-8137.1968.tb06386.x

Björck, S., Kromer, B., Johnsen, S., Bennike, O., Hammarlund, D., Lemdahl, G., Possnert, G., Rasmussen, T.L., Wohlfarth, B., Hammer, C.U., Spurk, M., 1996. Synchronized terrestrial atmospheric deglacial records around the North Atlantic. Science. 274, 1155–1160. https://doi.org/10.1126/science.274.5290.1155

Björck, S., Walker, M.J.C., Cwynar, L.C., Johnsen, S., Knudsen, K.-L., Lowe, J.J., Wohlfarth, B., 1998. An event stratigraphy for the Last Termination in the North Atlantic region based on the Greenland ice-core record: a proposal by the INTIMATE group. J. Quat. Sci. 13, 283–292. https://doi.org/10.1002/(SICI)1099-1417(199807/08)13:4<283::AID-JQS386>3.0.CO;2-A

Blaauw, M., Christen, J.A., 2011. Flexible paleoclimate age-depth models using an autoregressive gamma process. Bayesian Anal. 6, 457–474. https://doi.org/10.1214/11-BA618

Blaga, C.I., Reichart, G.J., Heiri, O., Sinninghe Damsté, J.S., 2009. Tetraether membrane lipid distributions in water-column particulate matter and sediments: A study of 47 European lakes along a north-south transect. J. Paleolimnol. 41, 523–540. https://doi.org/10.1007/s10933-008-9242-2

Bligh, E.G., Dyer, W.J., 1959. A Rapid Method of Total Lipid Extraction and Purification. Can. J. Biochem. Physiol. 37, 911–917. https://doi.org/10.1139/o59-099

Bloemsma, M., Croudace, I., Daly, J.S., Francus, P., Galloway, J.M., Gregory, B.R.B., Steven Huang, J.-J., Jones, A.F., Kylander, M., Löwemark, L., Luo, Y., Maclachlan, S., Ohlendorf, C., Patterson, R.T., Pearce, C., Profe, J., Reinhardt, E.G., Stranne, C., Tjallingii, R., Turner, J.N., 2018. Practical guidelines and recent advances in the Itrax

XRF core-scanning procedure. Quat. Int. https://doi.org/10.1016/j.quaint.2018.10.044

Blumer, M., Omenn, G.S., 1961. Fossil porphyrins: uncomplexed chlorins in a triassic sediment. Geochim. Cosmochim. Acta 25, 81–90. https://doi.org/10.1016/0016-7037(61)90124-7

Blumer, M., Guillard, R.R.L., Chase, T., 1971. Hydrocarbons of marine phytoplankton. Mar. Biol. 8, 183–189. https://doi.org/10.1007/BF00355214

Bogaard, A., Fraser, R., Heaton, T.H.E., Wallace, M., Vaiglova, P., Charles, M., Jones, G., Evershed, R.P., Styring, A.K., Andersen, N.H., Arbogast, R.-M., Bartosiewicz, L., Gardeisen, A., Kanstrup, M., Maier, U., Marinova, E., Ninov, L., Schafer, M., Stephan, E., 2013. Crop manuring and intensive land management by Europe's first farmers. Proc. Natl. Acad. Sci. 110, 12589–12594. https://doi.org/10.1073/pnas.1305918110

Bond, G., Broecker, W., Johnsen, S., McManus, J., Labeyrie, L., Jouzel, J., Bonani, G., 1993. Correlations between climate records from North Atlantic sediments and Greenland ice. Nature 365, 143–147. https://doi.org/10.1038/365143a0

Bos, J.A.A., van Geel, B., van der Plicht, J., Bohncke, S.J.P., 2007. Preboreal climate oscillations in Europe: Wiggle-match dating and synthesis of Dutch high-resolution multi-proxy records. Quat. Sci. Rev. 26, 1927–1950. https://doi.org/10.1016/J.QUASCIREV.2006.09.012

Boyd, M., 2015. Speleothems in Warm Climates : Holocene records from the Caribbean and Mediterranean.

Bozan, B., Temelli, F., 2008. Chemical composition and oxidative stability of flax, safflower and poppy seed and seed oils. Bioresour. Technol. 99, 6354–6359. https://doi.org/10.1016/j.biortech.2007.12.009

Bradley, R.S., Wanner, H., Diaz, H.F., 2016. The Medieval Quiet Period. The Holocene 26, 990–993. https://doi.org/10.1177/0959683615622552

Brassell, S.C., Eglinton, G., Marlowe, I.T., Pflaumann, U., Sarnthein, M., 1986. Molecular stratigraphy: a new tool for climatic assessment. Nature 320, 129–133. https://doi.org/10.1038/320129a0

Brauer, A., Endres, C., Günter, C., Litt, T., Stebich, M., Negendank, J.F.W., 1999. High resolution sediment and vegetation responses to Younger Dryas climate change in varved lake sediments from Meerfelder Maar, Germany. Quat. Sci. Rev. 18, 321–329. https://doi.org/10.1016/S0277-3791(98)00084-5

Brauer, A., Litt, T., Negendank, J.F.W., Zolitschka, B., 2001. Lateglacial varve chronology and biostratigraphy of lakes Holzmaar and Meerfelder Maar, Germany. Boreas 30, 83–88. https://doi.org/10.1111/j.1502-3885.2001.tb00991.x

Brauer, A., Haug, G.H., Dulski, P., Sigman, D.M., Negendank, J.F.W., 2008. An abrupt wind shift in western Europe at the onset of the Younger Dryas cold period. Nat. Geosci. 1,

520–523. https://doi.org/10.1038/ngeo263

Broecker, W.S., 2006. Was the Younger Dryas Triggered by a Flood? Science. 312, 1146–1148. https://doi.org/10.1126/science.1123253

Bronk Ramsey, C., 2009. Bayesian Analysis of Radiocarbon Dates. Radiocarbon 51, 337–360.

Brooke, J.L., 2014. Climate Change and the Course of Global History: A Rough Journey. Cambridge University Press, New York.

Brown, A.G., Walsh, K., 2017. Societal stability and environmental change: Examining the archaeology-soil erosion paradox. Geoarchaeology 32, 23–35. https://doi.org/10.1002/gea.21611

Brown, T.A., Belt, S.T., Cabedo-Sanz, P., 2014. Identification of a novel di-unsaturated C25highly branched isoprenoid in the marine tube-dwelling diatom Berkeleya rutilans. Environ. Chem. Lett. 12, 455–460. https://doi.org/10.1007/s10311-014-0472-4

Brozio, J.P., Dörfler, W., Feeser, I., Kirleis, W., Klooß, S., Müller, J., 2014. A Middle Neolithic well from Northern Germany: a precise source to reconstruct water supply management, subsistence economy, and deposition practices. J. Archaeol. Sci. 51, 135–153. https://doi.org/10.1016/j.jas.2013.03.029

Brozio, J.P., 2016. Megalithanlagen und Siedlungsmuster im trichterbecherzeitlichen Ostholstein. Frühe Monumentalitat und soziale Differenzierung. Verlag Dr. Rudolf Habelt, Bonn.

Brozio, J.P., Müller, J., Furholt, M., Kirleis, W., Dreibrodt, S., Feeser, I., Dörfler, W., Weinelt, M., Raese, H., Bock, A., 2019. Monuments and economies: What drove their variability in the middle-Holocene Neolithic? The Holocene 29, 1558–1571. https://doi.org/10.1177/0959683619857227

Brozio, J.P., 2019. Megalithic And Settlement Patterns Of Funnel Beaker Times In Eastern Holstein , Germany. Dr. Rudolf Habelt GmbH, Bonn.

Büntgen, U., Tegel, W., Nicolussi, K., McCormick, M., Frank, D., Trouet, V., Kaplan, J.O., Herzig, F., Heussner, K.U., Wanner, H., Luterbacher, J., Esper, J., 2011. 2500 years of European climate variability and human susceptibility. Science. 331, 578–582. https://doi.org/10.1126/science.1197175

Büntgen, U., Myglan, V.S., Ljungqvist, F.C., McCormick, M., Di Cosmo, N., Sigl, M., Jungclaus, J., Wagner, S., Krusic, P.J., Esper, J., Kaplan, J.O., De Vaan, M.A.C., Luterbacher, J., Wacker, L., Tegel, W., Kirdyanov, A. V., 2016. Cooling and societal change during the Late Antique Little Ice Age from 536 to around 660 AD. Nat. Geosci. 9, 231–236. https://doi.org/10.1038/ngeo2652

Büntgen, U., Myglan, V.S., Ljungqvist, F.C., McCormick, M., Di Cosmo, N., Sigl, M., Jungclaus, J., Wagner, S., Krusic, P.J., Esper, J., Kaplan, J.O., De Vaan, M.A.C.,

Luterbacher, J., Wacker, L., Tegel, W., Solomina, O.N., Nicolussi, K., Oppenheimer, C., Reinig, F., Kirdyanov, A. V., 2017. Reply to “Limited Late Antique cooling.” Nat. Geosci. https://doi.org/10.1038/ngeo2927

Buschhaus, C., Herz, H., Jetter, R., 2007. Chemical Composition of the Epicuticular and Intracuticular Wax Layers on Adaxial Sides of Rosa canina Leaves. Ann. Bot. 100, 1557–1564. https://doi.org/10.1093/aob/mcm255

Bush, R.T., McInerney, F.A., 2013. Leaf wax *n*-alkane distributions in and across modern plants: Implications for paleoecology and chemotaxonomy. Geochim. Cosmochim. Acta 117, 161–179. https://doi.org/10.1016/j.gca.2013.04.016

Busta, L., Hegebarth, D., Kroc, E., Jetter, R., 2017. Changes in cuticular wax coverage and composition on developing Arabidopsis leaves are influenced by wax biosynthesis gene expression levels and trichome density. Planta 245, 297–311. https://doi.org/10.1007/s00425-016-2603-6

Butzer, K.W., 2012. Collapse, environment, and society. Proc. Natl. Acad. Sci. U. S. A. 109, 3632–3639. https://doi.org/10.1073/pnas.1114845109

Campbell, S., 2018. Overview of the Site, Daily Life, and Small Finds, in: Campbell, S. (Ed.), The Cistercian Monastery of Zaraka, Greece. Western Michigan University, p. 259.

Carlson, A.E., Clark, P.U., Haley, B.A., Klinkhammer, G.P., Simmons, K., Brook, E.J., Meissner, K.J., 2007. Geochemical proxies of North American freshwater routing during the Younger Dryas cold event. Proc. Natl. Acad. Sci. U. S. A. 104, 6556–61. https://doi.org/10.1073/pnas.0611313104

Casana, J., 2008. Mediterranean valleys revisited: Linking soil erosion, land use and climate variability in the Northern Levant. Geomorphology 101, 429–442. https://doi.org/10.1016/j.geomorph.2007.04.031

Caseldine, C., 2001. Changes in Betula in the Holocene record from Iceland—a palaeoclimatic record or evidence for early Holocene hybridisation? Rev. Palaeobot. Palynol. 117, 139–152. https://doi.org/10.1016/S0034-6667(01)00082-3

Castañeda, I.S., Mulitza, S., Schefuss, E., Lopes dos Santos, R.A., Sinninghe Damste, J.S., Schouten, S., 2009a. Wet phases in the Sahara/Sahel region and human migration patterns in North Africa. Proc. Natl. Acad. Sci. 106, 20159–20163. https://doi.org/10.1073/pnas.0905771106

Castañeda, I.S., Werne, J.P., Johnson, T.C., Filley, T.R., 2009b. Late Quaternary vegetation history of southeast Africa: The molecular isotopic record from Lake Malawi. Palaeogeogr. Palaeoclimatol. Palaeoecol. 275, 100–112. https://doi.org/10.1016/j.palaeo.2009.02.008

Castañeda, I.S., Schouten, S., 2011. A review of molecular organic proxies for examining modern and ancient lacustrine environments. Quat. Sci. Rev.

https://doi.org/10.1016/j.quascirev.2011.07.009

Castenholz, R.W., 2015. General Characteristics of the Cyanobacteria, in: Bergey's Manual of Systematics of Archaea and Bacteria. John Wiley & Sons, Ltd, Chichester, UK, pp. 1–23. https://doi.org/10.1002/9781118960608.cbm00019

Chapman, J., Gaydarska, B., Nebbia, M., 2019. The Origins of Trypillia Megasites. Front. Digit. Humanit. 6, 1–20. https://doi.org/10.3389/fdigh.2019.00010

Chen, J., An, Z., Head, J., 1999. Variation of Rb/Sr Ratios in the Loess-Paleosol Sequences of Central China during the Last 130,000 Years and Their Implications for Monsoon Paleoclimatology. Quat. Res. 51, 215–219. https://doi.org/10.1006/qres.1999.2038

Chen, J., Chen, Y., Liu, L., Ji, J., Balsam, W., Sun, Y., Lu, H., 2006. Zr/Rb ratio in the Chinese loess sequences and its implication for changes in the East Asian winter monsoon strength. Geochim. Cosmochim. Acta 70, 1471–1482. https://doi.org/10.1016/j.gca.2005.11.029

Chikaraishi, Y., Naraoka, H., 2003. Compound-specific δD–δ13C analyses of n-alkanes extracted from terrestrial and aquatic plants. Phytochemistry 63, 361–371. https://doi.org/10.1016/S0031-9422(02)00749-5

Chu, G., Sun, Q., Li, S., Zheng, M., Jia, X., Lu, C., Liu, J., Liu, T., 2005. Long-chain alkenone distributions and temperature dependence in lacustrine surface sediments from China. Geochim. Cosmochim. Acta 69, 4985–5003. https://doi.org/10.1016/j.gca.2005.04.008

Chu, G., Sun, Q., Wang, X., Liu, M., Lin, Y., Xie, M., Shang, W., Liu, J., 2012. Seasonal temperature variability during the past 1600 years recorded in historical documents and varved lake sediment profiles from northeastern China. Holocene 22, 785–792. https://doi.org/10.1177/0959683611430413

Coates, R.C., Podell, S., Korobeynikov, A., Lapidus, A., Pevzner, P., Sherman, D.H., Allen, E.E., Gerwick, L., Gerwick, W.H., 2014. Characterization of Cyanobacterial Hydrocarbon Composition and Distribution of Biosynthetic Pathways. PLoS One 9, e85140. https://doi.org/10.1371/journal.pone.0085140

Cohen, A.S., 2003. Paleolimnology: the history and evolution of lake systems, 1st ed. Oxford University Press, Oxford.

Colombini, M.P., Modugno, F., 2009. Organic Mass Spectrometry in Art and Archaeology. John Wiley & Sons, Ltd, Chichester, UK. https://doi.org/10.1002/9780470741917

Colonese, A.C., Hendy, J., Lucquin, A., Speller, C.F., Collins, M.J., Carrer, F., Gubler, R., Kühn, M., Fischer, R., Craig, O.E., 2017. New criteria for the molecular identification of cereal grains associated with archaeological artefacts. Sci. Rep. 7, 6633. https://doi.org/10.1038/s41598-017-06390-x

Condron, A., Winsor, P., 2012. Meltwater routing and the Younger Dryas. Proc. Natl. Acad. Sci. 109, 19928–19933. https://doi.org/10.1073/pnas.1207381109

Cooke, M.P., Talbot, H.M., Farrimond, P., 2008. Bacterial populations recorded in bacteriohopanepolyol distributions in soils from Northern England. Org. Geochem. 39, 1347–1358. https://doi.org/10.1016/j.orggeochem.2008.05.003

Copley, M.S., Rose, P.J., Clapham, A., Edwards, D.N., Horton, M.C., Evershed, R.P., 2001. Detection of palm fruit lipids in archaeological pottery from Qasr Ibrim, Egyptian Nubia. Proc. R. Soc. London. Ser. B Biol. Sci. 268, 593–597. https://doi.org/10.1098/rspb.2000.1394

Copley, M.S., Berstan, R., Dudd, S.N., Docherty, G., Mukherjee, A.J., Straker, V., Payne, S., Evershed, R.P., 2003. Direct chemical evidence for widespread dairying in prehistoric Britain. Proc. Natl. Acad. Sci. 100, 1524–1529. https://doi.org/10.1073/pnas.0335955100

Copley, M.S., Berstan, R., Mukherjee, A.J., Dudd, S.N., Straker, V., Payne, S., Evershed, R.P., 2005a. Dairying in antiquity. III. Evidence from absorbed lipid residues dating to the British Neolithic. J. Archaeol. Sci. 32, 523–546. https://doi.org/10.1016/j.jas.2004.08.006

Copley, M.S., Bland, H.A., Rose, P., Horton, M., Evershed, R.P., 2005b. Gas chromatographic, mass spectrometric and stable carbon isotopic investigations of organic residues of plant oils and animal fats employed as illuminants in archaeological lamps from Egypt. Analyst 130, 860. https://doi.org/10.1039/b500403a

Correa-Ascencio, M., Evershed, R.P., 2014. High throughput screening of organic residues in archaeological potsherds using direct acidified methanol extraction. Anal. Methods 6, 1330–1340. https://doi.org/10.1039/c3ay41678j

Craig, O.E., Chapman, J., Heron, C., Willis, L.H., Bartosiewicz, L., Taylor, G., Whittle, A., Collins, M., 2005. Did the first farmers of central and eastern Europe produce dairy foods? Antiquity 79, 882–894. https://doi.org/10.1017/S0003598X00115017

Craig, O.E., Forster, M., Andersen, S.H., Koch, E., Crombe, P., Milner, N.J., Stern, B., Bailey, G.N., Heron, C.P., 2007. Molecular and isotopic demonstration of the processing of aquatic products in northern European prehistoric pottery. Archaeometry 49, 135–152. https://doi.org/10.1111/j.1475-4754.2007.00292.x

Craig, O.E., Steele, V.J., Fischer, A., Hartz, S., Andersen, S.H., Donohoe, P., Glykou, A., Saul, H., Jones, D.M., Koch, E., Heron, C.P., 2011. Ancient lipids reveal continuity in culinary practices across the transition to agriculture in Northern Europe. Proc. Natl. Acad. Sci. 108, 17910–17915. https://doi.org/10.1073/pnas.1107202108

Craig, O.E., Allen, R.B., Thompson, A., Stevens, R.E., Steele, V.J., Heron, C., 2012. Distinguishing wild ruminant lipids by gas chromatography/combustion/isotope ratio mass spectrometry. Rapid Commun. Mass Spectrom. 26, 2359–2364. https://doi.org/10.1002/rcm.6349

Cramp, L., Evershed, R.P., 2014. Reconstructing Aquatic Resource Exploitation in Human Prehistory Using Lipid Biomarkers and Stable Isotopes, in: Treatise on Geochemistry.

Elsevier, pp. 319–339. https://doi.org/10.1016/B978-0-08-095975-7.01225-0

Cramp, L.J.E., Ethier, J., Urem-Kotsou, D., Bonsall, C., Borić, D., Boroneanţ, A., Evershed, R.P., Perić, S., Roffet-Salque, M., Whelton, H.L., Ivanova, M., 2019. Regional diversity in subsistence among early farmers in Southeast Europe revealed by archaeological organic residues. Proc. R. Soc. B Biol. Sci. 286, 20182347. https://doi.org/10.1098/rspb.2018.2347

Crane, P.R., Stockey, R.A., 1987. Betula leaves and reproductive structures from the Middle Eocene of British Columbia, Canada. Can. J. Bot. 65, 2490–2500. https://doi.org/10.1139/b87-338

Cranwell, P.A., 1973. Chain-length distribution of n-alkanes from lake sediments in relation to post-glacial environmental change. Freshw. Biol. 3, 259–265. https://doi.org/10.1111/j.1365-2427.1973.tb00921.x

Cranwell, P.A., Volkman, J.K., 1981. Alkyl and steryl esters in a recent lacustrine sediment. Chem. Geol. 32, 29–43. https://doi.org/10.1016/0009-2541(81)90126-1

Cranwell, P.A., Eglinton, G., Robinson, N., 1987. Lipids of aquatic organisms as potential contributors to lacustrine sediments-II. Org. Geochem. 11, 513–527. https://doi.org/10.1016/0146-6380(87)90007-6

Cruz, F.W., Burns, S.J., Jercinovic, M., Karmann, I., Sharp, W.D., Vuille, M., 2007. Evidence of rainfall variations in Southern Brazil from trace element ratios (Mg/Ca and Sr/Ca) in a Late Pleistocene stalagmite. Geochim. Cosmochim. Acta 71, 2250–2263. https://doi.org/10.1016/j.gca.2007.02.005

Cuven, S., Francus, P., Lamoureux, S.F., 2010. Estimation of grain size variability with micro X-ray fluorescence in laminated lacustrine sediments, Cape Bounty, Canadian High Arctic. J. Paleolimnol. 44, 803–817. https://doi.org/10.1007/s10933-010-9453-1

D'Andrea, W.J., Huang, Y., 2005. Long chain alkenones in Greenland lake sediments: Low δ13C values and exceptional abundance. Org. Geochem. 36, 1234–1241. https://doi.org/10.1016/j.orggeochem.2005.05.001

D'Andrea, W.J., Huang, Y., Fritz, S.C., Anderson, N.J., 2011. Abrupt Holocene climate change as an important factor for human migration in West Greenland. Proc. Natl. Acad. Sci. 108, 9765–9769. https://doi.org/10.1073/pnas.1101708108

Dal Corso, M., Out, W.A., Ohlrau, R., Hofmann, R., Dreibrodt, S., Videiko, M., Müller, J., Kirleis, W., 2018. Where are the cereals? Contribution of phytolith analysis to the study of subsistence economy at the Trypillia site Maidanetske (ca. 3900-3650 BCE), central Ukraine. J. Arid Environ. 157, 137–148. https://doi.org/10.1016/j.jaridenv.2018.06.009

Dang, X., Xue, J., Yang, H., Xie, S., 2016. Environmental impacts on the distribution of microbial tetraether lipids in Chinese lakes with contrasting pH: Implications for lacustrine paleoenvironmental reconstructions. Sci. China Earth Sci. 59, 939–950.

https://doi.org/10.1007/s11430-015-5234-z

Daniels, W.C., Russell, J.M., Giblin, A.E., Welker, J.M., Klein, E.S., Huang, Y., 2017. Hydrogen isotope fractionation in leaf waxes in the Alaskan Arctic tundra. Geochim. Cosmochim. Acta 213, 216–236. https://doi.org/10.1016/j.gca.2017.06.028

Dansgaard, W., White, J.W.C., Johnsen, S.J., 1989. The abrupt termination of the Younger Dryas climate event. Nature 339, 532–534. https://doi.org/10.1038/339532a0

Davies, P., 2008. Snails: Archaeology and Landscape Change. Oxbow Books.

Davison, W., 1993. Iron and manganese in lakes. Earth Sci. Rev. 34, 119–163. https://doi.org/10.1016/0012-8252(93)90029-7

Dawson, L.A., Towers, W., Mayes, R.W., Craig, J., Väisänen, R.K., Waterhouse, E.C., 2004. The use of plant hydrocarbon signatures in characterizing soil organic matter. Geol. Soc. London, Spec. Publ. 232, 269–276. https://doi.org/10.1144/GSL.SP.2004.232.01.24

De Jong, P.C., 1993. An introduction to Betula: Its morphology, evolution, classification and distribution with a survey of recent work. IDS Betula Symp. Int. Dendrol. Soc. Susses, U.K.

De Jonge, C., Hopmans, E.C., Stadnitskaia, A., Rijpstra, W.I.C., Hofland, R., Tegelaar, E., Sinninghe Damsté, J.S., 2013. Identification of novel penta- and hexamethylated branched glycerol dialkyl glycerol tetraethers in peat using HPLC–MS2, GC–MS and GC–SMB-MS. Org. Geochem. 54, 78–82. https://doi.org/10.1016/j.orggeochem.2012.10.004

De Jonge, C., Hopmans, E.C., Zell, C.I., Kim, J.-H., Schouten, S., Sinninghe Damsté, J.S., 2014. Occurrence and abundance of 6-methyl branched glycerol dialkyl glycerol tetraethers in soils: Implications for palaeoclimate reconstruction. Geochim. Cosmochim. Acta 141, 97–112. https://doi.org/10.1016/j.gca.2014.06.013

de Klerk, P., Theuerkauf, M., Joosten, H., 2017. Vegetation, recent pollen deposition, and distribution of some non-pollen palynomorphs in a degrading ice-wedge polygon mire complex near Pokhodsk (NE Siberia), including size-frequency analyses of pollen attributable to Betula. Rev. Palaeobot. Palynol. 238, 122–143. https://doi.org/10.1016/j.revpalbo.2016.11.015

de Leeuw, J.W., v.d. Meer, F.W., Rijpstra, W.I.C., Schenck, P.A., 1980. On the occurrence and structural identification of long chain unsaturated ketones and hydrocarbons in sediments. Phys. Chem. Earth 12, 211–217. https://doi.org/10.1016/0079-1946(79)90105-8

Depciuch, J., Kasprzyk, I., Drzymała, E., Parlinska-Wojtan, M., 2018. Identification of birch pollen species using FTIR spectroscopy. Aerobiologia (Bologna). 34, 525–538. https://doi.org/10.1007/s10453-018-9528-4

di Lernia, S., 2006. Building monuments, creating identity: Cattle cult as a social response to

rapid environmental changes in the Holocene Sahara. Quat. Int. 151, 50–62. https://doi.org/10.1016/j.quaint.2006.01.014

Diefendorf, A.F., Mueller, K.E., Wing, S.L., Koch, P.L., Freeman, K.H., 2010. Global patterns in leaf 13C discrimination and implications for studies of past and future climate. Proc. Natl. Acad. Sci. 107, 5738–5743. https://doi.org/10.1073/pnas.0910513107

Diefendorf, A.F., Freeman, K.H., Wing, S.L., Graham, H. V., 2011. Production of n-alkyl lipids in living plants and implications for the geologic past. Geochim. Cosmochim. Acta 75, 7472–7485. https://doi.org/10.1016/j.gca.2011.09.028

Diefendorf, A.F., Leslie, A.B., Wing, S.L., 2015. Leaf wax composition and carbon isotopes vary among major conifer groups. Geochim. Cosmochim. Acta 170, 145–156. https://doi.org/10.1016/j.gca.2015.08.018

Diefendorf, A.F., Freimuth, E.J., 2017. Extracting the most from terrestrial plant-derived n-alkyl lipids and their carbon isotopes from the sedimentary record: A review. Org. Geochem. 103, 1–21. https://doi.org/10.1016/j.orggeochem.2016.10.016

Dove, H., Mayes, R.W., 2006. Protocol for the analysis of n-alkanes and other plant-wax compounds and for their use as markers for quantifying the nutrient supply of large mammalian herbivores. Nat. Protoc. 1, 1680–1697. https://doi.org/10.1038/nprot.2006.225

Drake, B.L., 2012. The influence of climatic change on the Late Bronze Age Collapse and the Greek Dark Ages. J. Archaeol. Sci. 39, 1862–1870. https://doi.org/10.1016/j.jas.2012.01.029

Dudd, S.N., Evershed, R.P., 1998. Direct Demonstration of Milk as an Element of Archaeological Economies. Science. 282, 1478–1481. https://doi.org/10.1126/science.282.5393.1478

Dulf, F. V., 2012. Fatty acids in berry lipids of six sea buckthorn (Hippophae rhamnoides L., subspecies carpatica) cultivars grown in Romania. Chem. Cent. J. 6, 106. https://doi.org/10.1186/1752-153X-6-106

Dunne, J., Evershed, R.P., Salque, M., Cramp, L., Bruni, S., Ryan, K., Biagetti, S., di Lernia, S., 2012. First dairying in green Saharan Africa in the fifth millennium bc. Nature 486, 390–394. https://doi.org/10.1038/nature11186

Durand, B., 2003. A History of Organic Geochemistry. Oil Gas Sci. Technol. 58, 203–231. https://doi.org/10.2516/ogst:2003014

Dypvik, H., Harris, N.B., 2001. Geochemical facies analysis of fine-grained siliciclastics using Th/U, Zr/Rb and (Zr + Rb)/Sr ratios. Chem. Geol. 181, 131–146. https://doi.org/10.1016/S0009-2541(01)00278-9

Eganhouse, R.P., 1997. Molecular Markers and Environmental Organic Geochemistry: An Overview, in: ACS Symposium Series. pp. 1–20. https://doi.org/10.1021/bk-1997-

0671.ch001

Eglinton, G., Gonzalez, A.G., Hamilton, R.J., Raphael, R.A., 1962. Hydrocarbon constituents of the wax coatings of plant leaves: A taxonomic survey. Phytochemistry 1, 89–102. https://doi.org/10.1016/S0031-9422(00)88006-1

Eglinton, G., Calvin, M., 1967. Chemical Fossils. Sci. Am. 216, 32–43. https://doi.org/10.1038/scientificamerican0167-32

Eglinton, G., Hamilton, R.J., 1967. Leaf Epicuticular Waxes. Science. 156, 1322–1335. https://doi.org/10.1126/science.156.3780.1322

Eley, Y.L., Hren, M.T., 2018. Reconstructing vapor pressure deficit from leaf wax lipid molecular distributions. Sci. Rep. 8, 3967. https://doi.org/10.1038/s41598-018-21959-w

Elkington, T.T., 1968. Introgressive hybridization between Betula nana L. and B. pubescens Ehrh. in North-West Iceland. New Phytol. 67, 109–118. https://doi.org/10.1111/j.1469-8137.1968.tb05459.x

Emmanouilidis, A., Katrantsiotis, C., Norström, E., Risberg, J., Kylander, M., Sheik, T.A., Iliopoulos, G., Avramidis, P., 2018. Middle to late Holocene palaeoenvironmental study of Gialova Lagoon, SW Peloponnese, Greece. Quat. Int. 476, 46–62. https://doi.org/10.1016/j.quaint.2018.03.005

Ertel, J.R., Hedges, J.I., 1985. Sources of sedimentary humic substances: vascular plant debris. Geochim. Cosmochim. Acta 49, 2097–2107. https://doi.org/10.1016/0016-7037(85)90067-5

Eusterhues, K., Lechterbeck, J., Schneider, J., Wolf-Brozio, U., 2002. Late- and Post-Glacial evolution of Lake Steisslingen. Palaeogeogr. Palaeoclimatol. Palaeoecol. 187, 341–371. https://doi.org/10.1016/S0031-0182(02)00486-8

Eusterhues, K., Heinrichs, H., Schneider, J., 2005. Geochemical response on redox fluctuations in Holocene lake sediments, Lake Steisslingen, Southern Germany. Chem. Geol. 222, 1–22. https://doi.org/10.1016/j.chemgeo.2005.06.006

Evershed, R.P., Heron, C., Goad, L.J., 1990. Analysis of organic residues of archaeological origin by high-temperature gas chromatography and gas chromatography-mass spectrometry. Analyst 115, 1339. https://doi.org/10.1039/an9901501339

Evershed, R.P., Heron, C., Goad, L.J., 1991a. Epicuticular wax components preserved in potsherds as chemical indicators of leafy vegetables in ancient diets. Antiquity 65, 540–544. https://doi.org/10.1017/S0003598X00080145

Evershed, R.P., Heron, C., Charters, S., Goad, L.J., 1991b. The Survival of Food Residues: New Methods of Analysis, Interpretation and Application. Proc. Br. Acad. Br. Acad. 77, 187–208.

Evershed, R.P., 1993. Biomolecular archaeology and lipids. World Archaeol. 25, 74–93. https://doi.org/10.1080/00438243.1993.9980229

Evershed, R.P., Stott, A.W., Raven, A., Dudd, S.N., Charters, S., Leyden, A., 1995. Formation of long-chain ketones in ancient pottery vessels by pyrolysis of acyl lipids. Tetrahedron Lett. 36, 8875–8878. https://doi.org/10.1016/0040-4039(95)01844-8

Evershed, R.P., Dudd, S.N., Copley, M.S., Berstan, R., Stott, A.W., Mottram, H., Buckley, S.A., Crossman, Z., 2002. Chemistry of Archaeological Animal Fats. Acc. Chem. Res. 35, 660–668. https://doi.org/10.1021/ar000200f

Evershed, R.P., 2008. Organic Residue Analysis in Archaeology: The Archaeological Biomarker Revolution. Archaeometry 50, 895–924. https://doi.org/10.1111/j.1475-4754.2008.00446.x

Evershed, R.P., Copley, M.S., Dickson, L., Hansel, F.A., 2008a. Experimental evidence for the processing of marine animal products in pottery vessels. Archaeometry 50, 101–113. https://doi.org/10.1111/j.1475-4754.2007.00368.x

Evershed, R.P., Payne, S., Sherratt, A.G., Copley, M.S., Coolidge, J., Urem-Kotsu, D., Kotsakis, K., Özdoğan, M., Özdoğan, A.E., Nieuwenhuyse, O., Akkermans, P.M.M.G., Bailey, D., Andeescu, R.R., Campbell, S., Farid, S., Hodder, I., Yalman, N., Özbaşaran, M., Biçakci, E., Garfinkel, Y., Levy, T., Burton, M.M., 2008b. Earliest date for milk use in the Near East and southeastern Europe linked to cattle herding. Nature 455, 528–531. https://doi.org/10.1038/nature07180

Fairbanks, R.G., 1990. The age and origin of the “Younger Dryas climate event” in Greenland ice cores. Paleoceanography 5, 937–948. https://doi.org/10.1029/PA005i006p00937

Farrimond, P., Flanagan, R.L., 1996. Lipid stratigraphy of a Flandrian peat bed (Northumberland, UK): comparison with the pollen record. The Holocene 6, 69–74. https://doi.org/10.1177/095968369600600108

Fatima, T., Snyder, C.L., Schroeder, W.R., Cram, D., Datla, R., Wishart, D., Weselake, R.J., Krishna, P., 2012. Fatty Acid Composition of Developing Sea Buckthorn (Hippophae rhamnoides L.) Berry and the Transcriptome of the Mature Seed. PLoS One 7, e34099. https://doi.org/10.1371/journal.pone.0034099

Ficken, K.., Li, B., Swain, D.., Eglinton, G., 2000. An n-alkane proxy for the sedimentary input of submerged/floating freshwater aquatic macrophytes. Org. Geochem. 31, 745–749. https://doi.org/10.1016/S0146-6380(00)00081-4

Ficken, K.J., Barber, K.E., Eglinton, G., 1998. Lipid biomarker, δ13C and plant macrofossil stratigraphy of a Scottish montane peat bog over the last two millennia. Org. Geochem. 28, 217–237. https://doi.org/10.1016/S0146-6380(97)00126-5

Filipović, D., Brozio, J.P., Ditchfield, P., Klooß, S., Müller, J., Kirleis, W., 2019. Middle-Neolithic agricultural practices in the Oldenburger Graben wetlands, northern Germany: First results of the analysis of arable weeds and stable isotopes. The Holocene 29, 1587–1595. https://doi.org/10.1177/0959683619857224

Filzmoser, P., Hron, K., Reimann, C., 2009. Principal components analysis for compositional data with outliers. Environmetrics 20, 621–632. https://doi.org/10.1002/env.966

Finné, M., Holmgren, K., Sundqvist, H.S., Weiberg, E., Lindblom, M., 2011. Climate in the eastern Mediterranean, and adjacent regions, during the past 6000 years – A review. J. Archaeol. Sci. 38, 3153–3173. https://doi.org/10.1016/j.jas.2011.05.007

Finné, M., Bar-Matthews, M., Holmgren, K., Sundqvist, H.S., Liakopoulos, I., Zhang, Q., 2014. Speleothem evidence for late Holocene climate variability and floods in Southern Greece. Quat. Res. 81, 213–227. https://doi.org/10.1016/j.yqres.2013.12.009

Finné, M., Holmgren, K., Shen, C.-C., Hu, H.-M., Boyd, M., Stocker, S., 2017. Late Bronze Age climate change and the destruction of the Mycenaean Palace of Nestor at Pylos. PLoS One 12, e0189447. https://doi.org/10.1371/journal.pone.0189447

Firestone, R.B., West, A., Kennett, J.P., Becker, L., Bunch, T.E., Revay, Z.S., Schultz, P.H., Belgya, T., Kennett, D.J., Erlandson, J.M., Dickenson, O.J., Goodyear, A.C., Harris, R.S., Howard, G.A., Kloosterman, J.B., Lechler, P., Mayewski, P.A., Montgomery, J., Poreda, R., Darrah, T., Hee, S.S.Q., Smith, A.R., Stich, A., Topping, W., Wittke, J.H., Wolbach, W.S., 2007. Evidence for an extraterrestrial impact 12,900 years ago that contributed to the megafaunal extinctions and the Younger Dryas cooling. Proc. Natl. Acad. Sci. U. S. A. 104, 16016–21. https://doi.org/10.1073/pnas.0706977104

Fischer, A., Olsen, J., Richards, M., Heinemeier, J., Sveinbjörnsdóttir, Á.E., Bennike, P., 2007. Coast–inland mobility and diet in the Danish Mesolithic and Neolithic: evidence from stable isotope values of humans and dogs. J. Archaeol. Sci. 34, 2125–2150. https://doi.org/10.1016/j.jas.2007.02.028

Fleitmann, D., Cheng, H., Badertscher, S., Edwards, R.L., Mudelsee, M., Göktürk, O.M., Fankhauser, A., Pickering, R., Raible, C.C., Matter, A., Kramers, J., Tüysüz, O., 2009. Timing and climatic impact of Greenland interstadials recorded in stalagmites from northern Turkey. Geophys. Res. Lett. 36, L19707. https://doi.org/10.1029/2009GL040050

Francke, A., Wagner, B., Leng, M.J., Rethemeyer, J., 2013. A Late Glacial to Holocene record of environmental change from Lake Dojran (Macedonia, Greece). Clim. Past 9, 481–498. https://doi.org/10.5194/cp-9-481-2013

Franich, R.A., Goodin, S.J., Volkman, J.K., 1985. Alkyl esters from pinus radiata foliage epicuticular wax. Phytochemistry 24, 2949–2952. https://doi.org/10.1016/0031-9422(85)80033-9

Freund, H., Birks, H.H., Birks, H.J.B., 2001. The identification of wingless Betula fruits in Weichselian sediments in the Gross Todtshorn borehole (Lower Saxony, Germany) – the occurrence of Betula humilis Schrank. Veg. Hist. Archaeobot. 10, 107–115. https://doi.org/10.1007/PL00006919

Friedli, H., Lötscher, H., Oeschger, H., Siegenthaler, U., Stauffer, B., 1986. Ice core record of the 13C/12C ratio of atmospheric CO2 in the past two centuries. Nature 324, 237–238. https://doi.org/10.1038/324237a0

Fuchs, M., Lang, A., Wagner, G.A., 2004. The history of Holocene soil erosion in the Phlious Basin, NE Peloponnese, Greece, based on optical dating. The Holocene 14, 334–345. https://doi.org/10.1191/0959683604hl710rp

Fuchs, M., 2007. An assessment of human versus climatic impacts on Holocene soil erosion in NE Peloponnese, Greece. Quat. Res. 67, 349–356. https://doi.org/10.1016/j.yqres.2006.11.008

Furholt, Martin, Müller, Johannes, 2011. The earliest monuments in Europe e architecture and social structures (5000-3000 cal BC), in: Furholt, M., Lüth, F., Müller, J. (Eds.), Megaliths and Identities. Early Monuments and Neolithic Societies from the Atlantic to the Baltic. Habelt, Bonn, pp. 15–32.

Furlow, J.J., 1990. The genera of Betulaceae in the southeastern United States. J. Arnold Arboretum. 71, 1–67. https://doi.org/10.5962/bhl.part.24925

Gambacorta, A., Pagnotta, E., Romano, I., Sodano, G., Trincone, A., 1998. Heterocyst glycolipids from nitrogen-fixing cyanobacteria other than nostocaceae. Phytochemistry 48, 801–805. https://doi.org/10.1016/S0031-9422(97)00954-0

Gambacorta, A., Trincone, A., Soriente, A., Sodano, G., 1999. Chemistry of glycolipids from the heterocysts of nitrogen-fixing cyanobacteria. Curr. Top. Phytochem. 2, 145–150.

Gelpi, E., Schneider, H., Mann, J., Oró, J., 1970. Hydrocarbons of geochemical significance in microscopic algae. Phytochemistry 9, 603–612. https://doi.org/10.1016/S0031-9422(00)85700-3

Giger, W., Schaffner, C., Wakeham, S.G., 1980. Aliphatic and olefinic hydrocarbons in recent sediments of Greifensee, Switzerland. Geochim. Cosmochim. Acta 44, 119–129. https://doi.org/10.1016/0016-7037(80)90182-9

Gogou, A., Triantaphyllou, M., Xoplaki, E., Izdebski, A., Parinos, C., Dimiza, M., Bouloubassi, I., Luterbacher, J., Kouli, K., Martrat, B., Toreti, A., Fleitmann, D., Rousakis, G., Kaberi, H., Athanasiou, M., Lykousis, V., 2016. Climate variability and socio-environmental changes in the northern Aegean (NE Mediterranean) during the last 1500 years. Quat. Sci. Rev. 136, 209–228. https://doi.org/10.1016/j.quascirev.2016.01.009

Göktürk, O.M., Fleitmann, D., Badertscher, S., Cheng, H., Edwards, R.L., Leuenberger, M., Fankhauser, A., Tüysüz, O., Kramers, J., 2011. Climate on the southern Black Sea coast during the Holocene: Implications from the Sofular Cave record. Quat. Sci. Rev. 30, 2433–2445. https://doi.org/10.1016/j.quascirev.2011.05.007

Goñi, M.A., Hartz, D.M., Thunell, R.C., Tappa, E., 2001. Oceanographic considerations for the application of the alkenone-based paleotemperature U37K′ index in the Gulf of California.

Geochim. Cosmochim. Acta 65, 545–557. https://doi.org/10.1016/S0016-7037(00)00559-7

Goslar, T., Arnold, M., Bard, E., Kuc, T., Pazdur, M.F., Ralska-Jasiewiczowa, M., Różanski, K., Tisnerat, N., Walanus, A., Wicik, B., Więqkowski, K., 1995. High concentration of atmospheric 14C during the Younger Dryas cold episode. Nature 377, 414–417. https://doi.org/10.1038/377414a0

Grachev, A.M., Severinghaus, J.P., 2005. A revised +10±4°C magnitude of the abrupt change in Greenland temperature at the Younger Dryas termination using published GISP2 gas isotope data and air thermal diffusion constants. Quat. Sci. Rev. 24, 513–519. https://doi.org/10.1016/J.QUASCIREV.2004.10.016

Gregg, M.W., Banning, E.B., Gibbs, K., Slater, G.F., 2009. Subsistence practices and pottery use in Neolithic Jordan: molecular and isotopic evidence. J. Archaeol. Sci. 36, 937–946. https://doi.org/10.1016/j.jas.2008.09.009

Grootes, P.M., Nadeau, M.J., Rieck, A., 2004. ^{14}C-AMS at the Leibniz-Labor: Radiometric dating and isotope research, in: Nuclear Instruments and Methods in Physics Research, Section B: Beam Interactions with Materials and Atoms. North-Holland, pp. 55–61. https://doi.org/10.1016/j.nimb.2004.04.015

Guasch-Jané, M.R., Andrés-Lacueva, C., Jáuregui, O., Lamuela-Raventós, R.M., 2006. First evidence of white wine in ancient Egypt from Tutankhamun's tomb. J. Archaeol. Sci. 33, 1075–1080. https://doi.org/10.1016/j.jas.2005.11.012

Gulliksen, S., Birks, H.H., Possnert, G., Mangerud, J., 1998. A calendar age estimate of the Younger Dryas-Holocene boundary at Kråkenes, western Norway. The Holocene 8, 249–259. https://doi.org/10.1191/095968398672301347

Gülz, P.-G., 1994. Epicuticular Leaf Waxes in the Evolution of the Plant Kingdom. J. Plant Physiol. 143, 453–464. https://doi.org/10.1016/S0176-1617(11)81807-9

Guo, Y., Li, J.J., Busta, L., Jetter, R., 2018. Coverage and composition of cuticular waxes on the fronds of the temperate ferns Pteridium aquilinum, Cryptogramma crispa, Polypodium glycyrrhiza, Polystichum munitum and Gymnocarpium dryopteris. Ann. Bot. 122, 555–568. https://doi.org/10.1093/aob/mcy078

Haldon, J., Mordechai, L., Newfield, T.P., Chase, A.F., Izdebski, A., Guzowski, P., Labuhn, I., Roberts, N., 2018. History meets palaeoscience: Consilience and collaboration in studying past societal responses to environmental change. Proc. Natl. Acad. Sci. U. S. A. https://doi.org/10.1073/pnas.1716912115

Hammann, S., Cramp, L.J.E., 2018. Towards the detection of dietary cereal processing through absorbed lipid biomarkers in archaeological pottery. J. Archaeol. Sci. 93, 74–81. https://doi.org/10.1016/j.jas.2018.02.017

Hammann, S., Cramp, L.J.E., Whittle, M., Evershed, R.P., 2018. Cholesterol degradation in

archaeological pottery mediated by fired clay and fatty acid pro-oxidants. Tetrahedron Lett. 59, 4401–4404. https://doi.org/10.1016/j.tetlet.2018.10.071

Hammer, Ø., Harper, D.A.T., Ryan, P.D., 2001. Past: Paleontological statistics software package for education and data analysis. Palaeontol. Electron. 4.

Hammer, S., Levin, I., 2017. Monthly mean atmospheric D14CO2 at Jungfraujoch and Schauinsland from 1986 to 2016, heiDATA. https://doi.org/10.11588/data/10100

Hammond, M.D., 2015. Late Roman Ceramics from the Panayia Field, Corinth. University of Missouri.

Han, J., Calvin, M., 1969. Hydrocarbon Distribution of Algae and Bacteria, and Microbiological Activity in Sediments. Proc. Natl. Acad. Sci. 64, 436–443. https://doi.org/10.1073/pnas.64.2.436

Hansel, F.A., Copley, M.S., Madureira, L.A.S., Evershed, R.P., 2004. Thermally produced ω-(o-alkylphenyl)alkanoic acids provide evidence for the processing of marine products in archaeological pottery vessels. Tetrahedron Lett. 45, 2999–3002. https://doi.org/10.1016/j.tetlet.2004.01.111

Hansel, F.A., Bull, I.D., Evershed, R.P., 2011. Gas chromatographic mass spectrometric detection of dihydroxy fatty acids preserved in the 'bound' phase of organic residues of archaeological pottery vessels. Rapid Commun. Mass Spectrom. 25, 1893–1898. https://doi.org/10.1002/rcm.5038

He, D., Simoneit, B.R.T., Xu, Y., Jaffé, R., 2016. Occurrence of unsaturated C25highly branched isoprenoids (HBIs) in a freshwater wetland. Org. Geochem. 93, 59–67. https://doi.org/10.1016/j.orggeochem.2016.01.006

Heiri, O., Cremer, H., Engels, S., Hoek, W.Z., Peeters, W., Lotter, A.F., 2007. Lateglacial summer temperatures in the Northwest European lowlands: a chironomid record from Hijkermeer, the Netherlands. Quat. Sci. Rev. 26, 2420–2437. https://doi.org/10.1016/j.quascirev.2007.06.017

Helama, S., Jones, P.D., Briffa, K.R., 2017a. Dark Ages Cold Period: A literature review and directions for future research. The Holocene 16, 095968361769389. https://doi.org/10.1177/0959683617693898

Helama, S., Jones, P.D., Briffa, K.R., 2017b. Limited Late Antique cooling. Nat. Geosci. https://doi.org/10.1038/ngeo2926

Herbin, G.A., Robins, P.A., 1969. Patterns of variation and development in leaf wax alkanes. Phytochemistry 8, 1985–1998. https://doi.org/10.1016/S0031-9422(00)88085-1

Heron, C., Evershed, R.P., Goad, L.J., 1991. Effects of migration of soil lipids on organic residues associated with buried potsherds. J. Archaeol. Sci. 18, 641–659. https://doi.org/10.1016/0305-4403(91)90027-M

Heron, C., Nemcek, N., Bonfield, K.M., Dixon, D., Ottaway, B.S., 1994. The chemistry of

neolithic beeswax. Naturwissenschaften 81, 266–269. https://doi.org/10.1007/BF01131579

Heron, C., Craig, O.E., Luquin, A., Steele, V.J., Thompson, A., Piličiauskas, G., 2015. Cooking fish and drinking milk? Patterns in pottery use in the southeastern Baltic, 3300–2400 cal BC. J. Archaeol. Sci. 63, 33–43. https://doi.org/10.1016/j.jas.2015.08.002

Heymann, C., Nelle, O., Dörfler, W., Zagana, H., Nowaczyk, N., Xue, J., Unkel, I., 2013. Late Glacial to mid-Holocene palaeoclimate development of Southern Greece inferred from the sediment sequence of Lake Stymphalia (NE-Peloponnese). Quat. Int. 302, 42–60. https://doi.org/10.1016/j.quaint.2013.02.014

Ho, L.-H., Bhat, R., 2015. Exploring the potential nutraceutical values of durian (Durio zibethinus L.) – An exotic tropical fruit. Food Chem. 168, 80–89. https://doi.org/10.1016/j.foodchem.2014.07.020

Hodell, D.A., Channeil, J.E.T., Curtis, J.H., Romero, O.E., Röhl, U., 2008. Onset of “Hudson Strait” Heinrich events in the eastern North Atlantic at the end of the middle Pleistocene transition (~640 ka)? Paleoceanography 23. https://doi.org/10.1029/2008PA001591

Hoekman-Sites, H.A., Giblin, J.I., 2012. Prehistoric animal use on the Great Hungarian Plain: A synthesis of isotope and residue analyses from the Neolithic and Copper Age. J. Anthropol. Archaeol. 31, 515–527. https://doi.org/10.1016/j.jaa.2012.05.002

Hoffmann, B., Kahmen, A., Cernusak, L.A., Arndt, S.K., Sachse, D., 2013. Abundance and distribution of leaf wax n-alkanes in leaves of Acacia and Eucalyptus trees along a strong humidity gradient in northern Australia. Org. Geochem. 62, 62–67. https://doi.org/10.1016/j.orggeochem.2013.07.003

Hofmann, R., Müller, J., Shatilo, L., Videiko, M., Ohlrau, R., Rud, V., Burdo, N., Dal Corso, M., Dreibrodt, S., Kirleis, W., 2019. Governing Tripolye: Integrative architecture in Tripolye settlements. PLoS One 14, e0222243. https://doi.org/10.1371/journal.pone.0222243

Honch, N. V., Higham, T.F.G., Chapman, J., Gaydarska, B., Hedges, R.E.M., 2006. A palaeodietary investigation of carbon (13C/12C) and nitrogen (15N/14N) in human and faunal bones from the Copper Age cemeteries of Varna I and Durankulak, Bulgaria. J. Archaeol. Sci. 33, 1493–1504. https://doi.org/10.1016/j.jas.2006.02.002

Hopmans, E.C., Weijers, J.W.., Schefuß, E., Herfort, L., Sinninghe Damsté, J.S., Schouten, S., 2004. A novel proxy for terrestrial organic matter in sediments based on branched and isoprenoid tetraether lipids. Earth Planet. Sci. Lett. 224, 107–116. https://doi.org/10.1016/j.epsl.2004.05.012

Hopmans, E.C., Schouten, S., Sinninghe Damsté, J.S., 2016. The effect of improved chromatography on GDGT-based palaeoproxies. Org. Geochem. 93, 1–6. https://doi.org/10.1016/j.orggeochem.2015.12.006

Hou, L., Liu, Y., Wei, A., 2019. Geographical variations in the fatty acids of Zanthoxylum seed

oils: A chemometric classification based on the random forest algorithm. Ind. Crops Prod. 134, 146–153. https://doi.org/10.1016/j.indcrop.2019.03.070

Huang, Y., Lockheart, M.J., Collister, J.W., Eglinton, G., 1995. Molecular and isotopic biogeochemistry of the Miocene Clarkia Formation: hydrocarbons and alcohols. Org. Geochem. 23, 785–801. https://doi.org/10.1016/0146-6380(95)80001-8

Huang, Y., Eglinton, G., Ineson, P., Bol, R., Harkness, D.D., 1999. The effects of nitrogen fertilisation and elevated CO2 on the lipid biosynthesis and carbon isotopic discrimination in birch seedlings (Betula pendula). Plant Soil 216, 35–45. https://doi.org/10.1023/A:1004771431093

Isaksson, S., Karlsson, C., Eriksson, T., 2010. Ergosterol (5, 7, 22-ergostatrien-3β-ol) as a potential biomarker for alcohol fermentation in lipid residues from prehistoric pottery. J. Archaeol. Sci. 37, 3263–3268. https://doi.org/10.1016/j.jas.2010.07.027

Isaksson, S., Hallgren, F., 2012. Lipid residue analyses of Early Neolithic funnel-beaker pottery from Skogsmossen, eastern Central Sweden, and the earliest evidence of dairying in Sweden. J. Archaeol. Sci. 39, 3600–3609. https://doi.org/10.1016/j.jas.2012.06.018

Isarin, R.F.B., Bohncke, S.J.P., 1999. Mean July Temperatures during the Younger Dryas in Northwestern and Central Europe as Inferred from Climate Indicator Plant Species. Quat. Res. 51, 158–173. https://doi.org/10.1006/qres.1998.2023

Izdebski, A., Pickett, J., Roberts, N., Waliszewski, T., 2016. The environmental, archaeological and historical evidence for regional climatic changes and their societal impacts in the Eastern Mediterranean in Late Antiquity. Quat. Sci. Rev. 136, 189–208. https://doi.org/10.1016/j.quascirev.2015.07.022

Jacob, J., Disnar, J.-R., Boussafir, M., Spadano Albuquerque, A.L., Sifeddine, A., Turcq, B., 2005. Pentacyclic triterpene methyl ethers in recent lacustrine sediments (Lagoa do Caçó, Brazil). Org. Geochem. 36, 449–461. https://doi.org/10.1016/j.orggeochem.2004.09.005

Jahns, S., 1993. On the Holocene vegetation history of the Argive Plain (Peloponnese, southern Greece). Veg. Hist. Archaeobot. 2, 187–203. https://doi.org/10.1007/BF00198161

Jahns, S., 2000. Late-glacial and Holocene woodland dynamics and land-use history of the Lower Oder valley, north-eastern Germany, based on two, AMS14C-dated, pollen profiles. Veg. Hist. Archaeobot. 9, 111–123. https://doi.org/10.1007/BF01300061

Jansen, B., Nierop, K.G.J., Hageman, J.A., Cleef, A.M., Verstraten, J.M., 2006. The straight-chain lipid biomarker composition of plant species responsible for the dominant biomass production along two altitudinal transects in the Ecuadorian Andes. Org. Geochem. 37, 1514–1536. https://doi.org/10.1016/j.orggeochem.2006.06.018

Jansen, B., de Boer, E.J., Cleef, A.M., Hooghiemstra, H., Moscol-Olivera, M., Tonneijck, F.H., Verstraten, J.M., 2013. Reconstruction of late Holocene forest dynamics in northern Ecuador from biomarkers and pollen in soil cores. Palaeogeogr. Palaeoclimatol. Palaeoecol. 386, 607–619. https://doi.org/10.1016/j.palaeo.2013.06.027

Jansen, B., Wiesenberg, G.L.B., 2017. Opportunities and limitations related to the application of plant-derived lipid molecular proxies in soil science. SOIL 3, 211–234. https://doi.org/10.5194/soil-3-211-2017

Järvinen, P., Palme, A., Orlando Morales, L., Lannenpaa, M., Keinanen, M., Sopanen, T., Lascoux, M., 2004. Phylogenetic relationships of Betula species (Betulaceae) based on nuclear ADH and chloroplast matK sequences. Am. J. Bot. 91, 1834–1845. https://doi.org/10.3732/ajb.91.11.1834

Jenks, M.A., Joly, R.J., Peters, P.J., Rich, P.J., Axtell, J.D., Ashworth, E.N., 1994. Chemically Induced Cuticle Mutation Affecting Epidermal Conductance to Water Vapor and Disease Susceptibility in Sorghum bicolor (L.) Moench. Plant Physiol. 105, 1239–1245. https://doi.org/10.1104/pp.105.4.1239

Jetter, R., Kunst, L., 2008. Plant surface lipid biosynthetic pathways and their utility for metabolic engineering of waxes and hydrocarbon biofuels. Plant J. 54, 670–683. https://doi.org/10.1111/j.1365-313X.2008.03467.x

Jin, Z., Wang, S., Shen, J., Zhang, E., Li, F., Ji, J., Lu, X., 2001. Chemical weathering since the little ice age recorded in lake sediments: A high-resolution proxy of past climate. Earth Surf. Process. Landforms 26, 775–782. https://doi.org/10.1002/esp.224

Jin, Z., Cao, J., Wu, J., Wang, S., 2006. A Rb/Sr record of catchment weathering response to Holocene climate change in Inner Mongolia. Earth Surf. Process. Landforms 31, 285–291. https://doi.org/10.1002/esp.1243

Johannsen, N., Laursen, S., 2010. Routes and Wheeled Transport in Late 4th–Early 3rd Millennium Funerary Customs of the Jutland Peninsula: Regional Evidence and European Context. Praehist. Zeitschrift 85, 135–153. https://doi.org/10.1515/pz.2010.004

Johnsen, S.J., Clausen, H.B., Dansgaard, W., Fuhrer, K., Gundestrup, N., Hammer, C.U., Iversen, P., Jouzel, J., Stauffer, B., Steffensen, J.P., 1992. Irregular glacial interstadials recorded in a new Greenland ice core. Nature 359, 311–313. https://doi.org/10.1038/359311a0

Johnsen, S.J., Dahl-Jensen, D., Gundestrup, N., Steffensen, J.P., Clausen, H.B., Miller, H., Masson-Delmotte, V., Sveinbjörnsdottir, A.E., White, J., 2001. Oxygen isotope and palaeotemperature records from six Greenland ice-core stations: Camp Century, Dye-3, GRIP, GISP2, Renland and NorthGRIP. J. Quat. Sci. 16, 299–307. https://doi.org/10.1002/jqs.622

Julkunen-Tiitto, R., Rousi, M., Bryant, J., Sorsa, S., Keinänen, M., Sikanen, H., 1996. Chemical diversity of several Betulaceae species: comparison of phenolics and terpenoids in northern birch stems. Trees 11, 16. https://doi.org/10.1007/s004680050053

Kaniewski, D., Van Campo, E., Guiot, J., Le Burel, S., Otto, T., Baeteman, C., 2013. Environmental Roots of the Late Bronze Age Crisis. PLoS One 8, e71004. https://doi.org/10.1371/journal.pone.0071004

Karlsdóttir, L., Thórsson, Æ.T., Hallsdóttir, M., Sigurgeirsson, A., Eysteinsson, T., Anamthawat-Jónsson, K., 2007. Differentiating pollen of Betula species from Iceland. Grana 46, 78–84. https://doi.org/10.1080/00173130701237832

Katrantsiotis, C., Norström, E., Holmgren, K., Risberg, J., Skelton, A., 2016. High-resolution environmental reconstruction in SW Peloponnese, Greece, covering the last c. 6000 years: Evidence from Agios Floros fen, Messenian plain. The Holocene 26, 188–204. https://doi.org/10.1177/0959683615596838

Katrantsiotis, C., Kylander, M.E., Smittenberg, R., Yamoah, K.K.A., Hättestrand, M., Avramidis, P., Strandberg, N.A., Norström, E., 2018. Eastern Mediterranean hydroclimate reconstruction over the last 3600 years based on sedimentary n-alkanes, their carbon and hydrogen isotope composition and XRF data from the Gialova Lagoon, SW Greece. Quat. Sci. Rev. 194, 77–93. https://doi.org/10.1016/j.quascirev.2018.07.008

Katrantsiotis, C., Norström, E., Smittenberg, R.H., Finne, M., Weiberg, E., Hättestrand, M., Avramidis, P., Wastegård, S., 2019. Climate changes in the Eastern Mediterranean over the last 5000 years and their links to the high-latitude atmospheric patterns and Asian monsoons. Glob. Planet. Change 175, 36–51. https://doi.org/10.1016/j.gloplacha.2019.02.001

Keinänen, M., Julkunen-Tiitto, R., Rousi, M., Tahvanainen, J., 1999. Taxonomic implications of phenolic variation in leaves of birch (Betula L.) species. Biochem. Syst. Ecol. 27, 243–254. https://doi.org/10.1016/S0305-1978(98)00086-6

Keinänen, M., Käkelä, R., Ritvanen, T., Myllylä, T., Pönni, J., Vuorinen, P.J., 2017. Fatty acid composition of sprat (Sprattus sprattus) and herring (Clupea harengus) in the Baltic Sea as potential prey for salmon (Salmo salar). Helgol. Mar. Res. 71, 4. https://doi.org/10.1186/s10152-017-0484-0

Kiel, M., 1987. Population growth and food production in 16th century Athens and Attica according to the Ottoman Tahrir Defters, in: Bacque-Grammont, J.-L., van Donzel, E. (Eds.), Proceedings of the VIth Cambridge CIEPO Symposium. The Divit Press, Istanbul-Paris-Leiden, pp. 115–133.

Kiel, M., 1997. The rise and decline of Turkish Boeotia, 15th-19th century, in: Bintliff, J.L. (Ed.), Recent Developments in the History and Archaeology of Central Greece. Tempus Reparatum, Oxford, pp. 315–358.

Killops, S., Killops, V., 2005. Introduction to Organic Geochemistry. Blackwell Publishing Ltd., Malden, MA USA. https://doi.org/10.1002/9781118697214

Kim, J.-H., Rimbu, N., Lorenz, S.J., Lohmann, G., Nam, S.-I., Schouten, S., Rühlemann, C., Schneider, R.R., 2004. North Pacific and North Atlantic sea-surface temperature variability during the Holocene. Quat. Sci. Rev. 23, 2141–2154. https://doi.org/10.1016/j.quascirev.2004.08.010

Kimble, B.J., Maxwell, J.R., Philp, R.P., Eglinton, G., 1974. Identification of steranes and tritepanes in geolipid extracts by high-resolution gas chromatography and mass spectrometry. Chem. Geol. 14, 173–198. https://doi.org/10.1016/0009-2541(74)90127-2

Kirkels, F.M.S.A., Jansen, B., Kalbitz, K., 2013. Consistency of plant-specific n- alkane patterns in plaggen ecosystems: A review. The Holocene 23, 1355–1368. https://doi.org/10.1177/0959683613486943

Kirleis, W., Klooß, S., Kroll, H., Müller, J., 2012. Crop growing and gathering in the northern German Neolithic: a review supplemented by new results. Veg. Hist. Archaeobot. 21, 221–242. https://doi.org/10.1007/s00334-011-0328-9

Kirleis, W., Klooß, S., 2014. More than simply fallback food? Social context of plant use in the northern German Neolithic., in: Plants and People. Choices and Diversity through Time. Early Agricultural Remnants and Technical Heritage 1. pp. 428–438.

Kirleis, W., Dal Corso, M., 2016. Trypillian Subsistence Economy: Animal and Plant Exploitation, in: Müller, J., Rassmann, K., Videiko, M. (Eds.), Trypillia Mega-Sites and European Prehistory: 4100-3400 BCE. London, pp. 195–206.

Knapp, A.B., Manning, S.W., 2016. Crisis in Context: The End of the Late Bronze Age in the Eastern Mediterranean. Am. J. Archaeol. 120, 99. https://doi.org/10.3764/aja.120.1.0099

Knauss, J., 1990. Der Graben des Herakles im Becken von Pheneos und die Vertreibung der stymphalischen Vögel 105.

Koch, K., Ensikat, H.-J., 2008. The hydrophobic coatings of plant surfaces: Epicuticular wax crystals and their morphologies, crystallinity and molecular self-assembly. Micron 39, 759–772. https://doi.org/10.1016/j.micron.2007.11.010

Koinig, K.A., Shotyk, W., Lotter, A.F., Ohlendorf, C., Sturm, M., 2003. 9000 years of geochemical evolution of lithogenic major and trace elements in the sediment of an alpine lake – the role of climate, vegetation, and land- use history. J. Paleolimnol. 30, 307–320. https://doi.org/10.1023/A:1026080712312

Kolodziej, B., 2011. Pochówki zwierzęce w neolicie na terenie ziem Polski". Mater. i Spraw. 32, 55–106.

Kontopoulos, N., Avramidis, P., 2003. A late Holocene record of environmental changes from the Aliki lagoon, Egion, North Peloponnesus, Greece. Quat. Int. 111, 75–90. https://doi.org/10.1016/S1040-6182(03)00016-8

Kotthoff, U., Müller, U.C., Pross, J., Schmiedl, G., Lawson, I.T., van de Schootbrugge, B., Schulz, H., 2008. Lateglacial and Holocene vegetation dynamics in the Aegean region: an integrated view based on pollen data from marine and terrestrial archives. The Holocene 18, 1019–1032. https://doi.org/10.1177/0959683608095573

Kotthoff, U., Koutsodendris, A., Pross, J., Schmiedl, G., Bornemann, A., Kaul, C., Marino, G., Peyron, O., Schiebel, R., 2011. Impact of Lateglacial cold events on the northern Aegean region reconstructed from marine and terrestrial proxy data. J. Quat. Sci. 26, 86–96. https://doi.org/10.1002/jqs.1430

Kourelis, K., 2018. Zaraka Surrounded: The Archaeology of Settlements in the Peloponnesian Countryside, in: Campell, S. (Ed.), The Cistercian Monastery of Zaraka, Greece. Western Michigan University, pp. 193–213.

Krüger, S., Damrath, M., 2019. In search of the Bølling-Oscillation: a new high resolution pollen record from the locus classicus Lake Bølling, Denmark. Veg. Hist. Archaeobot. https://doi.org/10.1007/s00334-019-00736-3

Kuhnt, T., Schmiedl, G., Ehrmann, W., Hamann, Y., Andersen, N., 2008. Stable isotopic composition of Holocene benthic foraminifers from the Eastern Mediterranean Sea: Past changes in productivity and deep water oxygenation. Palaeogeogr. Palaeoclimatol. Palaeoecol. 268, 106–115. https://doi.org/10.1016/j.palaeo.2008.07.010

Kvenvolden, K.A., 2006. Organic geochemistry – A retrospective of its first 70 years. Org. Geochem. 37, 1–11. https://doi.org/10.1016/j.orggeochem.2005.09.001

Kylander, M.E., Ampel, L., Wohlfarth, B., Veres, D., 2011. High-resolution X-ray fluorescence core scanning analysis of Les Echets (France) sedimentary sequence: New insights from chemical proxies. J. Quat. Sci. 26, 109–117. https://doi.org/10.1002/jqs.1438

Lane, C.S., Brauer, A., Blockley, S.P.E., Dulski, P., 2013. Volcanic ash reveals time-transgressive abrupt climate change during the Younger Dryas. Geology 41, 1251–1254. https://doi.org/10.1130/G34867.1

Langgut, D., Finkelstein, I., Litt, T., 2013. Climate and the Late Bronze collapse: New evidence from the southern Levant. Tel Aviv 40, 149–175. https://doi.org/10.1179/033443513X13753505864205

Lazarova, M., Koutsios, A., Kontopoulos, N., 2012. Holocene vegetation history of the Kotihi lagoon (northwest Peloponnesus, Greece). Quat. Int. 261, 138–145. https://doi.org/10.1016/j.quaint.2009.10.036

Leininger, S., Urich, T., Schloter, M., Schwark, L., Qi, J., Nicol, G.W., Prosser, J.I., Schuster, S.C., Schleper, C., 2006. Archaea predominate among ammonia-oxidizing prokaryotes in soils. Nature 442, 806–809. https://doi.org/10.1038/nature04983

Leng, M.J., Marshall, J.D., 2004. Palaeoclimate interpretation of stable isotope data from lake sediment archives. Quat. Sci. Rev. 23, 811–831.

https://doi.org/10.1016/j.quascirev.2003.06.012

Leroy, S.A.G., Tudryn, A., Chalié, F., López-Merino, L., Gasse, F., 2013. From the Allerød to the mid-Holocene: palynological evidence from the south basin of the Caspian Sea. Quat. Sci. Rev. 78, 77–97. https://doi.org/10.1016/j.quascirev.2013.07.032

Lichtfouse, É., Derenne, S., Mariotti, A., Largeau, C., 1994. Possible algal origin of long chain odd n-alkanes in immature sediments as revealed by distributions and carbon isotope ratios. Org. Geochem. 22, 1023–1027. https://doi.org/10.1016/0146-6380(94)90035-3

Lihavainen, J., Ahonen, V., Keski-Saari, S., Sõber, A., Oksanen, E., Keinänen, M., 2017. Low vapor pressure deficit reduces glandular trichome density and modifies the chemical composition of cuticular waxes in silver birch leaves. Tree Physiol. 37, 1166–1181. https://doi.org/10.1093/treephys/tpx045

Lionello, P., 2012. The climate of the Mediterranean region: From the past to the future. Elsevier.

Lipp, J.S., Hinrichs, K., 2009. Structural diversity and fate of intact polar lipids in marine sediments. Geochim. Cosmochim. Acta 73, 6816–6833. https://doi.org/10.1016/j.gca.2009.08.003

Little, L.K., 2007. Plague and the End of Antiquity - the Pandemic of 541-750.

Liu, W., Liu, Z., Fu, M., An, Z., 2008. Distribution of the C37 tetra-unsaturated alkenone in Lake Qinghai, China: A potential lake salinity indicator. Geochim. Cosmochim. Acta 72, 988–997. https://doi.org/10.1016/j.gca.2007.11.016

Liu, W., Liu, Z., Wang, H., He, Y., Wang, Z., Xu, L., 2011. Salinity control on long-chain alkenone distributions in lake surface waters and sediments of the northern Qinghai-Tibetan Plateau, China. Geochim. Cosmochim. Acta 75, 1693–1703. https://doi.org/10.1016/j.gca.2010.10.029

Lockheart, M.J., van Bergen, P.F., Evershed, R.P., 2000. Chemotaxonomic classification of fossil leaves from the Miocene Clarkia lake deposit, Idaho, USA based on n -alkyl lipid distributions and principal component analyses. Org. Geochem. 31, 1223–1246. https://doi.org/10.1016/S0146-6380(00)00107-8

Lolos, Y.A., 1997. The Hadrianic Aqueduct of Corinth. Hesperia 66, 271–314.

Long, L.M., Patel, H.P., Cory, W.C., Stapleton, A.E., 2003. The maize epicuticular wax layer provides UV protection. Funct. Plant Biol. 30, 75. https://doi.org/10.1071/FP02159

Longo, W.M., Theroux, S., Giblin, A.E., Zheng, Y., Dillon, J.T., Huang, Y., 2016. Temperature calibration and phylogenetically distinct distributions for freshwater alkenones: Evidence from northern Alaskan lakes. Geochim. Cosmochim. Acta 180, 177–196. https://doi.org/10.1016/j.gca.2016.02.019

Longo, W.M., Huang, Y., Yao, Y., Zhao, J., Giblin, A.E., Wang, X., Zech, R., Haberzettl, T., Jardillier, L., Toney, J., Liu, Z., Krivonogov, S., Kolpakova, M., Chu, G., D'Andrea, W.J.,

Harada, N., Nagashima, K., Sato, M., Yonenobu, H., Yamada, K., Gotanda, K., Shinozuka, Y., 2018. Widespread occurrence of distinct alkenones from Group I haptophytes in freshwater lakes: Implications for paleotemperature and paleoenvironmental reconstructions. Earth Planet. Sci. Lett. 492, 239–250. https://doi.org/10.1016/j.epsl.2018.04.002

Lotter, A.F., Eicher, U., Siegenthaler, U., Birks, H.J.B., 1992. Late-glacial climatic oscillations as recorded in Swiss lake sediments. J. Quat. Sci. 7, 187–204. https://doi.org/10.1002/jqs.3390070302

Lotter, A.F., 1999. Late-glacial and Holocene vegetation history and dynamics as shown by pollen and plant macrofossil analyses in annually laminated sediments from Soppensee, central Switzerland. Veg. Hist. Archaeobot. 8, 165–184. https://doi.org/10.1007/BF02342718

Lotter, A.F., Birks, H.J.B., Eicher, U., Hofmann, W., Schwander, J., Wick, L., 2000. Younger Dryas and Allerod summer temperatures at Gerzensee (Switzerland) inferred from fossil pollen and cladoceran assemblages. Palaeogeogr. Palaeoclimatol. Palaeoecol. 159, 349–361. https://doi.org/10.1016/S0031-0182(00)00093-6

Lowell, T., Waterson, N., Fisher, T., Loope, H., Glover, K., Comer, G., Hajdas, I., Denton, G., Schaefer, J., Rinterknecht, V., Broecker, W., Teller, J., 2005. Testing the Lake Agassiz meltwater trigger for the Younger Dryas. Eos, Trans. Am. Geophys. Union 86, 365. https://doi.org/10.1029/2005EO400001

Löwemark, L., Chen, H.F., Yang, T.N., Kylander, M., Yu, E.F., Hsu, Y.W., Lee, T.Q., Song, S.R., Jarvis, S., 2011. Normalizing XRF-scanner data: A cautionary note on the interpretation of high-resolution records from organic-rich lakes. J. Asian Earth Sci. 40, 1250–1256. https://doi.org/10.1016/j.jseaes.2010.06.002

LUBW, 2016. ISF Arbeitsbericht 2014.

Lucas, G., McGovern, T., 2007. Bloody slaughter: Ritual decapitation and display at the Viking settlement of Hofstaðir, Iceland. Eur. J. Archaeol. 10, 7–30. https://doi.org/10.1177/1461957108091480

Lucke, B., Sprafke, T., 2015. Correlation of soil color, redness ratings, and weathering indices of Terrae Calcis along a precipitation gradient in northern Jordan. Erlanger Geogr. Arb. 53–68.

Luterbacher, J., García-Herrera, R., Akcer-On, S., Allan, R., Alvarez-Castro, M.C., Benito, G., Booth, J., Büntgen, U., Cagatay, N., Colombaroli, D., Davis, B., Esper, J., Felis, T., Fleitmann, D., Frank, D., Gallego, D., Garcia-Bustamante, E., Glaser, R., Gonzalez-Rouco, F.J., Goosse, H., Kiefer, T., Macklin, M.G., Manning, S.W., Montagna, P., Newman, L., Power, M.J., Rath, V., Ribera, P., Riemann, D., Roberts, N., Sicre, M.A., Silenzi, S., Tinner, W., Tzedakis, P.C., Valero-Garcés, B., van der Schrier, G., Vannière,

B., Vogt, S., Wanner, H., Werner, J.P., Willett, G., Williams, M.H., Xoplaki, E., Zerefos, C.S., Zorita, E., 2012. A review of 2000 years of paleoclimatic evidence in the mediterranean, in: The Climate of the Mediterranean Region. Elsevier Inc., pp. 87–185. https://doi.org/10.1016/B978-0-12-416042-2.00002-1

Maffei, M., 1996. Chemotaxonomic significance of leaf wax alkanes in the gramineae. Biochem. Syst. Ecol. 24, 53–64. https://doi.org/10.1016/0305-1978(95)00102-6

Maffei, M., Badino, S., Bossi, S., 2004. Chemotaxonomic significance of leaf wax n-alkanes in the Pinales (Coniferales). J. Biol. Res. (Thessaloniki, Greece) 1, 3–19.

Magny, M., Vannière, B., de Beaulieu, J.L., Bégeot, C., Heiri, O., Millet, L., Peyron, O., Walter-Simonnet, A.V., 2007a. Early-Holocene climatic oscillations recorded by lake-level fluctuations in west-central Europe and in central Italy. Quat. Sci. Rev. 26, 1951–1964. https://doi.org/10.1016/j.quascirev.2006.04.013

Magny, M., de Beaulieu, J.-L., Drescher-Schneider, R., Vannière, B., Walter-Simonnet, A.-V., Miras, Y., Millet, L., Bossuet, G., Peyron, O., Brugiapaglia, E., Leroux, A., 2007b. Holocene climate changes in the central Mediterranean as recorded by lake-level fluctuations at Lake Accesa (Tuscany, Italy). Quat. Sci. Rev. 26, 1736–1758. https://doi.org/10.1016/j.quascirev.2007.04.014

Magny, M., 2013. Orbital, ice-sheet, and possible solar forcing of Holocene lake-level fluctuations in west-central Europe: A comment on Bleicher. The Holocene 23, 1202-1212. https://doi.org/10.1177/0959683613483627

Maguire, L.S., O'Sullivan, S.M., Galvin, K., O'Connor, T.P., O'Brien, N.M., 2004. Fatty acid profile, tocopherol, squalene and phytosterol content of walnuts, almonds, peanuts, hazelnuts and the macadamia nut. Int. J. Food Sci. Nutr. 55, 171–178. https://doi.org/10.1080/09637480410001725175

Mäkelä, E.M., 1996. Size distinctions between Betula pollen types — A review. Grana 35, 248–256. https://doi.org/10.1080/00173139609430011

Maliouchenko, O., Palmé, A.E., Buonamici, A., Vendramin, G.G., Lascoux, M., 2007. Comparative phylogeography and population structure of European Betula species, with particular focus on B. pendula and B. pubescens. J. Biogeogr. 34, 1601–1610. https://doi.org/10.1111/j.1365-2699.2007.01729.x

Manning, S.W., 2013. The Roman World and Climate: Context, Relevance of Climate Change, and Some Issues, in: The Ancient Mediterranean Environment between Science and History. BRILL. https://doi.org/10.1163/9789004254053_007

Manning, S.W., 2018. Some Perspectives on the Frequency of Significant, Historically Forcing Drought and Subsistence Crises in Anatolia and Region, in: Holt, E. (Ed.), Water and Power in Past Societies: IEMA Proceedings, Volume 7. State University of New York Press, Albany, pp. 279–295.

Marseille, F., Disnar, J.R., Guillet, B., Noack, Y., 1999. n-Alkanes and free fatty acids in humus and A1 horizons of soils under beech, spruce and grass in the Massif-Central (Mont-Lozère), France. Eur. J. Soil Sci. 50, 433–441. https://doi.org/10.1046/j.1365-2389.1999.00243.x

Martrat, B., Jimenez-Amat, P., Zahn, R., Grimalt, J.O., 2014. Similarities and dissimilarities between the last two deglaciations and interglaciations in the North Atlantic region. Quat. Sci. Rev. 99, 122–134. https://doi.org/10.1016/j.quascirev.2014.06.016

Mayer, B., Schwark, L., 1999. A 15,000-year stable isotope record from sediments of Lake Steisslingen, Southwest Germany. Chem. Geol. 161, 315–337. https://doi.org/10.1016/S0009-2541(99)00093-5

Mayes, R.W., Beresford, N.A., Lamb, C.S., Barnett, C.L., Howard, B.J., Jones, B.-E.V., Eriksson, O., Hove, K., Pedersen, Ø., Staines, B.W., 1994. Novel approaches to the estimation of intake and bioavailability of radiocaesium in ruminants grazing forested areas. Sci. Total Environ. 157, 289–300. https://doi.org/10.1016/0048-9697(94)90592-4

Mayewski, P.A., Rohling, E.E., Stager, J.C., Karlén, W., Maasch, K.A., Meeker, L.D., Meyerson, E.A., Gasse, F., van Kreveld, S., Holmgren, K., Lee-Thorp, J., Rosqvist, G., Rack, F., Staubwasser, M., Schneider, R.R., Steig, E.J., 2004. Holocene climate variability. Quat. Res. 62, 243–255. https://doi.org/10.1016/j.yqres.2004.07.001

Mayr, C., Lücke, A., Maidana, N.I., Wille, M., Haberzettl, T., Corbella, H., Ohlendorf, C., Schäbitz, F., Fey, M., Janssen, S., Zolitschka, B., 2009. Isotopic fingerprints on lacustrine organic matter from Laguna Potrok Aike (southern Patagonia, Argentina) reflect environmental changes during the last 16,000 years. J. Paleolimnol. 42, 81–102. https://doi.org/10.1007/s10933-008-9249-8

Mayyas, A.S., Al-Qudah, M.A., Douglas, K.A., Al-Ajlouny, and F.K., 2012. Beeswax Preserved in Archaeological Ceramics: Function and Use. Ann. Fac. Arts, Ain Shams Univ. 40, 343–371.

McCormick, M., Büntgen, U., Cane, M.A., Cook, E.R., Harper, K., Huybers, P., Litt, T., Manning, S.W., Mayewski, P.A., More, A.F.M., Nicolussi, K., Tegel, W., 2012. Climate Change during and after the Roman Empire: Reconstructing the Past from Scientific and Historical Evidence. J. Interdiscip. Hist. 43, 169–220. https://doi.org/10.1162/JINH_a_00379

McCorriston, J., Harrower, M., Martin, L., Oches, E., 2012. Cattle Cults of the Arabian Neolithic and Early Territorial Societies. Am. Anthropol. 114, 45–63. https://doi.org/10.1111/j.1548-1433.2011.01396.x

Meriam, E.O., Aurélia, H., Héléne, L., Volkan, K., Jacqueline, V.A., Gilles, L., Olivier, D., Sabine, S., 2017. Soil erosion in relation to land-use changes in the sediments of Amik Lake near Antioch antique city during the last 4 kyr. The Holocene 1–15.

https://doi.org/10.1177/0959683617715702

Meyers, P., 2003. Application of organic geochemistry to paleolimnological reconstruction: a summary of examples from the Laurention Great Lakes. Org. Geochem. 34, 261–289. https://doi.org/10.1016/S0146-6380(02)00168-7

Meyers, P.A., 1994. Preservation of elemental and isotopic source identification of sediemntary organic matter. Chem. Geol. 114, 289–302. https://doi.org/10.1016/0009-2541(94)90059-0

Mischke, S., Ginat, H., Al-Saqarat, B.S., Faershtein, G., Porat, N., Braun, P., Rech, J.A., 2017. Fossil-Based Reconstructions of Ancient Water Bodies in the Levantine Deserts, in: Quaternary of the Levant. pp. 381–390. https://doi.org/10.1017/9781316106754.045

Mook, W.G., Van Der Plicht, J., 1999. Reporting 14C activities and concentrations. Radiocarbon 41, 227–239. https://doi.org/10.1017/S0033822200057106

Morfis, A., Zojer, H., 1986. Karst hydrogeology of the Central and Eastern Peloponnesus (Greece), Steirische Beiträge zur Hydrogeologie.

Mortensen, M.F., Birks, H.H., Christensen, C., Holm, J., Noe-Nygaard, N., Odgaard, B.V., Olsen, J., Rasmussen, K.L., 2011. Lateglacial vegetation development in Denmark – New evidence based on macrofossils and pollen from Slotseng, a small-scale site in southern Jutland. Quat. Sci. Rev. 30, 2534–2550. https://doi.org/10.1016/j.quascirev.2011.04.018

Moschen, R., Kühl, N., Peters, S., Vos, H., L̈cke, A., 2011. Temperature variability at Düarres Maar, Germany during the Migration Period and at High Medieval Times, inferred from stable carbon isotopes of *Sphagnum* cellulose. Clim. Past 7, 1011–1026. https://doi.org/10.5194/cp-7-1011-2011

Mueller-Niggemann, C., Schwark, L., 2015. Chemotaxonomy and diagenesis of aliphatic hydrocarbons in rice plants and soils from land reclamation areas in the Zhejiang Province, China. Org. Geochem. 83–84, 215–226. https://doi.org/10.1016/j.orggeochem.2015.03.016

Mueller-Niggemann, C., Utami, S.R., Marxen, A., Mangelsdorf, K., Bauersachs, T., Schwark, L., 2016. Distribution of tetraether lipids in agricultural soils – differentiation between paddy and upland management. Biogeosciences 13, 1647–1666. https://doi.org/10.5194/bg-13-1647-2016

Mukherjee, A.J., Berstan, R., Copley, M.S., Gibson, A.M., Evershed, R.P., 2007. Compound-specific stable carbon isotopic detection of pig product processing in British Late Neolithic pottery. Antiquity 81, 743–754. https://doi.org/10.1017/S0003598X00095703

Müller, E., Schunke, T., 2014. Die Rinderopfer von Niederwünsch – Belege eines umfangreichen Ritualgeschehens im späten 4. Jahrtausend v. Chr. H. Meller, 85–92.

Müller, J., 2011. Megaliths and Funnel Beakers: Societies in Change 4100-2700 BC., in:

Stichting Nederlands Museum Voor Anthropologie En Praehistorie. Stichting Nederlands Museum voor Anthropologie en Praehistorie, Amsterdam, p. 92.

Müller, J., 2013. Mesolithisch – neolithisch: Zur Entwicklung von Hütten und Häusern im südlichen Skandinavien und nördlichen Mitteleuropa. Offta 69/70.

Munsell, A.H., 2000. Munsell Soil Color Charts, Munsell Color.

Muschitiello, F., Andersson, A., Wohlfarth, B., Smittenberg, R.H., 2015. The C20highly branched isoprenoid biomarker - A new diatom-sourced proxy for summer trophic conditions? Org. Geochem. 81, 27–33. https://doi.org/10.1016/j.orggeochem.2015.01.007

Naafs, B.D.A., Inglis, G.N., Zheng, Y., Amesbury, M.J., Biester, H., Bindler, R., Blewett, J., Burrows, M.A., del Castillo Torres, D., Chambers, F.M., Cohen, A.D., Evershed, R.P., Feakins, S.J., Gałka, M., Gallego-Sala, A., Gandois, L., Gray, D.M., Hatcher, P.G., Honorio Coronado, E.N., Hughes, P.D.M., Huguet, A., Könönen, M., Laggoun-Défarge, F., Lähteenoja, O., Lamentowicz, M., Marchant, R., McClymont, E., Pontevedra-Pombal, X., Ponton, C., Pourmand, A., Rizzuti, A.M., Rochefort, L., Schellekens, J., De Vleeschouwer, F., Pancost, R.D., 2017a. Introducing global peat-specific temperature and pH calibrations based on brGDGT bacterial lipids. Geochim. Cosmochim. Acta 208, 285–301. https://doi.org/10.1016/j.gca.2017.01.038

Naafs, B.D.A., Gallego-Sala, A.V., Inglis, G.N., Pancost, R.D., 2017b. Refining the global branched glycerol dialkyl glycerol tetraether (brGDGT) soil temperature calibration. Org. Geochem. 106, 48–56. https://doi.org/10.1016/j.orggeochem.2017.01.009

Naeher, S., Gilli, A., North, R.P., Hamann, Y., Schubert, C.J., 2013. Tracing bottom water oxygenation with sedimentary Mn/Fe ratios in Lake Zurich, Switzerland. Chem. Geol. 352, 125–133. https://doi.org/10.1016/j.chemgeo.2013.06.006

Naeher, S., Peterse, F., Smittenberg, R.H., Niemann, H., Zigah, P.K., Schubert, C.J., 2014. Sources of glycerol dialkyl glycerol tetraethers (GDGTs) in catchment soils, water column and sediments of Lake Rotsee (Switzerland) – Implications for the application of GDGT-based proxies for lakes. Org. Geochem. 66, 164–173. https://doi.org/10.1016/j.orggeochem.2013.10.017

Nanou, E.-A., Zagana, E., 2018. Groundwater Vulnerability to Pollution Map for Karst Aquifer Protection (Ziria Karst System, Southern Greece). Geosciences 8, 125. https://doi.org/10.3390/geosciences8040125

Needham, S., Evans, J., 1987. Honey and Dripping: Neolithic Food Residues from Runnymede Bridge. Oxford J. Archaeol. 6, 21–28. https://doi.org/10.1111/j.1468-0092.1987.tb00138.x

Neugebauer, I., Brauer, A., Dräger, N., Dulski, P., Wulf, S., Plessen, B., Mingram, J., Herzschuh, U., Brande, A., 2012. A Younger Dryas varve chronology from the Rehwiese

palaeolake record in NE-Germany. Quat. Sci. Rev. 36, 91–102. https://doi.org/10.1016/j.quascirev.2011.12.010

Neugebauer, I., Brauer, A., Schwab, M.J., Dulski, P., Frank, U., Hadzhiivanova, E., Kitagawa, H., Litt, T., Schiebel, V., Taha, N., Waldmann, N.D., 2015. Evidences for centennial dry periods at ~3300 and ~2800 cal. yr BP from micro-facies analyses of the Dead Sea sediments. The Holocene 25, 1358–1371. https://doi.org/10.1177/0959683615584208

Norström, E., Katrantsiotis, C., Smittenberg, R.H., Kouli, K., 2017. Chemotaxonomy in some Mediterranean plants and implications for fossil biomarker records. Geochim. Cosmochim. Acta 219, 96–110. https://doi.org/10.1016/j.gca.2017.09.029

Norström, E., Katrantsiotis, C., Finné, M., Risberg, J., Smittenberg, R.H., Bjursäter, S., 2018. Biomarker hydrogen isotope composition (δD) as proxy for Holocene hydroclimatic change and seismic activity in SW Peloponnese, Greece. J. Quat. Sci. 33, 563–574. https://doi.org/10.1002/jqs.3036

Nowaczyk, N.R., Minyuk, P., Melles, M., Brigham-Grette, J., Glushkova, O., Nolan, M., Lozhkin, A. V., Stetsenko, T. V., Andersen, P.M., Forman, S.L., 2002. Magnetostratigraphic results from impact crater Lake El'gygytgyn, northeastern Siberia: a 300 kyr long high-resolution terrestrial palaeoclimatic record from the Arctic. Geophys. J. Int. 150, 109–126. https://doi.org/10.1046/j.1365-246X.2002.01625.x

Nowaczyk, N.R., 2005. Logging of Magnetic Susceptibility, in: Tracking Environmental Change Using Lake Sediments. Kluwer Academic Publishers, pp. 155–170. https://doi.org/10.1007/0-306-47669-x_8

O'Leary, M.H., 1988. Carbon Isotopes in Photosynthesis Fractionation techniques may reveal new aspects of carbon dynamics in plants. Bioscience 38, 328–336. https://doi.org/jstor.org/stable/1310735

Ohlendieck, U., Stuhr, A., Siegmund, H., 2000. Nitrogen fixation by diazotrophic cyanobacteria in the Baltic Sea and transfer of the newly fixed nitrogen to picoplankton organisms. J. Mar. Syst. 25, 213–219. https://doi.org/10.1016/S0924-7963(00)00016-6

Orav, A., Arak, E., Boikova, T., Raal, A., 2011. Essential oil in Betula spp. leaves naturally growing in Estonia. Biochem. Syst. Ecol. 39, 744–748. https://doi.org/10.1016/j.bse.2011.06.013

Orland, I.J., Bar-Matthews, M., Kita, N.T., Ayalon, A., Matthews, A., Valley, J.W., 2009. Climate deterioration in the Eastern Mediterranean as revealed by ion microprobe analysis of a speleothem that grew from 2.2 to 0.9??ka in Soreq Cave, Israel. Quat. Res. 71, 27–35. https://doi.org/10.1016/j.yqres.2008.08.005

Orsavova, J., Misurcova, L., Ambrozova, J., Vicha, R., Mlcek, J., 2015. Fatty Acids Composition of Vegetable Oils and Its Contribution to Dietary Energy Intake and Dependence of Cardiovascular Mortality on Dietary Intake of Fatty Acids. Int. J. Mol. Sci.

16, 12871–12890. https://doi.org/10.3390/ijms160612871

Otto, A., Simpson, M.J., 2005. Degradation and Preservation of Vascular Plant-derived Biomarkers in Grassland and Forest Soils from Western Canada. Biogeochemistry 74, 377–409. https://doi.org/10.1007/s10533-004-5834-8

Ourisson, G., Albrecht, P., 1992. Hopanoids. 1. Geohopanoids: the most abundant natural products on Earth? Acc. Chem. Res. 25, 398–402. https://doi.org/10.1021/ar00021a003

Ourisson, G., Rohmer, M., 1992. Hopanoids. 2. Biohopanoids: A Novel Class of Bacterial Lipids. Acc. Chem. Res. 25, 403–408. https://doi.org/10.1021/ar00021a004

Outram, A.K., Stear, N.A., Bendrey, R., Olsen, S., Kasparov, A., Zaibert, V., Thorpe, N., Evershed, R.P., 2009. The Earliest Horse Harnessing and Milking. Science. 323, 1332–1335. https://doi.org/10.1126/science.1168594

Outram, A.K., Stear, N.A., Kasparov, A., Usmanova, E., Varfolomeev, V., Evershed, R.P., 2011. Horses for the dead: funerary foodways in Bronze Age Kazakhstan. Antiquity 85, 116–128. https://doi.org/10.1017/S0003598X00067478

Özogul, Y., Özogul, F., 2007. Fatty acid profiles of commercially important fish species from the Mediterranean, Aegean and Black Seas. Food Chem. 100, 1634–1638. https://doi.org/10.1016/j.foodchem.2005.11.047

Pagani, M., Pedentchouk, N., Huber, M., Sluijs, A., Schouten, S., Brinkhuis, H., Sinninghe Damsté, J.S., Dickens, G.R., 2006. Arctic hydrology during global warming at the Palaeocene/Eocene thermal maximum. Nature 442, 671–675. https://doi.org/10.1038/nature05043

Palme, A.E., Su, Q., Palsson, S., Lascoux, M., 2004. Extensive sharing of chloroplast haplotypes among European birches indicates hybridization among Betula pendula, B. pubescens and B. nana. Mol. Ecol. 13, 167–178. https://doi.org/10.1046/j.1365-294X.2003.02034.x

Palmisano, A., Bevan, A., Shennan, S., 2017. Comparing archaeological proxies for long-term population patterns : An example from central Italy Comparing archaeological proxies for long-term population patterns : An example from central Italy. J. Archaeol. Sci. 87, 59–72. https://doi.org/10.1016/j.jas.2017.10.001

Palmisano, A., Woodbridge, J., Roberts, C.N., Bevan, A., Fyfe, R., Shennan, S., Cheddadi, R., Greenberg, R., Kaniewski, D., Langgut, D., Leroy, S.A., Litt, T., Miebach, A., 2019. Holocene landscape dynamics and long-term population trends in the Levant. The Holocene 29, 708–727. https://doi.org/10.1177/0959683619826642

Panagiotopoulos, V., 1985. Plithismos Kai Oikismoi Tis Peloponnisou. Athens.

Pancost, R.D., Baas, M., van Geel, B., Sinninghe Damsté, J.S., 2002. Biomarkers as proxies for plant inputs to peats: an example from a sub-boreal ombrotrophic bog. Org. Geochem. 33, 675–690. https://doi.org/10.1016/S0146-6380(02)00048-7

Papakosta, V., Oras, E., Isaksson, S., 2019. Early pottery use across the Baltic – A comparative lipid residue study on Ertebølle and Narva ceramics from coastal hunter-gatherer sites in southern Scandinavia, northern Germany and Estonia. J. Archaeol. Sci. Reports 24, 142–151. https://doi.org/10.1016/j.jasrep.2019.01.003

Papastergiadou, E.S., Retalis, A., Kalliris, P., Georgiadis, T., 2007. Land use changes and associated environmental impacts on the Mediterranean shallow Lake Stymfalia, Greece. Hydrobiologia 584, 361–372. https://doi.org/10.1007/s10750-007-0606-9

Pawłowski, D., Płóciennik, M., Brooks, S.J., Luoto, T.P., Milecka, K., Nevalainen, L., Peyron, O., Self, A., Zieliński, T., 2015. A multiproxy study of Younger Dryas and Early Holocene climatic conditions from the Grabia River paleo-oxbow lake (central Poland). Palaeogeogr. Palaeoclimatol. Palaeoecol. 438, 34–50. https://doi.org/10.1016/j.palaeo.2015.07.031

Pecci, A., Giorgi, G., Salvini, L., Cau Ontiveros, M.Á., 2013. Identifying wine markers in ceramics and plasters using gas chromatography–mass spectrometry. Experimental and archaeological materials. J. Archaeol. Sci. 40, 109–115. https://doi.org/10.1016/j.jas.2012.05.001

Peters, K.E., Walters, C.C., Moldowan, J.M., 2005. The Biomarker Guide (Vol 1). Cambridge University Press, New York. https://doi.org/10.1017/S0016756806212056

Peterse, F., van der Meer, J., Schouten, S., Weijers, J.W.H., Fierer, N., Jackson, R.B., Kim, J., Sinninghe Damsté, J.S., 2012. Revised calibration of the MBT–CBT paleotemperature proxy based on branched tetraether membrane lipids in surface soils. Geochim. Cosmochim. Acta 96, 215–229. https://doi.org/10.1016/j.gca.2012.08.011

Peyron, O., Goring, S., Dormoy, I., Kotthoff, U., Pross, J., de Beaulieu, J.-L., Drescher-Schneider, R., Vannière, B., Magny, M., 2011. Holocene seasonality changes in the central Mediterranean region reconstructed from the pollen sequences of Lake Accesa (Italy) and Tenaghi Philippon (Greece). The Holocene 21, 131–146. https://doi.org/10.1177/0959683610384162

Philippson, A., 1892. Der Peloponnes Versuch einer Landeskunde auf geologischer Grundlage. Nature 47, 6–6. https://doi.org/10.1038/047006b0

Pitcher, A., Hopmans, E.C., Mosier, A.C., Park, S.-J., Rhee, S.-K., Francis, C.A., Schouten, S., Sinninghe Damsté, J.S., 2011. Core and Intact Polar Glycerol Dibiphytanyl Glycerol Tetraether Lipids of Ammonia-Oxidizing Archaea Enriched from Marine and Estuarine Sediments. Appl. Environ. Microbiol. 77, 3468–3477. https://doi.org/10.1128/AEM.02758-10

Pollard, A.M., Batt, C.M., Stern, B., Young, S.M.M., 2007. Analytical Chemistry in Archaeology. Cambridge University Press, Cambridge. https://doi.org/10.1017/CBO9780511607431

Pollex, A., 1999. Comments on the interpretation of the so-called cattle burials of Neolithic Central Europe. Antiquity 73, 542–550. https://doi.org/10.1017/S0003598X00065091

Poynter, J., Eglinton, G., 1990. Molecular Composition of Three Sediments from Hole 717C: The Bengal Fan, in: Proceedings of the Ocean Drilling Program, 116 Scientific Results. Ocean Drilling Program, pp. 155–161. https://doi.org/10.2973/odp.proc.sr.116.151.1990

Prahl, F.G., Wakeham, S.G., 1987. Calibration of unsaturation patterns in long-chain ketone compositions for palaeotemperature assessment. Nature 330, 367–369. https://doi.org/10.1038/330367a0

Prahl, F.G., Pilskaln, C.H., Sparrow, M.A., 2001. Seasonal record for alkenones in sedimentary particles from the Gulf of Maine. Deep. Res. Part I Oceanogr. Res. Pap. 48, 515–528. https://doi.org/10.1016/S0967-0637(00)00057-1

R Core Team, 2017. R: A language and environment for statistical computing. R Foundation for Statistical Computing, Vienna, Austria, Austria.

Rach, O., Brauer, A., Wilkes, H., Sachse, D., 2014. Delayed hydrological response to Greenland cooling at the onset of the Younger Dryas in western Europe. Nat. Geosci. 7, 109–112. https://doi.org/10.1038/ngeo2053

Rajčević, N., Janaćković, P., Dodoš, T., Tešević, V., Marin, P.D., 2014. Biogeographic Variation of Foliar n- Alkanes of Juniperus communis var . saxatilis Pallas from the Balkans. Chem. Biodivers. 11, 1923–1938. https://doi.org/10.1002/cbdv.201400048

Ramsey, C.B., 2008. Deposition models for chronological records. Quat. Sci. Rev. 27, 42–60. https://doi.org/10.1016/j.quascirev.2007.01.019

Ramsey, C.B., Lee, S., 2013. Recent and Planned Developments of the Program OxCal. Radiocarbon 55, 720–730. https://doi.org/10.1017/s0033822200057878

Randlett, M.È., Coolen, M.J.L., Stockhecke, M., Pickarski, N., Litt, T., Balkema, C., Kwiecien, O., Tomonaga, Y., Wehrli, B., Schubert, C.J., 2014. Alkenone distribution in Lake Van sediment over the last 270ka: Influence of temperature and haptophyte species composition. Quat. Sci. Rev. 104, 53–62. https://doi.org/10.1016/j.quascirev.2014.07.009

Rao, S.J., Iason, G.R., Hulbert, I.A., Mayes, R.W., Racey, P.A., 2003. Estimating diet composition for mountain hares in newly established native woodland: development and application of plant-wax faecal markers. Can. J. Zool. 81, 1047–1056. https://doi.org/10.1139/z03-093

Raven, A.M., van Bergen, P.F., Stott, A.W., Dudd, S.N., Evershed, R.P., 1997. Formation of long-chain ketones in archaeological pottery vessels by pyrolysis of acyl lipids. J. Anal. Appl. Pyrolysis 40–41, 267–285. https://doi.org/10.1016/S0165-2370(97)00036-3

Reimer, P.J., Bard, E., Bayliss, A., Beck, J.W., Blackwell, P.G., Ramsey, C.B., Buck, C.E., Cheng, H., Edwards, R.L., Friedrich, M., Grootes, P.M., Guilderson, T.P., Haflidason, H.,

Hajdas, I., Hatté, C., Heaton, T.J., Hoffmann, D.L., Hogg, A.G., Hughen, K.A., Kaiser, K.F., Kromer, B., Manning, S.W., Niu, M., Reimer, R.W., Richards, D.A., Scott, E.M., Southon, J.R., Staff, R.A., Turney, C.S.M., van der Plicht, J., 2013. IntCal13 and Marine13 Radiocarbon Age Calibration Curves 0–50,000 Years cal BP. Radiocarbon 55, 1869–1887. https://doi.org/10.2458/azu_js_rc.55.16947

Roberts, N., Moreno, A., Valero-Garcés, B.L., Corella, J.P., Jones, M., Allcock, S., Woodbridge, J., Morellón, M., Luterbacher, J., Xoplaki, E., Türkeş, M., 2012. Palaeolimnological evidence for an east–west climate see-saw in the Mediterranean since AD 900. Glob. Planet. Change 84–85, 23–34. https://doi.org/10.1016/j.gloplacha.2011.11.002

Roberts, N., Allcock, S.L., Arnaud, F., Dean, J.R., Eastwood, W.J., Jones, M.D., Leng, M.J., Metcalfe, S.E., Malet, E., Woodbridge, J., Yiğitbaşıoğlu, H., 2016. A tale of two lakes: a multi-proxy comparison of Lateglacial and Holocene environmental change in Cappadocia, Turkey. J. Quat. Sci. 31, 348–362. https://doi.org/10.1002/jqs.2852

Robinson, S.A., Black, S., Sellwood, B.W., Valdes, P.J., 2006. A review of palaeoclimates and palaeoenvironments in the Levant and Eastern Mediterranean from 25,000 to 5000 years BP: setting the environmental background for the evolution of human civilisation. Quat. Sci. Rev. 25, 1517–1541. https://doi.org/10.1016/j.quascirev.2006.02.006

Roffet-Salque, M., Regert, M., Evershed, R.P., Outram, A.K., Cramp, L.J.E., Decavallas, O., Dunne, J., Gerbault, P., Mileto, S., Mirabaud, S., Pääkkönen, M., Smyth, J., Šoberl, L., Whelton, H.L., Alday-Ruiz, A., Asplund, H., Bartkowiak, M., Bayer-Niemeier, E., Belhouchet, L., Bernardini, F., Budja, M., Cooney, G., Cubas, M., Danaher, E.M., Diniz, M., Domboróczki, L., Fabbri, C., González-Urquijo, J.E., Guilaine, J., Hachi, S., Hartwell, B.N., Hofmann, D., Hohle, I., Ibáñez, J.J., Karul, N., Kherbouche, F., Kiely, J., Kotsakis, K., Lueth, F., Mallory, J.P., Manen, C., Marciniak, A., Maurice-Chabard, B., Mc Gonigle, M.A., Mulazzani, S., Özdoğan, M., Perić, O.S., Perić, S.R., Petrasch, J., Pétrequin, A.-M., Pétrequin, P., Poensgen, U., Joshua Pollard, C., Poplin, F., Radi, G., Stadler, P., Stäuble, H., Tasić, N., Urem-Kotsou, D., Vuković, J.B., Walsh, F., Whittle, A., Wolfram, S., Zapata-Peña, L., Zoughlami, J., 2015. Widespread exploitation of the honeybee by early Neolithic farmers. Nature 527, 226–230. https://doi.org/10.1038/nature15757

Roffet-Salque, M., Lee, M.R.F., Timpson, A., Evershed, R.P., 2017. Impact of modern cattle feeding practices on milk fatty acid stable carbon isotope compositions emphasise the need for caution in selecting reference animal tissues and products for archaeological investigations. Archaeol. Anthropol. Sci. 9, 1343–1348. https://doi.org/10.1007/s12520-016-0357-5

Rohling, E., Mayewski, P., Abu-Zied, R., Casford, J., Hayes, A., 2002. Holocene atmosphere-ocean interactions: records from Greenland and the Aegean Sea. Clim. Dyn. 18, 587–

593. https://doi.org/10.1007/s00382-001-0194-8

Romanus, K., Poblome, J., Verbeke, K., Luypaerts, A., Jacobs, P., De Vos, D., Waelkens, M., 2007. An evaluation of analytical and interpretative methodologies for the extraction and identification of lipids associated with pottery sherds from the site of sagalassos, Turkey. Archaeometry 49, 729–747. https://doi.org/10.1111/j.1475-4754.2007.00332.x

Rommerskirchen, F., Plader, A., Eglinton, G., Chikaraishi, Y., Rullkötter, J., 2006. Chemotaxonomic significance of distribution and stable carbon isotopic composition of long-chain alkanes and alkan-1-ols in C4 grass waxes. Org. Geochem. 37, 1303–1332. https://doi.org/10.1016/j.orggeochem.2005.12.013

Ronkainen, T., Väliranta, M., McClymont, E., Biasi, C., Salonen, S., Fontana, S., Tuittila, E.S., 2015. A combined biogeochemical and palaeobotanical approach to study permafrost environments and past dynamics. J. Quat. Sci. 30, 189–200. https://doi.org/10.1002/jqs.2763

Rösch, M., Lechterbeck, J., 2016. Seven Millennia of human impact as reflected in a high resolution pollen profile from the profundal sediments of Litzelsee, Lake Constance region, Germany. Veg. Hist. Archaeobot. 25, 339–358. https://doi.org/10.1007/s00334-015-0552-9

Ross, A.B., Shepherd, M.J., Schüpphaus, M., Sinclair, V., Alfaro, B., Kamal-Eldin, A., Åman, P., 2003. Alkylresorcinols in Cereals and Cereal Products. J. Agric. Food Chem. 51, 4111–4118. https://doi.org/10.1021/jf0340456

Rossell, J.B., 1991. Purity Criteria in Edible Oils and Fats. Fett Wiss. Technol. Sci. Technol. 93, 526–531. https://doi.org/10.1002/lipi.19910931311

Rowland, S.J., Yon, D.A., Lewis, C.A., Maxwell, J.R., 1985. Occurrence of 2,6,10-trimethyl-7-(3-methylbutyl)-dodecane and related hydrocarbons in the green alga Enteromorpha prolifera and sediments. Org. Geochem. 8, 207–213. https://doi.org/10.1016/0146-6380(85)90028-2

Russell, J.M., Hopmans, E.C., Loomis, S.E., Liang, J., Sinninghe Damsté, J.S., 2018. Distributions of 5- and 6-methyl branched glycerol dialkyl glycerol tetraethers (brGDGTs) in East African lake sediment: Effects of temperature, pH, and new lacustrine paleotemperature calibrations. Org. Geochem. 117, 56–69. https://doi.org/10.1016/j.orggeochem.2017.12.003

Rütters, H., Sass, H., Cypionka, H., Rullkötter, J., 2002. Phospholipid analysis as a tool to study complex microbial communities in marine sediments. J. Microbiol. Methods 48, 149–160. https://doi.org/10.1016/S0167-7012(01)00319-0

Sachse, D., Radke, J., Gleixner, G., 2006. δD values of individual n-alkanes from terrestrial plants along a climatic gradient – Implications for the sedimentary biomarker record. Org. Geochem. 37, 469–483. https://doi.org/10.1016/j.orggeochem.2005.12.003

Sachse, D., Billault, I., Bowen, G.J., Chikaraishi, Y., Dawson, T.E., Feakins, S.J., Freeman, K.H., Magill, C.R., McInerney, F.A., van der Meer, M.T.J., Polissar, P., Robins, R.J., Sachs, J.P., Schmidt, H.-L., Sessions, A.L., White, J.W.C., West, J.B., Kahmen, A., 2012. Molecular Paleohydrology: Interpreting the Hydrogen-Isotopic Composition of Lipid Biomarkers from Photosynthesizing Organisms. Annu. Rev. Earth Planet. Sci. 40, 221–249. https://doi.org/10.1146/annurev-earth-042711-105535

Sadori, L., Zanchetta, G., Giardini, M., 2008. Last Glacial to Holocene palaeoenvironmental evolution at Lago di Pergusa (Sicily, Southern Italy) as inferred by pollen, microcharcoal, and stable isotopes. Quat. Int. 181, 4–14. https://doi.org/10.1016/j.quaint.2007.02.024

Sadori, L., Giraudi, C., Masi, A., Magny, M., Ortu, E., Zanchetta, G., Izdebski, A., 2016. Climate, environment and society in southern Italy during the last 2000 years. A review of the environmental, historical and archaeological evidence. Quat. Sci. Rev. 136, 173–188. https://doi.org/10.1016/j.quascirev.2015.09.020

Salque, M., 2012. Was milk processed in these ceramic pots? Organic residue analyses of European prehistoric cooking vessels, in: Feulner, F. (Ed.), May Contain Traces of Milk – Investigating the Role of Dairy Farming and Milk Consumption in the European Neolithic. University of York, York, pp. 127–141.

Schäfer, I.K., Lanny, V., Franke, J., Eglinton, T.I., Zech, M., Vysloužilová, B., Zech, R., 2016. Leaf waxes in litter and topsoils along a European transect. SOIL 2, 551–564. https://doi.org/10.5194/soil-2-551-2016

Schaus, G.P. (Ed.), 2014. Symphalos: The Acropolis Sanctuary, Volume 1. University of Toronto Press.

Schellekens, J., Buurman, P., 2011. Geoderma n -Alkane distributions as palaeoclimatic proxies in ombrotrophic peat : The role of decomposition and dominant vegetation. Geoderma 164, 112–121. https://doi.org/10.1016/j.geoderma.2011.05.012

Schenk, M.F., Thienpont, C.-N., Koopman, W.J.M., Gilissen, L.J.W.J., Smulders, M.J.M., 2008. Phylogenetic relationships in Betula (Betulaceae) based on AFLP markers. Tree Genet. Genomes 4, 911. https://doi.org/10.1007/s11295-008-0162-0

Scheu, A., Powell, A., Bollongino, R., Vigne, J.-D., Tresset, A., Çakırlar, C., Benecke, N., Burger, J., 2015. The genetic prehistory of domesticated cattle from their origin to the spread across Europe. BMC Genet. 16, 54. https://doi.org/10.1186/s12863-015-0203-2

Schlolaut, G., Brauer, A., Nakagawa, T., Lamb, H.F., Tyler, J.J., Staff, R.A., Marshall, M.H., Bronk Ramsey, C., Bryant, C.L., Tarasov, P.E., 2017. Evidence for a bi-partition of the Younger Dryas Stadial in East Asia associated with inversed climate characteristics compared to Europe. Sci. Rep. 7, 44983. https://doi.org/10.1038/srep44983

Schouten, S., Hopmans, E.C., Schefuß, E., Sinninghe Damsté, J.S., 2002. Distributional variations in marine crenarchaeotal membrane lipids: a new tool for reconstructing

ancient sea water temperatures? Earth Planet. Sci. Lett. 204, 265–274. https://doi.org/10.1016/S0012-821X(02)00979-2

Schouten, S., Woltering, M., Rijpstra, W.I.C., Sluijs, A., Brinkhuis, H., Sinninghe Damsté, J.S., 2007. The Paleocene-Eocene carbon isotope excursion in higher plant organic matter: Differential fractionation of angiosperms and conifers in the Arctic. Earth Planet. Sci. Lett. 258, 581–592. https://doi.org/10.1016/j.epsl.2007.04.024

Schouten, S., Hopmans, E.C., Sinninghe Damsté, J.S., 2013a. The organic geochemistry of glycerol dialkyl glycerol tetraether lipids: A review. Org. Geochem. 54, 19–61. https://doi.org/10.1016/j.orggeochem.2012.09.006

Schouten, S., Villareal, T.A., Hopmans, E.C., Mets, A., Swanson, K.M., Sinninghe Damsté, J.S., 2013b. Endosymbiotic heterocystous cyanobacteria synthesize different heterocyst glycolipids than free-living heterocystous cyanobacteria. Phytochemistry 85, 115–121. https://doi.org/10.1016/j.phytochem.2012.09.002

Schreiner, A., 1973a. Erläuterungen zu Blatt 8219 Singen.

Schreiner, A., 1973b. Geologische Karte von Baden-Württemberg 1:25000.

Schwander, J., Eicher, U., Ammann, B., 2000. Oxygen isotopes of lake marl at Gerzensee and Leysin (Switzerland), covering the Younger Dryas and two minor oscillations, and their correlation to the GRIP ice core. Palaeogeogr. Palaeoclimatol. Palaeoecol. 159, 203–214. https://doi.org/10.1016/S0031-0182(00)00085-7

Schwark, L., Zink, K., Lechterbeck, J., 2002. Reconstruction of postglacial to early Holocene vegetation history in terrestrial Central Europe via cuticular lipid biomarkers and pollen records from lake sediments. Geology 30, 463. https://doi.org/10.1130/0091-7613(2002)030<0463:ROPTEH>2.0.CO;2

Seguin, J., Bintliff, J.L., Grootes, P.M., Bauersachs, T., Dörfler, W., Heymann, C., Manning, S.W., Müller, S., Nadeau, M.J., Nelle, O., Steier, P., Weber, J., Wild, E.M., Zagana, E., Unkel, I., 2019. 2500 years of anthropogenic and climatic landscape transformation in the Stymphalia polje, Greece. Quat. Sci. Rev. 213, 133–154. https://doi.org/10.1016/j.quascirev.2019.04.028

Seifert, W.K., Michael Moldowan, J., 1978. Applications of steranes, terpanes and monoaromatics to the maturation, migration and source of crude oils. Geochim. Cosmochim. Acta 42, 77–95. https://doi.org/10.1016/0016-7037(78)90219-3

Shepherd, T., Robertson, G.W., Griffiths, D.W., Birch, A.N.E., 1999. Epicuticular wax ester and triacylglycerol composition in relation to aphid infestation and resistance in red raspberry (Rubus idaeus L.). Phytochemistry 52, 1255–1267. https://doi.org/10.1016/S0031-9422(99)00414-8

Sherratt, A., 1983. The secondary exploitation of animals in the Old World. World Archaeol. 15, 90–104. https://doi.org/10.1080/00438243.1983.9979887

Shukurov, A., Videiko, M.Y., Sarson, G.R., Davison, K., Shiel, R., Dolukhanov, P.M., Pashkevich, G.A., 2015. Productivity of pre-modern agriculture in the Cucuteni-Trypillia area.

Sieber, P., Schorderet, M., Ryser, U., Buchala, A., Kolattukudy, P., Métraux, J.-P., Nawrath, C., 2000. Transgenic Arabidopsis Plants Expressing a Fungal Cutinase Show Alterations in the Structure and Properties of the Cuticle and Postgenital Organ Fusions. Plant Cell 12, 721–737. https://doi.org/10.1105/tpc.12.5.721

Sigalos, E., 2004. Housing in Medieval and Post-Medieval Greece. Br. Archaeol. Reports Int. Ser.

Sinninghe Damsté, J.S., Rampen, S.W., Masse, G., Allard, G.W., Belt, S.T., Robert, J., Rowland, S.J., Moldowan, J.M., Barbanti, S.M., Fago, F.J., Denisevich, P., Dahl, J., Trindade, L.A.F., Schouten, S., 2004. The Rise of the Rhizosolenid Diatoms. Science. 304, 584–587.

Sinninghe Damsté, J.S., Rijpstra, W.I.C., Hopmans, E.C., Weijers, J.W.H., Foesel, B.U., Overmann, J., Dedysh, S.N., 2011. 13,16-Dimethyl Octacosanedioic Acid (iso -Diabolic Acid), a Common Membrane-Spanning Lipid of Acidobacteria Subdivisions 1 and 3. Appl. Environ. Microbiol. 77, 4147–4154. https://doi.org/10.1128/AEM.00466-11

Sinninghe Damsté, J.S., Ossebaar, J., Schouten, S., Verschuren, D., 2012a. Distribution of tetraether lipids in the 25-ka sedimentary record of Lake Challa: extracting reliable TEX86 and MBT/CBT palaeotemperatures from an equatorial African lake. Quat. Sci. Rev. 50, 43–54. https://doi.org/10.1016/j.quascirev.2012.07.001

Sinninghe Damsté, J.S., Rijpstra, W.I.C., Hopmans, E.C., Jung, M.-Y., Kim, J.-G., Rhee, S.-K., Stieglmeier, M., Schleper, C., 2012b. Intact Polar and Core Glycerol Dibiphytanyl Glycerol Tetraether Lipids of Group I.1a and I.1b Thaumarchaeota in Soil. Appl. Environ. Microbiol. 78, 6866–6874. https://doi.org/10.1128/AEM.01681-12

Sinninghe Damsté, J.S., Rijpstra, W.I.C., Hopmans, E.C., Foesel, B.U., Wüst, P.K., Overmann, J., Tank, M., Bryant, D.A., Dunfield, P.F., Houghton, K., Stott, M.B., 2014. Ether- and ester-bound iso-diabolic acid and other lipids in members of Acidobacteria subdivision 4. Appl. Environ. Microbiol. 80, 5207–5218. https://doi.org/10.1128/AEM.01066-14

Sinninghe Damsté, J.S., Rijpstra, W.I.C., Foesel, B.U., Huber, K.J., Overmann, J., Nakagawa, S., Kim, J.J., Dunfield, P.F., Dedysh, S.N., Villanueva, L., 2018a. An overview of the occurrence of ether- and ester-linked iso-diabolic acid membrane lipids in microbial cultures of the Acidobacteria: Implications for brGDGT paleoproxies for temperature and pH. Org. Geochem. 124, 63–76. https://doi.org/10.1016/j.orggeochem.2018.07.006

Sinninghe Damsté, J.S., Rijpstra, W.I.C., Foesel, B.U., Huber, K.J., Overmann, J., Nakagawa, S., Kim, J.J., Dunfield, P.F., Dedysh, S.N., Villanueva, L., 2018b. An overview of the

occurrence of ether- and ester-linked iso-diabolic acid membrane lipids in microbial cultures of the Acidobacteria: Implications for brGDGT paleoproxies for temperature and pH. Org. Geochem. 124, 63–76. https://doi.org/10.1016/j.orggeochem.2018.07.006

Sirocko, F., 2009. Wetter, Klima, Menschheitsentwicklung: von der Eiszeit bis ins 21. Jahrhundert. Konrad Theiss Verlag, Stuttgart.

Skvortsov, A.K., 2002. A new system of the genus Betula L. Bull. Mosc. Natur. Soc 107, 73–76.

Słowiński, M., Zawiska, I., Ott, F., Noryśkiewicz, A.M., Plessen, B., Apolinarska, K., Rzodkiewicz, M., Michczyńska, D.J., Wulf, S., Skubała, P., Kordowski, J., Błaszkiewicz, M., Brauer, A., 2017. Differential proxy responses to late Allerød and early Younger Dryas climatic change recorded in varved sediments of the Trzechowskie palaeolake in Northern Poland. Quat. Sci. Rev. 158, 94–106. https://doi.org/10.1016/j.quascirev.2017.01.005

Smith, F., Wing, S., Freeman, K., 2007. Magnitude of the carbon isotope excursion at the Paleocene–Eocene thermal maximum: The role of plant community change. Earth Planet. Sci. Lett. 262, 50–65. https://doi.org/10.1016/j.epsl.2007.07.021

Smith, F.M.J., Wood, S.A., van Ginkel, R., Broady, P.A., Gaw, S., 2011. First report of saxitoxin production by a species of the freshwater benthic cyanobacterium, Scytonema Agardh. Toxicon 57, 566–573. https://doi.org/10.1016/j.toxicon.2010.12.020

Sollai, M., Hopmans, E.C., Bale, N.J., Mets, A., Warden, L., Moros, M., Sinninghe Damsté, J.S., 2017. The Holocene sedimentary record of cyanobacterial glycolipids in the Baltic Sea: an evaluation of their application as tracers of past nitrogen fixation. Biogeosciences 14, 5789–5804. https://doi.org/10.5194/bg-14-5789-2017

Spangenberg, J.E., Ogrinc, N., 2001. Authentication of Vegetable Oils by Bulk and Molecular Carbon Isotope Analyses with Emphasis on Olive Oil and Pumpkin Seed Oil. J. Agric. Food Chem. 49, 1534–1540. https://doi.org/10.1021/jf001291y

Spangenberg, J.E., Jacomet, S., Schibler, J., 2006. Chemical analyses of organic residues in archaeological pottery from Arbon Bleiche 3, Switzerland – evidence for dairying in the late Neolithic. J. Archaeol. Sci. 33, 1–13. https://doi.org/10.1016/j.jas.2005.05.013

Stal, L.J., 2012. Cyanobacterial Mats and Stromatolites, in: Ecology of Cyanobacteria II. Springer Netherlands, Dordrecht, pp. 65–125. https://doi.org/10.1007/978-94-007-3855-3_4

Stammitti, L., Derridj, S., Garrec, J.P., 1996. Leaf epicuticular lipids of Prunus laurocerasus: importance of extraction methods. Phytochemistry 43, 45–48. https://doi.org/10.1016/0031-9422(96)00241-5

Stansell, N.D., Abbott, M.B., Rull, V., Rodbell, D.T., Bezada, M., Montoya, E., 2010. Abrupt Younger Dryas cooling in the northern tropics recorded in lake sediments from the

Venezuelan Andes. Earth Planet. Sci. Lett. 293, 154–163. https://doi.org/10.1016/J.EPSL.2010.02.040

Starkel, L., Michczyńska, D.J., Krąpiec, M., Margielewski, W., Nalepka, D., Pazdur, A., 2012. Progress in the holocene chrono-climatostratigraphy of Polish territory. Geochronometria 40, 1–21. https://doi.org/10.2478/s13386-012-0024-2

Staubwasser, M., Weiss, H., 2006. Holocene climate and cultural evolution in late prehistoric-early historic West Asia. Quat. Res. 66, 372–387. https://doi.org/10.1016/j.yqres.2006.09.001

Steele, V.J., Stern, B., Stott, A.W., 2010. Olive oil or lard?: Distinguishing plant oils from animal fats in the archeological record of the eastern Mediterranean using gas chromatography/combustion/isotope ratio mass spectrometry. Rapid Commun. Mass Spectrom. 24, 3478–3484. https://doi.org/10.1002/rcm.4790

Steffens, J., 2005. Die Bedeutung der Jagd in der Trichterbecherkultur. J. Neolit. Archaeol. 7, 1–12. https://doi.org/10.12766/jna.2005.14

Sümmchen, P., Markstädter, C., Wienhaus, O., 1995. Composition of the Epicuticular Wax Esters of Picea abies (L.) Karst. Zeitschrift für Naturforsch. C 50, 11–14. https://doi.org/10.1515/znc-1995-1-203

Sun, Q., Chu, G., Liu, G., Li, S., Wang, X., 2007. Calibration of alkenone unsaturation index with growth temperature for a lacustrine species, Chrysotila lamellosa (Haptophyceae). Org. Geochem. 38, 1226–1234. https://doi.org/10.1016/j.orggeochem.2007.04.007

Sun, Q., Chu, G., Xie, M., Ling, Y., Su, Y., Zhu, Q., Shan, Y., Liu, J., 2018. Long-chain alkenone-inferred temperatures from the last deglaciation to the early Holocene recorded by annually laminated sediments of the maar lake Sihailongwan, northeastern China. The Holocene 28, 1173–1180. https://doi.org/10.1177/0959683618761546

Szczepanek, K., Myszkowska, D., Worobiec, E., Piotrowicz, K., Ziemianin, M., Bielec-Bąkowska, Z., 2017. The long-range transport of Pinaceae pollen: an example in Kraków (southern Poland). Aerobiologia (Bologna). 33, 109–125. https://doi.org/10.1007/s10453-016-9454-2

Talbot, H.M., Farrimond, P., 2007. Bacterial populations recorded in diverse sedimentary biohopanoid distributions. Org. Geochem. 38, 1212–1225. https://doi.org/10.1016/j.orggeochem.2007.04.006

Talbot, M.R., 1990. A review of the palaeohydrological interpretation of carbon and oxygen isotopic ratios in primary lacustrine carbonates. Chem. Geol. Isot. Geosci. Sect. 80, 261–279. https://doi.org/10.1016/0168-9622(90)90009-2

Talbot, M.R., Johannessen, T., 1992. A high resolution palaeoclimatic record for the last 27,500 years in tropical West Africa from the carbon and nitrogen isotopic composition of lacustrine organic matter. Earth Planet. Sci. Lett. 110, 23–37.

https://doi.org/10.1016/0012-821X(92)90036-U

Tarasov, P.E., Bezrukova, E. V., Krivonogov, S.K., 2009. Late Glacial and Holocene changes in vegetation cover and climate in southern Siberia derived from a 15 kyr long pollen record from Lake Kotokel. Clim. Past 5, 285–295. https://doi.org/10.5194/cp-5-285-2009

Tarasov, P.E., Müller, S., Zech, M., Andreeva, D., Diekmann, B., Leipe, C., 2013. Last glacial vegetation reconstructions in the extreme-continental eastern Asia: Potentials of pollen and n-alkane biomarker analyses. Quat. Int. 290–291, 253–263. https://doi.org/10.1016/j.quaint.2012.04.007

Terberger, T., Burger, J., Lüth, F., Müller, J., Piezonka, H., 2018. Step by step – The neolithisation of Northern Central Europe in the light of stable isotope analyses. J. Archaeol. Sci. 99, 66–86. https://doi.org/10.1016/j.jas.2018.08.004

Theroux, S., D'Andrea, W.J., Toney, J., Amaral-Zettler, L., Huang, Y., 2010. Phylogenetic diversity and evolutionary relatedness of alkenone-producing haptophyte algae in lakes: Implications for continental paleotemperature reconstructions. Earth Planet. Sci. Lett. 300, 311–320. https://doi.org/10.1016/j.epsl.2010.10.009

Thomson, A.M., Dick, C.W., Pascoini, A.L., Dayanandan, S., 2015. Despite introgressive hybridization, North American birches (Betula spp.) maintain strong differentiation at nuclear microsatellite loci. Tree Genet. Genomes 11, 101. https://doi.org/10.1007/s11295-015-0922-6

Thórsson, A.T., Salmela, E., Anamthawat-Jónsson, K., 2001. Morphological, cytogenetic, and molecular evidence for introgressive hybridization in birch. J. Hered. 92, 404–8. https://doi.org/10.1093/jhered/92.5.404

Tierney, J.E., Russell, J.M., 2009. Distributions of branched GDGTs in a tropical lake system: Implications for lacustrine application of the MBT/CBT paleoproxy. Org. Geochem. 40, 1032–1036. https://doi.org/10.1016/j.orggeochem.2009.04.014

Tipple, B.J., Pagani, M., 2013. Environmental control on eastern broadleaf forest species' leaf wax distributions and d/h ratios. Geochim. Cosmochim. Acta 111, 64–77. https://doi.org/10.1016/j.gca.2012.10.042

Tjallingii, R., 2006. Application and quality of X-Ray Fluorescence core scanning in reconstructing late Pleistocene NW African continental margin sedimentation patterns and paleoclimate variations. Dep. Geosci. Univ. Bremen 1–114.

Tjallingii, R., Röhl, U., Kölling, M., Bickert, T., 2007. Influence of the water content on X-ray fluorescence corescanning measurements in soft marine sediments. Geochemistry, Geophys. Geosystems 8, n/a-n/a. https://doi.org/10.1029/2006GC001393

Tralau, H., 1963. The recent and fossil distribution of some boreal and arctic montane plants in Europe. Ark. Bot. Ser. 2.

Treibs, A., 1934. Chlorophyll- und Häminderivate in bituminösen Gesteinen, Erdölen,

Erdwachsen und Asphalten. Ein Beitrag zur Entstehung des Erdöls. Justus Liebigs Ann. Chem. 510, 42–62. https://doi.org/10.1002/jlac.19345100103

Tsuda, Y., Semerikov, V., Sebastiani, F., Vendramin, G.G., Lascoux, M., 2017. Multispecies genetic structure and hybridization in the Betula genus across Eurasia. Mol. Ecol. 26, 589–605. https://doi.org/10.1111/mec.13885

Tyson, R. V., 1995. Sedimentary Organic Matter. Springer Netherlands, Dordrecht. https://doi.org/10.1007/978-94-011-0739-6

Unkel, I., Heymann, C., Nelle, O., Zagana, E., 2011. Climatic influence on Lake Stymphalia during the last 15 000 years, in: Advances in the Research of Aquatic Environment. Springer Berlin Heidelberg, pp. 75–82. https://doi.org/10.1007/978-3-642-19902-8_8

Unkel, I., Schimmelmann, A., Shriner, C., Forsén, J., Heymann, C., Brückner, H., 2014. The environmental history of the last 6500 years in the Asea Valley (Peloponnese, Greece) and its linkage to the local archaeological record. Zeitschrift für Geomorphol. Suppl. Issues 58, 89–107. https://doi.org/10.1127/0372-8854/2014/S-00160

van Asch, N., Kloos, M.E., Heiri, O., de Klerk, P., Hoek, W.Z., 2012. The younger dryas cooling in northeast Germany: summer temperature and environmental changes in the Friedländer Groβe Wiese region. J. Quat. Sci. 27, 531–543. https://doi.org/10.1002/jqs.2547

van Bergen, P.F., Bull, I.D., Poulton, P.R., Evershed, R.P., 1997. Organic geochemical studies of soils from the Rothamsted Classical Experiments—I. Total lipid extracts, solvent insoluble residues and humic acids from Broadbalk Wilderness. Org. Geochem. 26, 117–135. https://doi.org/10.1016/S0146-6380(96)00134-9

van den Bos, V., Engels, S., Bohncke, S.J.P., Cerli, C., Jansen, B., Kalbitz, K., Peterse, F., Renssen, H., Sachse, D., 2018. Late Holocene changes in vegetation and atmospheric circulation at Lake Uddelermeer (The Netherlands) reconstructed using lipid biomarkers and compound-specific δD analysis. J. Quat. Sci. 33, 100–111. https://doi.org/10.1002/jqs.3006

van Dinter, M., Birks, H.H., 1996. Distinguishing fossil Betula nana and B. pubescens using their wingless fruits: implications for the late-glacial vegetational history of western Norway. Veg. Hist. Archaeobot. 5, 229–240. https://doi.org/10.1007/BF00217500

Veski, S., Amon, L., Heinsalu, A., Reitalu, T., Saarse, L., Stivrins, N., Vassiljev, J., 2012. Lateglacial vegetation dynamics in the eastern Baltic region between 14,500 and 11,400 cal yr BP: A complete record since the Bølling (GI-1e) to the Holocene. Quat. Sci. Rev. 40, 39–53. https://doi.org/10.1016/j.quascirev.2012.02.013

Volkman, J.K., Eglinton, G., Corner, E.D.S., Sargent, J.R., 1980. Novel unsaturated straight-chain C37-C39 methyl and ethyl ketones in marine sediments and a coccolithophore Emiliania huxleyi. Phys. Chem. Earth 12, 219–227. https://doi.org/10.1016/0079-

1946(79)90106-X

Volkman, J.K., Barrett, S.M., Dunstan, G.A., 1994. C25 and C30 highly branched isoprenoid alkenes in laboratory cultures of two marine diatoms. Org. Geochem. 21, 407–414. https://doi.org/10.1016/0146-6380(94)90202-X

Volkman, J.K., Barrerr, S.M., Blackburn, S.I., Sikes, E.L., 1995. Alkenones in Gephyrocapsa oceanica: Implications for studies of paleoclimate. Geochim. Cosmochim. Acta 59, 513–520. https://doi.org/10.1016/0016-7037(95)00325-T

Von Grafenstein, U., Erlenkeuser, Brauer, Jouzel, Johnsen, 1999. A mid-european decadal isotope-climate record from 15,500 to 5000 years B.P. Science 284, 1654–7. https://doi.org/10.1126/science.284.5420.1654

Vött, A., Brückner, H., Zander, A.M., May, S.M., Mariolakos, I., Lang, F., Fountoulis, I., Dunkel, A., 2009. Late Quaternary evolution of Mediterranean poljes – the Vatos case study (Akarnania, NW Greece) based on geo-scientific core analyses and IRSL dating. Zeitschrift für Geomorphol. 53, 145–169. https://doi.org/10.1127/0372-8854/2009/0053-0145

Wada, E., Hattori, A., 1991. Nitrogen in the sea: Forms, abundances, and rate processes. CRC Press, Boca Raton.

Walsh, K., Brown, A.G., Gourley, B., Scaife, R., 2017a. Archaeology, hydrogeology and geomythology in the Stymphalos valley. J. Archaeol. Sci. Reports 15, 446–458. https://doi.org/10.1016/j.jasrep.2017.03.058

Walsh, K., Brown, A.G., Gourley, B., Scaife, R., 2017b. Archaeology, hydrogeology and geomythology in the Stymphalos valley. J. Archaeol. Sci. Reports 15, 446–458. https://doi.org/10.1016/j.jasrep.2017.03.058

Wang, N., McAllister, H.A., Bartlett, P.R., Buggs, R.J.A., 2016. Molecular phylogeny and genome size evolution of the genus Betula (Betulaceae). Ann. Bot. 117, 1023–1035. https://doi.org/10.1093/aob/mcw048

Weber, Y., De Jonge, C., Rijpstra, W.I.C., Hopmans, E.C., Stadnitskaia, A., Schubert, C.J., Lehmann, M.F., Sinninghe Damsté, J.S., Niemann, H., 2015. Identification and carbon isotope composition of a novel branched GDGT isomer in lake sediments: Evidence for lacustrine branched GDGT production. Geochim. Cosmochim. Acta 154, 118–129. https://doi.org/10.1016/j.gca.2015.01.032

Weiberg, E., Unkel, I., Kouli, K., Holmgren, K., Avramidis, P., Bonnier, A., Dibble, F., Finné, M., Izdebski, A., Katrantsiotis, C., Stocker, S.R., Andwinge, M., Baika, K., Boyd, M., Heymann, C., 2016. The socio-environmental history of the Peloponnese during the Holocene: Towards an integrated understanding of the past. Quat. Sci. Rev. 136, 40–65. https://doi.org/10.1016/j.quascirev.2015.10.042

Weidenbach, K., Nickel, L., Neve, H., Alkhnbashi, O.S., Künzel, S., Kupczok, A., Bauersachs,

T., Cassidy, L., Tholey, A., Backofen, R., Schmitz, R.A., 2017. Methanosarcina Spherical Virus, a Novel Archaeal Lytic Virus Targeting Methanosarcina Strains. J. Virol. 91, e00955-17. https://doi.org/10.1128/JVI.00955-17

Weijers, J.W.H., Schouten, S., van den Donker, J.C., Hopmans, E.C., Sinninghe Damsté, J.S., 2007. Environmental controls on bacterial tetraether membrane lipid distribution in soils. Geochim. Cosmochim. Acta 71, 703–713. https://doi.org/10.1016/j.gca.2006.10.003

Weltje, G.J., Tjallingii, R., 2008. Calibration of XRF core scanners for quantitative geochemical logging of sediment cores: Theory and application. Earth Planet. Sci. Lett. 274, 423–438. https://doi.org/10.1016/j.epsl.2008.07.054

Weninger, B., Clare, L., Rohling, E.J., Bar-Yosef, O., Böhner, U., Budja, M., Bundschuh, M., Feurdean, A., Gebel, H.G., Jöris, O., Linstädter, J., Mayewski, P., Mühlenbruch, T., Reingruber, A., Rollefson, G., Schyle, D., Thissen, L., Todorova, H., Zielhofer, C., 2009. The Impact of Rapid Climate Change on prehistoric societies during the Holocene in the Eastern Mediterranean. Doc. Praehist. 36, 7–59. https://doi.org/10.4312/dp.36.2

White, S.A., 2013. The Climate of Rebellion in the Early Modern Ottoman Empire, Cambridge. ed. Cambridge.

Whiticar, M.J., 1999. Carbon and hydrogen isotope systematics of bacterial formation and oxidation of methane. Chem. Geol. 161, 291–314. https://doi.org/10.1016/S0009-2541(99)00092-3

Wick, L., Lemcke, G., Sturm, M., 2003. Evidence of Lateglacial and Holocene climatic change and human impact in eastern Anatolia: High-resolution pollen, charcoal, isotopic and geochemical records from the laminated sediments of Lake Van, Turkey. Holocene 13, 665–675. https://doi.org/10.1191/0959683603hl653rp

Wiesenberg, G.L.B., Andreeva, D.B., Chimitdorgieva, G.D., Erbajeva, M.A., Zech, W., 2015. Reconstruction of environmental changes during the late glacial and Holocene reflected in a soil-sedimentary sequence from the lower Selenga River valley, Lake Baikal region, Siberia, assessed by lipid molecular proxies. Quat. Int. 365, 190–202. https://doi.org/10.1016/j.quaint.2015.01.042

Wild, E.M., Steier, P., Fischer, P., Höflmayer, F., 2013. 14C Dating of Humic Acids from Bronze and Iron Age Plant Remains from the Eastern Mediterranean. Radiocarbon 55, 599–607. https://doi.org/10.2458/azu_js_rc.55.16450

Williams, E.H., 1983. Stymphalos: A Planned City of Ancient Arcadia. Echos du Monde Class. Class. Views 27, 194–205.

Williams, H., 1984a. Investigations at Stymphalos. Echos du Monde Class. Class. Views 26, 215–224.

Williams, H., 1984b. Investigations at Mytilene and Stymphalos. Echos du Monde Class. Class. Views 169–183.

Williams, H., Cronkite Price, S.-M., 1995. Excavations at Stymphalos, 1994. Echos du Monde Class. Class. Views 39, 1–22.

Williams, H., 1996. Excavations at Stymphalos, 1995. Echos du Monde Class. Class. Views 40, 75–98.

Williams, H., Schaus, G., Cronkite Price, S.-M., Gourley, B., Lutomsky, H., 1997. Excavations at Ancient Stymphalos, 1996. Echos du Monde Class. Class. Views 41, 23–73.

Williams, H., Schaus, G., Cronkite Price, S.-M., Gourley, B., Hagerman, C., 1998. Excavations at Ancient Stymphalos, 1997. Echos du Monde Class. Class. Views 42, 261–319.

Williams, H., Schaus, G., Gourley, B., Cronkite Price, S.-M., Sherwood, K.D., Lolos, Y., 2002. Excavations at Ancient Stymphalos, 1999-2002. Mouseion 2, 135–187. https://doi.org/10.1353/mou.2002.0016

Williams, H., 2003. The Exploration of Ancient Stymphalos, 1982 - 2002 397–411.

Williams, H., 2005. Excavations at Stymphalos. Preliminary Reports 1983 - 2005. Museion.

Williams, H., Gouley, B., 2005. The Fortifications of Stymphalos. Mouseion III, 5, 213–259.

Winkler, H., 1904. Betulaceae, in: Engler, A. (Ed.), Das Pflanzenreich. Wilhelm Engelmann.

Woidich, M., 2014. Die Westliche Kugelamphorenkultur: Untersuchungen zu ihrer raumzeitlichen Differenzierung, kulturellen und anthropologischen Identität.

Wolbach, W.S., Ballard, J.P., Mayewski, P.A., Adedeji, V., Bunch, T.E., Firestone, R.B., French, T.A., Howard, G.A., Israde-Alcántara, I., Johnson, J.R., Kimbel, D., Kinzie, C.R., Kurbatov, A., Kletetschka, G., LeCompte, M.A., Mahaney, W.C., Melott, A.L., Maiorana-Boutilier, A., Mitra, S., Moore, C.R., Napier, W.M., Parlier, J., Tankersley, K.B., Thomas, B.C., Wittke, J.H., West, A., Kennett, J.P., 2018a. Extraordinary biomass-burning episode and impact winter triggered by the younger dryas cosmic impact ~12,800 years ago. 1. Ice cores and glaciers. J. Geol. 126, 165–184. https://doi.org/10.1086/695703

Wolbach, W.S., Ballard, J.P., Mayewski, P.A., Parnell, A.C., Cahill, N., Adedeji, V., Bunch, T.E., Domínguez-Vázquez, G., Erlandson, J.M., Firestone, R.B., French, T.A., Howard, G., Israde-Alcántara, I., Johnson, J.R., Kimbel, D., Kinzie, C.R., Kurbatov, A., Kletetschka, G., Lecompte, M.A., Mahaney, W.C., Melott, A.L., Mitra, S., Maiorana-Boutilier, A., Moore, C.R., Napier, W.M., Parlier, J., Tankersley, K.B., Thomas, B.C., Wittke, J.H., West, A., Kennett, J.P., 2018b. Extraordinary biomass-burning episode and impact winter triggered by the younger dryas cosmic impact ~12,800 years ago. 2. Lake, marine, and terrestrial sediments. J. Geol. 126, 185–205. https://doi.org/10.1086/695704

Wolf, U., 1994. Nähr- und Schadstoffbelastung kleiner Seen in Baden-Württemberg unter Berücksichtigung der Sedimentationsgeschichte. Die Rolle der kleinen Stehgewässer im regionalen Verbund. Cuvillier-Verlag, Göttingen.

Woodbury, S.E., Evershed, R.P., Barry Rossell, J., 1998. Purity assessments of major vegetable oils based on δ 13 C values of individual fatty acids. J. Am. Oil Chem. Soc. 75,

371–379. https://doi.org/10.1007/s11746-998-0055-2

Wörmer, L., Cirés, S., Velázquez, D., Quesada, A., Hinrichs, K.U., 2012. Cyanobacterial heterocyst glycolipids in cultures and environmental samples: Diversity and biomarker potential. Limnol. Oceanogr. 57, 1775–1788. https://doi.org/10.4319/lo.2012.57.06.1775

Xoplaki, E., Fleitmann, D., Luterbacher, J., Wagner, S., Haldon, J.F., Zorita, E., Telelis, I., Toreti, A., Izdebski, A., 2016. The Medieval Climate Anomaly and Byzantium: A review of the evidence on climatic fluctuations, economic performance and societal change. Quat. Sci. Rev. 136, 229–252. https://doi.org/10.1016/j.quascirev.2015.10.004

Xu, H., Liu, B., Wu, F., Dasch, E., Liu, C., Zhang, J., Li, C., Chen, J., An, Z., Head, J., Chen, J., An, Z., Liu, L., Ji, J., Yang, J., Chen, Y., Jin, Z., Cao, J., Wu, J., Wang, S., Xu, H., Liu, X., An, Z., Hou, Z., Dong, J., Xu, H., Ai, L., Tan, L., An, Z., Xu, H., Hou, Z., An, Z., Liu, X., Dong, J., Pang, J., Huang, C., Zhang, Z., Li, F., Xie, C., Pan, G., Xu, H., Hou, Z., Ai, L., Tan, L., 2010. Spatial and temporal variations of Rb/Sr ratios of the bulk surface sediments in Lake Qinghai. Geochem. Trans. 11, 3. https://doi.org/10.1186/1467-4866-11-3

Yang, B., Kallio, H.P., 2001. Fatty Acid Composition of Lipids in Sea Buckthorn (Hippophaë rhamnoides L.) Berries of Different Origins. J. Agric. Food Chem. 49, 1939–1947. https://doi.org/10.1021/jf001059s

Yu, Z., Eicher, U., 1998. Abrupt climate oscillations during the last deglaciation in central North America. Science 282, 2235–2238. https://doi.org/10.1126/science.282.5397.2235

Zeb, A., 2004. Important Therapeutic Uses of Sea Buckthorn (Hippophae): A Review. J. Biol. Sci. 4, 687–693. https://doi.org/10.3923/jbs.2004.687.693

Zech, M., Andreev, A., Zech, R., Müller, S., Hambach, U., Frechen, M., Zech, W., 2010. Quaternary vegetation changes derived from a loess-like permafrost palaeosol sequence in northeast Siberia using alkane biomarker and pollen analyses. Boreas 39, 540–550. https://doi.org/10.1111/j.1502-3885.2009.00132.x

Zhang, Y., Su, Y., Liu, Z., Yu, J., Jin, M., 2017. Lipid biomarker evidence for determining the origin and distribution of organic matter in surface sediments of Lake Taihu, Eastern China. Ecol. Indic. 77, 397–408. https://doi.org/10.1016/J.ECOLIND.2017.02.031

Zhang, Y., Su, Y., Liu, Z., Kong, L., Yu, J., Jin, M., Yongdong, Z., Zhengwen, L., 2018. Aliphatic hydrocarbon biomarkers as indicators of organic matter source and composition in surface sediments from shallow lakes along the lower Yangtze River, Eastern China. Org. Geochem. 122, 29–40. https://doi.org/10.1016/j.orggeochem.2018.04.009

Zhang, Z., Smittenberg, R.H., Bradley, R.S., 2016. GDGT distribution in a stratified lake and implications for the application of TEX 86 in paleoenvironmental reconstructions. Sci. Rep. 6, 1–10. https://doi.org/10.1038/srep34465

Zielińska, A., Nowak, I., 2017. Abundance of active ingredients in sea-buckthorn oil. Lipids

Health Dis. 16, 95. https://doi.org/10.1186/s12944-017-0469-7

Zink, K.G., Leythaeuser, D., Melkonian, M., Schwark, L., 2001. Temperature dependency of long-chain alkenone distributions in Recent to fossil limnic sediments and in lake waters. Geochim. Cosmochim. Acta 65, 253–265. https://doi.org/10.1016/S0016-7037(00)00509-3

Zink, K.G., Vandergoes, M.J., Bauersachs, T., Newnham, R.M., Rees, A.B.H., Schwark, L., 2016. A refined paleotemperature calibration for New Zealand limnic environments using differentiation of branched glycerol dialkyl glycerol tetraether (brGDGT) sources. J. Quat. Sci. 31, 823–835. https://doi.org/10.1002/jqs.2908

Zolitschka, B., Francus, P., Ojala, A.E.K., Schimmelmann, A., 2015. Varves in lake sediments - a review. Quat. Sci. Rev. 117, 1-41. https://doi.org/10.1016/j.quascirev.2015.03.019

Eidesstattliche Erklärung

Hiermit erkläre ich, dass ich die vorliegende Abhandlung selbstständig, ohne unzulässige Hilfe Dritter und ohne Benutzung anderer als der angegebenen Quellen und Hilfsmittel angefertigt habe. Die Arbeit entstand unter Einhaltung der Regeln guter wissenschaftlicher Praxis der Deutschen Forschungsgemeinschaft. Ich erkläre, dass weder die ganze Arbeit noch Teile einer anderen Stelle im Rahmen eines Prüfungsverfahrens vorgelegt wurde, veröffentlicht wurde oder zur Veröffentlich eingereicht wurde. Mir wurde kein akademischer Grad entzogen.

Kiel, 09.03.2020 Jan Hendrik Weber